University of Southern Queensland

Faculty of Health, Engineering & Sciences

Fabrication and design of a Stirling Engine powered by hydrogen

A dissertation submitted by

Michael Sheehan

in fulfilment of the requirements of

ENG4111 and ENG4112 Engineering Research Project

towards the degree of

Bachelor of Engineering (Honours) (Mechanical)

Submitted October, 2022

Abstract

This dissertation investigates the potential for using hydrogen as a fuel to power a Stirling engine and generate useful energy for applications in industry. The Stirling engine is an excellent candidate for producing clean energy which is renewable and won't produce harmful by-products that pollute the environment. This type of engine only requires a heat source to operate and therefore can be powered by many alternative options available in the renewable energy space. Hydrogen as a fuel is compared with current solar technologies to assess its viability in being used as a fuel for a Stirling engine application. It was found that hydrogen combustion can produce significant flame temperatures without releasing harmful byproducts during combustion, and provides an attractive solution for generating power in various applications that won't harm the environment.

Stirling engine design and analytical theory is presented along with the relevant properties of hydrogen for use in calculations, and four different analyses have been used to assess the potential power output. The analyses used include the Pressure-Volume diagram, the Schmidt equation, the Beale number and the West number. An engine was designed for a target power output of 750 - 1000 Watts based on potential uses for the engine as found when comparing with solar energy technology. The flame temperature and energy produced by hydrogen combustion is used for selecting an appropriate configuration and designing the geometry of an alpha type Stirling engine with crank slider mechanism. All components of the engine were designed and analysed for safety in terms of stress and the material properties, and the decisions made throughout the design process are discussed. Finite element analysis has been conducted and the results are presented along with a comparison to the hand calculations. After completing design of the engine, technical detail and assembly drawings were produced and are presented as appendices. The engine was fabricated and assembled using the drawings produced, and testing was carried out by simulating a heat source comparable to hydrogen combustion. The heater head reached a maximum temperature of 800° C but unfortunately the engine failed to run. Various modifications were made to the engine in an attempt to improve its performance and these are discussed along with the results.

Although the engine failed to run, the potential for using hydrogen as a fuel to power a Stirling engine and generate clean power proves to be very promising. Potential applications have been discussed assuming that the target power output can be achieved, and various potential areas for optimisation are discussed.

University of Southern Queensland

Faculty of Health, Engineering and Sciences

ENG4111 & ENG4112 Research Project

Limitations of Use

The Council of the University of Southern Queensland, its Faculty of Health, Engineering and Sciences, and the staff of the University of Southern Queensland, do not accept any responsibility for the truth, accuracy or completeness of material contained within or associated with this dissertation.

Persons using all or any part of this material do so at their own risk, and not at the risk of the Council of the University of Southern Queensland, its Faculty of Health, Engineering and Sciences or the staff of the University of Southern Queensland.

This dissertation reports an educational exercise and has no purpose or validity beyond this exercise. The sole purpose of the course pair entitles “Research Project” is to contribute to the overall education within the student’s chosen degree program. This document, the associated hardware, software, drawings, and any other material set out in the associated appendices should not be used for any other purpose: if they are so used, it is entirely at the risk of the user.

Certification of Dissertation

I certify that the ideas, designs and experimental work, results, analyses and conclusions set out in this dissertation are entirely my own effort, except where otherwise indicated and acknowledged.

I further certify that the work is original and has not been previously submitted for assessment in any other course or institution, except where specifically stated.

Michael Sheehan
Student Number: [redacted]

Acknowledgements

I would like to acknowledge and thank everyone who has supported over the course of my university studies. Everyone in my family has always been extremely encouraging and I am truly grateful. While I have not always been able to attend events due to studies, we have always found the time to get together and you have all been so supportive.

In particular, I have to thank my Mum and Dad. You have both always supported me in every way that you can no matter what, and I feel very lucky. Thank you Dad for your advice over the years and for helping me out whenever I needed time to study. Completing this project has taken a lot of effort and I appreciate the assistance you have given me in terms of workshop resources and studying at work. Thank you Mum for all the help you have given me in getting through the tough periods. You are always there to help me however you can and it has made a huge difference.

I would like to thank my supervisor Dr. Belal Yousif. Thank you for all your help and suggestions in completing this project. You have always responded to my questions without hesitation and I am very grateful. Thank you also to the staff at Oztec Manufacturing for your assistance in completing the fabrication aspect of the project.

Contents

List of Figures

List of Tables

Chapter 1

Introduction

1.1 Project Background

Robert Stirling invented an external combustion engine in 1816 that is now known as the Stirling Engine (Walker, 1994). As it only requires a temperature differential to operate, it is a very versatile engine which can function using any heat source to provide the input energy. Traditionally it has found limited commercial success, however it has seen a few periods where improvements in steel and manufacturing methods have led to increases in efficiency and power output (Rinker 2018). While it has been unable to compete with internal combustion engines in many applications, it is finding increasing use in modern applications with the focus on renewable energy and sustainability becoming more and more important.

As the Stirling Engine only requires a heat source to operate, various renewable energy sources can be harnessed to supply heat to the engine. Significant power output can be achieved with high enough temperatures, and modern technology allows these kinds of temperatures to be generated from sustainable resources. Some potential applications where Stirling engines can be used include electricity generation, as a source of mechanical power, space heating, cryocooling, space applications and remote power generation (Thimsen, 2002). Although the technology lacks the ability to deliver instantaneous power which may be necessary in some applications, they are advantageous in other ways as they require little maintenance, run quietly and can be moveable depending on the heat source.

Current research and designs utilise heat sources such as solar energy, geothermal energy, natural gas, biofuels, waste heat and material waste as fuel (Furmanek & Kropiwnicki, 2021). Modern technology such as solar concentrators and innovations in biofuels are making Stirling engines more and more viable for commercial success. There are modern companies developing Stirling engine technology such as Genoa, Microgen, WhisperGen and Inspirit. For the most part these companies are utilising the engine for electricity production, and the power output ranges from 0.75 kWe in the case of the WhisperGen PPS16 to 6.4 kWe produced by the Inspirit Charger 3.1 (Furmanek & Kropiwnicki, 2021). The internal working gases used in these engines include nitrogen, air and helium and the most common fuels sources are natural gas, LPG and biomass (Furmanek & Kropiwnicki, 2021). For the lower power output engines, high temperatures of 180 – 525° C can be found while the higher power engines require

a working temperature of up to 900° C. Figure 1.1 shows an example of a modern Stirling engine produced by Genoa.

Figure 1.1: Genoa ML3000 Stirling engine with two cylinders and power output of 3 kWe (Furmanek & Kropiwnicki, 2021).

Another example of current developments in Stirling engine technology can be found in Dong et al. (2021), where a Stirling engine is used in combination with a solar thermal collector system and thermoelectric generator to produce and store electricity. The system used the heat collected by the solar thermal collector to power the engine and thus create electricity and was reportedly capable of producing 2.96 kW at 43.6% efficiency (Dong et al. 2021). This shows that the rise of renewable energy is providing designers with a multitude of opportunities for incorporating Stirling engines in modern industry.

One sustainable fuel source which has been largely overlooked for powering Stirling engines is that of hydrogen. When hydrogen burns in pure oxygen, the only byproduct is water. Some nitrous oxides appear in the byproducts when hydrogen is burned in air, however the amounts are negligible with proper design (Rand & Dell, 2007). Hydrogen technology is also gaining in popularity with many countries currently conducting research and development. Australia is one of these countries, as we are planning to commission the world's first hybrid gas-hydrogen turbine for generating grid electricity in 2023 (Australian Trade and Investment Commission 2022). Thus, the use of hydrogen as a fuel in powering a Stirling engine represents an exciting opportunity for generating clean power. Furthermore, high temperatures can be produced which leads to the possibility of producing an engine with high power density.

Traditional analysis techniques based on thermodynamic theory have been widely used in the past and are still relevant today. One of the most well-known methods is that of the Schmidt equations. Modern computers and technology allow for a better understanding of Stirling engine performance with the use of numerical techniques, known as third-order methods, which can analyse the complex processes which occur in a Stirling engine. Furthermore, the Stirling engine has been arranged into multiple configurations with various drive mechanisms to suit specific applications. For example, the configuration selection depends on the temperature differential available, and the power output required (Egas & Clucas 2018). Some literature currently exists on the best methods for selecting a configuration, however it is still relatively minimal.

1.2 Project Development

1.2.1 Aims, Objectives and Scope

AIM

As outlined in the Project Specification document, the overall aim of the project is "to investigate the potential of using hydrogen as a fuel source for powering a Stirling Engine, and to design and fabricate a Stirling Engine to evaluate its performance and suitability for use in real world applications."

OBJECTIVES

Also outlined in the Project Specification document, the objectives of the project are as follows.

1. Research background information relating to Stirling Engine types and applications.
2. Evaluate the literature on using hydrogen as a fuel source and identify the maximum difference in temperature which can be attained for powering the engine. Similarly, evaluate the literature on using solar concentration technology and compare the maximum temperature difference with that of hydrogen in order to the best engine configuration for the design.
3. Design engine parameters depending on power output requirements and research potential materials which could be utilised for engine components, before designing engine components and producing drawings for manufacture.
4. Fabricate and test the engine by simulating the temperature difference achievable with hydrogen as a fuel source and analyse the data from testing and compare results with expected values from earlier calculations.
5. Evaluate suitability of the engine for use in real world applications.

IF TIME AND RESOURCES PERMIT

6. Optimisation of the engine components and parameters.
7. Research the hydrogen combustion process and technology and consider its incorporation within the engine and compare with typical PV solar technology.

SCOPE

The scope of the project work includes the following.

1. **Research**. A literature review has been conducted to find the relevant background information, theory and analysis methods required for carrying out the objectives of the project.
2. **Analysis.** Based on the initial research, a theoretical analysis was carried out using data found for hydrogen combustion and solar energy, Stirling engine parameters and configuration selection.
3. **Design.** Based on the aforementioned analysis, a configuration was selected and design of the parameters for the Stirling engine was completed. Technical detail and assembly drawings have been produced and were utilised in manufacturing the engine.
4. **Fabrication** Once the design was completed, the engine was fabricated at the student's workplace.
5. **Testing** After the engine was been fabricated, the performance of the engine was assessed using a predetermined testing method.
6. **Results and Discussion** The results were analysed and a discussion written to meet the objective of evaluating the suitability of the engine in real world applications.
7. **Completion of dissertation.** Write-up of the dissertation was completed to present the project.

1.2.2 Outcomes and Benefits

It is hoped that the work completed in this research project will deliver outcomes and benefits that are useful and positive to modern industry, the environment and the wellbeing of human beings all over the world. Some potential outcomes and benefits are listed below.

- Reduce global carbon emissions by offering a viable alternative to traditional engines powered by fossil fuels.
- Reduce global carbon emissions by offering a potential environmentally friendly power source for generating electricity or other applications.

- Improving people's lives by making it easier for the general public to use environmentally friendly power sources.
- Identifying modern applications for Stirling engines.
- Validating the potential of using hydrogen with Stirling engines.
- Optimising the Stirling engine for use with hydrogen as a fuel.
- Offering a viable alternative engine to industry, which is environmentally friendly, and can be used in various applications.
- Prove the concept of a hydrogen fuelled Stirling engine by building a working prototype.
- Further understanding of the best principles in Stirling engine configuration selection and design.

1.3 Timeline

During the planning phase of the project, a timeline was produced as shown in Appendix A.

1.4 Dissertation Structure

The dissertation structure and a brief overview of each chapter is outlined below.

CHAPTER 2 – LITERATURE REVIEW

This chapter provides background information and theory on Stirling Engine technology, design and applications. Relevant data and information is outlined pertaining to hydrogen fuel and solar energy as an input fuel for a Stirling Engine. The literature is reviewed for thermodynamic theory, power equations and design requirements in regards to Stirling engines and is presented for analysis and design in subsequent chapters.

CHAPTER 3 – METHODOLOGY

This chapter outlines the overall methodology which was followed in completing the project. It outlines how Stirling Engine theory was utilised to produce a conceptual engine design initially based on the applied temperature and power output as main considerations. The methodology for designing, fabricating and testing the engine based on these initial calculations is then outlined, and how the results

were collected and analysed. Finally, the ways in which the results were interpreted and linked back to the aims and objectives is described.

CHAPTER 4 – INITIAL DESIGN AND POWER CALCULATIONS

This chapter draws on design criteria outlined in the literature to select a suitable Stirling Engine configuration and geometry based on the applied temperature difference and define a target power output. Further analysis is presented utilising analysis techniques found in the literature to determine work output, rotational speed and power output of the conceptual engine at various applied temperatures. The selected geometry of the engine is justified by comparing the calculated power output with the target value outlined at the beginning of the chapter.

CHAPTER 5 – ENGINE DESIGN AND FABRICATION

This chapter outlines the design choices made for each engine component and presents images of the 3D solid models which were produced. Calculations of stress in critical components is presented along with the results of the Finite Element Analyses which were carried out. Finally, photos and a discussion of the fabricated engine is presented.

CHAPTER 6 – TESTING AND DISCUSSION

This chapter outlines the results of testing the engine with applied temperature and discusses the engine performance. Modifications which were made to the engine are discussed and revised power calculations are presented for these variations. The results are discussed and suggestions for optimisation and real-world applications of the engine are outlined.

CHAPTER 7 – CONCLUSIONS AND FURTHER WORK

The outcomes achieved by the project are discussed and linked back to the aims and objectives. Potential further work in improving or continuing development of the engine is discussed.

REFERENCES

All references used in this dissertation are listed.

APPENDIX A – PROJECT SPECIFICATION

Appendix A contains the project specification and initial timeline which was produced in planning the project.

APPENDIX B – RISK ASSESSMENT

Appendix B presents the risk assessment which was carried out in planning the project, and covers all aspects of the work required.

APPENDIX C – DETAIL AND ASSEMBLY DRAWINGS OF ENGINE DESIGN

Appendix C contains detail and assembly drawings produced for fabrication of the engine, based on the initial design in Chapter 4.

APPENDIX D – DETAIL AND ASSEMBLY DRAWINGS OF MODIFIED COMPONENTS

As discussed in Chapter 6, some modifications were made to engine components to assess the engine's response. Appendix D contains drawings of the modified components and assemblies.

Chapter 2

Literature Review

2.1 Literature Review of relevant topics

2.1.1 Stirling Engine background and configurations

Stirling Engines are a type of heat engine which utilise a working fluid that is cycled between a hot and cold cylinder to generate power output. The engine operation can be described using the Stirling Cycle, which consists of two totally reversible isochoric and two totally reversible isothermal processes, which are all totally reversible. The Stirling Cycle requires the inclusion of a regenerator within the device, which extracts heat from the working fluid during one process within the cycle and returns it in another (Cengel et al. 2016). The four processes are shown in Figure 2.1 on a T-s diagram (temperature plotted against entropy) and P-v diagram (pressure plotted against volume) and can be described as: 1-2 isothermal expansion (external heat supply); 2-3 constant volume regeneration (working fluid transfers heat to regenerator internally); 3-4 isothermal compression (external heat sink); and 4-1 constant volume regeneration (regenerator transfers heat to working fluid) (Cengel & Boles 2015).

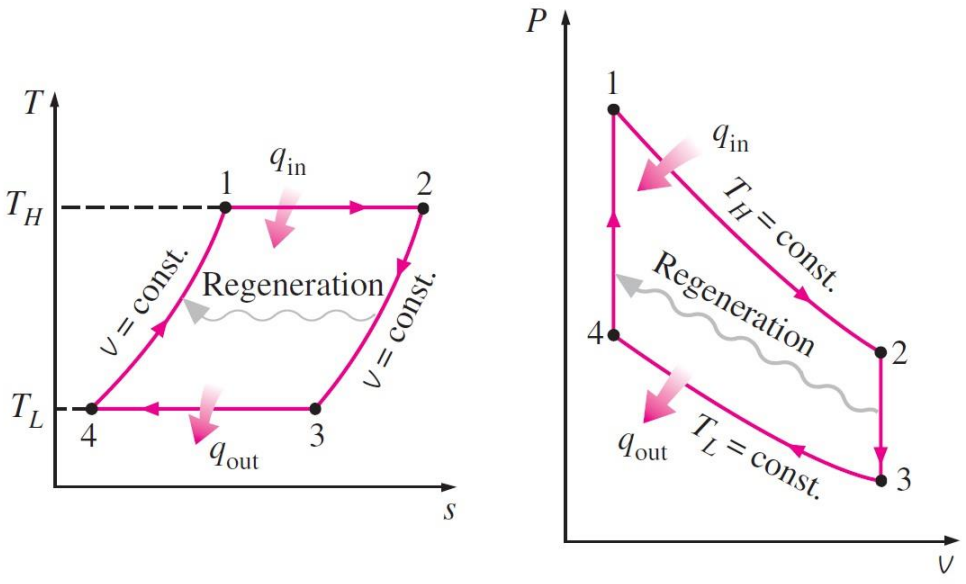

Figure 2.1: PV and TS diagrams for Stirling Cycle (Cengel & Boles 2015).

According to the Carnot principle, the thermal efficiency of the Stirling equal must be equal to the Carnot efficiency because it is also a totally reversible cycle. The Carnot efficiency, as shown in Figure 2.2 and denoted by $\eta_{th.rev}$, is the highest theoretically attainable efficiency of a heat engine operating between two temperatures of T_L (heat sink or low temperature) and T_H (heat source of high temperature), where the temperatures are given in Kelvin (Cengel & Boles 2015). It is impossible for the efficiency of any heat engine to exceed this value, and in practicality the efficiency of Stirling engines is lower than this value due to inefficiencies in the regenerator, heat exchangers, mechanical losses and other factors (Organ 2014). From this equation, one can deduce that in order to maximise the thermal efficiency of the engine, the temperature of the heat sink (T_L) must be minimised and the temperature of the heat source (T_H) must be maximised.

$$\eta_{\text{th.rev}} = 1 - \frac{T_L}{T_H}$$

Figure 2.2: Carnot cycle efficiency (Cengel et al. 2016)

According to Rutczyk, Szczygiel & Kabaj (2020), the efficiency of the regenerator significantly impacts the performance of the engine and should be considered one of the most important parameters. Various materials are used in their construction however are most commonly constructed from wire mesh screens and metal felts. In an analysis conducted on an alpha configuration engine with specified parameters, Rutczyk, Szczygiel & Kabaj (2020) determined the relationship between thermal efficiency and regenerator effectiveness. Figure 2.3 shows the results, and it is clear that the overall thermal efficiency increased significantly with a rise in regenerator effectiveness.

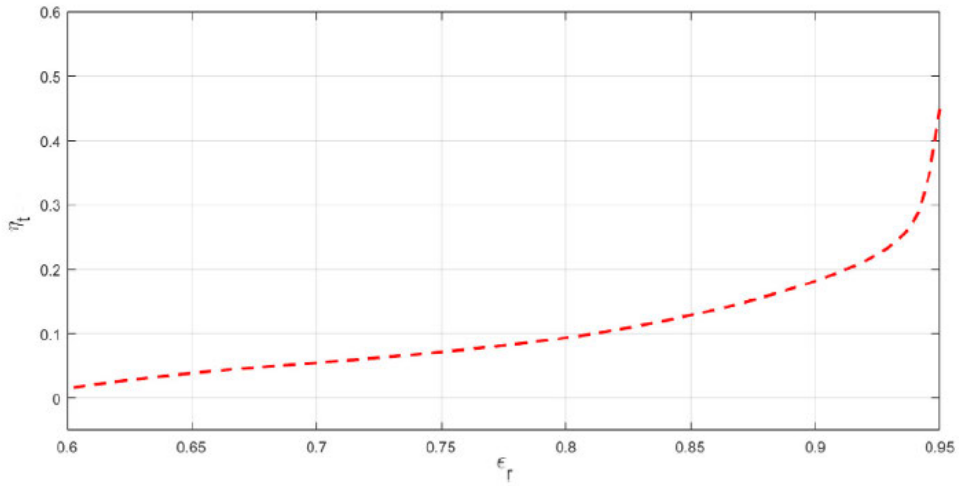

Figure 2.3: Evaluated Stirling engine's efficiency as a function of regenerator effectiveness (Rutczyk, Szczygiel & Kabaj 2020).

The regenerator is essentially a heat exchanger, and therefore it can be analysed using traditional theory, although various other discrete analyses have been proposed in the literature. When the number of transfer units (NTU) is known, the regenerator's effectiveness can be estimated using the equation in Figure 2.4. Where ε_r is the regenerator effectiveness, and NTU_O is the NTU value for the heat exchanger.

$$\varepsilon_r = \frac{NTU_o}{1 + NTU_o}$$

Figure 2.4: Regenerator effectiveness as a function of Number of Transfer Units (NTU) (Rutczyk, Szczygiel & Kabaj 2020).

It is desirable to use a material with a higher thermal conductivity so that the heat transfer rate between the working gas and the regenerator material is more efficient (Rutczyk, Szczygiel & Kabaj 2020). Furthermore, the porosity of the regenerator, which is determined by geometry such as wire diameter and mesh density, has a significant impact on its performance. A lower porosity value means it is more difficult for the working gas to penetrate the matrix and therefore a larger pressure drop occurs. However, a lower porosity leads to higher effectiveness and therefore a balance must be found when designing the regenerator to achieve the optimum result in terms of engine performance (Abdullah et al., 2005).

There are three main configurations of Stirling engine, namely: alpha; beta; and gamma. Each configuration offers different benefits for certain applications, and within each type there exists different designs and arrangements to further optimise the engine's performance. Alpha configuration engines typically use a crank drive mechanism or Ross yoke to convert the linear motion of the piston(s) to rotary motion of the output shaft, where Beta engines predominantly use a slider-crank drive or a rhombic drive (Egas & Clucas 2018). There are also other new configurations being developed such as delta and free piston which are briefly discussed later in the literature review. Figure 2.5 shows five different Stirling engine configurations, where the components of the engine can be identified using the colour scheme: hot and cold cylinders (expansion and compression volumes) are designated red and blue respectively; sealing pistons are gold; displacers are green pistons; and silver-grey cylinders represent regenerators (Egas & Clucas 2018).

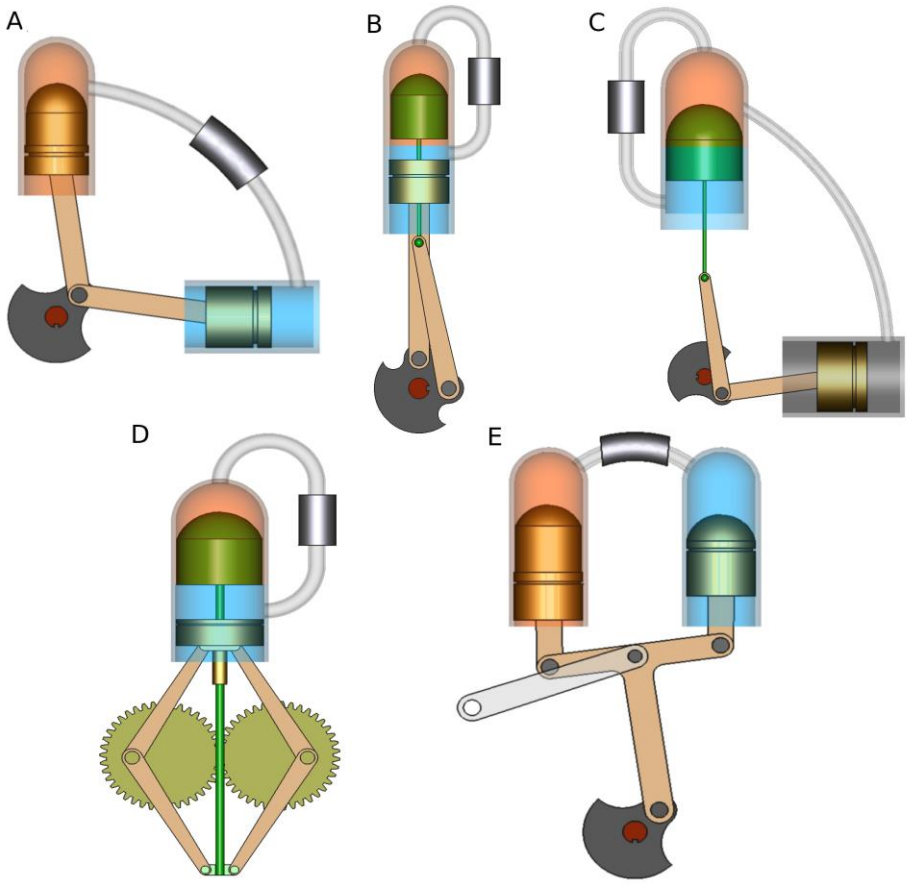

Figure 2.5: Five Stirling engine configurations (Egas & Clucas 2018).

Referring to Figure 2.5, diagram A shows the alpha type with crank slider mechanism. The pistons are out of phase by 90 degrees and a pipe housing the regenerator connects the hot and cold cylinders. Diagram B shows the beta configuration also fitted with a crank slider mechanism. Here there is a sealing piston and displacer both operating in the same cylinder. There is clearance between the cylinder and displacer allowing air to travel past the displacer from the hot end of the cylinder to the cold end, and vice versa. The two mechanisms are out of phase by 90 degrees. Diagram C shows a gamma configuration with crank drive. Here is there is a sealing piston a displacer operating however they are housed independently in two cylinders. Again, the two cylinders are connected by a pipe and phased by 90 degrees. Diagram D represents another beta configuration, this time with a rhombic drive, while diagram E shows an alpha configuration with a Ross yoke drive (Egas & Clucas 2018). Detailed explanation of each configuration is given in Section 2.1.2 where configuration selection is discussed.

The working fluid which is compressed and expanded within the cylinder(s) is another important consideration. A low heat capacity is desirable to maximise the increase in pressure for a given amount of heat (Vineeth 2012). A low viscosity is also favourable so that pressure drop is minimised as the fluid flows between the hot and cold regions. Finally, thermal conductivity is advantageous so that heat transfer to the gas is maximised (Vineeth 2012). Helium has a very low heat capacity and is therefore one of the best gases to use, however availability must also be considered. The gas will not always be

perfectly retained within the engine and therefore there must be a supply delivered to the expansion and compression spaces. Air is the most commonly used gas as it is readily available and has properties which are still viable. Hydrogen is a better choice because of its lower heat capacity, high thermal conductivity and low viscosity, however sealing is more difficult as it diffuses out of the engine more readily. Nitrogen and methane are other viable gases with attractive properties (Boretti 2021, pp. 16241-16247). Table 2.1 shows properties of some of the viable working fluids.

Table 2.1: Properties of some viable working fluids for use in a Stirling engine (Thombare & Karmare 2012).

Working fluid at 300 K	Thermal conductivity (W/m K)	Sp. Heat at const. volume (kJ/kg K)	Density (Kg/m^3)	Thermal diffusivity $TD = \frac{\text{thermal conductivity}}{\text{sp. heat} \times \text{density}}$
Air	0.0262	0.718	1.1700	0.03
Helium	0.7560	3.120	0.1620	1.50
CO_2	0.0168	0.657	1.7970	0.01
Nitrogen	0.0257	0.743	1.1380	0.03
Hydrogen	0.1858	10.200	0.0818	0.22

2.1.2 Configuration selection

Given the various configurations of Stirling engine and mechanical drives which have been devised, there are numerous prototypes which have been developed. Despite this, Egas & Clucas (2018) suggests that very few of these attempts have succeeded in being commercially viable due to their low power to weight ratio compared to internal combustion engines, poor correlation between empirical and theoretical performance and the lack of policies supporting new technologies and alternative energies. As a result, the final product is usually excessively priced and exhibits inferior performance when compared to other devices. Furthermore, selecting a configuration is difficult for modern designers due to the large number of possible options, the limited ways in which their fundamental properties can be compared, and most importantly the lack of selection criteria and a comparison method (Egas & Clucas 2018).

Thombare and Verma (2008, pp. 1-38) concur, stating that careful design and selection of various components including the heat exchangers, drive mechanism and engine configuration is essential to produce a successful engine with good efficiency. Considering how critical the choice of engine configuration is to its commercial viability and performance, the limited selection criteria which is available, according to the literature, may suggest why Stirling engines have failed to be more

prominent. A brief explanation of the three main configurations is outlined before presenting the selection criteria depending on the application.

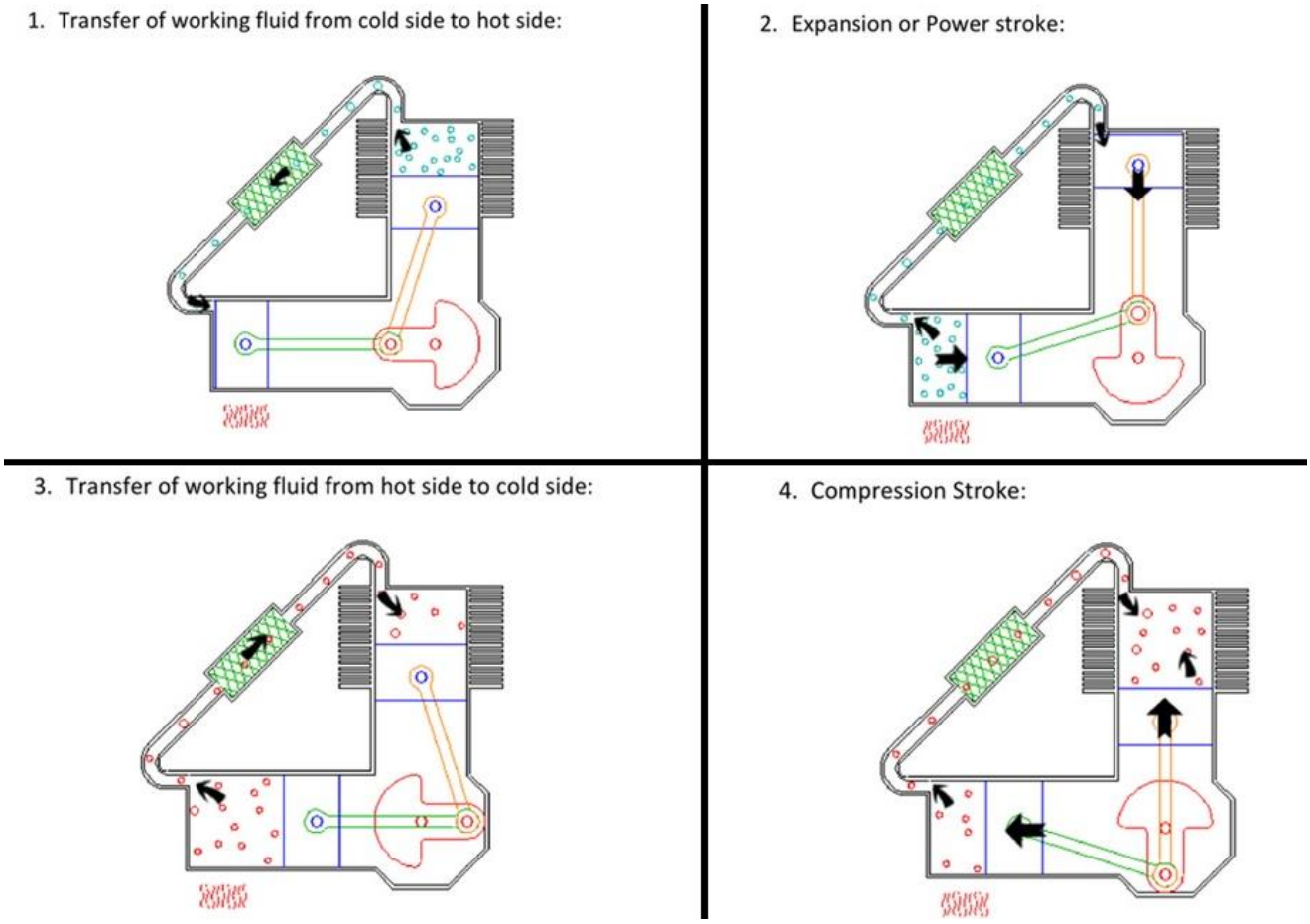

Figure 2.6: Four stages of Stirling cycle for alpha configuration (Keveny 2011).

Figure 2.6 shows the four stages of the Stirling cycle in an alpha configuration. Stage 1 corresponds to process 4-1 in Figure 2.1, where the working fluid is transferred in an isochoric process out of the cold cylinder and into the hot cylinder, while the regenerator transfers heat to the working fluid. Stage 2 corresponds to process 1-2 in Figure 2.1, where heat is transferred to the working fluid which is now in the hot cylinder (or heat source), causing it to expand isothermally and deliver work to the crank mechanism. This is the power stroke. Stage 3 corresponds to process 2-3 in Figure 2.1, where the working fluid is transferred in an isochoric process out of the hot cylinder and into the cold cylinder, while heat is transferred to the regenerator from the working fluid. Stage 4 corresponds to process 3-4 in Figure 2.1, where heat is rejected from the working fluid which is now in the cold cylinder (or heat sink), causing it to be compressed isothermally. The engine is now back in its original configuration and can begin the cycle again.

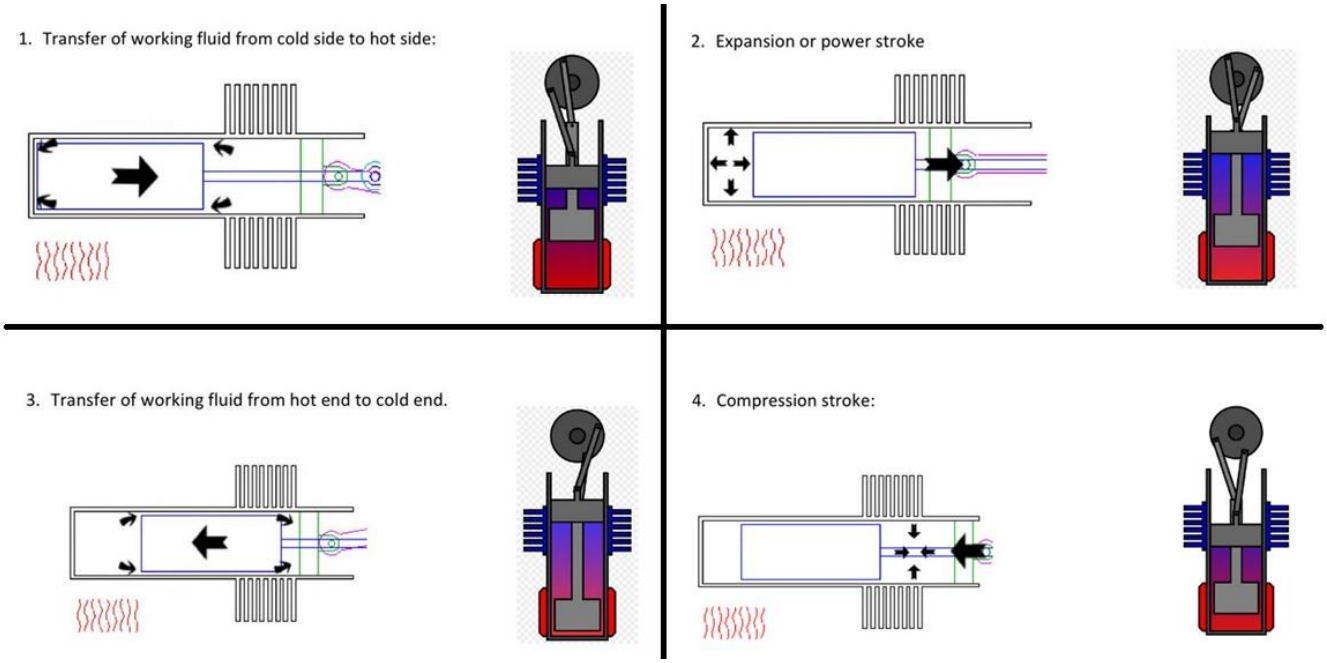

Figure 2.7: Four stages of Stirling cycle for beta configuration (Keveny 2011).

Figure 2.7 shows the four stages of the Stirling cycle in a beta configuration. A regenerator is more difficult to incorporate as the hot and cold ends of the cylinder are not insulated (Vineeth 2012). Figure 2.8 shows a schematic of a beta engine with regenerator included, while the diagrams in Figure 2.7 do not include a regenerator. As shown in Figure 2.7, Stage 1 corresponds to process 4-1 in Figure 2.1, where the working fluid is transferred in an isochoric process to the hot end of the cylinder from the cold end, and heat is transferred to the working fluid from the regenerator. Note that the clearance between the displacer and the cylinder allows air to move past it. The piston and displacer are timed so that the working fluid is displaced to the correct part of the cylinder to achieve the Stirling cycle. From here, the movements of the displacer and piston allow the cycle to proceed in the same manner as the alpha configuration (Vineeth 2012).

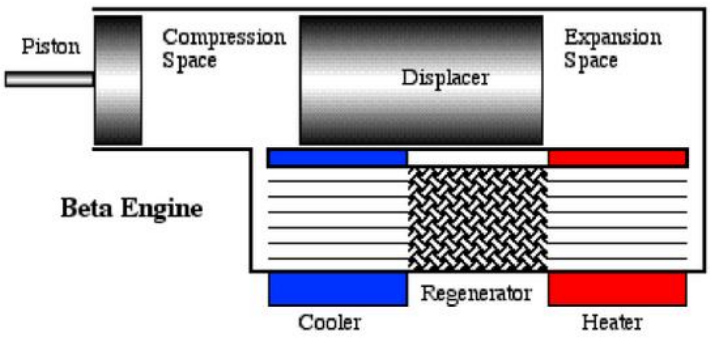

Figure 2.8: Schematic of beta Stirling engine with regenerator (Vineeth 2012).

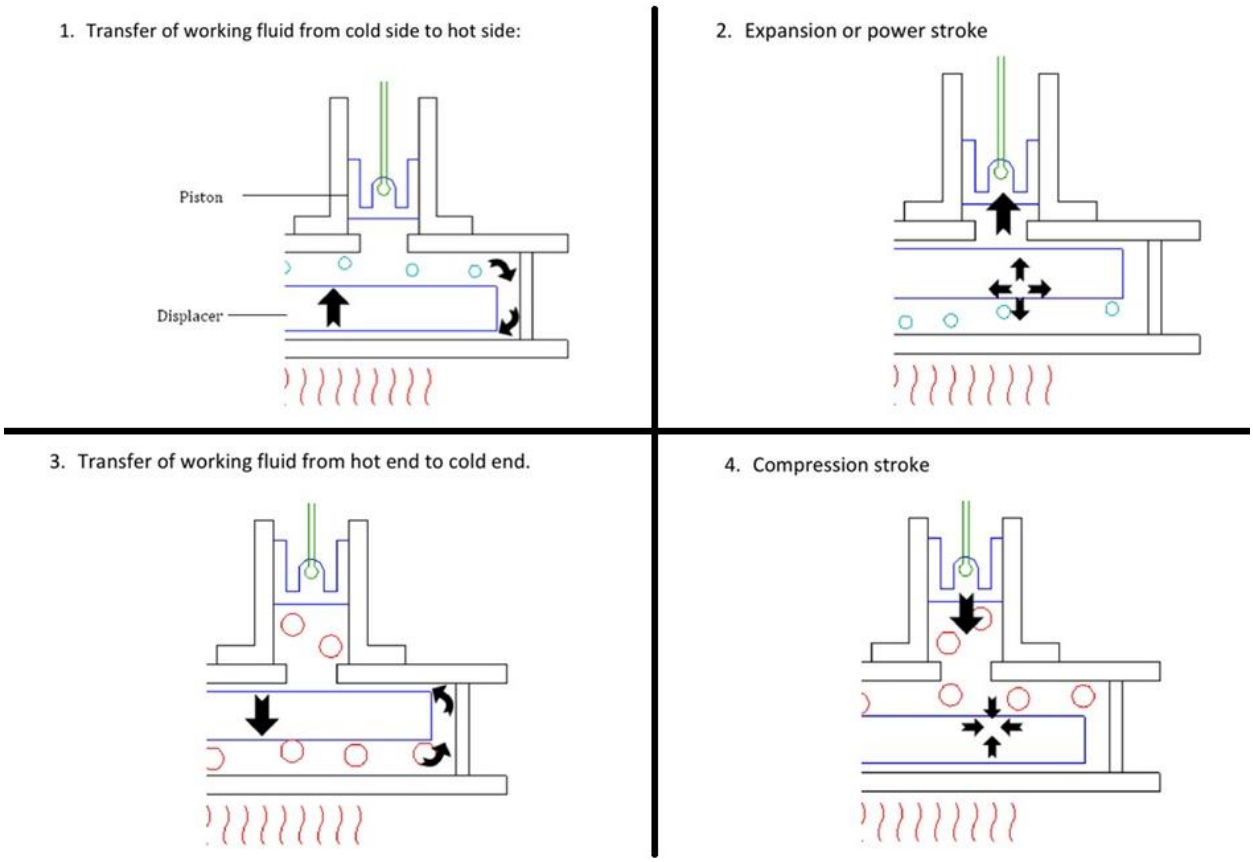

Figure 2.9: Four stages of Stirling cycle for gamma configuration (Keveny 2011).

Figure 2.9 shows the four stages of the Stirling cycle in gamma configuration. Here the engine is similar to the beta configuration in that there is a displacer and a piston, however in the gamma configuration the two are housed in independent cylinders. Similarly in Figure 2.9, Stage 1 corresponds to process 4-1 in Figure 2.1, where the working fluid is transferred from the cold end of the cylinder to the hot end in a constant volume process, and heat is transferred from the regenerator to the working fluid. Again, the piston and displacer are timed so that the working fluid is displaced to the correct part of each cylinder to achieve the Stirling cycle. From here, the movements of the displacer and piston allow the cycle to proceed in the same manner as the alpha and beta configuration (Vineeth 2012).

Table 2.2: Pros and cons of Stirling engine configurations (Rinker 2018).

Engine Configuration	Advantages	Disadvantages	Typical Drive Arrangements
Alpha	Conceptually the simplest.	Both pistons need to have seals to contain the working space.	V-arrangement and yoke drive (Ross linkage). Can be compounded into a multiple cylinder configuration.
Beta	High compression, efficiency, and power can be obtained due to lower dead volume.	Mechanical disadvantage of the drive rod from the displacer extends through the piston.	Rhombic drive.
Gamma	Mechanically more efficient than the other arrangements (simple crank mechanism).	Higher dead volumes, specifically the connecting pipe that connects both the compression space and the lower part of the expansion space.	Standard crank drive.

ALPHA CONFIGURATION

Table 2.2 lists advantages and disadvantages of each engine type as outlined in Rinker (2018). Thombare and Verma (2008, pp. 1-38) suggest that the alpha configuration is conceptually the simplest however may require more consideration when designing the pistons and cylinders for sealing, as the working fluid must be retained internally. Laazaar & Boutammachte (2020) suggests that an alpha machine will deliver the highest net work output of the three configurations, because its power-to-volume ratio is the largest. Unlike the other types of Stirling engine, the dead volume in the expansion and compression spaces is minimised by the inherent design of the alpha configuration, which means that high volumes yield a high pressure and thus power. There is a disadvantage in alpha type engines in that they must use a kinematic coupling, which by their nature require more maintenance, moving seals and lubrication to the mechanical components (Thimsen 2002).

The alpha is a versatile engine as it can achieve high specific power output by compounding it into a multi-cylinder engine and connecting the cold and hot ends of the cylinders together in series. The layout of a double-acting four-cylinder alpha Stirling engine is shown in Figure 2.10. The double-acting configuration enables a high specific power output, but increases the complexity of the design, is more expensive and makes it more difficult to couple an efficient drive mechanism (Thombare and Verma 2008, pp. 1-38). This configuration is also known as a Siemens configuration, and historically large size applications where Stirling engines are being considered, such as automotive applications, have utilised

this type (Martini 1983). The double-acting configuration is also suitable for low-temperature differential applications, for example using solar with an input temperature of 70° C yielding a differential of approximately 50° C (Abdullah et al. 2005, pp. 1923-1941).

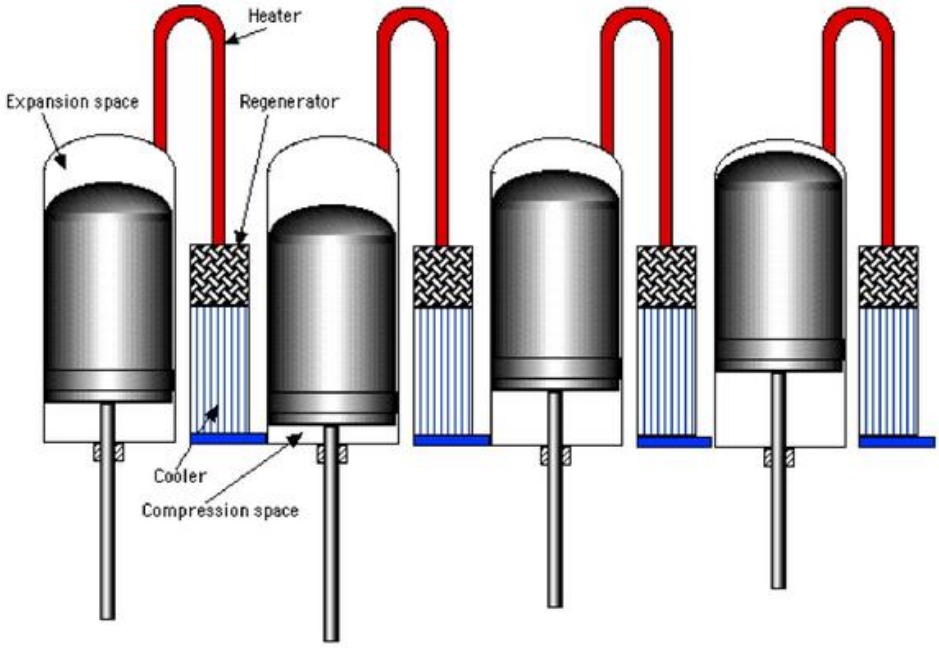

Figure 2.10: Schematic of a double-acting Stirling engine (Vineeth 2012).

BETA CONFIGURATION

From Table 2.2, it can be seen that a high compression efficiency is attainable when utilising the beta configuration, and a lower dead volume means that more power can be obtained. There is however a disadvantage in that the displacer drive rod is passed through the piston which may lead to sealing issues and mechanical losses (Rinker, 2018). Laazaar & Boutammachte (2020) suggests that the work output of the beta configuration is negatively impacted by the larger amount of dead volume within the expansion and compression spaces. This dead volume arises because of the clearance around the displacer which must exist to allow the working fluid to be shuttled from one end of the cylinder to the other. However, the problem of sealing is less significant when compared with the alpha type because there is only one power piston. According to Thimsen (2002), the beta type can be connected to a Rhombic drive or free piston coupling. Rhombic drive engines are advantageous because they can run at higher pressures, thus delivering higher specific power. Also, free piston engines offer benefits in that there are no cranks or rotating parts, meaning that lubrication and maintenance is reduced.

GAMMA CONFIGURATION

From Table 2.2, Rinker (2018) suggests that gamma engines are typically more mechanically efficient than the other types, however there is a larger dead volume. Laazaar & Boutammachte (2020) concurs, suggesting that similarly to beta engines, the gamma configuration has a higher dead volume when compared to alpha engines, again due to the inclusion of a clearance space around the displacer. This causes the net work output to be lower by comparison. Gamma engines do have the advantage of simpler sealing, for similar reasons to the beta type. Thimsen (2002) states that gamma configurations can be coupled using either kinematic or free-piston methods which offers flexibility in the design of the engine and comes with inherent advantages for each type.

TEMPERATURE CONSIDERATIONS

Egas & Clucas (2018) determined that for any Stirling engine the optimum compression ratio and the applied temperature ratio are directly related, and these ratios can be used as selection criteria for choosing the optimum configuration. Specifically, for a high temperature difference application, the engine configuration and drive mechanism should allow for a higher compression ratio, and similarly for a low temperature difference application a lower compression ratio should be used. Egas & Clucas (2018) analysed five different configuration and drive mechanism arrangements and determined the following.

1. **Alpha configuration with Ross yoke mechanism engines.** Best suited for high temperature difference applications. For example, highly concentrated solar power, nuclear power and high temperature geothermal.
2. **Beta with rhombic drive and alpha with crank-slider mechanism engines**. Best suited for applications with a medium to high temperature difference. An example fuel source for this type is LPG.
3. **Beta with crankshaft engines.** Best suited for applications where a medium to low temperature difference exists. For example, biogas or biodiesel.
4. **Gamma machines**. Are only suited for applications where a low to ultra-low temperature difference exists. Some example energy sources for this category low concentration solar power, waste energy or low temperature geothermal energy (Egas & Clucas 2018).

2.1.3 Thermodynamic theory and engine parameters

The differences in design between the alpha, beta and gamma configurations lead to different analyses when determining the volumetric compression ratio and performance of the engine. However, the overarching thermodynamic theory and analysis is applicable to all types as they all work according to

the Stirling cycle. Moreover, the net work and power output can be determined using analyses defined by various authors in the literature, and from this the engine parameters such as bore diameter, rotational speed, cylinder volumes and heat exchanger specifications, can be calculated depending on the temperatures available and the requirements of the engine application. The thermodynamic theory of the Stirling cycle is presented here, and some frequently used analyses are discussed, before final calculations are made in Chapter 4 once the engine configuration and drive mechanism have been selected.

In the operation of actual Stirling engines there is a significant departure from the ideal Stirling cycle, however Puech & Tishkova (2010, pp. 872-878) suggest that a simple thermodynamic analysis is useful in the first instance to determine a starting point for the engine parameters. The four processes of the Stirling cycle are shown using a PV and TS diagram in Figure 2.11 and using two opposing pistons in motion in Figure 2.12.

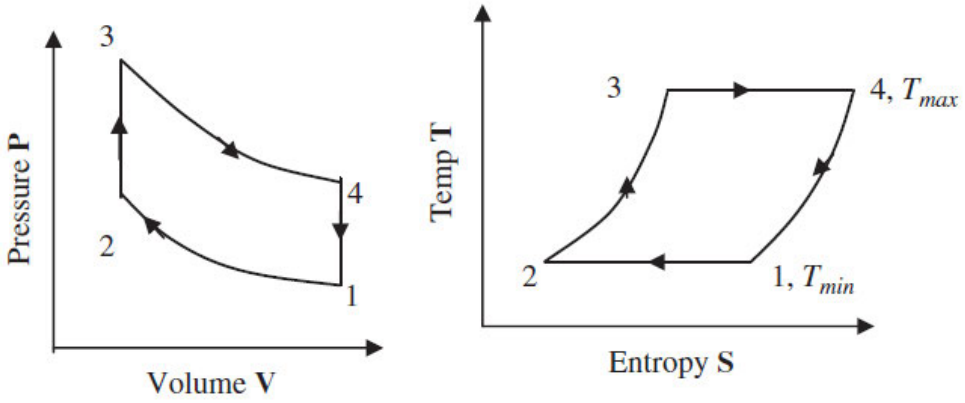

Figure 2.11: PV and TS diagrams for the Stirling cycle (Thombare and Verma 2008, pp. 1-38).

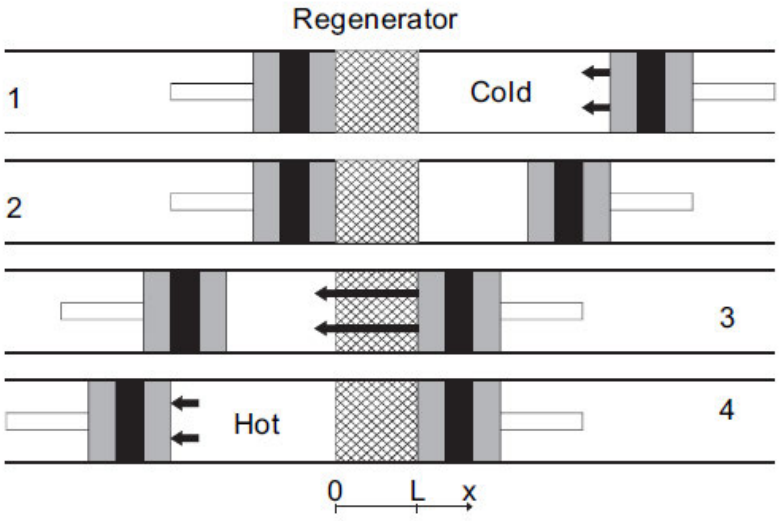

Figure 2.12: Stirling cycle demonstrated with motion of two opposing pistons (Puech & Tishkova 2010).

During process 1-2, the expansion piston remains approximately stationary while the compression piston is in motion. The regenerator is shown in the centre and the compression piston moves towards it in this process. The amount of heat rejected is theoretically equal to the work done to working fluid, while the temperature remains constant. The entropy decreases while the internal energy remains the same (Thombare & Verma 2008, pp. 1-38). Figure 2.13 shows the relevant equations for Process 1-2, where P_1 and P_2 are the pressures (in Pa), V_1 and V_2 are the volumes (in m^3) and T_1 and T_2 are the temperatures (in K) at the start and end of the process respectively. The term r_v is the ratio compression ratio, or the ratio of the two volumes. The heat transfer Q is equal to the work done W, where the units are Joules.

$$P_2 = \frac{P_1 V_1}{V_2} = P_1 r_v,$$

$$T_1 = T_2 = T_{min},$$

$$\text{Heat transfer } Q = \text{Work done } W,$$

$$Q = W_c = P_1 V_1 \ln(1/r_v) = mRT_1 \ln(1/r_v),$$

$$\text{Change in entropy} = (s_2 - s_2) = R \ln(1/r_v).$$

Figure 2.13: Equations for isothermal compression, process 1-2 (Thombare & Verma 2008, pp. 1-38).

During process 2-3, the two pistons are moving simultaneously in a common direction so maintain an approximately constant volume. During this motion, the working gas passes through the regenerator in moving from the cold cylinder to the hot cylinder, and picks up heat energy causing it to increase from T_{min} to T_{max} (Thombare & Verma 2008). Thus, constant volume regeneration is achieved. The increase in temperature causes the pressure to increase, and the entropy and internal energy also increases during this process. No work is done during this process (Thombare & Verma 2008, *pp. 1-38*). Figure 2.14 shows the relevant equations for process 2-3, where C_V is the constant volume heat capacity (in J/K).

$$P_3 = \frac{P_2 T_3}{T_2} = \frac{P_2}{\tau}; \quad V_3 = V_2.$$

$$\text{If } \tau = (T_2/T_3) \text{ The temperature ratio, } \tau \text{ defined by Gustav Schmidt}$$

$$\text{Heat transfer } Q = C_V(T_3 - T_2),$$

$$\text{Work done} = 0,$$

$$\text{Change in entropy} = (s_2 - s_2) = C_V \ln(1/\tau).$$

Figure 2.14: Equations for constant volume regeneration, process 2-3 (Thombare & Verma 2008, pp. 1-38).

During process 3-4, isothermal expansion occurs as the expansion piston continues moving away from the regenerator while the compression piston is approximately stationary. Heat is supplied to the hot cylinder at the high temperature of T_{max}, and the temperature of the working gas remains constant as it does work on the piston equal in magnitude to the heat energy supplied during this process. The volume increase causes the pressure to drop, while there is no change to the internal energy and an increase in the entropy of the working fluid is observed (Thombare & Verma 2008, pp. 1-38). Figure 2.15 shows the relevant equations for Process 3-4, where R is the gas constant (in J/kg.K) and m is the mass of the working gas (in kg).

$$P_4 = \frac{P_3 V_3}{V_4} = P_3(1/r_v); \quad T_4 = T_3 = T_{max},$$

$$\text{Heat transfer} = \text{Work done}, \quad Q = W = P_3 V_3 \ln r_v = mRT_3 \ln r_v,$$

$$\text{Change in entropy} = (s_3 - s_4) = R \ln r_v.$$

Figure 2.15: Equations for constant volume regeneration, process 3-4 (Thombare & Verma 2008, pp. 1-38).

During process 4-1, both pistons move simultaneously in a common direction, completing a constant volume process as the working gas is transferred to the cold cylinder from the hot cylinder. The temperature of the working fluid decreases from T_{max} to T_{min}. as it passes through the regenerator and rejects heat. Thus, constant volume regeneration is achieved. The decrease in temperature causes the pressure to drop, and the entropy and internal energy also decreases during this process. No work is done (Thombare & Verma 2008, pp. 1-38). Figure 2.16 shows the relevant equations for process 4-1.

$$P_1 = \frac{P_4 T_4}{T_1} = P_1 \tau; \quad V_1 = V_4,$$

$$\text{Heat transfer } Q = C_V(T_1 - T_4) \quad \text{and}$$

$$\text{Change in entropy} = (s_1 - s_4) = C_V \ln \tau$$

and if

$$r_v = V_4/V_3 = V_1/V_2$$

the total heat supplied $= RT_3 \ln r_v$ and the total heat rejected $= RT_1 \ln r_v$.

Figure 2.16: Equations for constant volume regeneration, process 4-1 (Thombare & Verma 2008, pp. 1-38).

The overall efficiency of the cycle is equal to the work done divided by the heat supplied and can be calculated using the equations developed in the analysis. Figure 2.17 shows the derivation of efficiency, and it can be seen that the equation is equal to the one presented earlier in Figure 2.2.

$$\eta_t = \frac{mRT_3 \ln(r_v) - mRT_1 \ln(r_v)}{mRT_3 \ln(r_v)},$$

$$\eta_t = 1 - \frac{T_1}{T_3} = 1 - \frac{T_{min}}{T_{max}} = 1 - \tau.$$

Figure 2.17: Derivation of Stirling cycle thermal efficiency (Thombare & Verma 2008, pp. 1-38).

In order to attain the value for effective heat transfer and determine the work done over a complete cycle, Urieli & Berchowitz (1984) modelled the ideal engine as five connected spaces, comprising the compression space, cooler, regenerator, heat and expansion spaces. This model is shown in Figure 2.18.

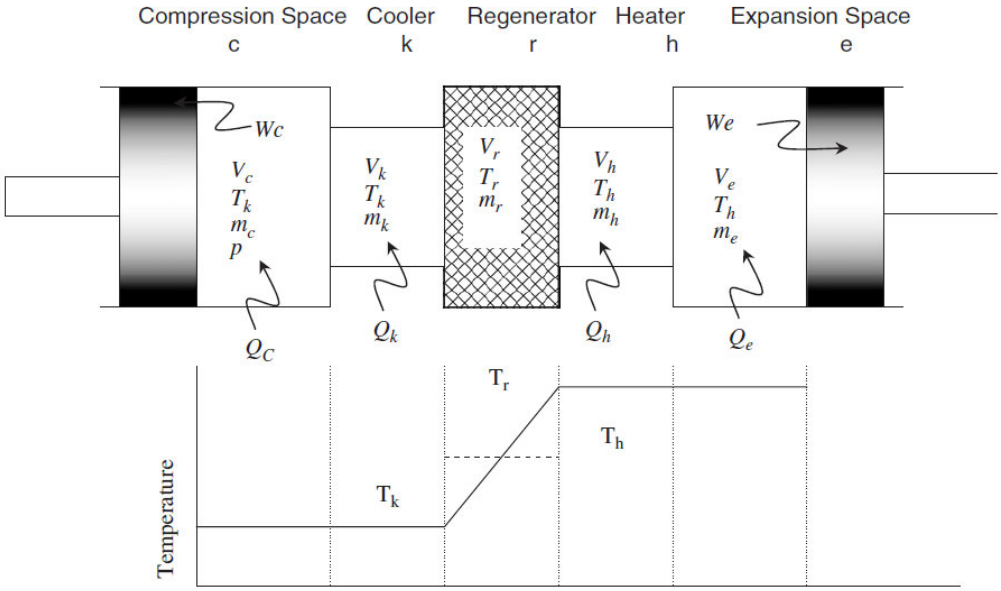

Figure 2.18: Ideal isothermal model used in analysis by Urieli & Berchowitz (1984).

A few assumptions are made, which include: constant mass of working gas; pressure is constant throughout the engine; cooler and compression space temperature is equal ($T_c = T_k$); and heater and expansion space temperature is equal ($T_h = T_e$). Using the ideal gas law, an equation for the mass of working fluid in the system can be found and subsequently the engine cycle pressure can be determined using the equation in Figure 2.19.

$$p = \mathrm{MR}\left(\frac{V_c}{T_k} + \frac{V_k}{T_k} + \frac{V_r \ln(T_h/T_k)}{(T_h - T_k)} + \frac{V_h}{T_h} + \frac{V_e}{T_h}\right)^{-1}$$

Figure 2.19: Equation for engine cycle pressure (Thombare & Verma 2008, pp. 1-38).

Where p is the pressure of the working fluid (Pa), M is the mass of the working fluid (kg), R is the gas constant (J/(kg.K)), and the other parameters are as shown in Figure 2.18. The total work done by the engine can be found by summing the work done in the expansion and compression spaces (Thombare & Verma 2008, pp. 1-38). Equations for the total work are shown in Figure 2.20, where P is pressure (in Pa) and V_c and V_e are the volumes of the expansion and compression spaces respectively (in m^3).

$$W = W_c + W_e,$$
$$W = \oint p\,dV_c + \oint p\,dV_e,$$
$$W = \oint p\left(\frac{dV_c}{d\phi} + \frac{dV_e}{d\phi}\right)d\phi \quad \text{where } \phi \text{ is crank angle.}$$

Figure 2.20: Equations for total work done by the engine (Thombare & Verma 2008, pp. 1-38).

Furthermore, Wu et al. (1998, pp. 727-732) established the relationship between net power output and efficiency shown in Figure 2.21 for Stirling engines with imperfect regeneration and heat transfer, where α is the heat conductance between the engine and the reservoirs, k is the ratio of the specific heats, and r_v is the volumetric ratio between the compression and expansion spaces.

$$P_i = \frac{\alpha\eta_t}{\{1/(T_H - T_{E\,av}) + \frac{(1-\eta_t)(1-\mu)}{(1-\mu\eta_t-\eta_t)T_{E\,av}-(1-\mu\eta_t)T_C} + A_r\eta_t\}},$$

where

$$A = \alpha(k_1 + k_2)/[nC_V(k-1)\ln r_v],$$
$$\mu = \frac{x}{[(k-1)\ln r_v]}.$$

Figure 2.21: Equation derived for new power output and efficiency (Wu et al. 1998, pp. 727-732).

Stirling engine design methods can be categorised into three groups: first-order; second-order; and third order. First-order methods include the simplest assumptions and are effective for calculating power and efficiency for a particular size engine when limited information is available. Second-order methods make more realistic assumptions, where various power losses are deducted from the final power output and it is assumed that a relatively simple Stirling cycle analysis can be used to determine power output and heat input (Martini 1983). Third-order analysis is generally referred to as nodal analysis. The engine is divided into sections, called nodes, and equations for conservation of mass, heat and momentum are derived for each node. These equations can then be used to run computational simulations and determine the engine performance (Martini 1983). First-order methods are likely to be the most useful for this project as the scope required for second-order and third-order methods may be too large.

One of the most widely used methods for designing Stirling engines has traditionally been the Schmidt analysis. It is one of the simplest methods and is limited in that some of the assumptions made are unrealistic, for example and isothermal working gas is assumed, zero regenerator volume and perfectly isothermal expansion and compression spaces (Abdullah et al. 2005). Nevertheless, the Schmidt analysis is useful for determining a good initial estimation for some critical engine parameters including: bore diameter; power required; and rotational frequency (Abdullah et al. 2005, pp. 1923-1941). Within the literature, there are numerous versions of the Schmidt equations which have been formulated by various authors. Furthermore, different equations are applicable for alpha and beta configurations. According to Martini (1983), the equation proposed by Walker is most adaptable to an alpha engine and is shown in (2.1).

$$W1 = (PX)(VT)\frac{\pi(AU-1)}{(K+1)}\left(\frac{(1-DL)}{(1+DL)}\right)^{1/2}\frac{DL\sin(ET)}{1+(1-(DL)^2)^{1/2}} \tag{2.1}$$

Where W1 is the work per cycle (Joules)

PX is the maximum pressure during cycle (MPa)

$VT = VL + VK = (1+K)VL$

VL is the swept volume in expansion space (cm^3)

VK is the swept volume in compression space (cm^3)

K is the swept volume ratio = $(VK)/(VL)$

$AU = TC/TH$

TC is the compression space gas temperature (K)

TH is the expansion space gas temperature (K)

TR is the dead space gas temperature (K) = $\frac{(TC)+(TH)}{2}$

$$DL = \frac{\left((AU)^2 + 2(AU)(K)\cos(AL) + K^2\right)^{1/2}}{(AU+K+2S)}$$

AL is the angle by which the volume variations in expansion space lead those in compression space (degrees)

$$S = \frac{2(RV)(AU)}{(AU+1)}$$

RV is the dead volume ratio = VD/VL

VD is the total dead volume (cm^3) = $HD + RD + CD$

$$ET = \tan^{-1}\left(\frac{K\sin(AL)}{(AU + K\cos(AL)}\right)$$

HD is the dead volume in the hot space (cm^3)

RD is the dead volume in the regenerator space (cm^3)

CD is the dead volume in the cold space (cm^3)

Once a preliminary design is outlined using first order methods, second and third order analysis can be used to optimise the design. Second-order methods account for power losses such as flow friction losses, regenerator pressure drop, heater and cooler pressure drop, windage losses, mechanical friction loss, heat and reheat losses, conduction losses, pumping losses and temperature swing losses (Martini 1983). These second-order methods provide a more realistic analysis without involving laborious computer simulation found with third-order methods. Third-order methods attempt to numerically compute the complex process occurring within a Stirling engine by writing differential equations and using computational methods to arrive at a numerical solution (Martini 1983). In the design method used by Abdullah et al. (2005, pp. 1923-1941), the Schmidt equation is used to initially size the critical components and a third-order method is subsequently used to optimise the design.

Senft (2002) suggests that six engine parameters primarily determine the optimum engine geometry, and they are: engine mechanism; cylinder arrangement; heater type; piston construction; regenerator properties; and crankcase construction. Thombare and Verma (2008, pp. 1-38) suggest some important engine parameters to be engine speed, pressure and displacement. The Beale number includes all of these parameters, however the West number may be more useful in the case of a Stirling engine as it also includes temperature. The equation for Beale number is shown in Figure 2.22 and the equation for West number is shown in Figure 2.23. Typically, the Beale number is 0.15 while the West number is approximately 0.25 for Stirling engines of power rating 5-150 kW (Thombare & Verma 2008, pp. 1-38). Hirata et al. (2001) suggests that for Stirling engines of a power output less than 5-150 kW, the West number is approximately 0.35.

$$B_{\mathrm{N}} = \frac{P_{\mathrm{i}}}{P_{\mathrm{M}} V_{\mathrm{se}} N}$$

Figure 2.22: Equation for Beale number (Thombare & Verma 2008, pp. 1-38).

Where B_N is the Beale number, P_i is the engine power (Watts), P_M is the mean engine pressure (Pa), V_{se} is the swept volume of the expansion space (m^3) and N is the rotational speed (revolutions per second).

$$W_S = \frac{P_i}{P_M V_{se} N(T_E - T_C / T_E + T_C)}$$

Figure 2.23: Equation for West number (Thombare & Verma 2008, pp. 1-38).

Where W_N is the West number, P_i is the engine power (Watts), P_M is the mean engine pressure (Pa), V_{se} is the swept volume of the expansion space (m^3), N is the rotational speed (revolutions per second), T_E is the temperature of the expansion space (K) and T_C is the temperature of the compression space (K).

The pressure of the working fluid is an important consideration when designing an engine. Theory and experimental evidence suggest that output power is approximately proportional to the fluid pressure, as shown by the equation in Figure 2.24, where W is work output (Joules), W_0 is the power factor, P_l is the fluid pressure (Pa) and V_s is the engine displacement volume (m^3) (Gicquel 2011).

$$\dot{W} = W_0 P_l V_s$$

Figure 2.24: Equation for work depending on fluid pressure and displacement volume (Gicquel 2011).

In general, a very high pressure in the realm of 100 to 200 bar should be used, where the sealing problems around the pistons and at the casing joint determine the limit. Not only does this increase the power output, but the thermal efficiency is also higher because heat transfer is improved within the engine (Senft 2002). Higher pressures can lead to issues with sealing, and therefore a balance should be found between power output and functionality (Gicquel 2011). Once the work per cycle has been found, the rotational speed of the engine needs to be determined to find the expected power output. Hirata et al. (2001) presents a non-dimensional analysis for determining the optimum rotational speed of a Stirling Engine using another non-dimensional term denoted as non-dimensional engine specification. (2.2) shows the equation determined experimentally by Hirata et al. (2001) for approximating the optimal non-dimensional rotational speed.

$$n_{opt}^{*} = 6.8 \times 10^{-5} S^{*0.6} \tag{2.2}$$

Where n_{opt}^{*} is the non-dimensional optimal rotational speed and S^{*} is the non-dimensional engine specification. The values in the equation shown in (2.2) are utilised to find the actual optimal rotation speed using (2.3) for non-dimensional engine specification and (2.4) for non-dimensional rotational speed as outlined in Hirata et al. (2001).

$$S^{*} = \frac{T_E R V_{SE}^{2/3}}{\nu^2} \tag{2.3}$$

Where T_E is the temperature of the expansion space (K), R is the individual gas constant of the working gas (J/(kg.K)), V_{SE} is the swept volume of the expansion space (m^3) and ν is the kinematic viscosity of the working gas at T_E and P_M (m^2/s).

$$n^* = \frac{nV_{SE}^{2/3}}{\nu} \tag{2.4}$$

Where n^* is the non-dimensional rotational speed and n is the rotational speed (rev/s).

2.1.4 Hydrogen as a fuel source

Hydrogen has been utilised as an attractive alternative to carbon-based fuels for many years due to its clean combustion products and effective energy carrying properties. Hydrogen is a highly abundant chemical element, making up approximately 75% of the universe by elemental mass and is the third most abundant on Earth (Aggarwal 2010, pp. 305-357). It can be utilised as a fuel in both fuel cells and internal combustion where the stored energy is converted into useful work. Fuel cell technologies utilise electrochemical reactions to convert the chemical energy within hydrogen into direct current electricity (FSEC 2014). Essentially, the fuel cell delivers electrical energy to some device that utilises this energy to output useful work (FSEC 2014). Hydrogen can also be utilised in internal combustion engines in a similar way to fossil fuels like petrol and diesel. However, when hydrogen is combusted in a flame of pure oxygen, the process is clean as the only by-product is water (*MEC4104 Renewable Energy Technology: course notes* 2021). The heat generated by hydrogen combustion can be used to power a Stirling Engine and deliver useul power output which is not harmful to the environment.

At normal conditions of atmospheric pressure and a temperature of 273.15 K, hydrogen exists as a non-toxic, odourless, tasteless and colourless gas of diatomic molecules having the formula H_2. Its molecular weight of 2.015 kg/kmol is the lowest of all the molecules, and consequently it has an exceptionally low density of 0.0899 kg/m^3 (Rand & Dell 2007). As a result of this low density, hydrogen as a fuel has the best energy-to-weight ratio, but its energy-to-volume ratio is poor (Rand & Dell 2007). The energy-to-volume ratio can be improved by storing the hydrogen as a liquid, however the transport and storage of hydrogen as a liquid presents a multitude of problems. For example, BMW (2006) opted for the liquid fuel option in their “BMW 7” as it represented an increase in energy of 75% over gaseous hydrogen stored in a compressed gas tank of the same volume, at a pressure of 700 bar. However, the design required a cryogenic hydrogen tank to maintain the liquid fuel at -250° C. This suggests that while efficiency might be improved by using hydrogen in liquid form, the viability of transporting and storing it for later use may be overly complicated and expensive.

Under stoichiometric conditions, the idealised combustion process of hydrogen in pure oxygen is shown in Figure 2.25.

$$H_2 + \frac{1}{2}O_2 \rightarrow H_2O$$

Figure 2.25: Stoichiometric combustion of hydrogen in pure oxygen (MEC4104 Renewable Energy Technology: course notes 2021).

When the combustion process takes place in air rather than pure oxygen, the existence of nitrogen (N_2) may cause harmful oxides of nitrogen (NOx) to form in the combustion products. The amount of NOx formation depends heavily on the air/fuel ratio which is denoted as λ and can be calculated using the equation in Figure 2.26.

$$\lambda = \frac{m_{\text{Air}}}{34.2 \cdot m_{\text{Hydrogen}}}$$

Figure 2.26: Air/fuel ratio of hydrogen combustion with air (Kiesgen, Leinhos & Rottengruber 2008).

Where m_{air} and $m_{hydrogen}$ are the mass of air and hydrogen respectively in the combustion process. The generation limit for oxides of nitrogen is observed at a ratio of $\lambda = 2.0\text{-}2.2$. For very lean homogeneous mixtures ($\lambda > 4$), very high efficiencies and minimal NOx levels are achieved, however the mixture burns at very low temperatures and the engines power density would be decreased significantly. On the other hand, with richer mixtures, better power density and higher flame temperatures are achieved but the NOx-emissions increase rapidly to levels which are significant. Therefore, the air/fuel ratio is an important parameter that must be selected to deliver an adequate flame temperature without causing unacceptable levels of NOx-emissions (Rand & Dell 2007).

The maximum amount of heat that can be derived from hydrogen combustion is known as the higher heating value (HHV), where the water product is condensed to a liquid with a temperature of 298.15 K. The practical value known as lower heating value (LHV) gives the effective (or engineering) heat of combustion where the steam is released at approximately 150° C (Rand & Dell 2007). As shown in Table 2.3, hydrogen has a HHV of 141.9 MJ/kg and a LHV of 120 MJ/kg. Other properties of hydrogen are given in Table 2.3 and compared with those of Petroleum.

Table 2.3: Comparison of hydrogen properties with petroleum (Rand & Dell 2007).

	Hydrogen	*Petroleum*
Boiling point/K	20.3	350–400
Liquid density/kg m^{-3}, NTP[a]	70.8	702
Gas density/kg m^{-3}, NTP[a]	0.0899	–
Heat of vaporization/kJ kg^{-1}	444	302
Higher heating value[b] (mass)/MJ kg^{-1}	141.9	46.7
Lower heating value[b] (mass)/MJ kg^{-1}	120.0	44.38
Lower heating value (liquid)[b] (volume)/MJ m^{-3}	8520	31 170
Diffusivity in air/cm^2 s^{-1}	0.63	0.08
Lower flammability limit/vol.% (in air)	4	1
Upper flammability limit/vol.% (in air)	75	6
Ignition temperature in air/°C	585	222
Ignition energy/mJ	0.02	0.25
Flame velocity/cm s^{-1}	270	30

[a] NTP=normal temperature (273.15 K) and pressure (101.325 kPa).
[b] Different authors give slightly different figures for the heating values.

The flame temperature which results from the combustion process is a function of the ratio of the oxidiser to the fuel. In this case, the ratio of the oxygen present to hydrogen. The flame temperature value peaks around stoichiometric conditions, generally slightly on the side of the curve where mixtures is slightly richer in fuel (Yetter, Glassman & Glumac 2014). Generally, the flame temperature is given as a function of the equivalence ratio, denoted ϕ, which can be found by dividing fuel/oxidiser ratio by the stoichiometric fuel/oxidiser ratio (Yetter, Glassman & Glumac 2014). As shown in Figure 2.27, the flame temperature decreases for mixtures which are both leaner in fuel ($\phi < 1$) and richer in fuel ($\phi > 1$) mixtures. Hydrogen has a wide flammability range of $0.7 < \phi < 7.1$, whereas gasoline only has a flammability range of $0.7 < \phi < 4$ (Schefer et al 2007).

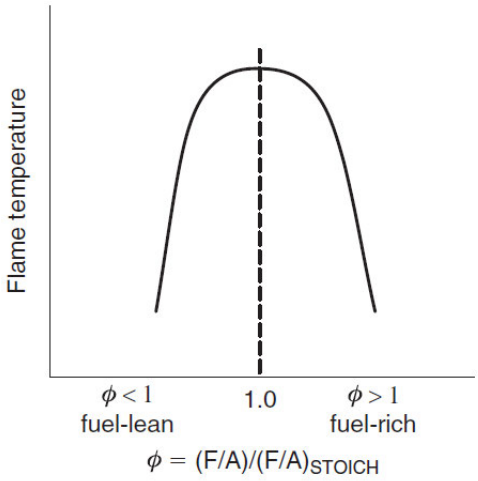

Figure 2.27: Variation of flame temperature with equivalence ratio (Yetter, Glassman & Glumac 2014).

Figure 2.28 shows the plot of flame temperature against equivalence ratio for hydrogen combustion in air. It can be seen that the flame temperature peaks at 2400 K at an equivalence ratio of approximately $\phi = 1$. This value is confirmed by a comparison of flame temperatures for various fuels as shown in Table 2.4. A higher flame temperature is achievable using pure oxygen as the oxidiser, however this will make the design of the combustion system more complicated and expensive. Therefore, once a desired temperature has been selected for the Stirling Engine, it will be necessary to assess the equivalence ratio to achieve this while ensuring that excess oxides of nitrogen will not be generated. Table 2.5 gives an indication of the levels of NOx in the combustion products at various equivalence ratios and pressures.

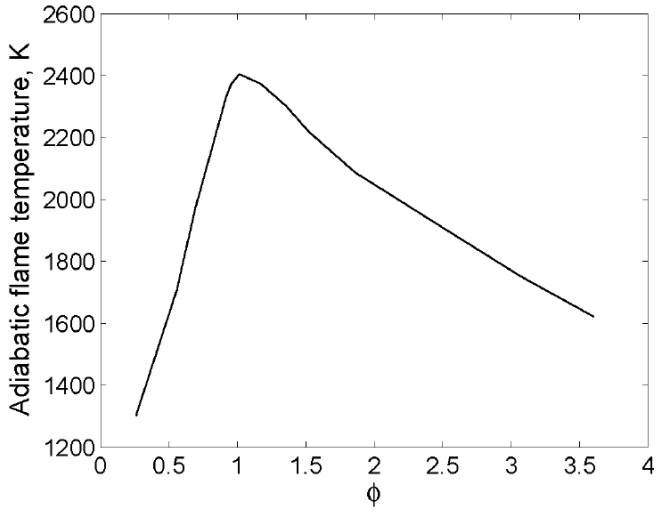

Figure 2.28: Adiabatic flame temperature for hydrogen-air mixtures (Drell & Belle 1958).

Table 2.4: Approximate flame temperatures of various stoichiometric mixtures (Yetter, Glassman & Glumac 2014)

Fuel	Oxidizer	Pressure (atm)	Temperature (K)
Acetylene	Air	1	2600[a]
Acetylene	Oxygen	1	3410[b]
Carbon monoxide	Air	1	2400
Carbon monoxide	Oxygen	1	3220
Heptane	Air	1	2290
Heptane	Oxygen	1	3100
Hydrogen	Air	1	2400
Hydrogen	Oxygen	1	3080
Methane	Air	1	2210
Methane	Air	20	2270
Methane	Oxygen	1	3030
Methane	Oxygen	20	3460

[a] *This maximum exists at $\phi = 1.3$.*
[b] *This maximum exists at $\phi = 1.7$.*

Table 2.5: Byproduct composition of hydrogen-air combustion (Yetter, Glassman & Glumac 2014).

ϕ	0.6	0.6	1.0	1.0	1.5	1.5
P (atm) species	1	10	1	10	1	10
H	0	0	0.002	0	0.003	0.001
H_2	0	0	0.015	0.009	0.147	0.148
H_2O	0.223	0.224	0.323	0.333	0.294	0.295
NO	0.003	0.003	0.003	0.002	0	0
N_2	0.700	0.700	0.644	0.648	0.555	0.556
O	0	0	0.001	0	0	0
OH	0.001	0	0.007	0.004	0.001	0
O_2	0.073	0.073	0.005	0.003	0	0
T (K)	1838	1840	2382	2442	2247	2252
Dissociation (%)			3	2		

2.1.5 Solar energy as a fuel source

Solar energy provides another viable source of heat for powering a Stirling engine to generate electricity or output mechanical power for another purpose. Collectors such as flat-plate collectors and evacuated collectors which are used in solar water heating applications can generate a temperature differential, and their use in a low temperature differential Stirling engine has been investigated by Abdullah et al. (2005, pp. 1923-1941) where a source temperature of 70° C was considered. It was shown that this temperature differential was viable for generating power using a double-acting alpha configuration, however the power is limited, and the maximum attainable thermal efficiency given by the Carnot equation is quite low. Higher temperatures can be achieved using solar concentrators to increase power output and improve the thermal efficiency.

In a solar concentrator, mirrors and lenses are used to collect insolation over a large area and focus the flux onto a small receiver. The flux can be focused onto a point, as in point concentrators, or onto a line as in linear concentrator (Twidell & Weir 2015). Added complexity is required if a concentrator is to be used as it must track the sun during the day to maximise the usage of available energy. Point concentrators must follow the sun in two directions, i.e. east/west and north/south, while linear concentrators only need to follow the sun in one direction, and rotate along the north/south axis (Twidell & Weir 2015). While solar concentrators can significantly increase the temperature available for a Stirling engine, there is a thermodynamic limit to the maximum concentration ratio which can be achieved. Furthermore, they add complexity to the design and operation of the device as tracking must be incorporated, and the location, time of day and time of year affects the available energy for power generation.

Using thermodynamic analysis, the maximum theoretical concentration ratio for a point concentrator is 46 000, while a linear concentrator can only achieve a maximum ratio of 210 (Twidell & Weir 2015). Moya (2012) suggests that a parabolic trough collector, which is a type of linear collector, is capable of delivering maximum temperatures of up to 500° C. Although the theoretical maximum is approximately 927° C for typical conditions in bright sunshine, the practical value is limited by modern technology in that the oils which are used as the working fluid cannot handle higher temperatures (Twidell & Weir 2015). Lovegrove, Nathan & Zapata (2022) suggests a similar figure, stating that typical parabolic trough collectors operate at a temperature of around 400° C. Figure 2.29 shows an image of a typical parabolic-trough solar collector.

Figure 2.29: Photo of a typical parabolic trough solar collector (Moya 2012).

Point concentrators can deliver higher temperatures again, with solar dishes and solar towers being modern examples of this type. Theoretically, the receiver temperature can reach up to around 3 000° C, but like the linear concentrators, only temperatures of up to around 1 000° C are usable due to the limitations of the materials used and limitations of the working fluid. Commercial solar tower plants use temperatures of up to around 600° C, with experimental systems reaching around 1 000° C (Lovegrove, Nathan & Zapata 2022). Boretti (2021, pp. 16241-16247) quotes a similar figure of 800° C using a concentrated solar dish for delivering heat to a Stirling engine. This is further supported by Reddy & Kahn (2021, pp. 5678-5702) who state that central tower receiver plants can achieve temperatures of over 1 000° C but are limited by receiver materials that can endure the elevated temperature and pressure. Figure 2.30 shows a picture of a concentrated solar dish with a Stirling engine mounted to utilise the heat at the focal point.

Figure 2.30: Concentrated solar dish with Stirling engine mounted at focal point (Boretti 2021, pp. 16241-16247).

2.1.6 Technologies, developments and applications

Stirling engines have been utilised for various applications and are seeing increased use in recent years with the current focus on renewable power sources. Many heat sources exist in nature and in industry that can be captured and used to power the engine which would otherwise go to waste. According to Furmanek & Kropiwnicki (2021, pp. 3-12), their main commercial application currently involves the production of heat and electricity from traditional energy sources such as diesel or natural gas. This is due to the technical problem of efficiently generating electricity which is economical from low-temperature energy sources that are commonly found with renewable applications.

Zhu et al. (2021) suggest that Stirling engine technology has great potential in the field of combined heat and power devices (CHP), in particular for residential applications due to their advantages of low maintenance, noise, vibration, emissions and high flexibility of fuel sources. A CHP device generates electricity for some purpose, while simultaneously generating heat for another application, for example heating water or space heating (Rinker 2018). Renewable fuel sources such as biomass and wood pellets have been utilised to supply heat to Stirling engine CHP devices, with high overall efficiencies of up to 90% achieved in some cases. While the Stirling engine is definitely proving feasible for this application, there are still obstacles such as considerable investment costs and low on-site operational efficiencies in some cases (Zhu et al. 2021).

Opportunities for use with a low and medium temperature differential application are also being investigated, especially for use with solar energy and waste heat recovery. Thombare and Verma (2008, pp. 1-38) suggest that a double-acting Stirling engine is a potentially attractive option for use with low-temperature solar energy, in particular with helium as the working fluid. Abdullah et al. (2005, pp. 1923-1941) also outline the design of a double-acting alpha configuration for generating power from a low temperature differential of 50° C. Waste heat recovery is another innovative way to reduce emissions by harnessing waste energy which would otherwise be useless. For example, Catapano et al. (2021) present an analysis for a Stirling engine which utilises waste heat from an internal combustion engine at temperatures in the range of 400-500° C for four-stroke engines. Given the large amounts of energy which is wasted in the form of heat, being able to use it for useful work will mean that fuel is saved elsewhere, thus promoting the efficient use of resources.

Stirling engines are also being developed for high power applications. While Thimsen (2002) suggests that the majority in development produce a power output of 25 kW_e or less, there are some companies developing Stirling engines with an output of 75 kW_e such as Quiet Revolution Motor Company, and even 200 kW_e which is being developed by Stirling Advantage. They have also been coupled with concentrated solar technologies which supply heat at high temperatures, yielding high power outputs. Boretti (2021, pp. 16241-16247) suggests that alpha configuration Stirling engines are being utilised in concentrated solar application to deliver power of 15-30 kW, however the designs have not been successful in delivering thermal efficiencies close to the Carnot efficiency. Typically, they have an efficiency of ~20%, however Boretti (2021, pp. 16241-16247) proposes a design with the cylinders in a V90° arrangement which could achieve thermal efficiency of 42% at 800° C.

When the Stirling cycle is operated in reverse, the engine becomes a cryocooler and some companies have produced devices for this purpose. The designs operate at very low temperatures in the realm of 30-80 K, and remove heat at around 29 W for a temperature of 77 K and 78 W for a temperature of 40 K (Rinker 2018).

The cost of power produced per kilowatt is another consideration when determining the viability of a product in the market. The cost depends on the size and application of the device, but some existing plants give an idea which can be compared to other energy sources. A large scale 50 MW power plant utilising Stirling Engine technology in combination with dish concentrated solar has been costed at $4,600 USD per kilowatt (Gadré & Maiorana 2014). This is substantially different to the values suggested by Thimsen (2002) who states that prototype systems at the time were available for as little as $2,000 USD per kilowatt, and even $500 USD per kilowatt for engines which were mass produced. This suggests that the cost depends heavily on the application and size of the engine, and it is difficult to determine an accurate cost in general.

2.2 Knowledge Gap

It has been identified from the literature that the Stirling engine offers great potential as a source of mechanical power in various applications. The nature of the device also means that it can be used as a sustainable alternative to other modern power sources such as internal combustion engines and coal fired electricity generation. This is because the only input required is heat, and this can come from a number of sustainable resources. As shown in the literature review, much research has been conducted into the utilisation of renewable energy for supplying heat to a Stirling engine. These renewable sources include solar energy, geothermal energy, waste heat and biofuels. The literature also includes research into numerical modelling and analysis of Stirling engine performance, and optimum configurations depending on the application.

Hydrogen as a fuel offers an environmentally friendly option for supplying heat to the engine at a high temperature. The only by-product of hydrogen combustion in pure oxygen is water, and therefore would not be harmful to the environment. After an extensive review of the literature, no sources were found that offered design or analysis of a Stirling engine coupled with a hydrogen combustion system. One article was found which proposed using a hydrogen combustion system with a Stirling engine, however this source focused on the design of the hydrogen combustion system and did not offer any design or analysis on the engine itself. Therefore, a knowledge gap exists in the design and analysis of a Stirling engine to select the optimal configuration and parameters for use with hydrogen combustion. This project aims to fill this gap in knowledge by utilising analysis and design techniques found in the literature to design, fabricate and test an environmentally friendly Stirling engine that operates by heat generated from hydrogen combustion.

2.3 Project Feasibility and Study Justification

The selection of configuration and parameters of a Stirling engine are critical to its success, depending on the application in which it is to be used and the temperature available. After a review of the literature, there exists traditional and emerging thermodynamic models which can be used to analyse and design the parameters of a Stirling engine. The selection of a configuration (alpha, beta or gamma) is also critical, and it was discovered that there is minimal literature available for this task. However, some recent sources have been found which offer useful information for this process. Hydrogen as a fuel and solar energy have also been researched to give background information to utilise with the analysis techniques discovered, and subsequently to assess the real-world potential of the engine design and compare with other renewable energy sources.

After reviewing the literature, it has been found that there is sufficient information as outlined above to analyse and design a Stirling engine for use with hydrogen combustion. Furthermore, the real world application and viability of such an engine will be determined by assessing current technology and comparing with other energy sources such as solar energy, using the information on solar power and modern applications found in the literature review. The fabrication and testing of the engine will establish a proof of concept and determine the validity of the theoretical analysis by comparing with the experimental results. Furthermore, given the lack of information in the literature for selecting a configuration which will best suit a certain application, this project aims to further current knowledge in this aspect. Access to a workshop and solid modelling software was utilised and greatly assisted in making the project feasible.

Chapter 3

Methodology

3.1 Chapter Overview

This chapter outlines the methodology utilised in completing the project which has been developed to best achieve the aims and objectives outlined in the Project Specification. An overall design process is presented in Section 3.2 which was used as a guide in structuring this methodology. Section 3.3 outlines the planning which was carried out before commencing the project and outlines requirements such as resources, data collection, risk management and ethical considerations. Section 3.4 outlines the initial calculations required before the design, fabrication and testing stages can be completed as outlined in Sections 3.5, 3.6, 3.7 and 3.8. Section 3.9 outlines the ways in which the results will be linked back to the aims and objectives and Section 3.10 provides a review of the methodology.

3.2 Design Process

Figure 3.1 shows the engineering design process as outlined by Ertas and Jones (1996). Given the complex and varying nature of engineering design projects, it was useful to have a defined process in place to use as a basis for the development of a methodology. While the process focuses more on product development within industry, it has been adapted for use in developing the methodology for this project. This project focuses on the development of a prototype engine to solve the design question of whether hydrogen can be used as a fuel source to power a Stirling Engine, and how it could then be utilised for applications within industry. Some of the steps are modified to suit the context of this project, and some additional steps are included as required. The following sections describe how the steps have been incorporated into the methodology for each stage of the project.

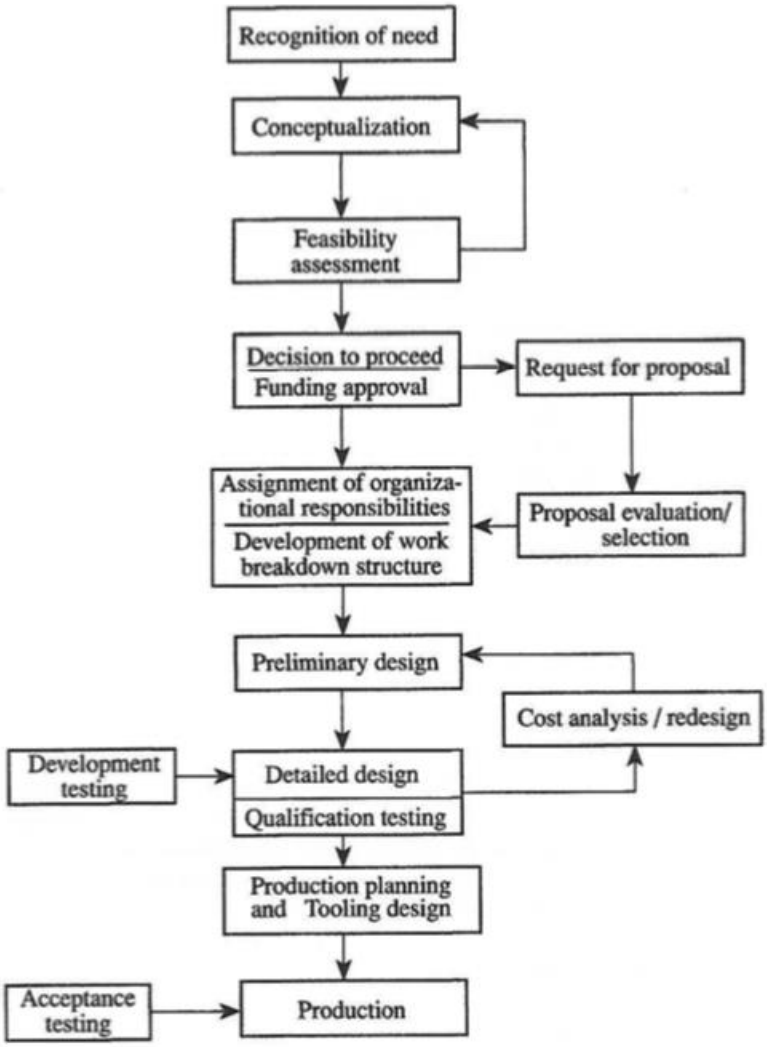

Figure 3.1: Engineering design process outlined by Ertas and Jones (1996).

3.3 Project Planning and Initial Stages

The initial stages of the project involved the recognition of a need, conceptualisation and a feasibility assessment before proceeding with the remainder of the project. In completing these stages, the aims and objectives were developed and thus a focus for the project was achieved, as well as a timeline for anticipated completion of each stage of the project. The project specification and timeline which was produced during the planning phase is contained in Appendix A. Both of these documents are important for the success of any engineering endeavour to ensure that things are completed on time and the objectives are being met. The following sections describe how these stages were achieved before the design, fabrication and testing stages were completed.

3.3.1 Background Information

RECOGNITION OF NEED

A literature review was conducted to find background information on the topic and identify a knowledge gap, which in this case was the use of hydrogen as a fuel source to power a Stirling Engine and an engine configuration and design to suit this fuel. Further information such as current technologies, potential applications and other Stirling Engine designs were investigated to assess the viability of a hydrogen powered Stirling Engine and to aid in the design for this project. Thus, the potential need in industry had been defined and some information had been gathered to proceed with conceptualisation of a solution and an assessment of the project feasibility. While an initial literature review was conducted, Chapter 2 presents the final literature review which contains all information gathered for completion of the project.

CONCEPTUALISATION

The conceptualisation of the project was initially completed concurrently with the recognition of need and presented in the Project Specification and timeline documents by outlining the aims and objectives. Once the initial conceptualisation had been completed, more information was gathered to further develop the scope of the project. Stirling Engine theory was gathered during this stage to provide an initial conceptual understanding of how to analyse the Stirling Cycle and ultimately design, build and test an engine in the later stages of the project. After defining the overall concept of the project, the work required and the timeframe available was outlined in detail to assess the feasibility of completing the project.

3.3.2 Resource Requirements

FEASIBILITY ASSESSMENT

An initial methodology was produced to assess the feasibility of the project in terms of scope and time available, as well as the ability to source the required resources and complete the necessary work. A timeline was produced as shown in Appendix A to show anticipated completion times for each stage of the project, and this aided in assessing whether the project could be completed in the required timeframe. It was assessed that sufficient time was available to complete the work and so an assessment of the required resources was made. During planning, the resources required for the project were outlined and their availability was assessed as shown below.

- **Materials for engine**. From the background information obtained, it was found that the engine would be made predominantly from steel. At the student's workplace, this was readily available in various forms and could be purchased if required. Other contacts could be utilised if other materials were required.
- **Machining and fabrication for engine.** Machining and fabrication of components for the engine would be required. In the first instance, the USQ workshop would be contacted for assistance. If the USQ workshop was unavailable, the student's workplace could complete the machining.
- **Fabrication of test jig.** For initial testing of the engine, it would need to be bolted down to a solid base. Steel benches were available at the student's workshop which could be utilised.
- **Testing equipment.** Discussion about testing at the USQ facilities was required with the student's USQ supervisor to ascertain what equipment is available at the university.
- **Heat source**. It was not intended that actual hydrogen combustion would be used during testing. Rather, the specified temperature was simulated using another method. Oxy-acetylene heating torches were available at the student's workplace and based on background information it was a suitable alternative.

3.3.3 Collection of data

The power output of the engine is the main consideration in assessing the performance and it would be compared with calculated values which are presented in Chapter 4. The high and low temperatures would need to be specified and reproduced in the test, and a temperature measuring device was required to verify the actual temperatures during testing. Other relevant parameters include engine rotational speed, torque, regenerator effectiveness and heat exchanger effectiveness.

3.3.4 Risk Management Plan

The Risk Management Plan can be found in Appendix B and it was produced to ensure safety of all personnel during all tasks required for the project.

3.3.5 Ethical Considerations

Ethical considerations were required to ensure the project was feasible in this aspect. The Code of Ethics outlined by Engineers Australia must not be breached by any aspects of the project. Some considerations were listed as shown below.

- **Research.** During the literature review and research stages, information is gathered from work completed by others. All ideas and information gathered from these outside sources must be cited in-text wherever they appear, and in the reference section of all documents. The "Academic Integrity Mandatory Training" course has been completed, and all requirements outlined in the course will be adhered to so that academic integrity is maintained.
- **Recommendations on engine applications.** Any potential hazards or risks associated with the engine should be discussed in the final dissertation. For example, hydrogen gas can explode if it is not handled properly or stored at certain concentrations. While no actual hydrogen will be used in carrying out the research project, there is an ethical responsibility to disclose the potential hazards if someone is to use this work in the future.
- **Safety**. At all stages of fabrication and testing, safety must be maintained at all times. If anyone else is to be involved, they must be notified of the hazards and risks.

DECISION TO PROCEED

After the project had been assessed as feasible given all the considerations listed above, the decision was made to proceed with the project and commence the remainder of work required. As the project is self-funded, no funding approval was required.

DEVELOPMENT OF WORK BREAKDOWN STRUCTURE

The work breakdown structure is essentially the methodology which was produced initially and the timeline which is shown in Appendix A. This chapter outlines the comprehensive methodology which represents the complete scope of the work breakdown. Some delegation was required when machining and fabrication was completed as professional tradesmen at the student's workplace were utilised.

3.4 Initial Design and Power Calculations

PRELIMINARY DESIGN

The preliminary design is outlined in Chapter 4. This covers the application of Stirling Engine theory found in the Literature Review to select an engine configuration based on the temperature achievable

with hydrogen fuel, and the calculation of work output, rotational speed and power output based on the theory. A target power output was decided based on Stirling Engine technology and potential applications found in the literature.

3.5 Engine Design

DETAILED DESIGN

Once the preliminary design had been completed, the values required for detailed design of the engine had been obtained. These include geometry, dimensions, temperature and pressures acting within the engine. This allowed for design of the various engine components which were required for the alpha configuration, after it was selected in Chapter 4. The detailed design of the engine was completed and is presented in Chapter 5. This chapter includes justification of material selection for each component as well as the manufacturing processes required. Decisions were made to optimise the functionality of each component as suggested in the literature, and stress analysis calculations are made to assess the safety and performance of each component. A 3D cad model was produced using SolidWorks and Chapter 5 presents images of the model, while Appendix C contains technical and assembly drawings which were produced for subsequent manufacture.

3.6 Design verification

Finite Element Analysis was conducted on all critical components to verify the stress analysis calculations and thus the safety of the design. The results are presented in Chapter 5. The agreement of the design with the Stirling Cycle as presented in the literature is verified by showing the motion of the pistons during operation. The considerations of cost, safety, fatigue and design life are discussed, which are important aspects of any engineering design verification.

3.7 Engine fabrication

PRODUCTION

The production stage was completed after detailed design had been completed. All the components were fabricated using the drawings and specified manufacturing processes and the engine was assembled

before being bolted to a steel bench for initial testing. Photos of the engine fabrication stage are presented in Chapter 5.

3.8 Testing

DEVELOPMENT TESTING

As the engine prototype is focused on proof of concept and is a new design, the testing carried out is best described as development testing. The acceptance testing mentioned in Figure 3.1 is more applicable to large scale productions and therefore is not required for this project. Testing of the engine was carried out by heating the heater head of the engine with an oxy-acetylene torch and attempting to crank start the engine at various design temperatures. Other crucial aspects of the design were assessed such as sealing of the working gas, minimisation of friction, performance of the mechanism and heat exchanger performance.

3.9 Analysis of Results

The performance of the engine at various temperatures was analysed and is discussed in Chapter 6. Modifications which were made in an attempt to improve the engine's performance are outlined and revised power calculations are presented for different geometrical configurations. If the engine had achieved operation under any applied temperature, the torque and rotational speed would have been measured using a dynamometer and thus the power output could have been determined and compared with the calculations in Chapter 4. Assuming the power values could be achieved, potential applications for the engine are discussed to provide an answer to the research question of whether a hydrogen powered Stirling engine is viable, and where it could be used. Potential optimisations for the engine are also discussed.

3.10 Evaluation of Methodology

Overall, the methodology adheres quite closely to the engineering design process outlined in Figure 3.1. This would suggest that the critical aspects have been covered in completing the project and a logical sequence of stages has been achieved. The work required for the project was planned in a fashion which ensured that all required values or data needed for a section had been found or determined in the

preceding section. This allowed each progressive stage to be completed without a significant amount of rework or redesign. Some redesign was required during the testing stage, but this is to be expected with any new engineering prototype. The planning stage was effective as a suitable focus was found for the project in the aims and objectives, and all resources required were identified to ensure that no delays occurred. The timeline was effective, but it was found that some stages took longer than expected. Fortunately, some stages also took less time than expected so the project was completed within the designated timeframe.

Some drawbacks of the methodology have been identified. Although the testing of the engine using an oxy-acetylene torch can provide adequate temperatures, it may behave slightly different than an actual hydrogen combustion system. While this is not ideal, the design and construction of a hydrogen combustion system was outside the scope of this project. Furthermore, as the engine requires significant optimisation to get it to run, this put pressure on time requirements and caused the testing stage to be a lot longer than anticipated. While the engine did not run in the end, the modifications which were attempted are discussed in Chapter 6.

3.11 Chapter summary

This chapter outlined the methodology which was used in completing this project. The design process in Figure 3.1 was used as a foundation for developing the methodology, and the correlation between the work in this dissertation and the stages in the process is discussed. Overall, the methodology adheres quite closely to the engineering design process outlined in Figure 3.1, and the positives and potential shortcomings have been reviewed.

Chapter 4

Initial Design and Power Calculations

4.1 Chapter Overview

This chapter sets out the initial design and power calculation of a Stirling Engine based on the specifications outlined in Section 4.2. The design criteria are chosen based on power output of the engine which could be utilised for a real-world application. The power output is calculated based on analysis techniques and Stirling Engine theory which has been outlined in the literature review, and the temperatures used in these calculations are based on flame temperatures which can be achieved by hydrogen combustion.

Part of the design process is choosing a configuration which would be most suited to the temperature difference attainable with hydrogen combustion. The criteria for determining configuration selection have been outlined in the literature review, and this will be used to decide on a configuration for the design in Section 4.3. Once a configuration has been selected, the relevant geometrical parameters will be outlined for use in the power calculations. Section 4.4 details the calculations of work per cycle, rotational speed and power output at various hot cylinder temperatures. Four different analysis techniques have been used to determine expected work per cycle values, namely: the P-V diagram; the Schmidt equation; Beale Number; and West Number. The theoretical rotational speed is calculated using non-dimensional method outlined in Chapter 2 and from these analyses power and efficiency is estimated.

4.2 Design Specifications

When an engine or motor is selected for an application, there are many factors which must be considered such as torque, rotational speed, rotational acceleration, running time, and others depending on the application. As stated in the literature review, it is difficult to determine an accurate cost per kilowatt for Stirling Engine technology as there are a wide range of applications and sizes. For this design, cost was not a major consideration as the main objective of the project is to fabricate a prototype and assess the potential for power output. Optimisation and affordability can be investigated for further work.

In order to choose a target power output, current Stirling Engine applications will be considered as well as a typical residential solar panel system. According to Thimsen (2002), the majority of Stirling engines in development have an output power of less than 25 kWe. Furthermore, Rinker (2018) gives several examples of Stirling Engine applications with output powers of between 500 W and 5 kW such as a 1 kW integrated absorption-chiller for a HDD4.1962-4 engine, a 1.38 kW Stirling Engine for a micro-CHP and an electric generator coupled Stirling engine generating around 511.5 W (Rinker, 2018). The Australian Government Department of Climate Change, Energy, the Environment and Water (DCCEEW) (2022) states that most Australian household install a solar panel system which generates 3-5 kW.

Given the power outputs that have been produced through other work, the target output power for the Stirling Engine design was chosen to be 750 – 1 000 Watts. This is lower than a typical residential solar panel installation but is in the realm of other Stirling Engine applications. If more power is required for a certain application, then multiple engines could be used. Output rotational speed is another consideration depending on the application, however for this design it will not be specified.

4.3 Configuration Selection

4.3.1 Temperature Difference

As determined in the literature, a flame temperature of 2 400 K is achieved when hydrogen is combusted at stoichiometric conditions and atmospheric pressure. As this is higher than most solar energy Stirling engine applications discussed in Chapter 2, clearly there is potential for hydrogen to be utilised as a fuel in powering a Stirling Engine. Given that the melting point of carbon steels is in the range of 1425 – 1540° C (1698 – 1813 K), clearly this flame temperature would be too high as many of the components are to be made of steel (Verhoeven, 2007). It was also found in the literature review that the flame temperature can be modified by adjusting the ratio of the fuel to the oxidiser. Even at the minimum equivalence ratio of $\phi = 0.7$ for hydrogen combustion, the flame temperature is approximately 1960 K. Therefore, a method would need to be devised for reducing the temperature at the cylinder as again this would be too high for the components of the engine.

For the purposes of this design, it will be assumed that the hot cylinder temperature can be heated to a temperature in the range of 500 – 1 100° C and the engine will be designed and tested based on these values. The temperature of the cold cylinder will be taken as room temperature of 27° C. This value is likely to be higher in practicality as the hot air will heat this space, however it has been adopted for

calculations in other work including Aksoy et al. (2010), Formosa & Despesse (2010) and Bataineh (2018).

In summary, the following values will be used for calculations.

- Hot Temperature = 500 – 1 100° C = 773 – 1 273 K
- Cold Temperature = 27° C = 300 K

4.3.2 Configuration Type

As found in the literature review, Egas & Clucas (2018) determined that for medium to high temperature difference applications the best Stirling Engine configurations are the beta with crankshaft or alpha with slider-crank. A typical heat source in this temperature range includes petrol or LPG, and as such the design temperature range of 500 – 1 100° C with hydrogen combustion would fit into this category.

In deciding between the alpha and beta options, the potential power output and simplicity of design has been considered. As shown in Table 2.2, Rinker (2018) suggests that the alpha configuration is conceptually the simplest, however can present problems with sealing the gas within the working space. Furthermore, Laazaar & Boutammachte (2020) suggests that the power-to-volume ratio of an alpha type engine is the largest of the three configurations, and as such it will deliver the highest net work output.

For these reasons, the **alpha type with slider crank mechanism** has been chosen as the optimum configuration for the temperatures supplied by hydrogen combustion, and the prototype engine was designed and fabricated based on this configuration. Figure 2.6 shows a diagram of the alpha type with slider crank mechanism.

4.3.3 Geometry and relevant parameters

Figure 4.1 shows the relevant geometry for performing calculations such as cylinder volumes, compression ratio, stroke length, work and ultimately power output.

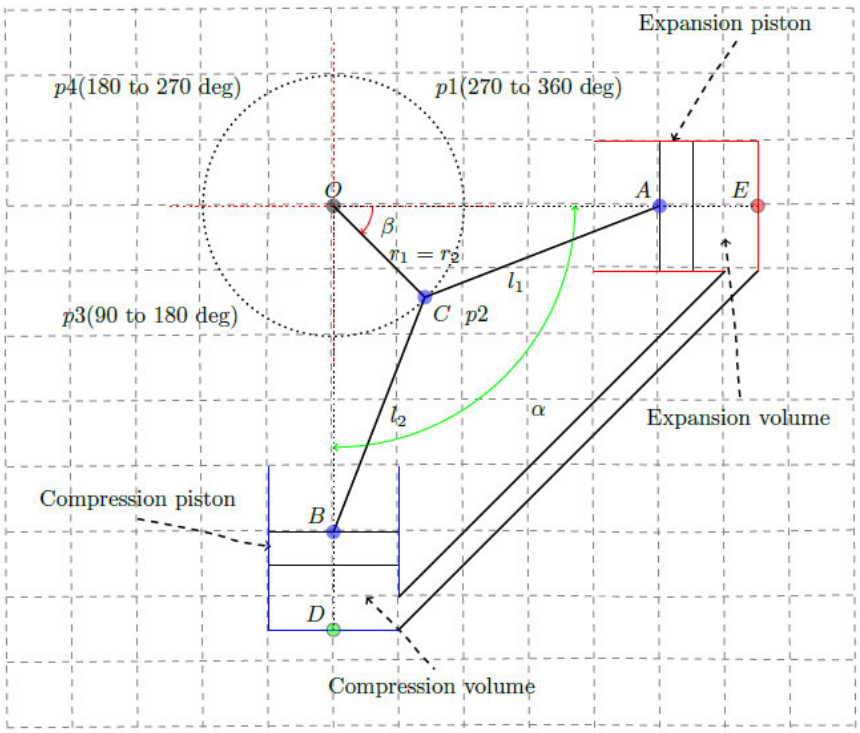

Figure 4.1: Geometry of alpha type Stirling Engine with slider crank mechanism (Egas & Clucas 2018).

The nomenclature for geometrical parameters as shown in Figure 4.1 is outlined below, as extracted from Egas & Clucas (2018).

- Point O = Crank rotation centre
- Segment OC = Crank radius of length $r_1 = r_2 = r$ (in cm)
- Segment CA = Connecting Rod Expansion Piston of length l_1 (in cm)
- Segment CB = Connecting Rod Compression Cylinder of length l_2 (in cm)
- Point E = Top Dead Centre Expansion Piston
- Point D = Top Dead Centre Compression Piston
- Angle ∠AOB = Phase angle represented by α (in degrees)
- Angle ∠AOC = Crank angle represented by β (in degrees)
- Segment AE = Length from expansion piston to top dead centre (in cm)
- Segment BD = Length from compression piston to top dead centre (in cm)
- Segment OE = Length from crank rotation centre to top dead centre of expansion piston (in cm)
- Segment OD = Length from crank rotation centre to top dead centre of compression piston (in cm)

The following assumptions are made for the calculations in Sections 4.4.1 and 4.4.2. The Schmidt equation is used in Section 4.4.3 which takes more factors into account but is still an idealisation,

before Sections 4.4.5 and 4.4.6 use the Beale and West numbers to estimate a more realistic power output.

- Dead volumes do not exist anywhere within the machine
- The working gas acts as an ideal gas
- There is infinite heat transfer time
- The temperature and pressure of the working gas is uniform (Egas & Clucas 2018)

The values of the crank radius, connecting rod lengths and top dead centre lengths will need to be chosen for the design. The phase angle chosen for the design is 90 degrees as this is standard for an alpha type Stirling Engine (Senviboon et al. 2018). The crank angle β varies as the crank rotates.

It can be seen from the diagram in Figure 4.1 that as the crank rotates, the length of segments AE and BD change in a cyclical fashion. This represents the motion of the piston, and the stroke length can be calculated by finding the difference between the minimum and maximum values of AE or BD. For an alpha configuration engine, the volume displaced by each piston is equal and therefore the stroke length of each piston is equal (Martini 1983). From the geometry, AE and BD can be represented as a function of β as shown in (4.1) and (4.2).

$$\overline{AE}(\beta) = \overline{OE} - (r_1.\cos(\beta) + \sqrt{l_1^2 - r_1^2.\sin(\beta)^2}) \text{ (Egas \& Clucas, 2018)} \quad (4.1)$$

$$\overline{BD}(\beta) = \overline{OD} - (r_2.\cos(\alpha - \beta) + \sqrt{l_2^2 - r_2^2.\sin(\alpha - \beta)^2}) \text{ (Egas \& Clucas 2018)} \quad (4.2)$$

As segments AE and BD change with β, the expansion and compression volumes also change. The expansion volume is defined as the swept volume of the expansion piston as it moves from top dead centre to bottom dead centre, and similarly for the compression volume. Therefore, the expansion and compression volumes can also be formulated as a function of β depending on the radius of the cylinder bores. The total working volume within the engine can be determined by summing the expansion and compression volumes. These values are denoted as shown (Egas & Clucas 2018).

- Expansion Cylinder Bore Radius = E_r (in cm)
- Compression Cylinder Bore Radius = C_r (in cm)
- Expansion Volume = V_e (in cm^3)
- Compression Volume = V_c (in cm^3)
- Total Volume = V_t (in cm^3)

Where the expansion and compression volumes are determined from (4.3) and (4.4) respectively.

$$V_e(\beta) = \pi.E_r^2.\overline{AE}(\beta) \text{ (Egas \& Clucas 2018)} \quad (4.3)$$

$$V_c(\beta) = \pi.C_r^2.\overline{BD}(\beta) \text{ (Egas \& Clucas, 2018)} \quad (4.4)$$

By substituting (4.1) into (4.3) and (4.2) into (4.4), a direct formulation of the expansion and compression volumes with respect to the crank angle can be found as shown in (4.5) and (4.6).

$$V_e(\beta) = \pi.E_r^2\left[\overline{OE} - (r_1.\cos(\beta) + \sqrt{l_1^2 - r_1^2.\sin(\beta)^2})\right] \text{ (Egas \& Clucas, 2018)} \quad (4.5)$$

$$V_c(\beta) = \pi.C_r^2\left[\overline{OD} - (r_2.\cos(\alpha - \beta) + \sqrt{l_2^2 - r_2^2.\sin(\alpha - \beta)^2})\right] \text{ (Egas \& Clucas, 2018)} \quad (4.6)$$

The total working volume is equal to the sum of the expansion and compression volumes and is expressed in (4.7).

$$V_t(\beta) = V_e(\beta) + V_c(\beta) \text{ (Egas \& Clucas, 2018)} \quad (4.7)$$

4.3.4 Compression Ratio

The compression ratio of an alpha Stirling Engine is defined as the ratio of the maximum total working volume to the minimum total working volume as shown in (4.8) (Thimsen, 2002).

$$CR = \frac{V_{t,\max}}{V_{t,\min}} \quad (4.8)$$

Where CR is the actual engine compression ratio

$V_{t,max}$ is the maximum total volume (in cm^3)

$V_{t,min}$ is the minimum total volume (in cm^3)

Egas & Clucas (2018) suggest that there is an optimum compression ratio which depends on the applied temperature difference. By considering the ideal Stirling Cycle it was determined that the

ideal compression ratio should be no larger than the ratio of the applied temperatures (where the temperatures are given in Kelvin) (4.9).

$$CR_i = \frac{T_h}{T_c} \text{ (Egas \& Clucas, 2018)} \quad (4.9)$$

Where CR_i is the ideal compression ratio

T_h is the temperature of the hot cylinder (K)

T_c is the temperature of the cold cylinder (K)

Upon further investigation, it was found that the empirical equation formulated by Kolin (1991) (4.10) gives a compression ratio which agreed with experimental results from engines that operated successfully. Even though this relationship was determined for low temperature difference engines, it can be used for high temperature difference engines as well.

$$CR_K = 1 + \frac{T_h - T_c}{1100} \text{ (Kolin 1991)} \quad (4.10)$$

Where CR_K is the empirical compression ratio suggested by Kolin (1991)

The optimum compression ratios suggested by (4.9) and (4.10) have been calculated for temperature differences at 100° C intervals between the design temperature range of 500 – 1 100° C, and the results are shown in Table 4.1.

Table 4.1: Ideal and empirical optimum compression ratio depending on temperature difference.

T_h (K)	773	873	973	1073	1173	1273	1373
T_c (K)	300	300	300	300	300	300	300
CR_i	2.58	2.91	3.24	3.58	3.91	4.24	4.58
CR_K	1.43	1.52	1.61	1.70	1.79	1.88	1.98

It can be seen that the compression ratios given by the empirical equation (4.10) are significantly lower than the ideal compression ratios suggested in (4.9). The calculations and design justification is outlined in Section 4.4.

4.4 Power Calculations

4.4.1 Volume calculations and Initial Design Values

A spreadsheet was produced in Excel to determine the volumes and compression ratio depending on the crank radius (r), connecting rod length ($l_1 = l_2$) and cylinder bore radius ($E_r = C_r$). These values are subsequently used to calculate pressures, work and power output. An iterative process was used by adjusting the geometric values until an acceptable compression ratio was achieved along with the desired power output.

It was found that it was very difficult to reduce the compression ratio to values anywhere near the empirical optimum values suggested in Table 4.1. This occurred because in order to reduce the compression ratio significantly, the crank radius needed to be almost equal to the connecting rod length. In practicality, this is very difficult to achieve because the bottom of the piston extends past the centre of the gudgeon pin and the cylinder would need to be extremely close to the crank mechanism as well. Another way to reduce the compression ratio is to change the phase angle. This could be achieved but was decided against for this design due to the increase in complexity.

The size of the engine was also a determining factor. A reasonably large cylinder bore was necessary to achieve the desired output, however as the size of the cylinder bore increased so did the size of all other components and therefore the potential cost. Making the engine larger also increases the weight which may be detrimental for portability and viability in some applications.

INITIAL DESIGN

The values in Table 4.2 satisfy the required output as demonstrated in Section 4.4.2 to 4.4.7 and were selected for the initial design.

Table 4.2: Values determined for initial design.

Description	Symbol	Value	Units
Crank Radius Expansion Piston	r_1	7.2	cm
Crank Radius Compression Piston	r_2	7.2	cm
Connecting Rod Length Expansion Piston	l_1	18.75	cm
Connecting Rod Length Compression Cylinder	l_2	18.75	cm
Phase Angle	α	90	degrees
Expansion Cylinder Radius	E_r	4.445	cm
Compression Cylinder Radius	C_r	4.445	cm
Length from crank centre to TDC of expansion piston	OE	25.95	cm
Length from crank centre to TDC of compression piston	OD	25.95	cm

Using the values in Table 4.2, the expansion, compression, and total volumes were calculated as a function of the crank angle β at increments of 1 degree and plotted as shown in Figure 4.2. As expected, the change in expansion volume leads the change in compression volume by 90 degrees.

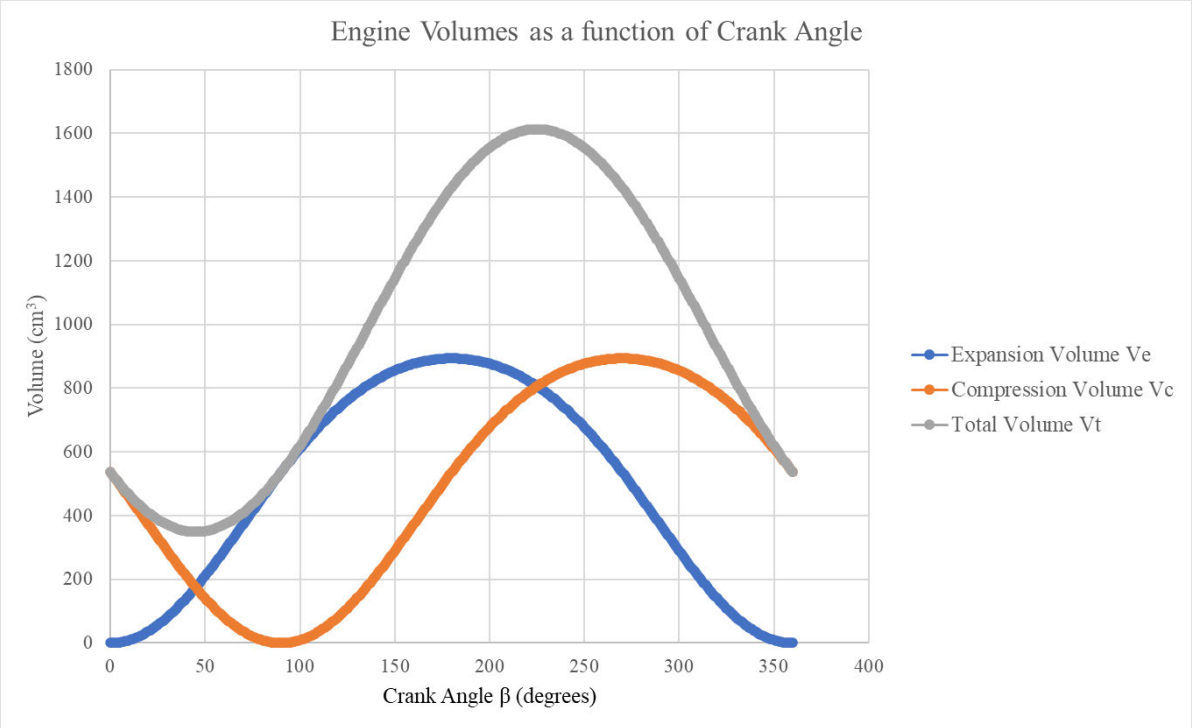

Figure 4.2: Graph of engine volumes as a function of crank angle using initial design values.

The minimum and maximum total volumes can be determined from the graph, however it could also be calculated by differentiating (4.7) and setting it equal to zero. The solutions to (4.11) would then give the minimum and maximum total volume, and the values of β at which they occur would give the angles of minimum and maximum total volume.

$$\frac{d(V_t(\beta))}{d\beta} = 0 \text{ (Egas \& Clucas, 2018)} \quad (4.11)$$

However, for the purposes of this design the maximum and minimum total volume have been determined from the calculated values and are shown in Table 4.3. The swept volumes in the expansion and compression cylinders were also determined by finding the difference between the maximum and minimum values respectively.

Table 4.3: Maximum and minimum total engine working volume, expansion volume and compression volume.

	Symbol	Value	Units	Crank Angle β (degrees)
Minimum Total Volume	$V_{t,\,min}$	349.25	cm^3	45
Maximum Total Volume	$V_{t,\,max}$	1613.3	cm^3	225
Expansion Volume	V_e	893.83	cm^3	180
Compression Volume	V_c	893.83	cm^3	270

Therefore, using (4.8) the compression ratio is found to be 4.62. This is only marginally higher than the ideal optimum compression ratio of 4.58 at a hot cylinder temperature of 1 100 K. Egas & Clucas (2018) state that engines with compression ratios higher than the temperature ratio can still operate, but will be less efficient. As the highest power output is achieved at the maximum temperature difference of 1 100 K, this compression ratio was accepted for the initial design.

4.4.2 Pressure-Volume diagrams

Given the assumption that the working gas can be treated as an ideal gas, the amount of working gas in in the internal space can be calculated. It was determined in the literature review that some gases offer advantages depending on their thermal conductivity, however as air is the most abundant it will be used for the design. Any gas will slowly leak past the pistons and so it is necessary to have a supply readily available, and therefore air presents the simplest and cheapest option. The engine will operate at atmospheric pressure, and therefore there is no need for a supply of air into the working space. For future work, an alternate working gas could be used or a pressurised system could be incorporated.

The ideal gas law (4.12) can be used to determine the amount of working gas in mol.

$$mol = \frac{P_{mean} V_{max}}{R T_{room}} \quad (4.12)$$

Where P_{mean} is atmospheric pressure for a non-pressurised engine (kPa)

V_{max} is the maximum total volume as per Table 4.3 (cm^3)

R = 8314 (cm^3.kPa)/(K.mol) is the universal gas constant

T_{room} is room temperature (K)

Therefore, the mol of air in the working space is 0.06598 mol as shown in (4.13).

$$mol = \frac{101.325 \times 1613.3}{8314 \times 298} = 0.06598 \tag{4.13}$$

From Egas and Clucas (2018), the working gas pressure can now be formulated with respect to the crank angle as shown in (4.14).

$$P(\beta) = \frac{mol.R}{\frac{V_c(\beta)}{T_c} + \frac{V_e(\beta)}{T_h}} \tag{4.14}$$

Where $P(\beta)$ is working gas pressure as a function of the crank angle β (kPa)

Using (4.14), the working gas pressure was calculated for $\beta = 0°$ to $\beta = 360°$ for the design temperatures of T_h = 500° C, 600° C, 700° C, 800° C, 900° C, 1 000° C and 1 100° C. The cold temperature was maintained at room temperature of T_c = 27° C. Figures 4.3 to 4.9 show the pressure-volume diagrams for each applied temperature. As determined in the literature review, the area enclosed by the pressure-volume diagram gives the theoretical work output per cycle. When comparing the diagrams in Figures 4.3 to 4.9 to the ideal case shown in Figure 2.1, it can be seen that the shape is different and the area enclosed by the curves in Figures 4.3 to 4.9 is smaller. This means that less work per cycle can be extracted when compared to the ideal cycle. This is a characteristic of the mechanisms within the engine because the physical movement of the pistons do not yield an ideal curve. In reality, the maximum pressure and actual work output for each case will not be as high as the values presented because of inefficiencies, losses and other factors which have not been considered in this analysis.

The maximum and minimum volume does not change with temperature as this is a function of the engine geometry only.

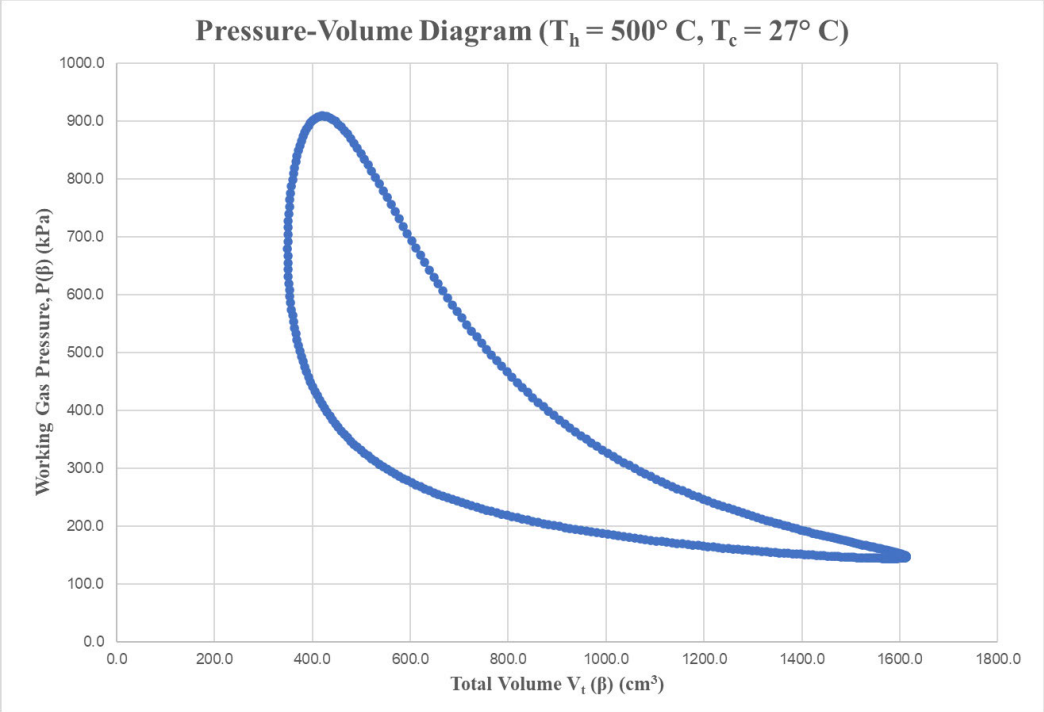

Figure 4.3: Pressure-volume diagram for hot cylinder temperature of 500° C.

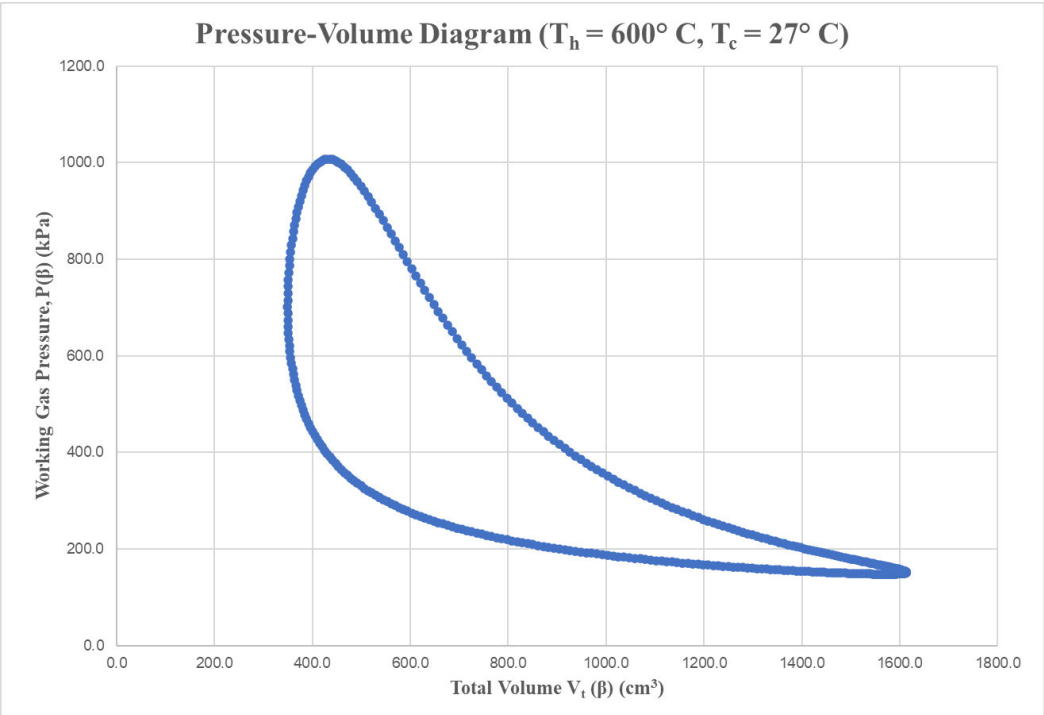

Figure 4.4: Pressure-volume diagram for hot cylinder temperature of 600° C.

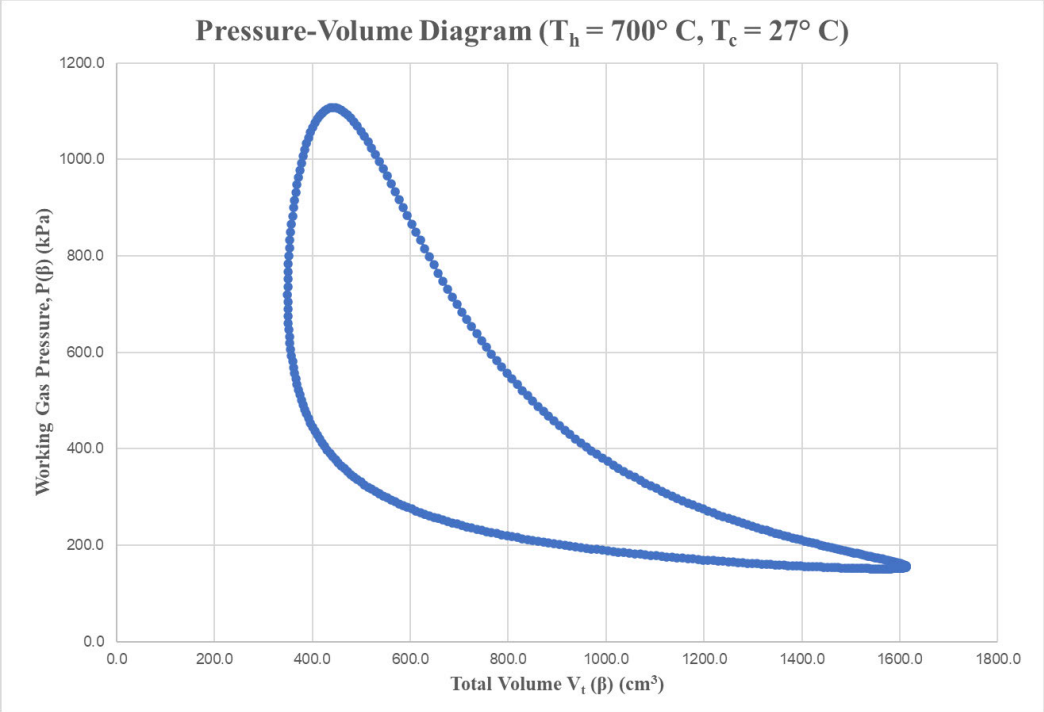

Figure 4.5: Pressure-volume diagram for hot cylinder temperature of 700° C.

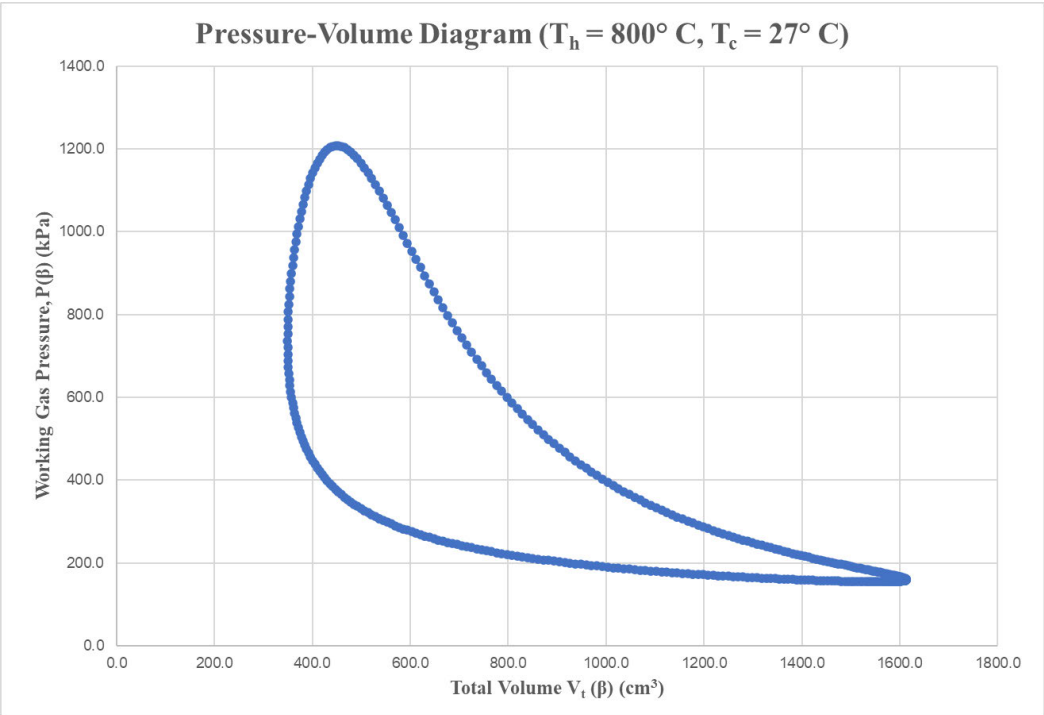

Figure 4.6: Pressure-volume diagram for hot cylinder temperature of 800° C.

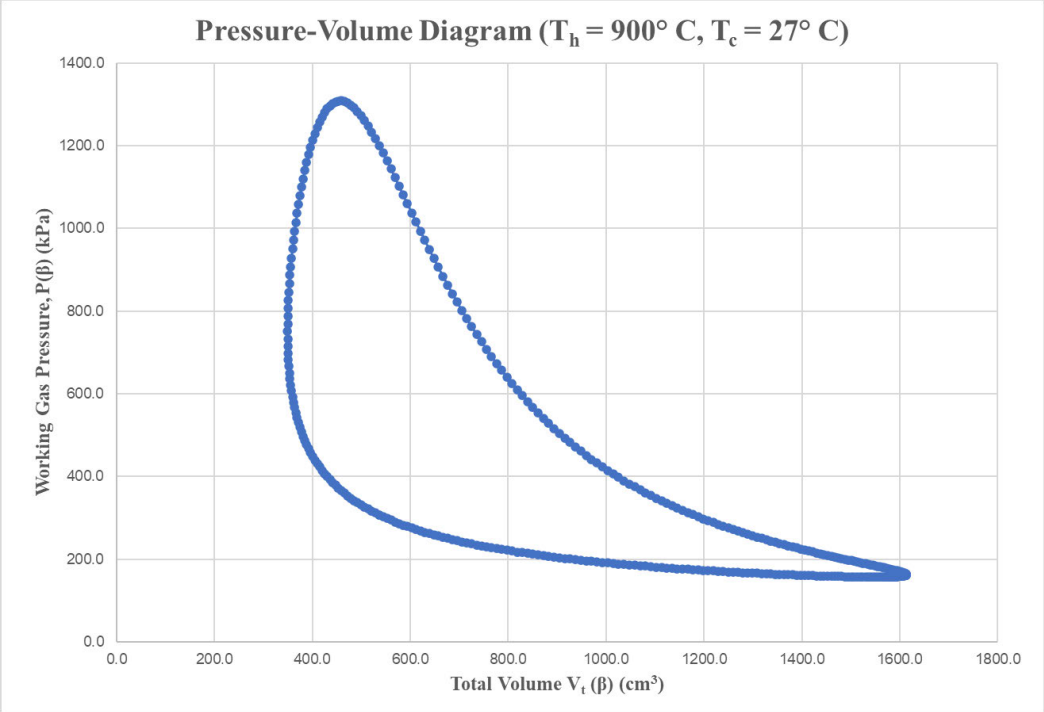

Figure 4.7: Pressure-volume diagram for hot cylinder temperature of 900° C.

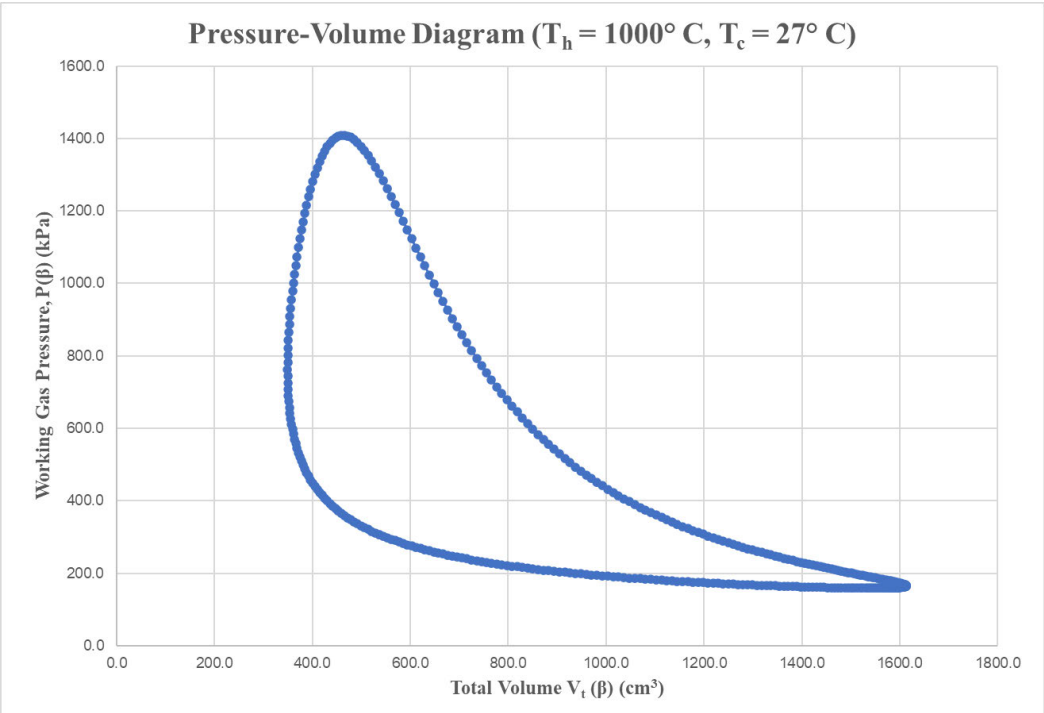

Figure 4.8: Pressure-volume diagram for hot cylinder temperature of 1000° C.

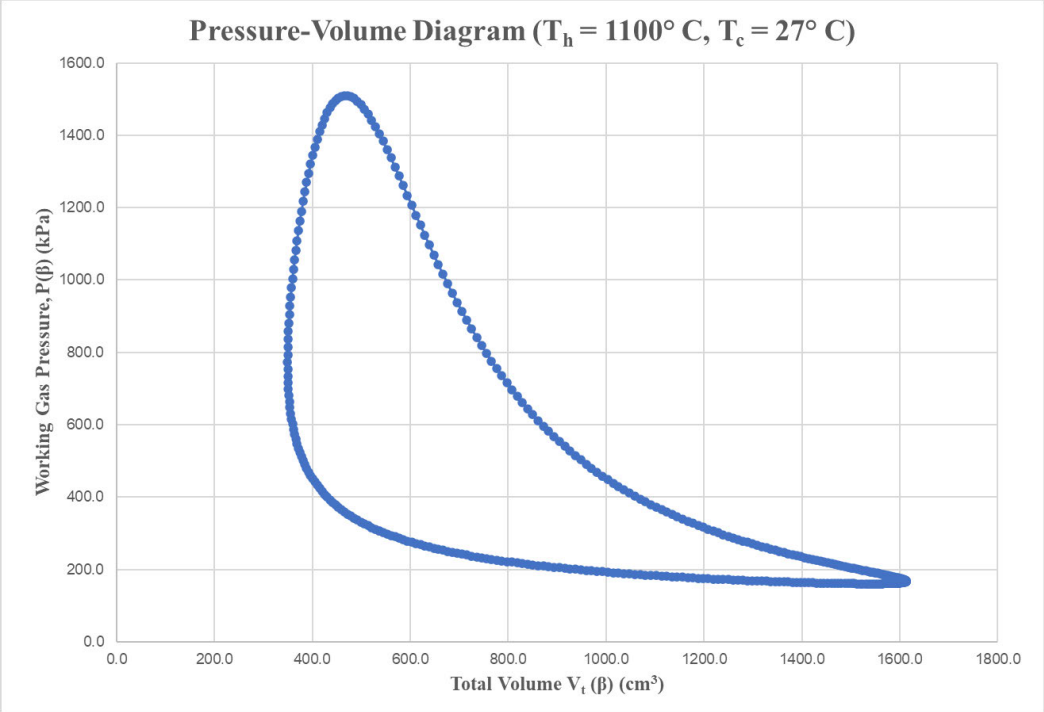

Figure 4.9: Pressure-volume diagram for hot cylinder temperature of 1100° C.

The maximum and minimum pressure for each case is summarised in Table 4.4, as well as the net work output per cycle. It can be seen that the minimum pressure remains approximately the same, ranging from 144.15 to 160.45 kPa, while the maximum pressure increases significantly with temperature, ranging from 908.48 to 1510.4 kPa. As expected, the working gas pressure increased with higher temperatures and this creates greater force on the expansion piston and thus more work output per cycle is generated.

The trapezoidal rule was used to find the area enclosed by each curve at 1 degree differentials, which represents the net work output per cycle for each hot cylinder temperature value. These values will be compared with the work determined using the Schmidt equation in Section 4.4.3. As expected, the net work output per cycle increases with temperature. The minimum work of 257.04 Joules is found at the minimum design temperature of 500° C, while the maximum work of 524.66 Joules is found at the maximum design temperature of 1 100° C.

Table 4.4: Minimum and maximum pressure and net work output per cycle at design hot cylinder temperatures.

T_h (° C)	Minimum Pressure (kPa)	Maximum Pressure (kPa)	Net work output per cycle (J)
500	144.15	908.48	257.04
600	148.13	1007.5	305.62
700	151.49	1107.4	352.43
800	154.29	1207.6	397.60
900	156.66	1308.3	441.29
1000	158.70	1409.2	483.60
1100	160.45	1510.4	524.66

4.4.3 Work Calculation using Schmidt Equation

As found in the literature, the Schmidt equation can be used to calculate the work per cycle of an alpha Stirling engine. This analysis makes assumptions which are unrealistic in a real engine but can be useful as a starting point for determining geometry and other parameters. Adapted from Martini (1983), an equation which can be utilised with a two-cylinder alpha Stirling engine is shown in (4.15) and is adapter here from (2.1).

$$W = P_{\max}(V_e + V_c)\frac{\pi(AU-1)}{(CR+1)}\left(\frac{(1-DL)}{(1+DL)}\right)^{1/2}\frac{DL\sin(ET)}{1+(1-(DL)^2)^{1/2}} \tag{4.15}$$

Where W is the work output per cycle (in Joules)

P_{max} is the maximum pressure of the working gas during cycle (MPa)

AU is the temperature ratio, which is found by $AU = \frac{T_h(K)}{T_c(K)}$

VD is the total dead volume, including dead volume in the heater, cooler and regenerator (cm^3)

RV is the dead volume ratio, which is found by $RV = \frac{VD(cm^3)}{V_e(cm^3)}$

S is found by $S = \frac{2(RV)(AU)}{(AU+1)}$

DL is found by $DL = \frac{((AU)^2 + 2(AU)(CR)\cos(\alpha) + CR^2)^{1/2}}{(AU+CR+S)}$

ET is found by $ET = \frac{\tan^{-1}(CR\sin(\alpha))}{(AU + CR\cos(\alpha))}$ (radians)

The maximum working pressure per cycle is determined using the values shown in Table 4.4. The dead volume was initially assumed to be zero for comparison with Section 4.4.3 but can be substituted with a value once the physical design is completed. Table 4.5 shows the net work output per cycle calculated using the Schmidt equation. It can be seen that the values found are quite similar to those found in Section 4.4.3, with a maximum difference of 4.36% at T_h = 500° C and a minimum difference of 0.910% at T_h = 1 100° C. It was found that as the temperature increased, the values found with the two methods converged. The agreement between Table 4.4 and Table 4.5 suggests that the calculations make similar assumptions, and the analysis was completed correctly in each case.

Table 4.5: Minimum and maximum pressure and net work output per cycle at design hot cylinder temperatures.

	Maximum Pressure (kPa)	**Schmidt work output per cycle W1 (J)**
500	908.48	246.30
600	1007.5	295.10
700	1107.4	342.60
800	1207.6	388.71
900	1308.3	433.64
1000	1409.2	477.34
1100	1510.4	519.93

After completing the initial design of the engine components, it was found that the dead volume in the regenerator tube is approximately 80.54 cm^3, the total dead volume in the ends of the cylinders when the pistons are at top dead centre is 283.92cm^3, and the dead volume in the heater is approximately 167.63 cm^3. These values were substituted into the Schmidt equation and the calculated values of work output per cycle are presented in Table 4.6. When compared with the values found in Table 4.5, an interesting result can be seen. The work output predicted at lower temperatures from 500° C to 800° C are higher in the case of zero dead volume, while the work output predicted at higher temperatures from 900° C to 1 100° C are higher in the case of dead volume included. Given that the values are approximately the same in any case, the values shown in Table 4.5 have been used for the remainder of the calculations.

Table 4.6: Schmidt equation values with dead volume included.

T_h (° C)	Maximum Pressure (kPa)	Schmidt work output per cycle W1 (J)
500	908.48	229.80
600	1007.5	281.76
700	1107.4	334.25
800	1207.6	386.95
900	1308.3	439.82
1000	1409.2	492.63
1100	1510.4	545.32

4.4.4 Work Calculation using Beale Number

As found in the literature, the Beale number is a method suggested by Beale in Hirata et al. (2001) for predicting the output power of a realistic Stirling engine. For engines with a hot cylinder temperature of approximately 650° C a typical Beale number is 0.15, however this is only an approximation and will vary depending on the efficiency of the engine. The equation for estimating output power using the Beale number is shown in (4.16) and is adapted from Figure 2.22.

$$B_N = \frac{L_S}{P_m V_e n} \tag{4.16}$$

Where B_N is the non-dimensional Beale number

L_S is the output power (Watts)

P_m is the mean pressure in the working space (MPa)

V_e is the expansion volume (cm^3)

n is the rotational speed (rev/s)

It can be shown that the work per cycle can be determined by dividing the power in Watts by the rotational speed in revolutions per second. This is because each revolution represents one complete cycle. Therefore, the Beale work per cycle can be represented by (4.17). The power will be calculated in Section 4.4.7 after rotational speed has been determined.

$$\left(\frac{L_S}{n}\right) = B_N P_m V_e$$
$$W_B = B_N P_m V_e \tag{4.17}$$

Where W_B is the Beale work per cycle (Joules)

The work per cycle for each design temperature according to the Beale number is presented in Table 4.7. The mean pressure is calculated by finding the average of the maximum and minimum pressure at each design temperature listed in Table 4.4, and the expansion volume is as shown in Table 4.3.

Table 4.7: Calculated values of Beale work output per cycle at design temperatures.

Th (° C)	Mean Pressure Pm (kPa)	Beale Number B_N	Beale work per cycle W_B (J)
500	526.32	0.15	70.559
600	577.82	0.15	77.470
700	629.45	0.15	84.393
800	680.95	0.15	91.294
900	732.48	0.15	98.207
1000	783.95	0.15	105.11
1100	835.43	0.15	112.01

It can be seen that the work output per cycle predicted by the Beale Number is significantly lower than the values calculated using the Schmidt equation. This is expected as the Schmidt equation makes unrealistic assumptions whereas the Beale Number uses experimental data to estimate the efficiency of a real engine. The actual Beale Number will vary depending on the engine.

4.4.5 Work Calculation using West Number

The West Number was also found in the literature review as a method for estimating power output of a Stirling Engine. It works on a similar principle to the Beale Number, however the equation includes terms for the hot cylinder and cold cylinder temperatures. The equation for estimating output power using the West number is shown in (4.18) as presented in Hirata et al. (2001) and is adapted from Figure 2.23. The literature states that for engines smaller than 5-150 kW the West Number is approximately 0.35 (Hirata et al., 2001).

$$W_N = \frac{L_S}{P_m V_e n \left(\frac{T_h - T_c}{T_h - T_c} \right)} \tag{4.18}$$

Where W_N is the non-dimensional West number

L_S is the output power (Watts)

P_m is the mean pressure in the working space (MPa)

V_e is the expansion volume (cm^3)

n is the rotational speed (rev/s)

T_h is the hot cylinder temperature (K)

T_c is the cold cylinder temperature (K)

Similarly, the work per cycle can be determined by dividing the power in Watts by the rotational speed in revolutions per second. Therefore, the West work per cycle can be represented by (4.19). The power will be calculated in Section 4.4.7 after rotational speed has been determined.

$$\left(\frac{L_S}{n}\right) = W_N P_m V_e \left(\frac{T_h - T_c}{T_h - T_c}\right)$$
$$W_W = W_N P_m V_e \left(\frac{T_h - T_c}{T_h - T_c}\right) \quad (4.19)$$

Where W_W is the West work per cycle (Joules)

The work per cycle for each design temperature according to the West number is presented in Table 4.8.

Table 4.8: Calculated values of West work output per cycle at design temperatures.

Th (° C)	**Mean Pressure Pm (kPa)**	**West Number W_N**	**West work per cycle W_W (J)**
500	526.32	0.35	72.575
600	577.82	0.35	88.302
700	629.45	0.35	104.100
800	680.95	0.35	119.930
900	732.48	0.35	135.810
1000	783.95	0.35	151.700
1100	835.43	0.35	167.620

It can be seen that the West equation predicts higher work per cycle than the Beale number, but still significantly less than the values suggested by the Schmidt equation. Figure 4.10 presents a summary of the work per cycle predicted by each analysis method. It can be seen that the P-V Diagram method and Schmidt equation predict similar values which are much higher than the values predicted by the Beale and West equations.

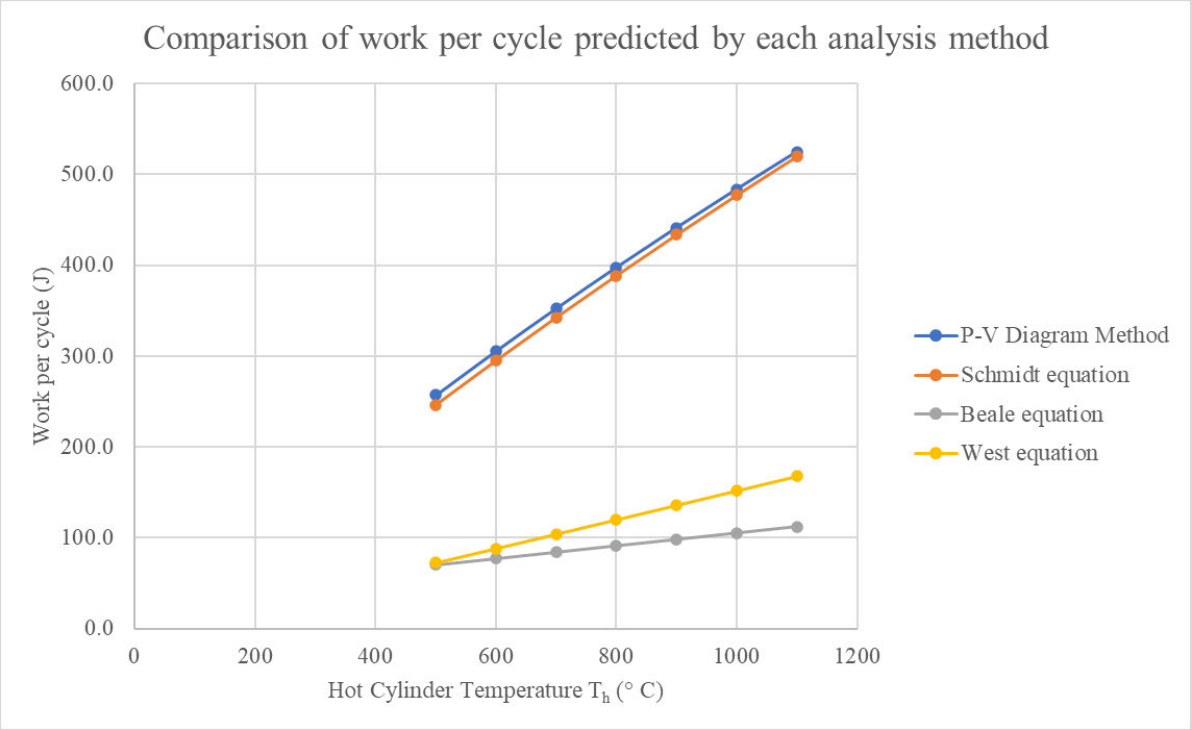

Figure 4.10: Comparison of work per cycle predicted by each analysis method.

4.4.6 Rotational Speed Calculation using Non-dimensional Analysis

In the literature review, a non-dimensional analysis method was found for determining the rotational speed of a Stirling engine depending on the expansion volume, hot cylinder temperature and gas properties. As described in Hirata et al. (2001), two non-dimensional terms are needed to find the rotational speed: non-dimensional speed and non-dimensional engine specification. The first term, non-dimensional speed, is calculated as shown in (4.20). The kinematic viscosity is determined using Wischnewski (2022) at each mean pressure and design temperature, and validated using Hirata (1998).

$$n^* = \frac{nV_e^{2/3}}{\nu} \tag{4.20}$$

Where n* is the non-dimensional speed

n is the rotational speed (rev/s)

V_e is the expansion volume (m^3)

ν is the kinematic viscosity coefficient of the working gas at T_h and P_m (m^2/s)

The second term is the non-dimensional engine specification, which is calculated as shown in (4.21).

$$S^* = \frac{T_h R V_e^{2/3}}{\nu^2} \tag{4.21}$$

Where S* is the non-dimensional engine specification

T_h is the hot cylinder temperature (K)

R is the individual gas constant of air (R_{air} = 287.3 J/(kg.K))

V_e is the expansion volume (m^3)

ν is the kinematic viscosity coefficient of the working gas at T_h and P_m (m^2/s)

Finally, the optimum non-dimensional rotational speed is found using the experimentally determined relation in (4.22) and substituted into (4.20) to find the optimum rotational speed as shown in (4.23).

$$n^*_{opt} = \left(6.8 \times 10^{-5}\right) S^{*0.6} \tag{4.22}$$

Where n^*_{opt} is the optimum non-dimensional speed

$$n_{opt} = \frac{n^*_{opt} \nu}{V_e^{2/3}} \tag{4.23}$$

Where n_{opt} is the optimum rotational speed (rev/s)

Table 4.9 shows the calculated values for the non-dimensional values, and finally the optimum rotational speed in revolutions per second. It can be seen that as the temperature increases, so does the optimum rotational speed. The minimum is found at T_h = 500° C where the optimum speed is 6.538 rev/s, which equates to 392.3 rpm. The maximum is found at T_h = 1 100° C where the optimum speed is 8.288 rev/s, which equates to 497.3 rpm. This is to be expected as more energy is being transferred into the engine at higher temperatures.

Table 4.9: Calculated values of West work output per cycle at design temperatures.

Th (° C)	Mean Pressure Pm (kPa)	v (m^2/s)	S*	n^*_{opt}	n_{opt} (rev/s)
500	526.32	1.5487E-05	8.5918E+12	3917.05	6.538
600	577.82	1.7284E-05	7.7905E+12	3693.58	6.880
700	629.45	1.8993E-05	7.1906E+12	3520.21	7.205
800	680.95	2.0642E-05	6.7133E+12	3378.08	7.515
900	732.48	2.2229E-05	6.3285E+12	3260.53	7.811
1000	783.95	2.3739E-05	6.0220E+12	3164.86	8.097
1100	835.43	2.6500E-05	5.2122E+12	2902.15	8.288

4.4.7 Power Estimation

Now that the work per cycle and rotational speed have been determined, the power output can be calculated. This is a simple matter of multiplying work per cycle by the rotational speed in revolutions per second because each revolution represents one cycle. Therefore, the power can be calculated as shown in (4.24).

$$L_S = W.n \tag{4.24}$$

Where L_S is the power output (Watts)

W is the work per cycle (Joules)

n is the rotational speed (rev/s)

The power output has been calculated using the work output calculated from each analysis method in the preceding sections, and the rotational speed calculated in Section 4.4.6. Table 4.10 and Figure 4.11 show the power output at each design temperature.

It can be seen that the Beale method predicts the lowest power output and ranges from 461.31 W at 500° C to 928.34 W and 1 100° C. The West method predicts slightly higher power output ranging from 474.50 W at 500° C to 1 389.2 W at 1 100° C. Not surprisingly, the P-V and Schmidt methods predict much higher power outputs due to the assumptions made. Here the power ranges from 1 610.3 W at 500° C using the Schmidt equation to 4 348.4 W at 1 100° C using the P-V method.

Given the target power output of 750 – 1 000 W outlined in Section 4.2, the design is considered adequate as the lowest predictor (being the Beale method) suggests values within this power range for

the upper design temperatures between 900° – 1 100° C. The West method predicts that the engine will achieve this performance between the design temperatures of 700° - 900° C.

Table 4.10: Calculated values of power output at design temperatures for each analysis method.

Th (° C)	n (rev/s)	P-V Power, $L_{S,PV}$ (W)	Schmidt Power $L_{S,S}$ (W)	Beale Power, $L_{S,B}$ (W)	West Power, $L_{S,W}$ (W)
500	6.538	1680.53	1610.31	461.31	474.50
600	6.880	2102.67	2030.29	532.99	607.52
700	7.205	2539.26	2468.43	608.05	750.04
800	7.515	2987.96	2921.16	686.07	901.27
900	7.811	3446.92	3387.16	767.09	1060.8
1000	8.097	3915.71	3865.02	851.08	1228.3
1100	8.288	4348.38	4309.18	928.34	1389.2

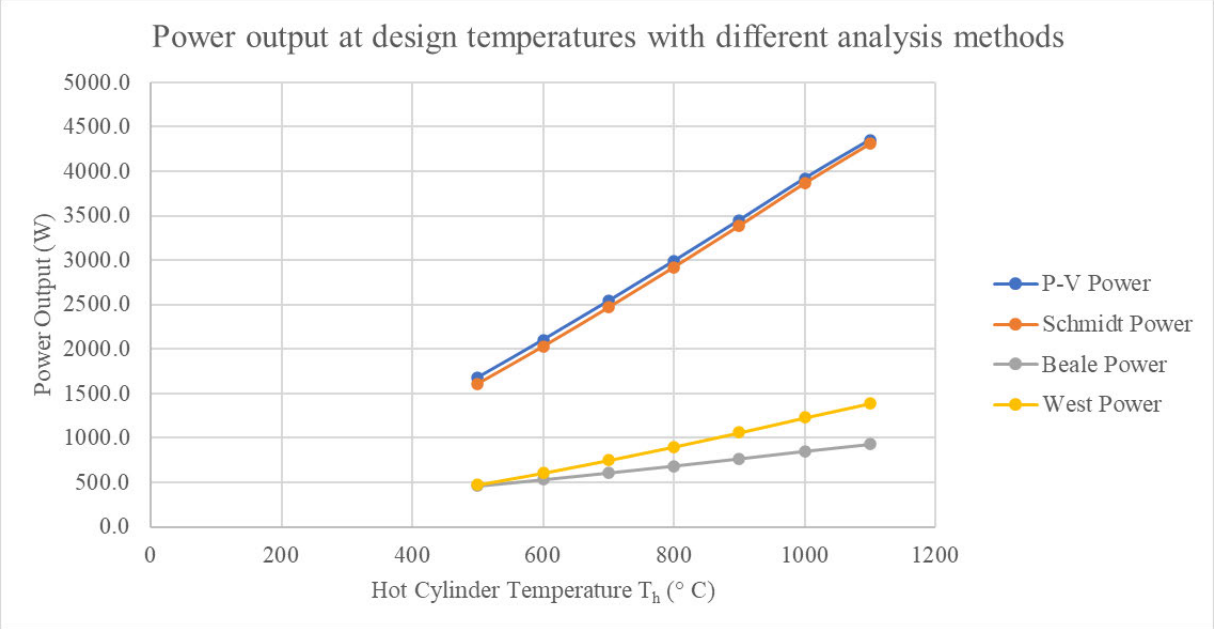

Figure 4.11: Comparison of power output predicted at design temperatures by each analysis method.

Chapter 5

Engine Design and Fabrication

5.1 Chapter Overview

This chapter outlines the design and fabrication of a Stirling Engine based on the initial design carried out in Chapter 4. The main geometrical parameters have been determined in Chapter 4 and the power output has been estimated based on these values. These values are incorporated into the design outlined in this chapter, as well as attempting to optimise the performance of all other components through best design practices.

Section 5.2 outlines detailed design of the various engine components with respect to functionality, stress, material selection and manufacturing processes. The cost of the engine is another important consideration for viability in the market, however it is not a primary consideration in this design as the aim is to prove viability of the engine in terms of its power output and potential in industrial applications. The cost, safety, fatigue and design life are discussed in Section 5.3. A 3D model of the components and assembly has been produced using SolidWorks. Finite Element Analysis (FEA) has also been performed on all critical components using SolidWorks Simulation to check the validity and safety of the design, and this is outlined in Section 5.4.

Section 5.5 outlines the production of detail drawings before the results of fabrication and assembly are presented in Sections 5.6 and 5.7.

5.2 Component Design and Analysis

A number of components are required for the functioning of an alpha Stirling Engine with a crank slider mechanism. In particular, the type of Stirling Engine chosen for this design is a two-cylinder alpha type. Furmanek & Kropiwnicki (2021) present the design of an alpha type Stirling engine and the necessary components have been identified as follows. A water cooling system was also incorporated in the design by Furmanek & Kropiwnicki (2021) however it has been decided to build a convection cooling system into the cold cylinder for this project.

- Engine body
- Hot cylinder
- Cold cylinder
- Two pistons
- Two connecting rods
- Connecting air tube
- Regenerator
- Crank mechanism
- Flywheel
- Heater
- Cooler

These are the major components, however there are other subcomponents which will be required such as bearings, bushes, pins, bolts, shaft keys and piston rings. Different material options are available for each component and the design choices are outlined in the following sections depending on stress, functionality and relevant material properties.

The design process was carried out with stress calculations and material properties governing the safety of components. Section 5.2.1 presents images of the final 3D solid model assembly produced in SolidWorks with diagrams showing how the Stirling cycle is achieved. Sections 5.2.2 to 5.2.12 outline the design of each component and how they are to be manufactured. For the purposes of stress analysis in the components, the maximum working gas pressure will be used to assess the forces acting on each component. From Table 4.4, it can be seen that the theoretical maximum working gas pressure is 1 510.4 kPa which occurs at a design temperature of 1 100° C.

5.2.1 3D Solid Model and Mechanical Simulation

Solid models of all components were produced in SolidWorks and a rendered image of the working assembly is shown in Figure 5.1. All components are shown except for the assembly bolts.

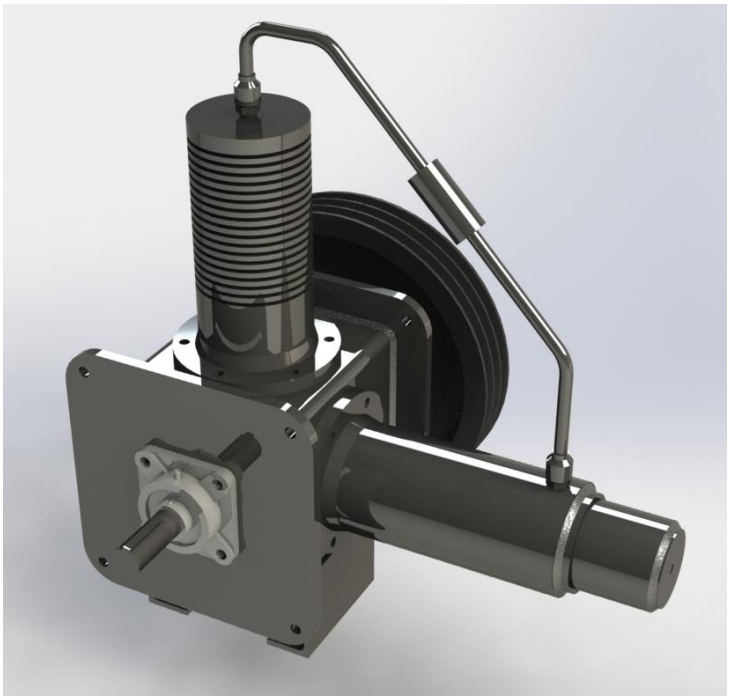

Figure 5.1: Rendered image of complete Stirling Engine assembly produced in SolidWorks.

Figure 5.2 shows an image of the working assembly with a section through the centre of the hot cylinder to reveal the internal components such as the pistons, connecting rods and crank mechanism.

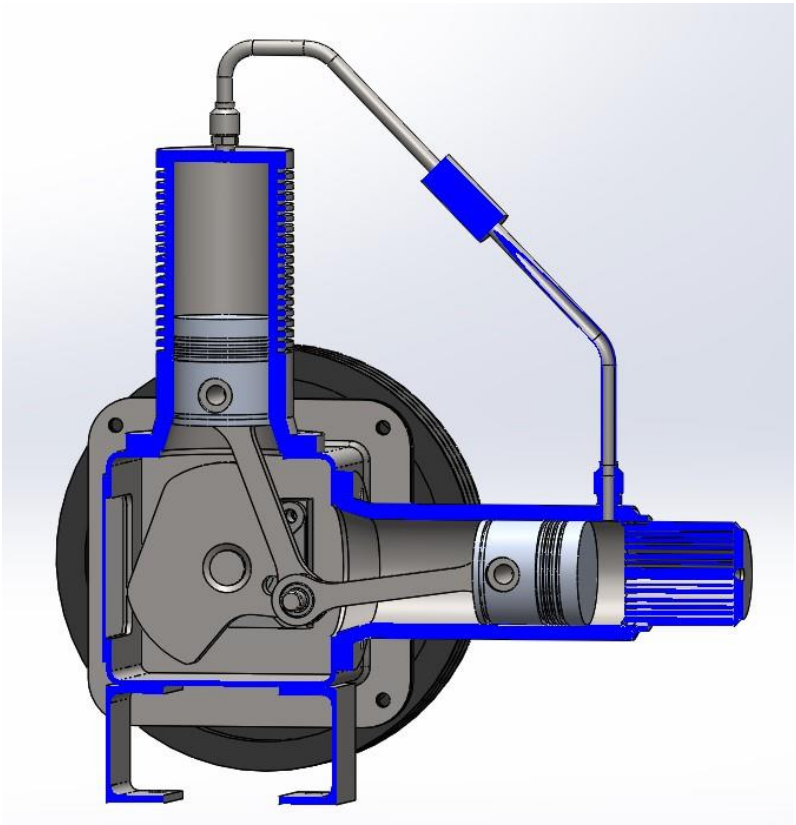

Figure 5.2: Section of Stirling engine assembly through centre of hot cylinder to show internal components.

Figure 5.3 shows the motion of the pistons within the cylinders and how the Stirling cycle is achieved when compared with diagrams found in the literature review such as Figure 2.6.

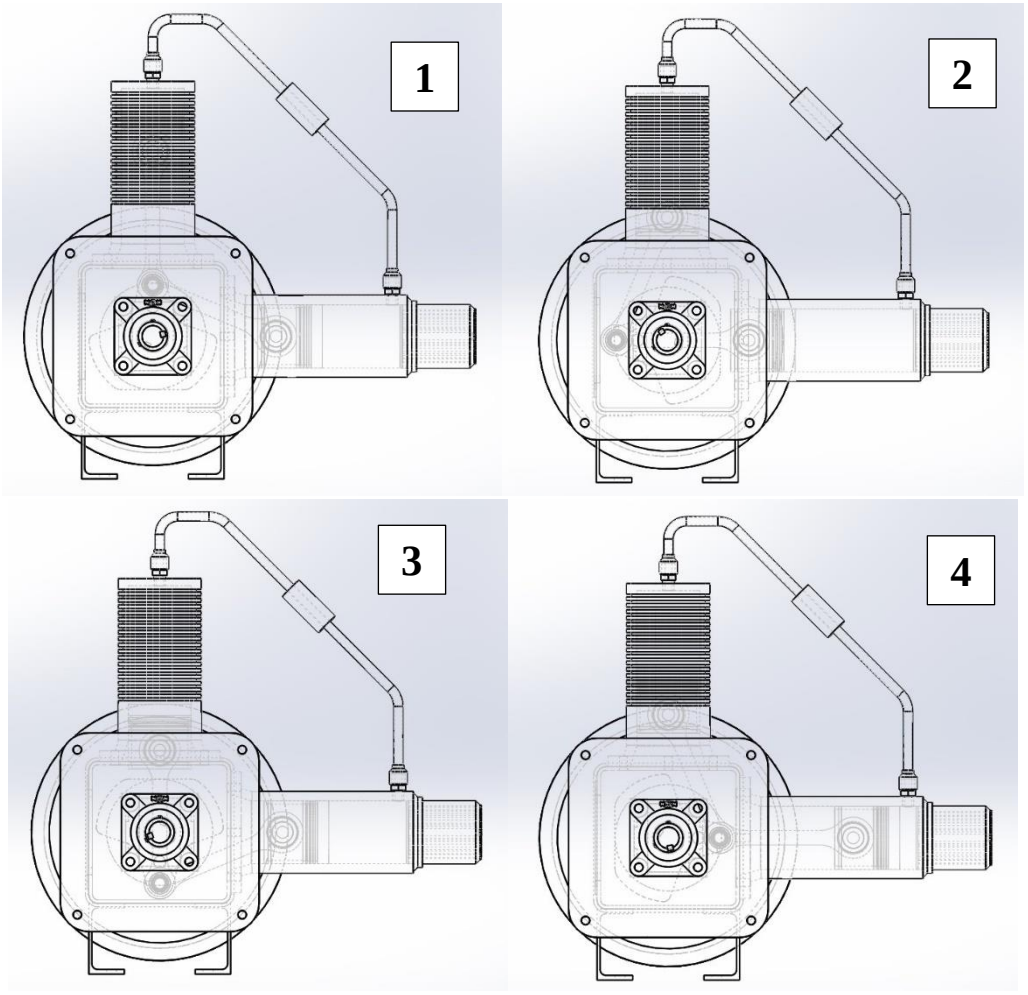

Figure 5.3: Stirling cycle represented in the engine design.

Figure 5.4 shows an image of the crank mechanism which is discussed in Section 5.2.9, and Figure 5.5 shows an image of the typical connection between the connecting rod and the piston.

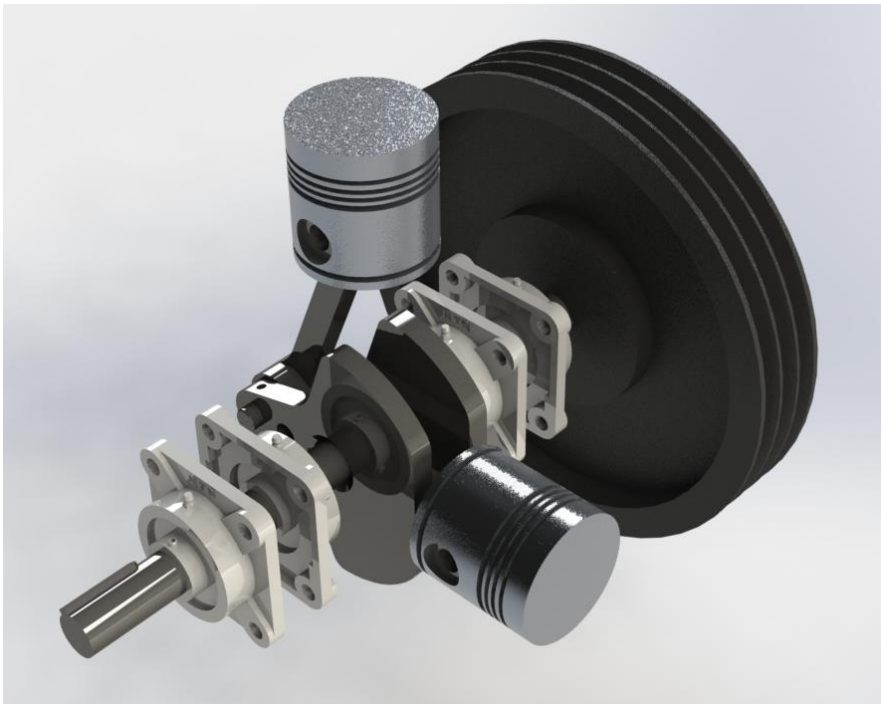

Figure 5.4: Crank mechanism including connecting rods, pistons and flywheel.

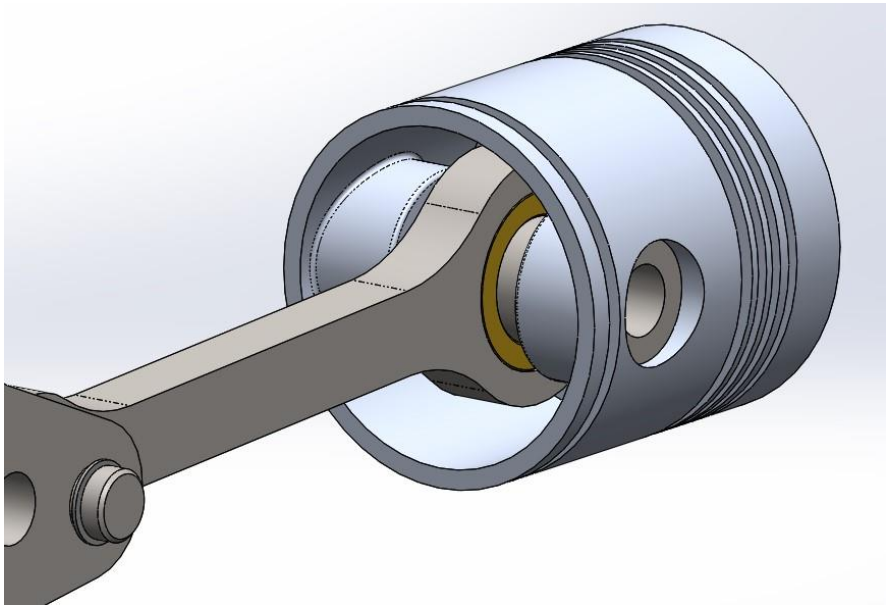

Figure 5.5: Connection between connecting rod and piston.

5.2.2 Engine body

DESIGN

Dinesh et al. (2014) states that the purpose of the engine body or frame is to support the connecting shaft, flywheel, cylinders and other rotating parts by allowing bearings to be fitted. With this in mind, the design considerations which are made for this project including the following.

1. Allow for mounting of cylinders at 90 degrees to each other. As outlined in Egas & Clucas (2018), the phase angle of 90 degrees determines the angle between the cylinder axes as the connecting rods are pinned at the same location on the crank shaft.
2. Sufficient space for housing of crank mechanism.
3. Allow for mounting bearings to support the crank shaft.
4. Allow access to internal components for assembly and disassembly.
5. Ability to bolt down engine to a jig or bench.

Figure 5.6 shows an image of the engine body weldment.

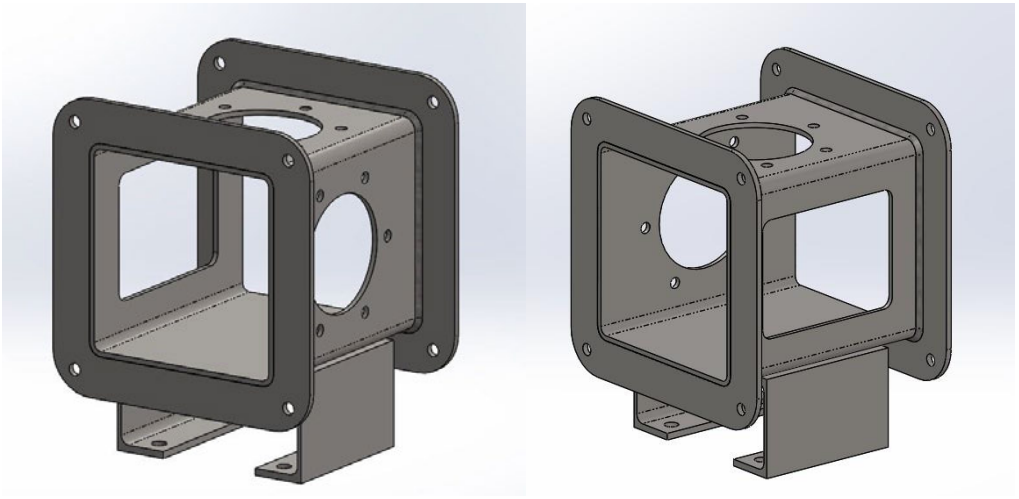

Figure 5.6: Engine body weldment.

The solution devised utilises 200 x 200 x 5 steel square hollow section (SHS) as the main body of the engine as the two cylinders can be bolted onto two walls which are perpendicular to each other, and the internal space was found to be large enough for the crank mechanism. A bolt hole pattern was drilled into the mating faces of the SHS for bolting the cylinders, and a large hole cut-out was made with adequate clearance for the piston to allow for assembly and disassembly.

A large rectangular cut-out was made in the wall opposing the horizontal cylinder for access to the internal components for assembly and disassembly. A guard is fitted to cover this cut-out with steel

mesh so that is impossible for a person to get their fingers into the working space during operation. Steel plates were welded onto the ends of the SHS with holes for bolting bearing plates onto each end to support the crank shafts. The centre of the cylinders are offset along the crank shaft axis so that the connecting rods are positioned at the centre of the gudgeon pins fitted to the pistons. The amount of offset is 8 mm which is equal to half the thickness of the connecting rods. Two pieces of parallel flange channel (PFC) were welded to the bottom of the SHS body and holes drilled in the bottom flanges so that the engine can be bolted down to a jig or bench.

MATERIALS

Steel is readily available as plate, PFC and SHS and can easily be joined into the desired configuration by welding. Furthermore, it is high strength and high stiffness and thus will not deform significantly. It has a relatively high density of 7800 kg/m^3 but by using structural profiles the overall weight can be minimised while retaining strength.

STRESS ANALYSIS

The stress on the bolts connecting the cylinders to the body are checked in Section 5.2.3 and 5.2.4. Furthermore, the stress in the bolts connecting the bearing plates to the body are checked in Section 5.2.9.

There are four M12 mounting bolts which fix the engine onto a jig or bench. As the pressures and forces are contained within the engine, the main purpose of these bolts is to stop rocking and vibration of the engine assembly. A vibration analysis has not been conducted for this design, however it may be necessary as future work.

MANUFACTURING PROCESSES

The holes and cut-outs in the SHS are created by drilling, oxy-cutting and mechanical means such as cut off wheels. There is also the potential for tubular laser cutting to be utilised for producing this part. The steel plate has been profiled using a laser cutter and welded onto the SHS body. The PFC and SHS were cut using a bandsaw and similarly welded together.

5.2.3 Hot cylinder

DESIGN

The hot cylinder has been designated the horizontal cylinder as it is easier to apply the heat source to the heater head at the end of the cylinder. It must have a mating flange on the bottom for bolting onto the SHS body and be bored and honed to suit the 88.9 mm piston. The key consideration for internal

machining is to meet the specified tolerance and the need for a cylinder hone to provide a low friction surface (Hoag & Dondlinger 2016). Figure 5.7 shows an image of the hot cylinder.

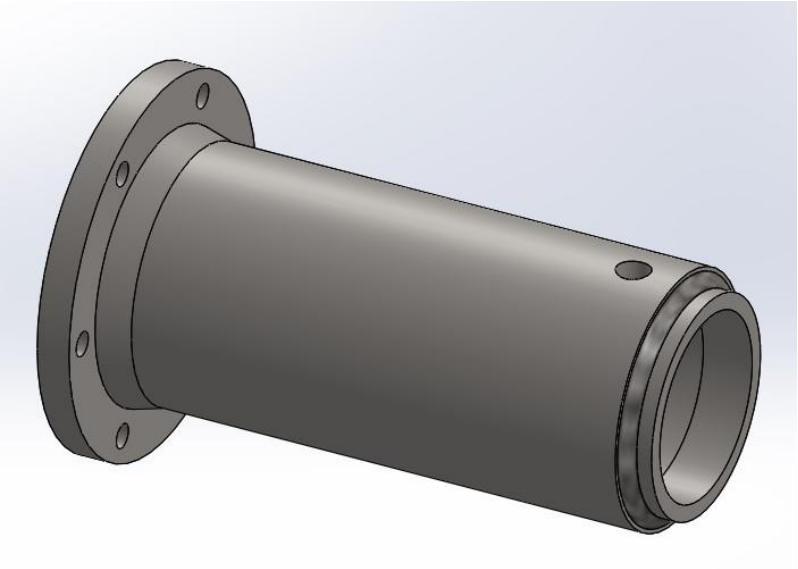

Figure 5.7: Hot cylinder solid model.

The clearance between the piston and cylinder wall is a key consideration as air leakage must be minimised. Although compression rings are utilised to aid in minimising air leakage, the specified clearance must be decided. Ross (1993) suggests a diametrical clearance of 3 to 4 thousandths of an inch, which equates to 0.0762 to 0.1016 mm. Other literature suggests similar values, as a clearance of 3 thousandths of an inch is also specified by He (2016) in the design of a gamma Stirling engine. This has been adopted for the design. While there is minimal literature on cylinder design, information is adapted from internal combustion (IC) engine design as this provides a useful starting point. Some considerations for cylinder design include cylinder wall distortion and thermal expansion of the piston as this will affect the clearance between the cylinder and piston (Hoag & Dondlinger 2016). This distortion can be affected by the pressures and temperatures present in the engine, initial machining and clamp bolting of the head (Hoag & Dondlinger 2016). Although these considerations are for an IC engine, high temperatures and pressures will be present in the Stirling engine design as well. Hoag & Dondlinger (2016) suggest that a cylinder cooling system should be incorporated to minimise the temperature variation across the cylinder wall. Although it was ultimately decided not to include a cooling system for the hot cylinder, it may be required if distortion occurs.

The cylinder must be long enough to accommodate the stroke of the piston as it travels from top dead centre to bottom dead centre and allow for the fitting of a heater to transfer the heat into the working gas. The heater design is shown in Section 5.2.11, and utilises a male 3” NPT threaded nipple. And therefore a 3” NPT female threaded socket is welded into the end of the hot cylinder to allow for fitting

of the heater. Furthermore, the working gas must be able to travel out of the cylinder and into the connecting air tube. A 3/8" BSPT tapped hole is made into the side wall of the cylinder to allow for a male 3/8" BSPT fitting to be screwed in and connected to the connecting air tube. BSPT thread is chosen as the tapered thread provides better sealing than its parallel thread counterpart (RedFluid, 2022). A sufficient gap must be left between the end of the heater and the piston when it is at top dead centre to ensure that the tapped hole is never covered, and the working gas is always free to travel in and out of the cylinder. The amount of clearance required here is unclear in the literature. Ipci & Karabulut (2018) present an analysis of an alpha type engine and specify a minimum distance of 2 mm between the top of the piston at top dead centre and the cylinder, however no justification is given. For this design, a minimum of 23 mm is required to clear the tapped hole, which is greater than 2 mm and therefore is considered acceptable.

MATERIALS

The pressure inside the cylinder will theoretically reach 1 510.4 kPa and therefore a material with sufficient strength must be chosen. Furthermore, the hardness of the material should be greater than the hardness of the piston and compression rings so that the bore of the cylinder doesn't wear. Johansson (2019) suggests that both material should have a high hardness and the difference in the hardness of the materials should be less than 10%. Typically, IC engine blocks are cast from aluminium alloy or gray cast iron to minimise weight and a cylinder liner is fitted to provide the sliding properties required (Hoag & Dondlinger 2016). This was considered out of the scope for this project and thus a material was selected to provide an adequate hardness with sufficient strength. Friction between the cylinder and piston should be minimised as much as possible and it must be machinable to the desired shape. It must also be able to withstand the high temperatures which will be applied from the heater and the hot working gas inside without excessive deformation.

Steel was the initial choice as it is readily available and can be machined to suit the piston. Furthermore, the female 3" NPT socket can be welded onto the end of the cylinder to take the heater. Steel has good strength, is relatively hard and can be drilled and tapped to take the fitting to connect the air tube. Steel has a relatively low coefficient of thermal expansion of $12 \times 10^{-6}/°$ C, and therefore shouldn't experience excessive deformation under the applied heat (Juvinall & Marshek 2012). For the prototype, 1045 round steel bar was available and it has been selected for the cylinder material. The wall thickness of the cylinder has been made quite large firstly to withstand the hoop stress, but also to provide insulation in an attempt to minimise heat loss through the cylinder walls. The chosen wall thickness is 13 mm.

STRESS ANALYSIS

The main considerations for stress in the hot cylinder are hoop stress in the cylinder walls resulting from the internal pressure, normal stress developed in the cylinder walls resulting from the axial force

generated by the internal pressure acting on the end face of the heater head and stress in the bolts holding the cylinder to the SHS body.

When the pressure builds within the cylinder, the worst stress case for the bolts is a direct axial force in-line with the axis of the cylinder. The maximum force is found in (5.1) using the relation between pressure and force.

$$P = \frac{F}{A} \tag{5.1}$$

Where P is the pressure (MPa)

F is force (N)

A is the area over which the pressure acts (mm^2)

Rearranging (5.1) and substituting the maximum pressure of 1 510.4 kPa and circular area with diameter of 88.9 mm, the force is found in (5.2).

$$F = PA = P\frac{\pi D^2}{4} = 1.5104 \times \frac{\pi \times 88.9^2}{4} = 9375.3N \tag{5.2}$$

Therefore, the maximum force acting in the axial direction of the cylinder is 9 375.3 N. Six M10 Grade 8.8 bolts have been specified for bolting the cylinder to the SHS body, and the force is assumed to be equally dispersed over all the bolts. The stress in each bolt is calculated using the relation for axial stress in (5.3).

$$\sigma = \frac{F}{A_s} \tag{5.3}$$

Where σ is the normal stress (MPa)

F is the force acting (N)

A_s is the stress area of the bolt (mm^2)

From Juvinall & Marshek (2012), the stress area of an M10 bolt is 58 mm^2 and Grade 8.8 specifies a yield strength of 660 MPa. Therefore, the safety factor can be found by dividing the strength of the bolt by the stress present. Firstly, the normal stress in each bolt is found to be 26.94 MPa as show in (5.4).

$$\sigma = \frac{9375.3}{6 \times 58} = 26.94MPa \tag{5.4}$$

Therefore, the safety factor is 24.5 as shown in (5.5). Clearly, this is a very high safety factor and will account for any uncertainty in loading and stress distribution.

$$SF = \frac{S_y}{\sigma} = \frac{660}{26.94} = 24.5 \tag{5.5}$$

Where SF is the safety factor

S_y is the yield strength (MPa)

The equation for hoop stress in a hollow cylinder is shown in (5.6) as defined in Air and Gas Duct Structural Design Committee (2020).

$$\sigma = \frac{Pr}{t} \tag{5.6}$$

Where P is the internal pressure (MPa)

σ is the normal stress within the walls of the cylinder (MPa)

r is the mean radius of the cylinder (mm)

t is the wall thickness of the cylinder (mm)

The total normal stress can be found by summing the hoop stress and the axial stress resulting from the force developed against the heater head and is found to be 8.17 MPa as shown in (5.7).

$$\sigma = \frac{1.5104 \times 50.95}{13} + \frac{9375.3}{\frac{\pi\left(114.9^2 - 88.9^2\right)}{4}} = 8.17 MPa \tag{5.7}$$

From Juvinall & Marshek (2012), the yield strength for 1045 hot rolled steel is 414 MPa. Therefore, the safety factor is found to be 50.7 as shown in (5.8). This is a very high safety factor in terms of stress, however the large wall thickness will help in reducing thermal losses through the wall of the cylinder. Furthermore, a larger wall thickness is likely to reduce costs as less machining is required. This is because the mounting flange is the largest diameter, and this dictates the stock steel bar from which the part must be machined.

$$SF = \frac{S_y}{\sigma} = \frac{414}{8.17} = 50.7 \tag{5.8}$$

MANUFACTURING PROCESSES

The outside profile of the cylinder will be produced by turning, while the internal surface needs to be bored and honed. This will give a smooth surface finish to reduce friction between the cylinder and the piston, and to produce an accurate dimension to achieve the necessary tolerance. According to Boundy (2012), the surface finish achievable with long-stroke honing in an average application ranges from approximately 0.05 to 0.8. For this application, a surface finish of 0.4 has been chosen to balance the machining cost and quality of the surface finish for minimising friction.

It is important that the cylinder walls do not distort as a result of heat input otherwise the piston will not be able to slide freely within the cylinder. Therefore, any welding must be done away from the section of cylinder in which the piston stroke is located. The only welding required is to join the female 3" NPT socket onto the end of the cylinder, and this is far enough away to avoid distortion of the cylinder. The tapped hole was drilled and tapped into the side wall of the cylinder.

5.2.4 Cold cylinder

DESIGN

The cold cylinder has been designated the vertical cylinder as in general the literature shows this layout. Similarly to the hot piston, it must have a mating flange on the bottom for bolting onto the SHS body and be bored and honed to suit the 88.9 mm piston. Figure 5.8 shows an image of the cold cylinder.

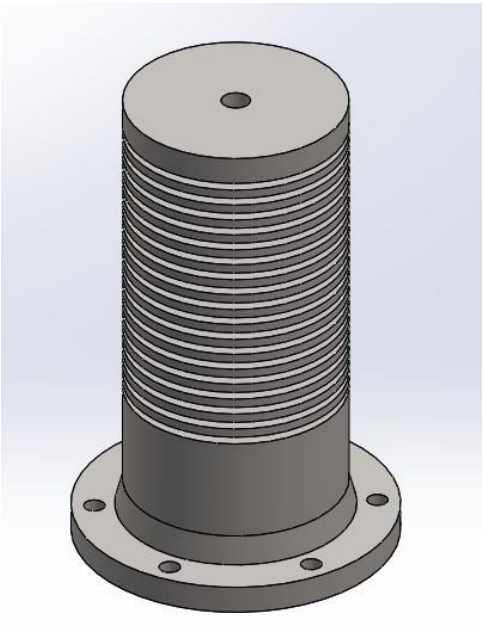

Figure 5.8: Cold cylinder solid model.

Some of the design considerations are the same as for the hot cylinder, including the clearance between the piston and cylinder wall and the length. As the stroke and crank radius is the same for both pistons, the length of both cylinders has been made the same. A cooler must be incorporated into the cold cylinder to minimise the temperature of the air in this space as this allows for greater compression. Some engines found in the literature incorporate intricate coolers such as air- or water-cooled systems, however for this design a more simplistic approach has been taken. Grooves have been machined into the cylinder walls to essentially create fins for heat to be rejected to the surrounding environment.

Similarly, the working gas must be able to travel out of the cylinder and into the connecting air tube. A 3/8" BSPT tapped hole has been made into the end wall of the cylinder to connect the other end of the air connecting tube.

MATERIALS

The material selected for the cold cylinder is the same as that chosen for the hot cylinder, being 1045 round steel bar. This is because the internal pressures and design requirements are the same, however no welding is required on the cold cylinder. The outside diameter of the cylinder has been made quite large to ensure that there is still sufficient wall thickness after the cooling fins have been machined. The maximum wall thickness is 14 mm with a groove depth of 7 mm, leaving a minimum wall thickness of 7 mm.

STRESS ANALYSIS

As the bolt pattern is the same for the hot cylinder, the stresses here will be the equal as the same internal pressure is experienced. Therefore, the normal stress in the cylinder walls is the only consideration and it can be calculated similarly to (5.7) and is shown in (5.9) with the minimum thickness of 7 mm substituted.

$$\sigma = \frac{1.5104 \times 50.95}{7} + \frac{9375.3}{\frac{\pi\left(102.9^2 - 88.9^2\right)}{4}} = 15.4MPa \tag{5.9}$$

Similarly, the safety factor can be calculated as shown in (5.10). Again, the safety factor of 26.8 is very high which ensures a safe design and leaving the outside diameter will reduce the amount of machining required and thus the cost.

$$SF = \frac{S_y}{\sigma} = \frac{414}{15.4} = 26.8 \tag{5.10}$$

The stress in the end of the cylinder can be determined by considering it a round disc with fixed edges and a uniform pressure applied. With these assumptions, the maximum stress can be calculated using (5.11) as defined in Hosford (2010).

$$\sigma_m = \frac{3pr^2}{4t^2} \tag{5.11}$$

Where σ_m is the maximum stress in the end wall of the cylinder (Pa)

p is the internal pressure (Pa)

r is the internal radius (m)

t is the thickness of the end wall (m)

The design thickness of the end wall is 10 mm, and therefore the maximum stress is found to be 22.382 MPa as shown in (5.12). This represents a safety factor of 18.5 and is considered safe.

$$\sigma_m = \frac{3\times 1510.4\times 10^3 \times 0.04445^2}{4\times 0.010^2} = 22.382 MPa \tag{5.12}$$

MANUFACTURING PROCESSES

The manufacturing processes utilised for the cold cylinder are the same as those utilised for the hot cylinder, however no welding is required.

5.2.5 Pistons

DESIGN

Pistons have been sourced off the shelf for the engine build with an outside diameter of 88.9 mm to suit the cylinder bore size decided in Chapter 4. The part number of the piston is 18018 000T1 and is taken from a Lister SR1, SR2 or SR3 diesel engine and has the following specifications.

Piston Diameter:	88.9 mm
Piston Length:	103.188 mm
Gudgeon Pin diameter:	29.37 mm
Compression Height:	65.138 mm

Three compression rings and two oil rings are included with the assembly, as well as the gudgeon pin with internal circlips to retain the pin in the piston. A balance must be found between sealing and friction in deciding how many rings to utilise. Better sealing is found when more rings are fitted however this will increase the friction between the piston and cylinder walls. Hoag & Dondlinger (2016) state that the clearance between the cylinder wall and the piston is an important consideration as excessive may cause side impact loading. Furthermore, a varying piston diameter should be incorporated so that the cold clearance at the crown is larger where more thermal expansion will occur (Hoag & Dondlinger 2016). This suggests that issues may occur with sealing of the cold piston as less heat will be present, and therefore less thermal expansion will occur. A custom designed piston may be required to rectify this issue.

It was found that the piston length was too long as interference with the crank mechanism would have occurred, and so 12 mm was machined off the bottom of the piston. Engine oil was applied to the piston and cylinder bores before testing reduce friction between the two components.

MATERIALS

The piston is made of aluminium alloy. This is a desirable material as it has a relatively low density when compared with steel but maintains a high strength-to-weight ratio and since the piston is lightweight, the inertial drag forces are minimised (Hoag & Dondlinger 2016). As the cylinders are made from 1045 steel bar, it is desirable to use pistons and compression rings which have a lower hardness so that the cylinder bore is not damaged as a result of the relative motion between the two. A typical hardness for 6061-T6 aluminium is 95 HB, while 1045 medium tensile carbon steel bar has a hardness of approximately 230 HB. Furthermore, the material specified for the compression rings is ASTM Class 25 cast iron which has a hardness of approximately 174 HB (Juvinall & Marshek, 2012). The difference in the hardness between the cylinder and compression ring material is higher than 10%, which may not be ideal as suggested by Johansson (2019). However, it is not excessively different and such is accepted for this design.

STRESS ANALYSIS

The maximum gross power of an SR1 Lister Diesel Engine with a single cylinder is listed as 8.15 hp (6.08 kW) and the B.M.E.P. (brake mean effective pressure) is 78.4 psi (540.55 kPa) (Lister 2000). It can be seen from Table 4.7 that in the Stirling engine design the largest mean pressure of 835.43 kPa occurs at 1 100° C. This mean pressure is larger than what occurs in the Lister SR1 Diesel Engine, however it is assumed that a sufficient safety factor has been allowed for in the diesel engine and as such it is safe for the engine prototype. A pressure test of 120 psi (827.37 kPa) was performed on the piston within the cylinder and no failure was observed. For further work, the piston could be modelled and analysed with FEA in order to determine the long term performance with respect to fatigue. A photo of the piston is shown in Figure 5.9.

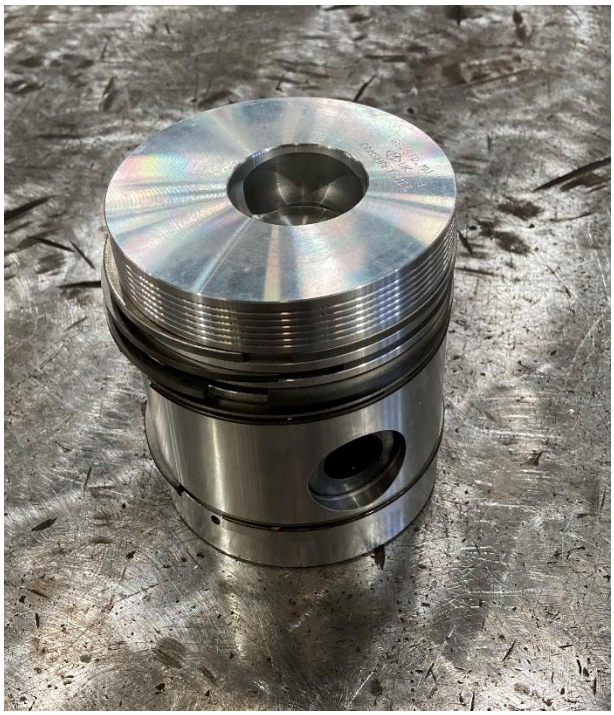

Figure 5.9: Lister 18018 000T1 piston for Stirling engine prototype.

5.2.6 Connecting rods

DESIGN

The connecting rods link the piston to the crank mechanism and pivot at both ends to convert the linear motion of the piston into rotary motion at the crank. Figure 5.10 shows the connecting rod assembly.

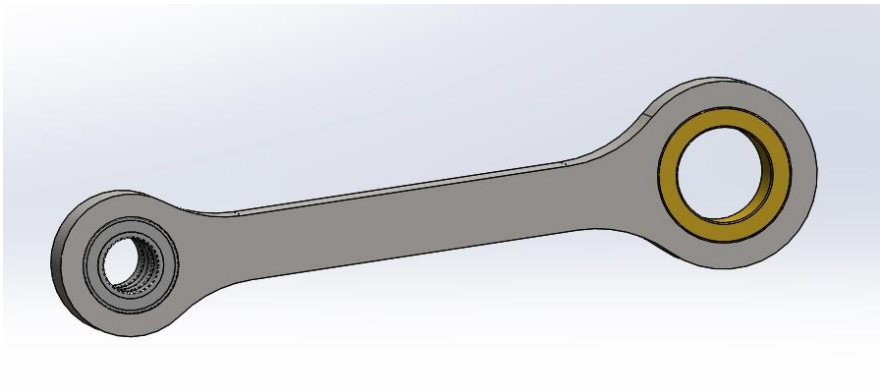

Figure 5.10: Connecting rod assembly including ball bearings and bronze bush.

As shown in Table 4.2, the length of the connecting rod 18.75 cm for both the expansion and compression pistons, and this represents the distance from the centre of the gudgeon pin on the piston to the centre of the connecting pin on the crank mechanism. The size of the gudgeon pin in the piston is 29.37 mm and the pin on the crank connection was designed with a diameter of 17 mm.

The friction that occurs as a result of the relative rotary motion between the connecting rods and the pins at each end must be minimised. Organ (2014) suggests that for engines with a temperature ratio of less than 3, plain bearings are suitable while rolling element bearings should be used when the temperature ratio is greater than 3. Therefore, as the temperature ratio is greater than 3 for all design cases, rolling element bearings are most suitable. Therefore, two ball bearings are pressed into the crank end to minimise friction, however a bronze bush is pressed into the piston end due to space requirements. At the piston end, a bronze bush was considered suitable as it has a low coefficient of friction and it essentially "rocks" back and forth at a relatively low frequency without completing full rotations.

MATERIALS

Typical materials used for connecting rods in other engine applications include cast iron, titanium, aluminium and steel and are historically forged, cast or machined from billet. Cast iron and aluminium are used in light-load applications while steel and titanium are reserved for high load or high-performance applications. In an internal combustion engine, they are one of the most highly stressed components and must be designed for fatigue loading as they experience fluctuating loads through every rotation of the engine. They experience tensile and compression loads (Hoag & Dondlinger 2016).

For the purposes of this design, steel has been chosen as it is readily available and has high strength and stiffness properties. For accuracy and ease of production, the connecting rods have been designed from 16 mm thick Grade 350 steel plate. The desired shape can be easily profiled by laser cutting with holes subsequently machined each end to press fit the bearings.

STRESS ANALYSIS

The rectangular cross section of the connecting rod has been checked for stress resulting from the tensile and compressive loads, assuming the maximum force is experienced as calculated in (5.2). The other consideration is buckling, and Euler's buckling equation has been used to check the safety in this aspect.

Assuming the maximum load of 9 375.3 N acts on the connecting rod, the normal stress in the rectangular cross section can be calculated. The dimensions of the cross section are 20 x 16 mm and as the rod is a two-force member, the tensile or compressive force must be equal and opposite and act along a line between the bearing centres. The normal stress of 29.30 MPa has been found as shown in (5.13). Given that the yield strength of the steel is 350 MPa, the safety factor here is 11.95. This is quite

high, but as mentioned there will be fatigue occurring in this component and a large safety factor is used for this reason. A thorough fatigue analysis should be conducted before any commercial production.

$$\sigma = \frac{F}{A} = \frac{9375.3}{20 \times 16} = 29.30 MPa \tag{5.13}$$

The critical buckling load can calculated using Euler's formula as shown in (5.14) (Beer et al., 2015).

$$P_{cr} = \frac{\pi^2 EI}{L_e^2} \tag{5.14}$$

Where P_{cr} is the critical buckling load (N)

E is the modulus of elasticity (Pa)

I is the second moment of area of the cross-section (m^4)

L_e is the effective length between the connections of the member (m)

For steel, the modulus of elasticity is 200 GPa, and as the rod has essentially pinned connections at each end the effective length is equal to the actual length (Beer et al., 2015). As the cross-section is a rectangle, the second moment of area has been calculated for the weak axis direction in (5.15) as buckling will occur about this axis first.

$$I = \frac{1}{12} bh^3 = \frac{1}{12} \times 0.020 \times 0.016^3 = 6.82 \times 10^{-9} m^4 \tag{5.15}$$

The critical buckling load was found to be 382.9 kN as shown in (5.16). This is significantly higher than the maximum force of 9.375 kN and therefore the design is safe from buckling.

$$P_{cr} = \frac{\pi^2 \times 200 \times 10^9 \times 6.82 \times 10^{-9}}{0.1875^2} = 382.9 kN \tag{5.16}$$

The thickness of the steel around the bearings at each end has been sized by assessing the stresses in the FEA and will be discussed in Section 5.4.

The bearings selected for the crank end of the connecting rod are 6903 open type deep groove ball bearings. As these bearings are 7 mm wide, two bearings are pressed into each rod to provide sufficient load bearing capacity. The dynamic capacity of each bearing is 4.65 kN and therefore the combined load capacity with two bearings is 9.3 kN (NTN Corporation, 2020). This is right on the boundary of

the maximum force and a better solution could be devised for future work. However, given that the maximum pressure is theoretical and is unlikely to be achieved in practice, it is considered adequate for this prototype.

A lubrication system for the bronze journal bearing at the piston end was considered outside of the scope for this project but could be considered in future work. The fit was designated H9/e9 which gives an easy running fit and is applicable to bearings in internal combustion engines such as camshaft and main bearings (Boundy 2012). As this application is similar, the fit was considered suitable. As the length of the bearing is 16 mm and the diameter of the pin is 29.37 mm, the L/D bearing ratio is equal to 0.5448. Synthetic lubricant was applied to the bush during assembly to reduce friction.

MANUFACTURING PROCESSES

The profile of the connecting rods has been produced by laser cutting steel plate, and the holes for fitting the bearings have been machined to achieve the desired tolerance. The bronze bush was machined from LG2 bronze hollow bar, and both the bronze bush and roller bearings were press fit into the connecting rod.

5.2.7 Connecting air tube

DESIGN

A tube connecting the two cylinder spaces is required so that the air can travel between the hot and cold cylinders. Figure 5.11 shows the design of the connecting air tube. The larger cylindrical piece in the centre represents the regenerator, which is discussed in Section 5.2.8.

Figure 5.11: Connecting air tube solid model.

From the literature review, it was found that the volume of the regenerator and connecting air tube should be as small as possible in order to minimise dead volume within the engine (Martini 1983). This can be achieved by minimising the internal diameter the tube. Making the cross-sectional area smaller will have a negative side effect however, in that the pressure loss will increase due to the increased resistance against the flow of the working gas (Abdullah et al. 2005). Therefore, a balance must be found between the two. A flexible tube is often used to allow for ease of manufacture and assembly, however for this application it was decided that this may not be appropriate due to the high temperatures present. The tube must be able to withstand the pressures within the engine and provide adequate sealing to avoid air loss from the working space.

The design of the connecting air tube utilises zinc plated steel tube with is used in high pressure hydraulic applications. The tube can be bent to the desired shape and standard hydraulic fittings can be utilised to connect the tube to the cylinders. These fittings are rated for high pressure hydraulic fluid so they have good sealing properties and are readily available. The chosen tube has an outside diameter of 12.7 mm and a wall thickness of 1.22 mm. The designated fittings on each end of the tube are 3/8" BSPT male to suit the tapped holes in the cylinders and the approximate dead volume contained within the connecting air tube is 80.54 cm^3. This was found by multiplying the internal cross-sectional area of the tube by the swept length and adding the internal volume of the socket which holds the regenerator material.

MATERIALS

As mentioned, flexible hose is often used for the connecting air tube. Steel is also commonly used due to its high strength properties. Hydraulic hose was also considered for the design, however the high design temperatures of this engine were outside of the working range of most typical hoses. By using hydraulic tube, JIC and BSPT threaded fittings could be utilised for connecting components to provide a tight seal.

STRESS ANALYSIS

According to Pirtek (2021), hydraulic tube with an outside diameter of 12.7 mm and a wall thickness of 1.22 mm has a working pressure of 24.8 MPa and a burst pressure of 74.4 MPa. Therefore, with respect to the working pressure there is a safety factor of 16.4 when considering the maximum pressure expected within the engine. Therefore, there is adequate safety with this tube size in terms of stress.

MANUFACTURING PROCESSES

The tube has been bent into the desired shape using a hand bender. Tube nuts and sleeves have been fitted to the tube ends for connecting by threaded fittings after flaring the ends according to standard specifications.

5.2.8 Regenerator

DESIGN

The regenerator has been made from a steel socket with fittings each end which connect to the connecting air tube. The socket is filled with copper mesh to withdraw heat from the air as it flows out of the cylinder and return the heat as the air flows back into the hot cylinder from the cold cylinder. The socket was incorporated so that the mesh is retained in this position and does not travel through the tube or into either of the cylinders. Figure 5.11 shows the size and location of the regenerator.

As found in the literature review, the regenerator is often made from a wire mesh screen or metal felt. Essentially the regenerator is a heat exchanger and there is a trade-off between heat transfer and pressure loss which results from forcing the air through the material (Abdullah et al. 2005). A decrease in the porosity of the material increases the regenerator effectiveness, but also increases the pressure drop which is undesirable.

For the regenerator material, a copper scourer has been utilised as shown in Figure 5.12. This is essentially a copper wire mesh which has been placed inside the socket in the centre of the connecting air tube. Determining the optimum porosity for this application was considered outside the scope of this

project and could be found for future work. The amount of mesh placed inside the socket was adjusted to ensure that air could still easily flow through the material.

Figure 5.12: Copper scourer utilised for the regenerator matrix.

MATERIALS

As outlined in the literature review, a high thermal conductivity is desirable for the regenerator material as the heat transfer between the working gas and the matrix will be increased (Rutczyk, Szczygiel & Kabaj 2020). According to Juvinall & Marshek (2012), carbon steel has a thermal conductivity of 47 W/m.°C while copper has a thermal conductivity of 381 W/m.°C. Therefore, the thermal conductivity of copper is significantly larger than that of carbon steel. Furthermore, the heat capacity of a material is another factor which should be considered. Bapat et al. (2011) analysed phosphor bronze, copper and stainless steel and determined that phosphor bronze effectiveness can achieve high effectiveness due to its high heat capacity, while copper is better than stainless steel. Although copper is more effective than stainless steel in terms of heat transfer, it is more likely to soften under high temperatures. Copper has been chosen for the regenerator material in this design as it will provides effective heat transfer properties and offers a good balance in terms of durability and heat capacity. The porosity and amount of mesh are other considerations which could be investigated in more detail as further work.

STRESS ANALYSIS

A steel socket with the same pressure rating as the hydraulic tube has been selected for the design to ensure it can hold the internal pressure without failing.

MANUFACTURING PROCESSES

As mentioned, a piece of copper mesh was removed from the scourer and pushed inside the steel socket. Fittings were screwed onto each to retain the mesh within the socket.

5.2.9 Crank mechanism

DESIGN

In designing the crank mechanism, various factors were taken into account and all components were checked for stress to ensure the safety of the design. The complete crank assembly is shown in Figures 5.13, 5.14 and 5.15.

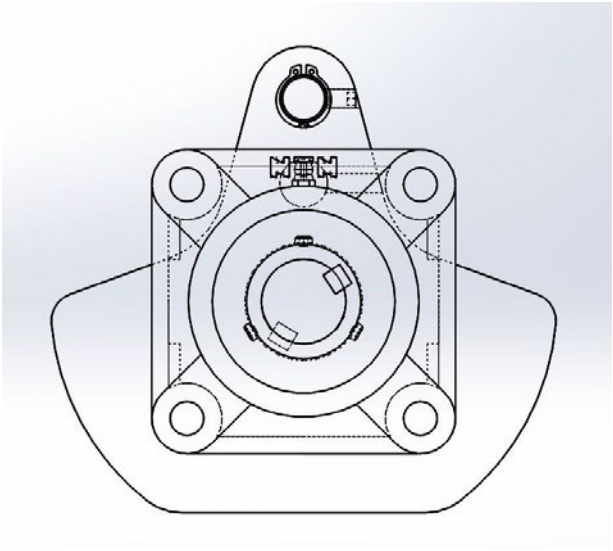

Figure 5.13: End view of the crank assembly.

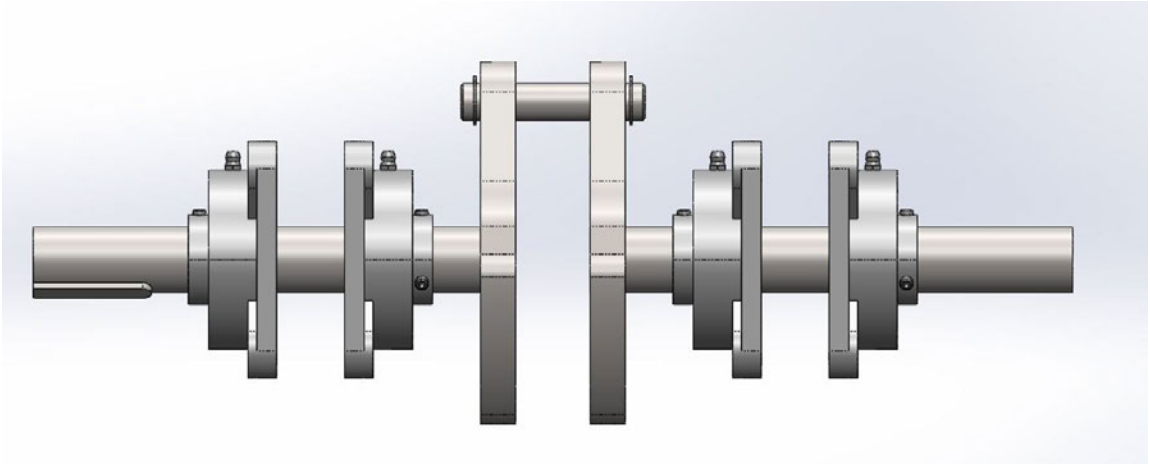

Figure 5.14: Side view of the crank assembly with bearing plates hidden.

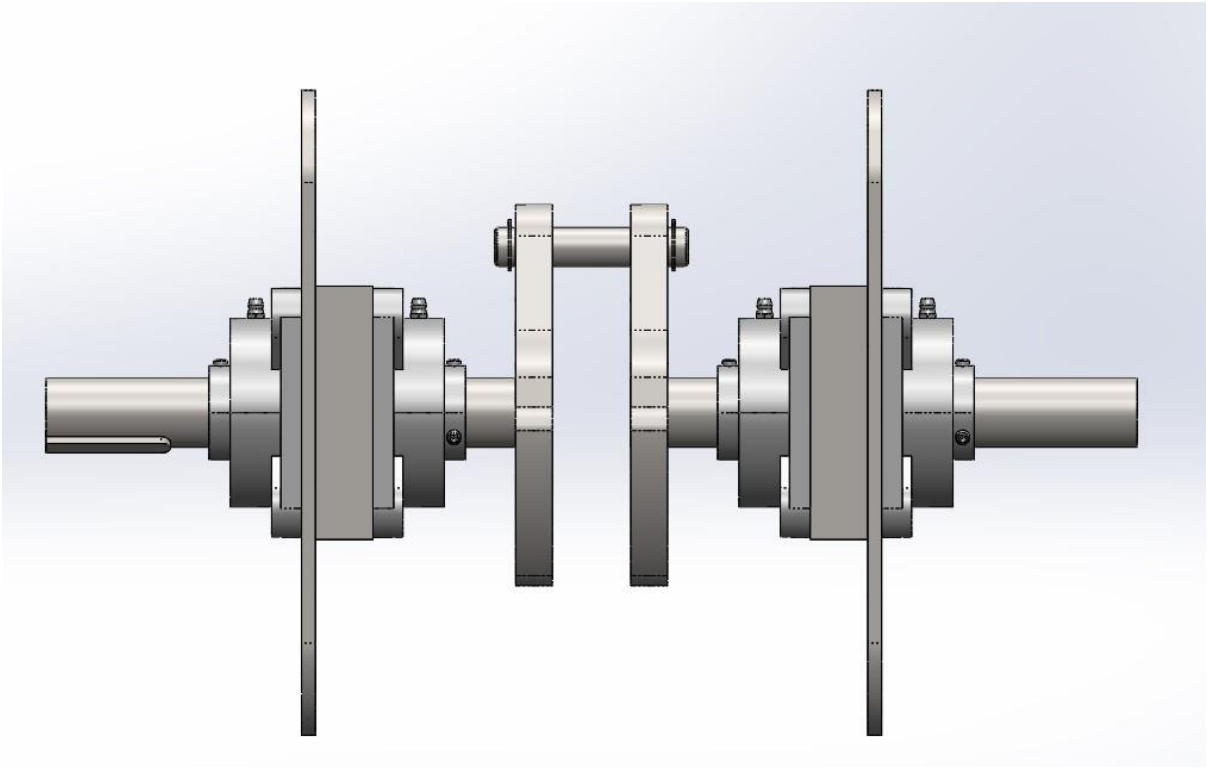

Figure 5.15: Side view of the crank assembly with bearing plates shown.

The crank shafts are supported by bearings which are bolted onto bearing plates as shown in Figure 5.16. The bearing plates are then bolted onto the engine body for support.

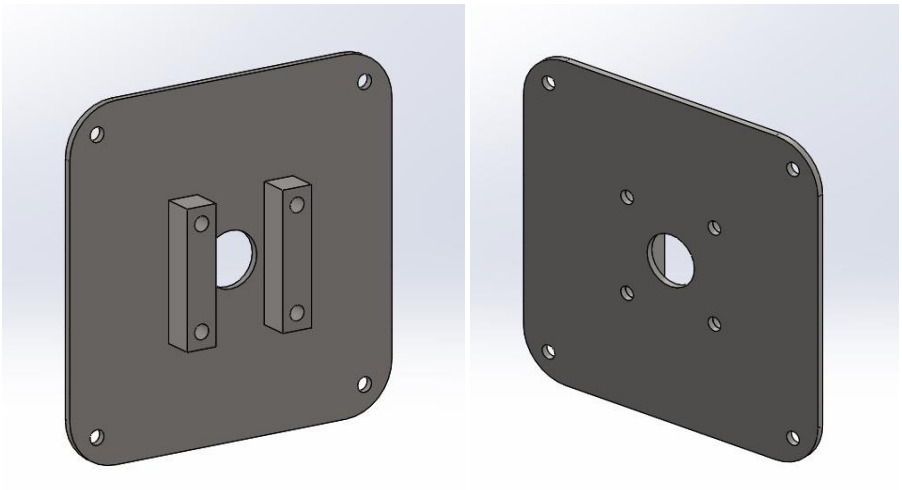

Figure 5.16: Bearing plate weldment solid body.

The purpose of the crank train is ultimately to produce output work by converting the linear motion of the pistons to rotary motion at the output shaft (Hoag & Dondlinger 2016). Typically, the material used is steel in IC engines and both journal and rolling element bearings are used depending on the application, and a key challenge is the assembly of components to the desired tolerance (Hoag & Dondlinger 2016). The diameter of the shafts used in the crank train must be sized to handle the loads

imposed by the connecting rods and suitable bearings must be chosen to minimise friction (He 2016). Furthermore, angular play in the connecting rod should be minimised (He 2016).

In the alpha Stirling engine configuration with a phase angle of 90 degrees, both connecting rods are connected to the crank mechanism at the same position (Egas & Clucas 2018). As shown in Table 4.2, the crank radius dimension for both pistons is equal to 7.2 cm. This means that the pivot point at the crank end of the connecting rods must be 7.2 cm from the centre of the output shaft. As the pistons move linearly within the cylinders, rotational motion occurs at the crank pin which turns the crank and produces output torque at some rotational speed.

In designing the crank slider mechanism, ease of assembly was a constant consideration as outlined in Hoag & Dondlinger (2016). The connecting rods need to be assembled and disassembled from the crank pin and the output shafts must be supported with bearings, as well as be easily assembled and disassembled from the engine body. It was decided to make the crank an assembly made up of components which could be assembled in position to ensure alignment of parts and the possibility of adjustment if necessary.

In order to position the crank pin offset from the centre of the output shafts, it was pinned through two steel plates which are welded to the output shafts. Therefore, the power is transmitted from the crank pin to the crank plates and to the output shafts through the welds. The output shaft which has the flywheel fitted is essentially an idler shaft as its only purpose is to transmit energy to the flywheel. The shaft which extends out the other end of the engine body is the output shaft which drives some external machine or device depending on the application. Keyways are used to transmit power through the shafts to some component such as a pulley or coupling. Insert bearings are utilised as they self-aligning and provide a high load capacity. As shown in Figure 5.13, two holes are drilled in the crank plates for fitting the crank pin. As will be discussed in Chapter 6, this was so that the engine could be tested with a shorter crank radius and subsequently shorter stroke. This is also shown in the drawings contained in Appendices C and D.

The crank pin has external circlips on the outside of the crank plates to retain it in position. Tapped holes have been made in the crank plates for grub screws which stop the pin from rotating in operation as this may wear out the hole in the plates and create slack. The crank plates have more material on the opposite side of the crank pin to act as a counterweight. Although the shafts are connected through the crank pin, two bearings are used to support each shaft to increase stability of the assembly and minimise flexing during operation. Square bar with side dimensions of 25 mm is welded on the back of the bearing plate to increase the distance between the centre of the bearings. Between the connecting rods and the crank plates, bronze shims were fitted to minimise sliding friction between the steel components.

MATERIALS

All components are made from steel as this is readily available, has good strength properties and is relatively inexpensive. The material selected for the shafts is 1045 steel round bar as it is machinable, can be welded and has good strength. Furthermore, connection to other power transmission components with the use of a keyway is typical and can be easily achieved using this material. The crank plates are laser cut from 16 mm Grade 350 steel plate to ensure sufficient strength. The crank pin is made from 4140 steel as it is a highly stressed component. Due to space restrictions, the diameter of the pin was made relatively small and after checking the stress the high tensile 4140 material was selected.

STRESS ANALYSIS

There are several areas of consideration in terms of stress.

- Shear and bending stresses in crank pin
- Shear and bending stresses in output shaft
- Shear stress in bolts
- Load capacity of bearings
- Bending stress in crank plate

The stresses in the crank plates have been determined using FEA as the geometry and loading is more complicated. The stresses in the crank pin and the output shaft have been calculated by hand and checked with FEA, while the stress in the bolts and load capacity of the bearings are checked by hand only.

To assess the stress in the crank pin, a conservative assumption has been made. It is assumed that the maximum force is acting in both of the connecting rods at the same time and in the same direction. This is the maximum possible force that the pin can be subject to and therefore the maximum stress that can occur. While the actual loading case is more complicated than this, it will be assumed safe if the stress is not too high for this analysis. Figure 5.17 shows the free body diagram of the pin where F represents the force of the connecting rod and R represents the reaction force of the crank plates. For the analysis, the supports will be treated as fixed ends and the forces will be treated as point loads. For the analysis, $F = R = 9\ 375.3$ N as calculated in (5.2).

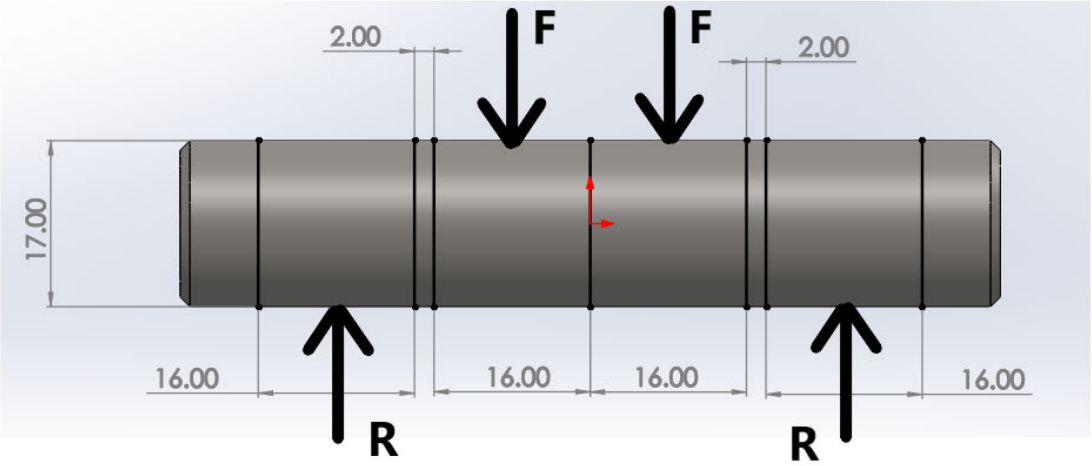

Figure 5.17: Free body diagram of crank pin. Dimensions are in mm.

Using standard beam formulae given in Juvinall & Marshek (2012), the maximum bending moment is found to act where the support begins on each of the pin. The bending moment here was found using (5.17).

$$M = \frac{Fa^2b}{L^2} + \frac{Fab^2}{L^2} \tag{5.17}$$

Where M is bending moment (Nm)

F is the force as shown in Figure 5.17 (9375.3 N)

a is the distance from the left support to the centre of the left force (0.010 m)

b is the distance from the right support to the centre of the left force (0.026 m)

L is the distance between the supports (0.036 m)

After substituting the above values into (5.17), the maximum bending moment was found to be 67.711 Nm. The normal stress which results from this bending moment is calculated using the bending stress equation as shown in (5.18).

$$\sigma = \frac{Mc}{I} = \frac{67.711 \times 0.0085}{\frac{\pi \times 0.017^4}{64}} = 140.38MPa \tag{5.18}$$

Where c is the radius of the pin (0.0085 m)

I is the moment of inertia of the circular section (m^4)

The maximum internal shear force also acts right next to the support at each end and is equal to F by geometry. The shear stress is calculated as shown in (5.19).

$$\tau = \frac{V}{A} = \frac{9375.3}{\frac{\pi \times 0.017^2}{4}} = 41.305MPa \tag{5.19}$$

The von mises equivalent stress at this location can be calculated using (5.20) as given in Juvinall & Marshek (2012).

$$\sigma_{vm} = \sqrt{\sigma_x{}^2 + 3\tau_{xy}{}^2} \tag{5.20}$$

The von mises equivalent stress was found to be 157.56 MPa as shown in (5.21).

$$\sigma_{vm} = \sqrt{\sigma_x{}^2 + 3\tau_{xy}{}^2} = \sqrt{140.38^2 + 3 \times 41.305^2} = 157.56MPa \tag{5.21}$$

According to Juvinall & Marshek (2012), the yield strength of normalized 4140 steel is 655 MPa. Therefore, the safety factor is 4.16. This component should be checked for fatigue as there will be cyclical stresses acting, however for the purposes of this prototype it is considered safe.

To check the stress in the four M12 Grade 8.8 bolts which connect the bearing plates to the engine body, it will be assumed that the maximum load is evenly distributed between the two and therefore a total force of 9 375.3 N is evenly distributed over the four bolts. The shear stress is calculated to be 27.803 MPa as shown in (5.22), which represents a safety factor of 23.74 given that the yield strength of a Grade 8.8 bolt is 660 MPa. The stress area of an M12 bolt is 84.3 mm^2 as given by Juvinall & Marshek (2012).

$$\tau = \frac{F}{4A} = \frac{9375.3}{4 \times 84.3} = 27.803MPa \tag{5.22}$$

The UC206 bearings selected for the design have a dynamic load rating of 21.6 kN (NTN Corporation, 2021). Figure 5.18 shows the free body diagram of the output shaft, however it should be noted that depending on the driven equipment there will likely be another force on the outer end of the shaft. The distance L_1 between F and R1 is equal to 49 mm, while the distance from R1 to R2 is 73 mm. Therefore, it can be shown by summation of moments that the maximum reaction force acts at R1 and is equal to 15.668 kN as shown in (5.23).

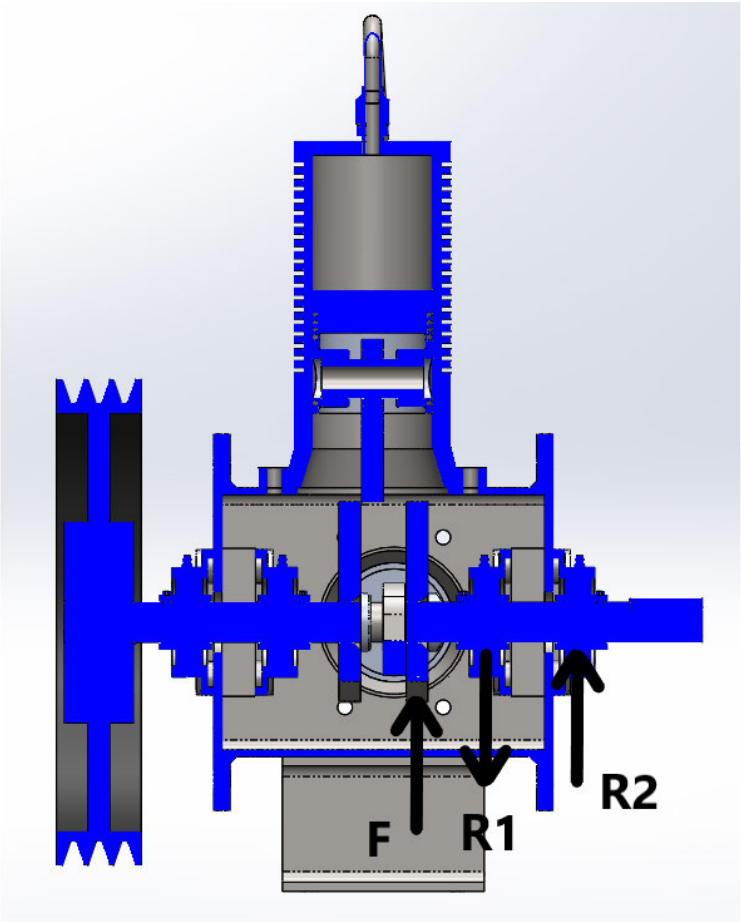

Figure 5.18: Cross section of engine assembly with forces shown.

$$R1 = \frac{F(L_1 + L_2)}{L_2} = \frac{9375.3(49+73)}{73} = 15668N \tag{5.23}$$

As the dynamic load capacity is higher than the maximum reaction force of 15.668 kN at R1, the bearings are considered suitable.

To assess the stress in the output shaft, the torque and bending moment resulting from the load applied to the crank plate by the connecting rod needs to be determined. It is assumed that the bearing supports allow rotation as self-aligning bearings are used, and the design material for the shaft is 30 mm diameter 1045 round steel bar.

By constructing a bending moment diagram for the load case in Figure 5.18, it can be seen that the maximum bending moment occurs at R1 and is equal to F multiplied by the centre distance between the load and the bearing support. Therefore, the maximum bending moment is equal to 459.39 Nm as shown in (5.24).

$$M_{\max} = Fd = 9375.3 \times 0.049 = 459.39 Nm \tag{5.24}$$

Where M_{max} is the maximum bending moment in the output shaft (Nm)

d is the centre distance between the applied force and the bearing support (m)

The bending stress at this point is calculated to be 173.31 MPa as shown in (5.25).

$$\sigma = \frac{Mc}{I} = \frac{459.39 \times 0.015}{\frac{\pi \times 0.030^4}{64}} = 173.31 MPa \tag{5.25}$$

The maximum shear stress is found by considering both the applied torque and force. The torque can be calculated using the relationship in (5.26). The P-V power is used as it predicted the highest power values and therefore will give the most conservative results for the stress analysis.

$$L_{S,PV} = Tn \tag{5.26}$$

Where T is torque (Nm)

n is rotational speed (rad/s)

The maximum torque was found to occur at the maximum design temperature of 1 100° C where the P-V power is 4 348.38 W and the rotational speed is 52.075 rad/s. Therefore, the maximum torque is calculated to be 83.502 Nm as shown in (5.27).

$$T = \frac{L_{S,PV}}{n} = 83.502 Nm \tag{5.27}$$

The shear stress which develops as a result of the applied force and torque was calculated to be 29.014 MPa using (5.28) as given in Juvinall & Marshek (2012) and the standard formula for shear stress resulting from the applied load, and which acts over the cross-sectional area of the shaft.

$$\tau = \frac{16T}{\pi d^3} + \frac{F}{A} = \frac{16 \times 83.502}{\pi \times 0.030^3} + \frac{9375.3}{\frac{\pi \times 0.030^2}{4}} = 29.014 MPa \tag{5.28}$$

Where τ is shear stress (Pa)

d is the outside diameter of the shaft (m)

Using the results from (5.27) and (5.28), the maximum von mises stress can be calculated using (5.21) and is shown to be 180.45 MPa in (5.29).

$$\sigma_{vm} = \sqrt{\sigma_x^{\ 2} + 3\tau_{xy}^{\ 2}} = \sqrt{173.31^2 + 3 \times 29.014^2} = 180.45 MPa \quad (5.29)$$

As the yield strength of the material is 414 MPa, the safety factor for the output shaft is 2.29. This safety factor is considered safe for the prototype as the shaft is unlikely to fail at this safety factor, however if fatigue were to be considered the shaft size and material may be insufficient. To increase the safety factor, a larger diameter shaft could be used or a stronger material such as 4140 steel.

MANUFACTURING PROCESSES

Multiple manufacturing processes are required to produce the crank mechanism components and assembly. The crank pin has been turned to size from 19.05 mm diameter 4140 steel round bar and circlip grooves have been machined on a lathe. The crank plates were laser cut from 16mm Grade 350 steel plate and the hole for fitting the crank pin was subsequently machined to achieve the required tolerance. To ensure that the axes of the two shafts were aligned after assembly, the crank plates were held back-to-back and drilled simultaneously. The two shafts were initially welded to the plates as one piece and parted after welding and drilling of the crank plates. The shafts were then welded to the back of the crank plates where a chamfer had been machined in the plate before the shaft had been welded on the outside.

The 25 x 25 mm steel square bar was welded to the bearings plates which had been laser cut from 5 mm Grade 250 steel plate. Keyways were cut in the output shafts using a milling machine. Tapped holes were made in the crank plates so that grub screws could be fitted to stop rotation of the crank pin during operation. The output shafts are locked to the insert bearings by way of grub screws which are already fitted to the bearings.

5.2.10 Flywheel

DESIGN

As determined in the literature review, a flywheel is required in a Stirling engine to rotate the crank through the transfer strokes where no power is generated by the engine (Martini 1983). During the power stroke of the hot piston, energy is absorbed by the flywheel in the form of rotational motion and

is given back to the system as momentum. The energy stored in a flywheel is given by (5.30) (Hoag & Dondlinger 2016).

$$E = \frac{I\omega^2}{2} \tag{5.30}$$

Where E is the energy stored in the flywheel (Joules)

I is the polar moment of inertia (kg.m^2)

ω is the rotational velocity (rad/s)

For ease of manufacture, a v-belt pulley which was readily available was utilised as the engine flywheel. The pulley is an SPB 3-groove 355mm pitch diameter v-belt pulley made of cast iron, with a 3020-30 mm taper lock bush to lock onto the shaft. As the geometry of the pulley is somewhat complex, it was modelled in SolidWorks to determine the polar moment of inertia. As shown in Figure 5.19 the polar moment of inertia about the z-axis (its axis of rotation) is 0.334879 kg.m^2. The pulley has a mass of 20.8 kg with the taper lock bush included.

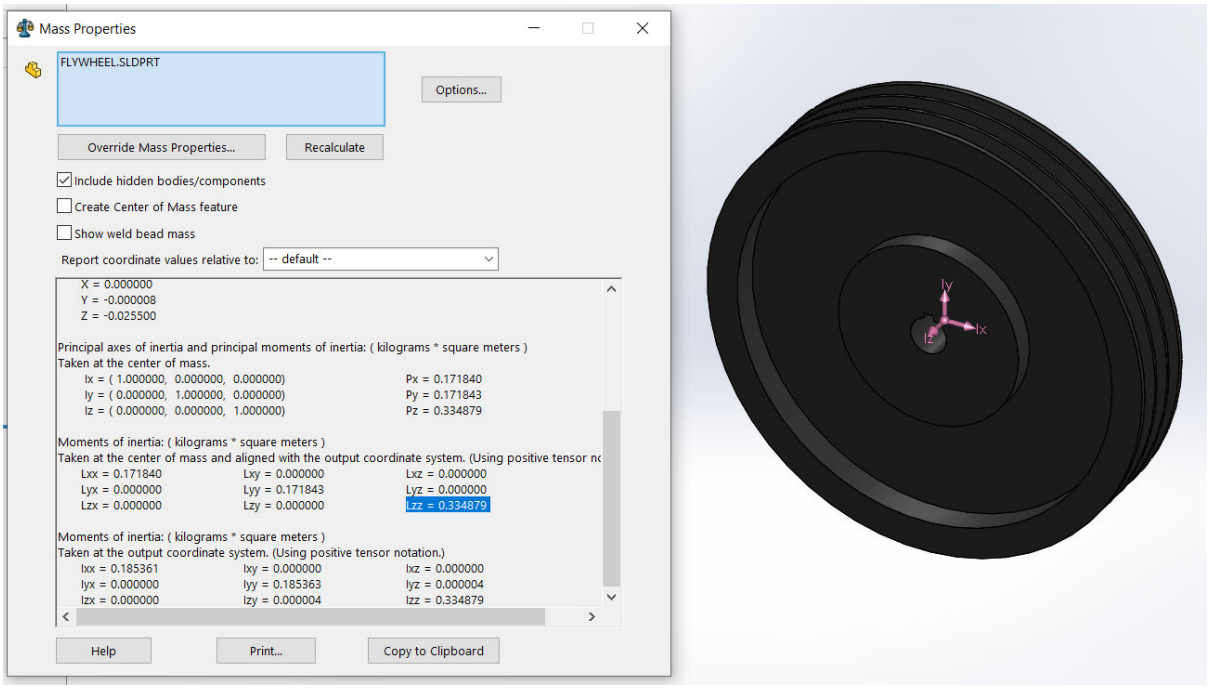

Figure 5.19: Solid model of pulley produced in SolidWorks with polar moment of inertia shown.

Table 5.1 shows the energy stored in the flywheel at the various rotational speeds calculated in Section 4 and shown in Table 4.7.

Table 5.1: Flywheel stored in energy at various rotational speeds.

Th (° C)	n (rev/s)	n (rad/s)	E (J)
500	6.538	41.079	282.56
600	6.880	43.228	312.89
700	7.205	45.270	343.15
800	7.515	47.218	373.32
900	7.811	49.078	403.30
1000	8.097	50.875	433.38
1100	8.288	52.075	454.06

MATERIALS

As stated previously, the pulley is made of cast iron and has a mass of approximately 20.8 kg. A larger polar moment of inertia is desirable in a flywheel as more momentum exists which can be imparted to the system, however more energy is required to continue rotating the flywheel.

STRESS ANALYSIS

There is no stress acting on the flywheel as no torque is developed in the body.

MANUFACTURING PROCESSES

The taper lock bush is utilised the lock the pulley onto the shaft. This requires a keyway and tightening of socket screws, however no other manufacturing processes are required.

5.2.11 Heater

DESIGN

Ideally, a heater is fitted to the hot cylinder to maximise the transfer of heat energy from the heat source into the working gas. The heater is essentially a heat exchanger, and the goal is to maximise heat transfer while minimising the amount of dead volume which reduces the power output of the engine. Figure 5.20 shows an image of the heater design.

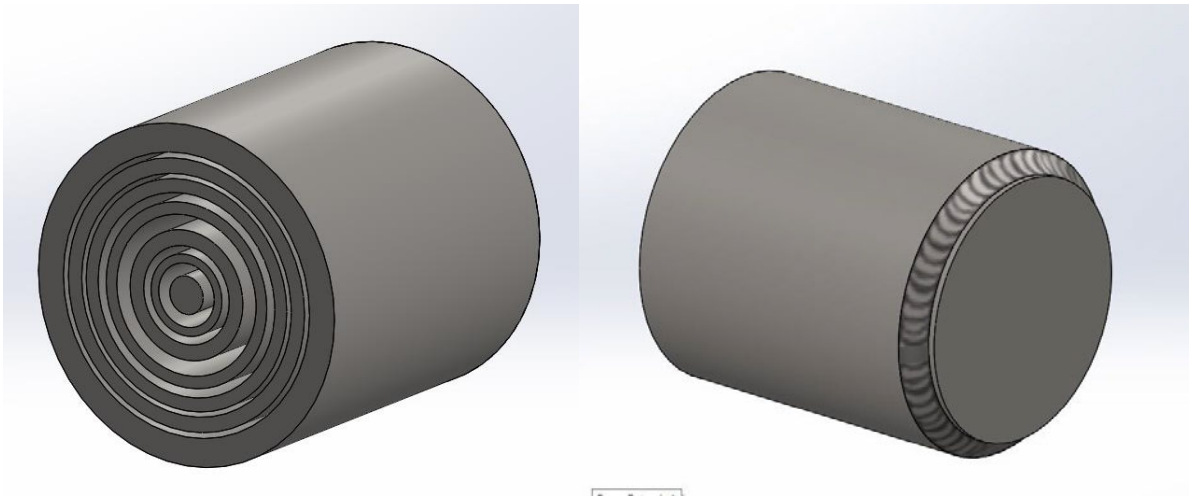

Figure 5.20: Heater head solid model.

As discussed, the heater is made out of a 3" NPT steel barrel nipple which has a male thread on one end to screw into the 3" NPT female socket which is welded into the hot cylinder. In designing the heater, the material selection and geometry is important to achieve effective heat exchanger properties (Rinker 2018). To achieve this, the surface area for heat transfer within the engine has been maximised by welding a series of concentric steel pipes onto a steel base plate. Therefore, when the base plate is heated, the heat energy will be conducted into the pipes and transferred to the working gas by convection. Furthermore, the close sizing of the pipes creates minimal dead volume inside the heater.

The internal surface area of the heater is 1 592.6 cm^2 while the internal dead volume created is 167.63 cm^3.

MATERIALS

All components used in the fabrication of the heater are made of steel. As the heat source will be directly applied to this component, it must be able to withstand the high temperatures and have good thermal conductivity to transfer the energy into the working gas. There are other materials which have better thermal conductivity than steel, however they are more expensive, more difficult to fabricate and not as readily available as steel. Also, materials such as copper do have a better thermal conductivity, but their melting point is lower than steel and so may not be suitable (Juvinall & Marshek 2012).

STRESS ANALYSIS

The heater will be subject to the same internal pressure as the cylinders and air connecting pipe. According to Valves Tubes Fittings (2022), the 3" NPT Sch 80 steel barrel nipple is rated to a pressure of 3000 psi, which equates to 20.68 MPa. This represents a safety factor of 13.7 when compared to the maximum internal pressure of 1.5104 MPa, which is considered safe for the design.

The end plate of the heater head which is welded to the barrel nipple can be analysed as a fixed round disc in a similar fashion to the end wall of the cold cylinder. Using (5.11), the normal stress is calculated to be 34.972 MPa as shown in (5.31). In this case, the thickness of the plate is 8 mm. This represents a safety factor of 11.8 as 1045 steel has been specified for the base plate.

$$\sigma_m = \frac{3pr^2}{4t^2} = \frac{3\times 1510.4\times 10^3 \times 0.04445^2}{4\times 0.008^2} = 34.972 MPa \tag{5.31}$$

MANUFACTURING PROCESSES

All pipes have been cut to length and subsequently welded to the base plate. The steel base plate was made by machining a disc from 1045 round steel bar for improved durability when exposed to the heat source.

5.2.12 Cooler

DESIGN

As discussed in Section 5.2.4, there is no cooler to be fitted to the cold cylinder as grooves have been machined in the cylinder walls to represent fins. To improve the cooling of the air in this cylinder, cool air or water could be forced to flow over the cylinder during operation to improve the convection of heat out of the air.

5.3 Cost, Safety, Fatigue and Design Life

COST

As this project is a prototype, cost was not the main consideration in designing the engine. However, for any engineering product to find success in the market it must be economically viable. The overall design was made as simple as possible with only the critical components included in the fabrication. If the engine was to be produced for industry, consideration would need to be given to making the cost as low as possible to provide value for money. As outlined in Chapter 2, the typical cost per kilowatt for Stirling Engine ranges from $500 USD to $4,600 USD per kilowatt (Thimsen, 2002). Given that the power target for this engine is 750 – 1 000 W, it should ideally cost somewhere in this range.

The total cost of the engine was found and can be broken down into materials and labour. The cost of materials was approximately $1,845 AUD and 20 hours of tradesman labour was required for welding and machining. Therefore, assuming a tradesman rate of $100 per hour, the total cost of the engine was approximately $3,845 AUD. However, the student also spent quite a lot of time assembling and disassembling the engine for the various tests. Given that this was a prototype, mass production would likely be able to reduce this figure significantly.

SAFETY

Safety is a critical consideration for any engineering device as engineers have a legal and ethical responsibility to produce designs that will not cause harm to any person or relevant stakeholder. A large safety factor has been incorporated into the design of all component with regards to stress for this purpose. The Risk Management Plan contained in Appendix A must be followed in any testing of the device to ensure that adequate personal protective equipment is worn and all safety measures are followed. The inspection window cover must be fitted at all times when testing the engine as the metal mesh which has been fitted is designed to prevent a person from being able to place any part of their body inside the crank case.

FATIGUE AND DESIGN LIFE

Wessels (2010) defines two approaches to design analysis: the safety factor approach; and the fatigue life approach. For the purposes of this project, the safety factor approach has been used as the stress analysis and FEA has considered a single maximum stress applied to each component which has then been compared to the yield strength of the material. This approach was chosen because the engine is a prototype and will not be required to operate continuously for many years, and as such as long as the yield strength of the material is significantly higher than the stress applied the design is considered safe.

For the purposes of a product which is to be released to the market, the fatigue life approach must be considered. Juvinall and Marshek (2012) defines the fatigue strength of a material as “the intensity of reversed stress causing failure after a given number of cycles”. Furthermore, the endurance limit is the stress value at which the component will endure 10^6 or more cycles. As dynamic loading is present within the engine, the reversed loading acting on each component must be considered, and the endurance limit should be determined to check the long-term safety of the design. Furthermore, engineers must consider other important factors such as reliability, maintenance, noise and end-of-life disposal before the engine can be a commercially viable product (Wessels 2010).

5.4 Finite Element Analysis

A finite element analysis (FEA) was conducted on all critical components to check the stress values calculated in Section 5.2 and assess the safety of the design. The safety factor with respect to the yield strength of the material has been determined and assessed for safety. The maximum stress of 1 510.4 kPa is used in the analysis where pressure is concerned, and the maximum force of 9 375.3 N which acts on the piston is used where force is concerned.

5.4.1 Hot Cylinder

In the FEA of the hot cylinder, the heater head is included as it will induce a normal stress in the walls of the cylinder because of the axial force developing due to the pressure acting on the internal end face of the heater. As shown in Figure 5.21, the bolt holes in the cylinder are fixed and an internal pressure is applied to the inside bore of the cylinder, the ends of the pipes in the heater and the internal faces of the base plate between the welded pipes.

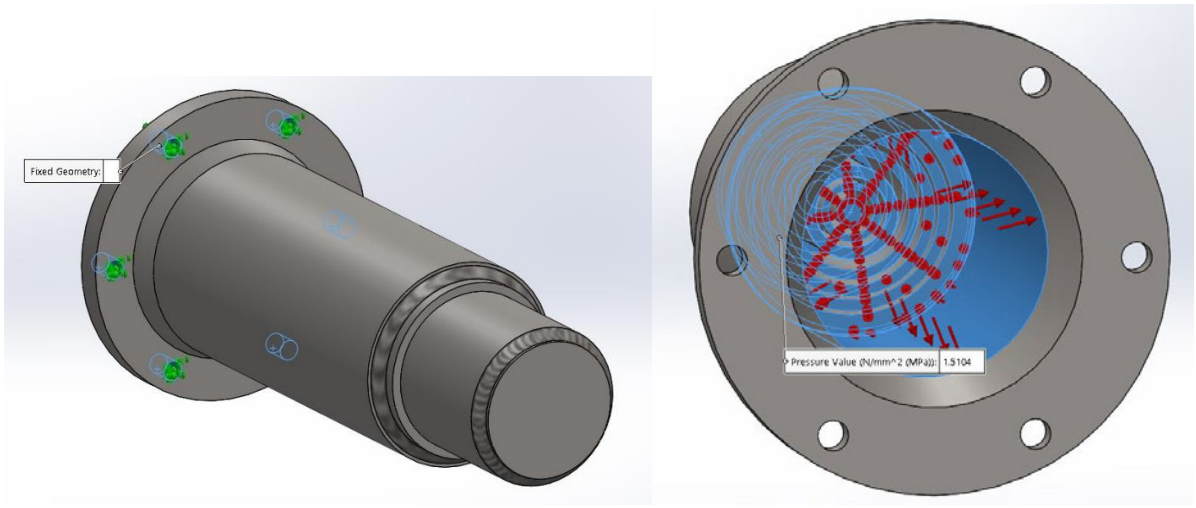

Figure 5.21: Hot cylinder fixed geometry and applied pressure.

A mesh control of 2.5 mm element size was applied to the welds to ensure a minimum of two elements across the width of the weld. The overall mesh was created with a maximum and minimum element size of 4 mm and a 1.2 mm respectively. Figure 5.22 shows the application of the mesh control and the final mesh.

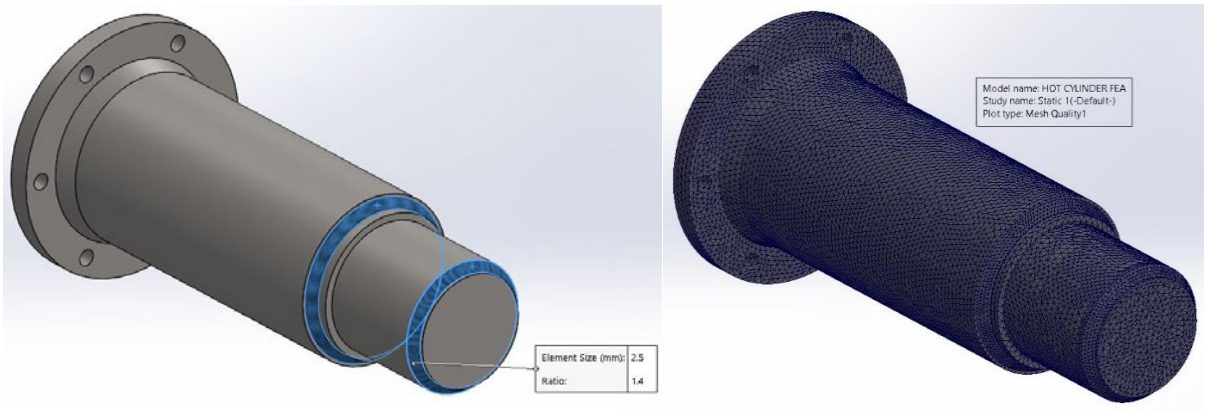

Figure 5.22: Hot cylinder mesh control and final mesh.

Figure 5.23 shows the von mises stress plot and a probe of the stress on the internal face of the cylinder bore. It can be seen that the maximum stress of 31.2 MPa occurs at the bolt holes, however this is unlikely as the fixed geometry at the bolt holes is an idealisation and the stress result here is likely because of the fixed edges. The stress on the base plate of the heater head is 13.7 MPa and therefore is well below the yield strength of 250 MPa for carbon steel. This is significantly lower than the calculated stress of 34.972 MPa found in (5.31). This is likely due to the welded pipes stiffening the plate and thus reducing the stress. The stress observed on the internal bore of the cylinder is approximately 6.64 MPa which is close to the calculated value of 8.17 MPa as shown in (5.7).

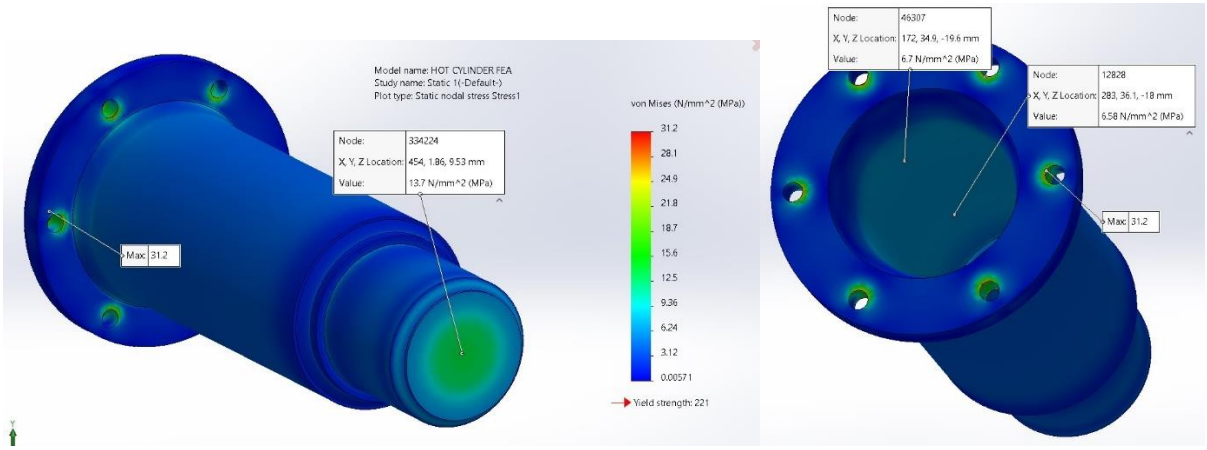

Figure 5.23: Hot cylinder von mises stress (MPa).

Figure 5.24 shows iso clipping of the stress at 10 MPa and 20 MPa. It can be seen that most of the stress above 10 MPa occurs in the end plate of the heater head and there is minimal stress above 20 MPa. This suggests that the stress concentrations at the bolt holes can be ignored, and in any case they are well below the yield strength of the material.

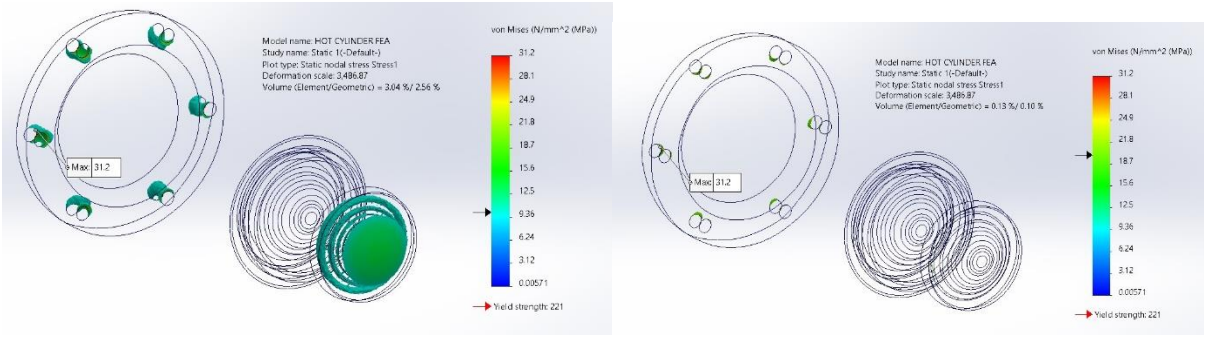

Figure 5.24: Hot cylinder iso clipping at 10 MPa (left) and 20 MPa (right).

5.4.2 Cold Cylinder

The FEA of the cold cylinder was carried out in a similar manner to the hot cylinder, with the tapped hole filled in to simulate the worst-case scenario in terms of axial force. The bolt holes were fixed and pressure applied to the internal surfaces as shown in Figure 5.25.

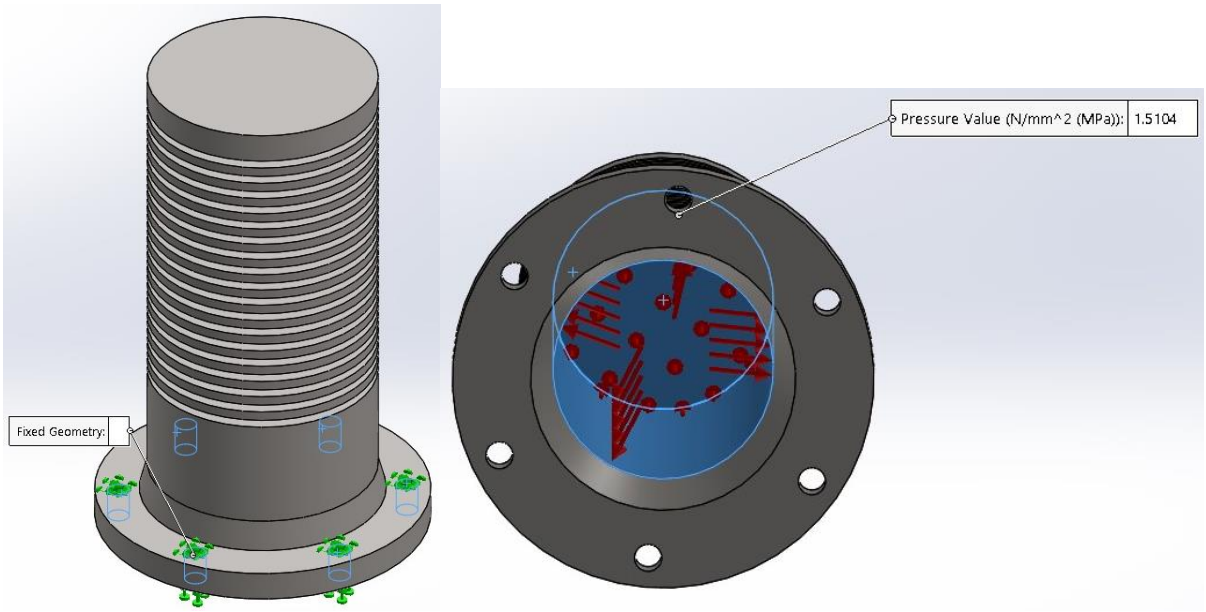

Figure 5.25: Cold cylinder fixed geometry and applied pressure.

No mesh control was required in this case as no welds are present. The mesh was produced with a maximum and minimum element size of 3 mm and 1.2 mm respectively. A smaller maximum element size was used to create a better-quality mesh in the fins. The final mesh and von mises stress plot are shown in Figure 5.26.

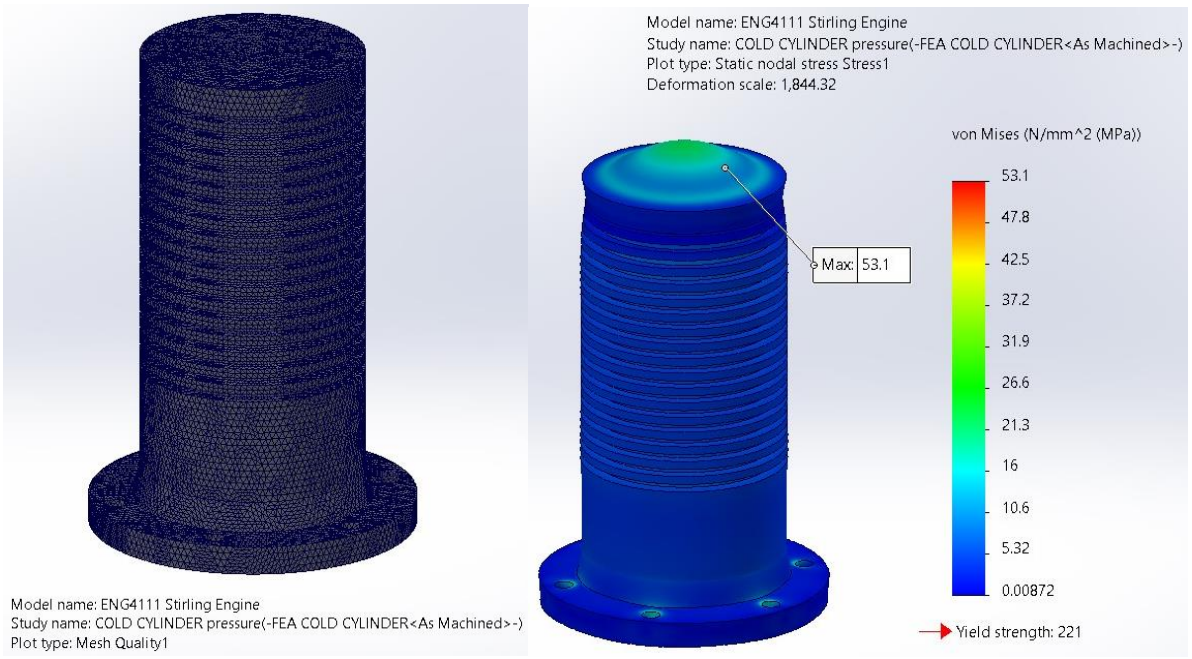

Figure 5.26: Cold cylinder final mesh and von mises stress plot (MPa).

The analysis suggests that the maximum stress of 53.1 MPa occurs at the edge of the cylinder end wall. However further inspection suggests that this is a stress singularity as shown in Figure 5.27, and the stresses in this region approximate 22.55 MPa. This seems more accurate as the calculated value of 22.38 MPa was found in (5.12). Probes taken from the inside bore of the cylinder suggest a von mises stress of approximately 8 MPa. This is significantly lower than the calculated values of 15.4 MPa shown in (5.9) and may be due to the fins present on the outside wall of the cylinder.

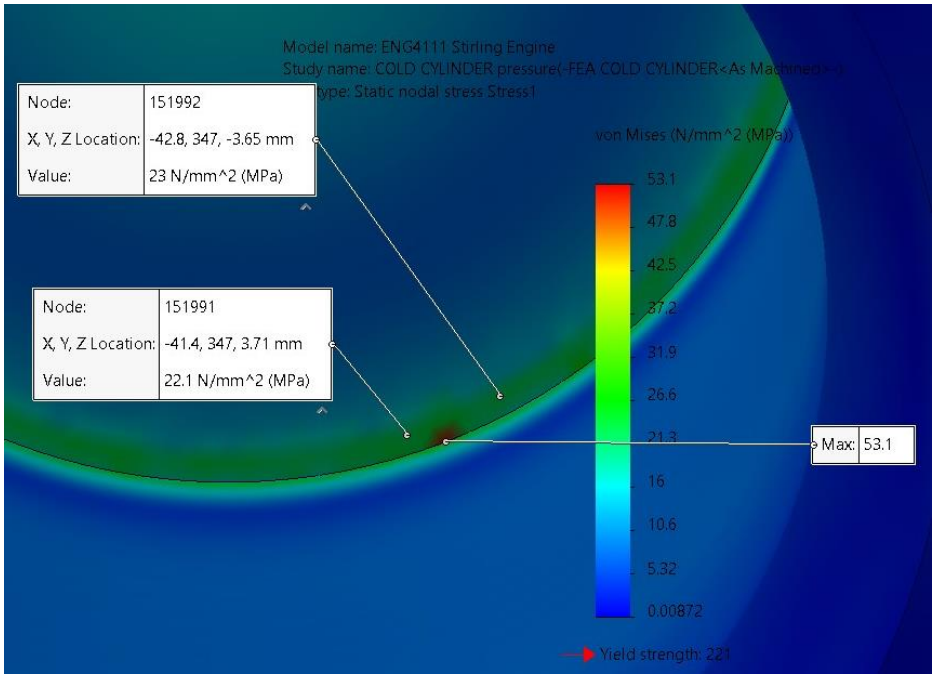

Figure 5.27: Von mises stress at edge of the cold cylinder end wall (MPa).

Figure 5.28 shows iso clipping of the stress at 10 MPa and 20 MPa. It can be seen that most of the stress above 10 MPa occurs in the end wall of the cylinder and there is minimal stress above 20 MPa. Again, the stress concentrations at the bolt holes can be ignored, and in any case they are still well below the yield strength of the material.

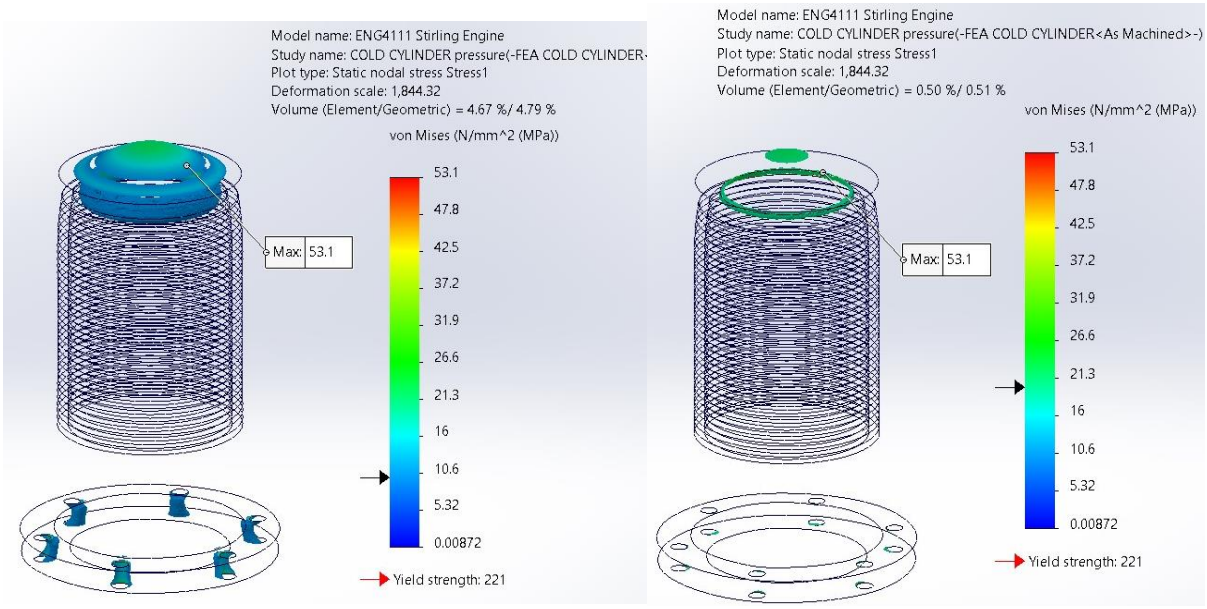

Figure 5.28: Cold cylinder iso clipping at 10 MPa (left) and 20 MPa (right).

5.4.3 Connecting Rod

The connecting rod was analysed assuming that a compressive force of 9 375.3 N is applied to the holes at each end. This is achieved by fixing the inside half of the larger hole and applying the force to the inside half of the smaller hole as shown in Figure 5.29.

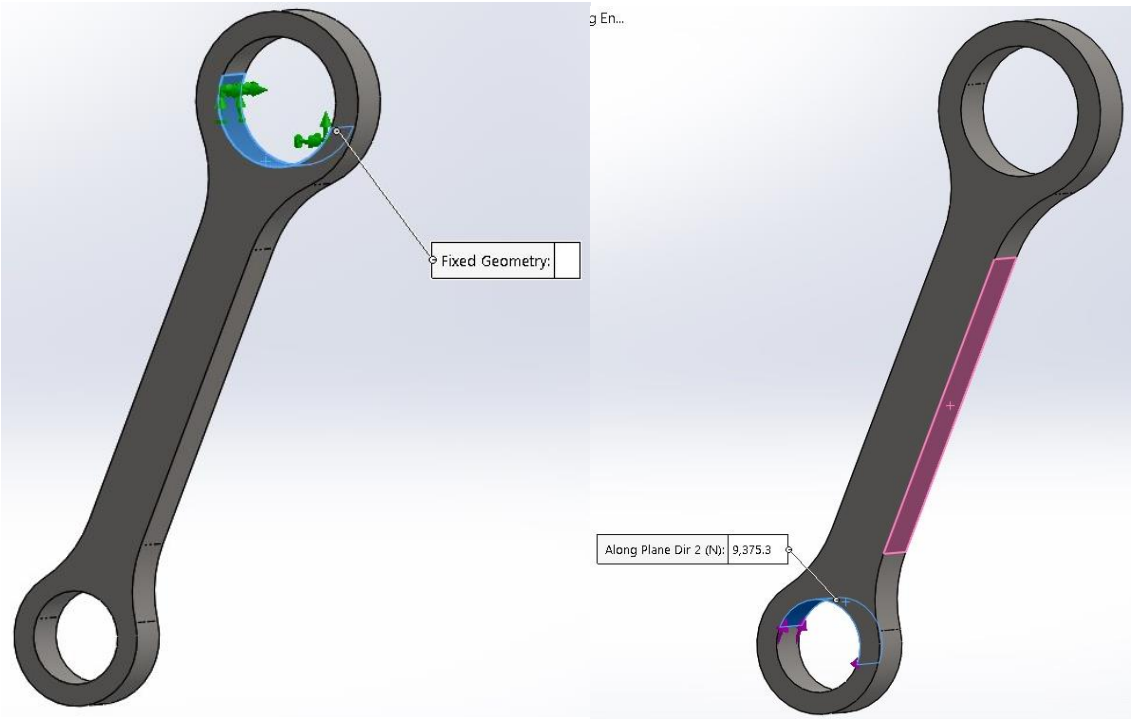

Figure 5.29: Load and fixed geometry in connecting rod analysis.

The mesh was produced with a maximum and minimum element size of 2 mm and 1 mm respectively as the part is quite small and therefore a fine mesh can be used without significant computational requirement. The meshed component is shown in Figure 5.30.

Figure 5.30: Meshed connecting rod for analysis.

Figure 5.31 shows the von mises stress plot for the connecting rod. It can be seen that the maximum stress of 48.6 MPa occurs at the transition from the main body to the hole where the bearings are fitted, and the nominal stress in the centre rectangular section is 29.3 MPa. This value exactly matches the compressive stress of 29.30 MPa found in (5.13). As Grade 350 plate with a yield strength of 350 MPa is used, the safety factor here with respect to the maximum stress of 48.6 MPa is 7.20. This is considered safe.

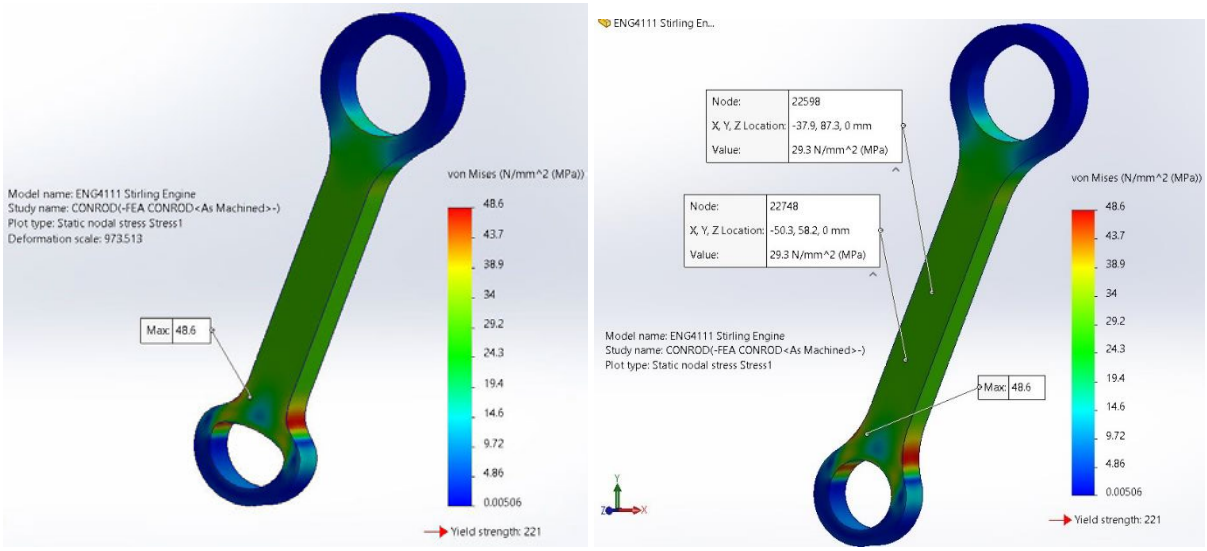

Figure 5.31: Von mises stress in connecting rod (MPa).

Figure 5.32 shows iso clipping of the stress at 25 MPa and 40 MPa. It can be seen that the body of the connecting rod and the transition to the smaller holes is stressed above 10 MPa, however there are only small areas at the radii around the hole which are stressed above 40 MPa. These stress values are well below the yield strength of the material and therefore considered safe.

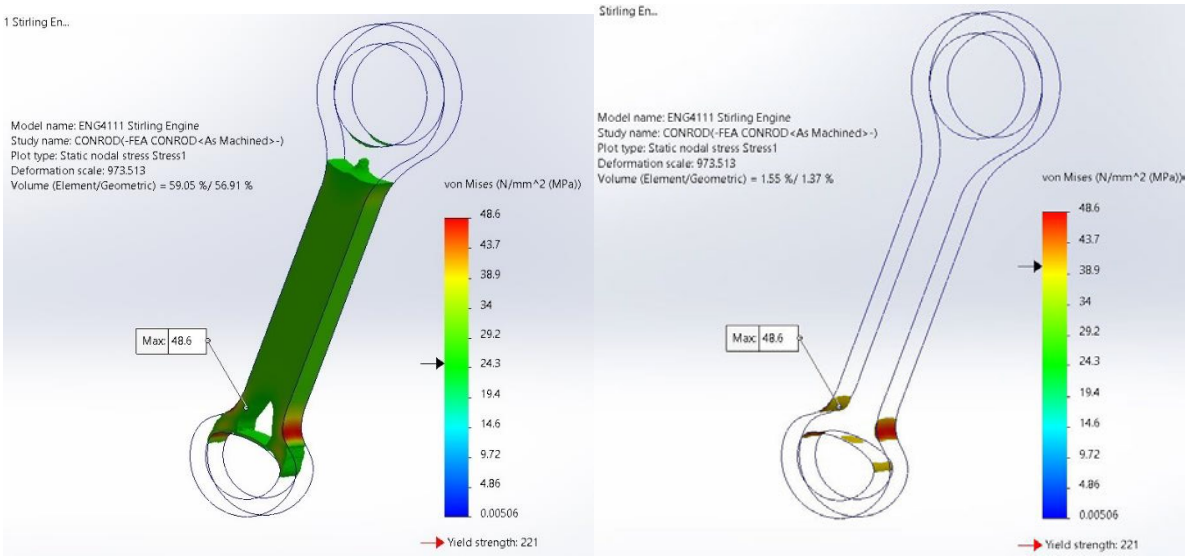

Figure 5.32: Connecting rod iso clipping at 25 MPa (left) and 40 MPa (right).

5.4.4 Crank Pin

Figure 5.33 shows the fixed geometry and applied loads on the crank pin. Here it is assumed that the pin is fixed axially and rotationally in the holes drilled in the crank plate. This is reasonable because the clearance between the pin and hole is small and grub screws are fitted to stop the pin from rotating. As discussed in Section 5.2.9, the worst-case scenario is assumed for analysing the stress in the pin. This is where the maximum force is applied by both connecting rods in the same direction. This will give a conservative estimate of stress.

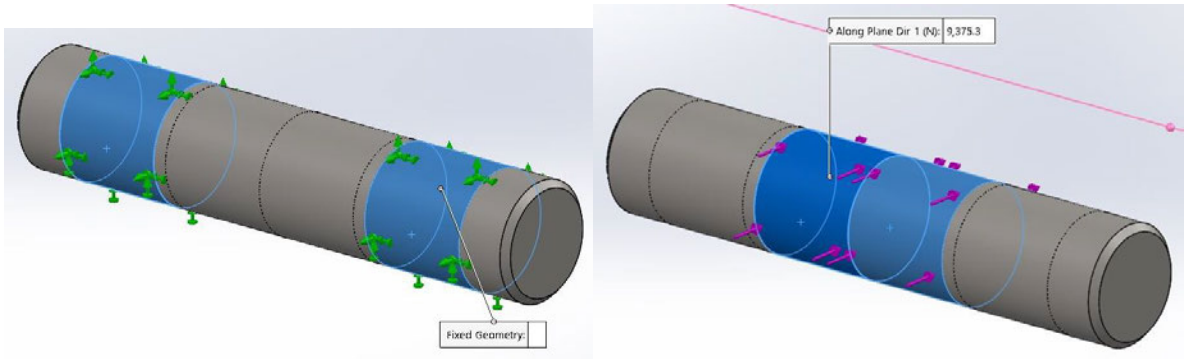

Figure 5.33: Fixed geometry and applied load on crank pin.

For producing the mesh, the maximum and minimum element sizes were 1.25 mm and 1 mm respectively. As the component is quite small, a very fine mesh could be utilised without a high computational requirement. The final mesh is shown in Figure 5.34.

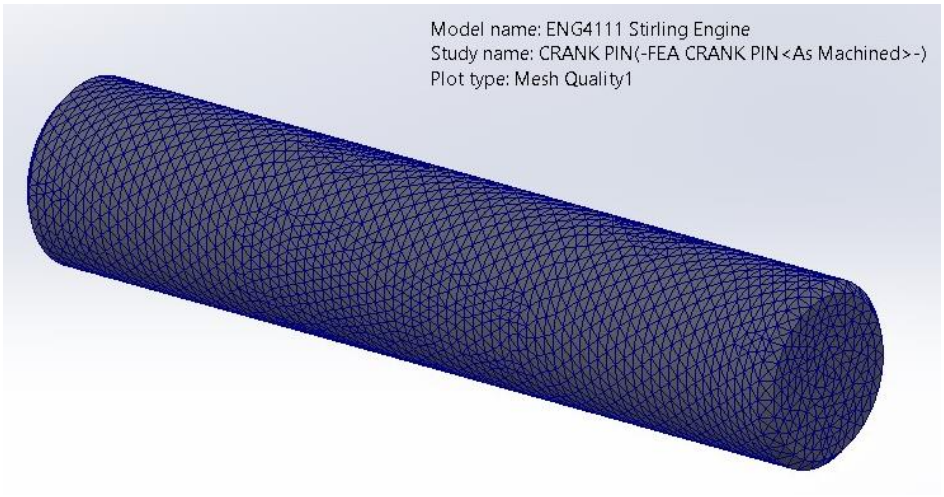

Figure 5.34: Final mesh of crank pin.

The von mises stress plot of the crank pin is shown in Figure 5.35. It can be seen that the maximum stresses occur at the edge of the supported faces. This matches the results found in the hand calculations. The analysis suggests a maximum stress of 345 MPa, however probing the values in the vicinity of this point suggest that the actual value is lower by Saint Venant's principle. As shown in Figure 5.36, the actual values of stress in this area are approximately 200 MPa. As the value found by hand calculations in (5.21) is 156.58 MPa, the lower values found by probing slightly away from the stress singularity are likely to be more realistic. Assuming a von mises stress value of 200 MPa, the safety factor is 3.3 when compared to the yield strength of 660 MPa for 4140 steel.

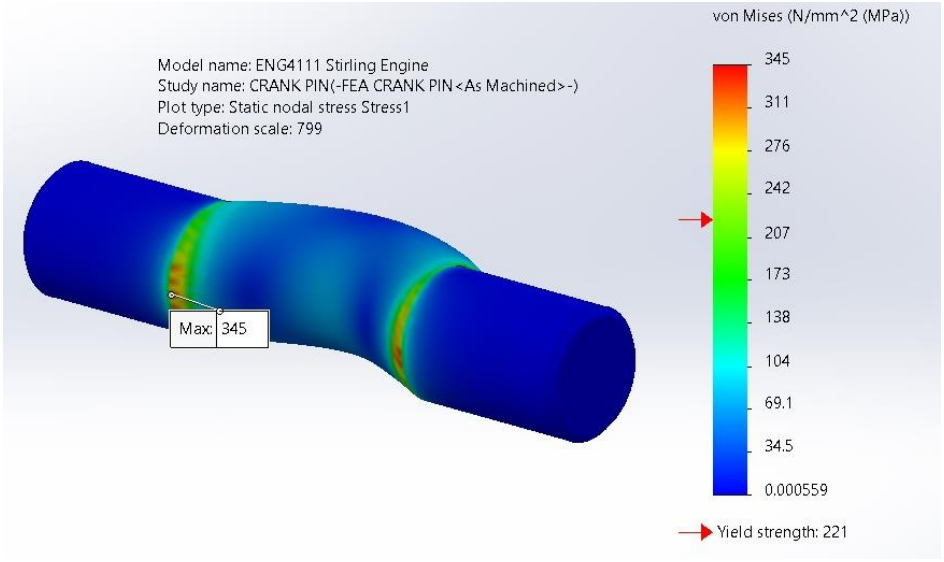

Figure 5.35: Von mises stress for crank pin analysis (MPa).

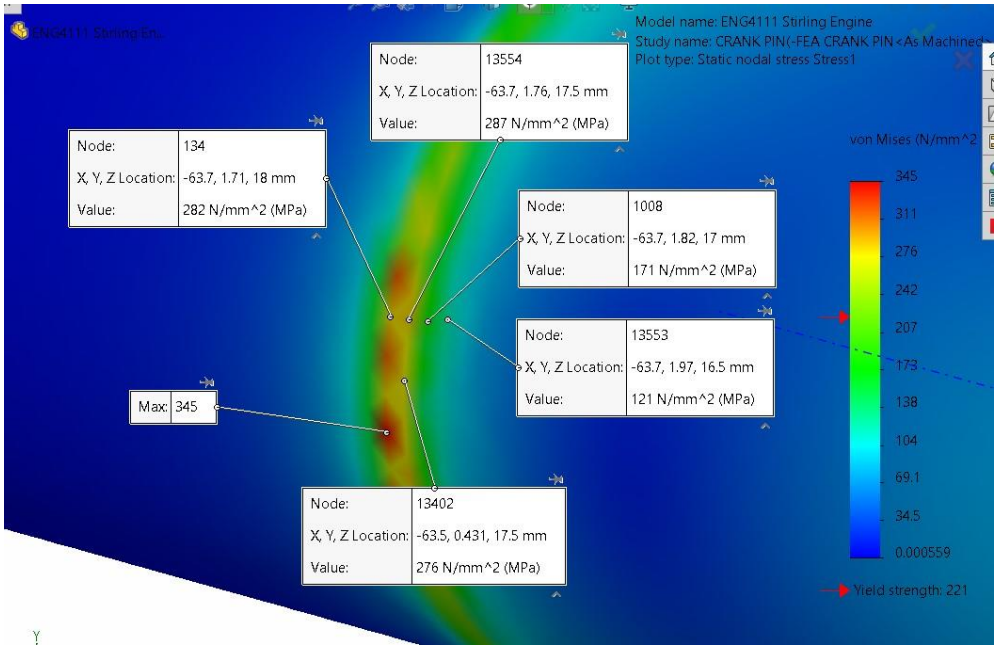

Figure 5.36: Von mises stress around edges of supported faces (MPa).

Figure 5.37 shows iso clipping of the crank pin stress at 100 MPa and 200 MPa. It can be seen that the stress values over 200 MPa are very localised and therefore may be unrealistic. Furthermore, as the load case is conservative and will not occur in actual operation, the design has a safety factor of approximately 3.3 even in this worst-case scenario. Therefore, it is considered safe.

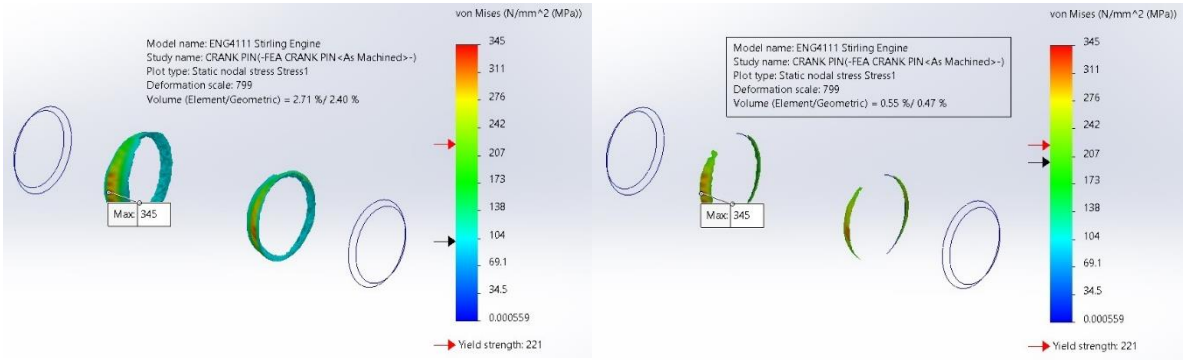

Figure 5.37: Crank pin iso clipping at 100 MPa (left) and 200 MPa (right).

5.4.5 Crank Plate

Figure 5.38 shows the setup of the analysis. The centre hole is fixed as the plate will be welded to the output shaft and therefore any torque will be transmitted through the centre hole. The load is applied to

the hole further from the centre as this will produce the highest bending moment in the plate and is applied to the bottom half of the hole to approximately the actual load distribution.

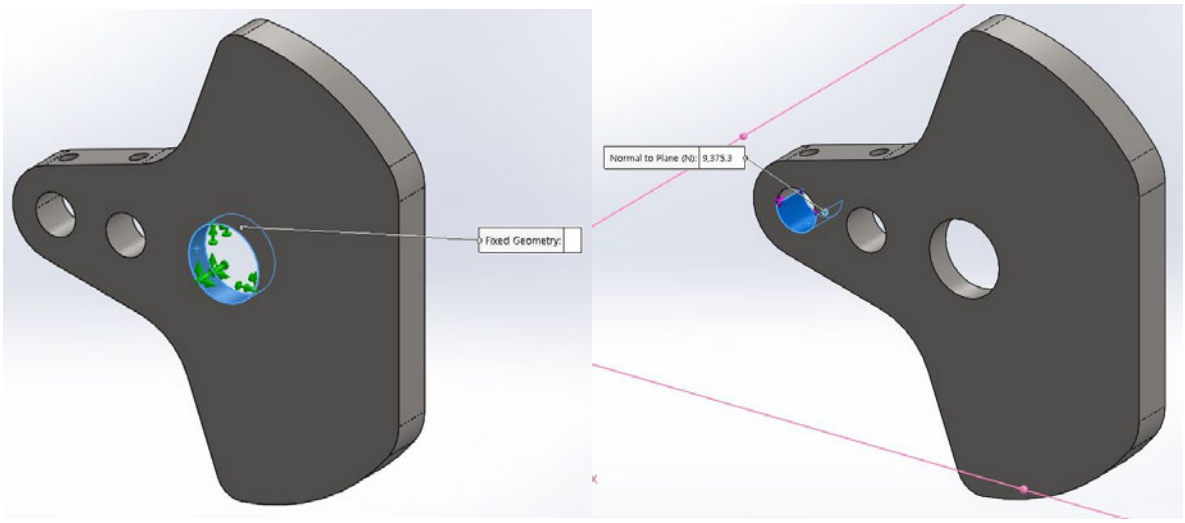

Figure 5.38: Fixed geometry and applied load on crank plate.

The mesh was produced with a maximum and minimum element sizes of 3 mm and 1.5 mm respectively. A relatively fine mesh could be utilised without a high computational requirement, while still producing accurate results. The final mesh is shown in Figure 5.39.

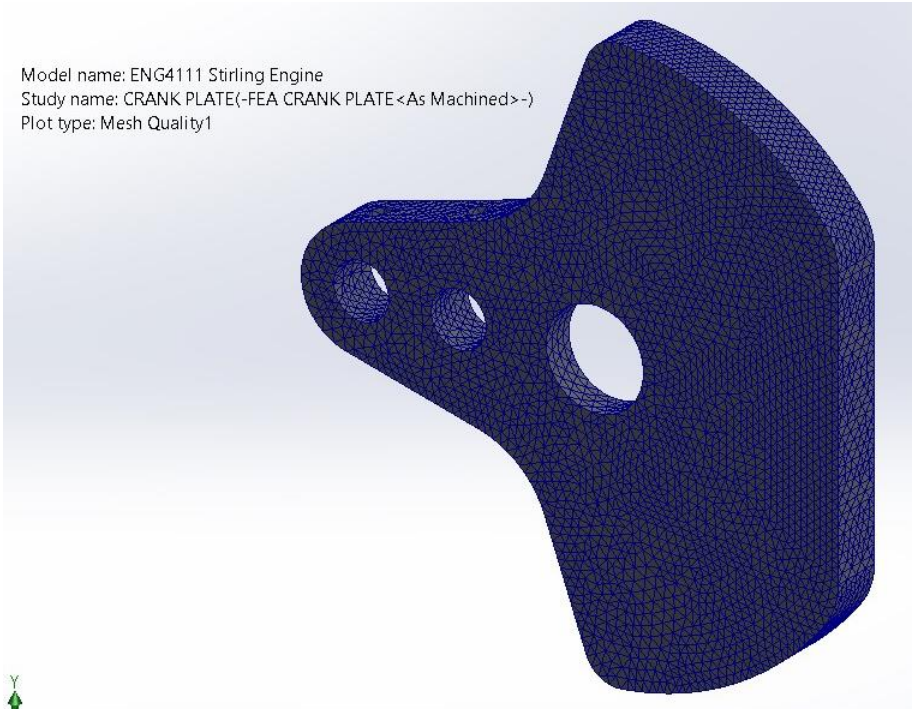

Figure 5.39: Final mesh of crank plate.

Figure 5.40 shows the von mises stress plot for the crank plate, while Figure 5.41 shows probes of the stress at the highly stressed locations. It can be seen that higher stresses are observed at the two 17 mm holes and the centre hole, however the shaft will be welded to the plate at the centre hole and therefore the stresses here will be lower in reality. The analysis suggests a maximum stress of 231.28 MPa, however by probing around this point the actual stress values here are approximately 120 MPa. This suggests that a stress singularity is occurring and can be ignored.

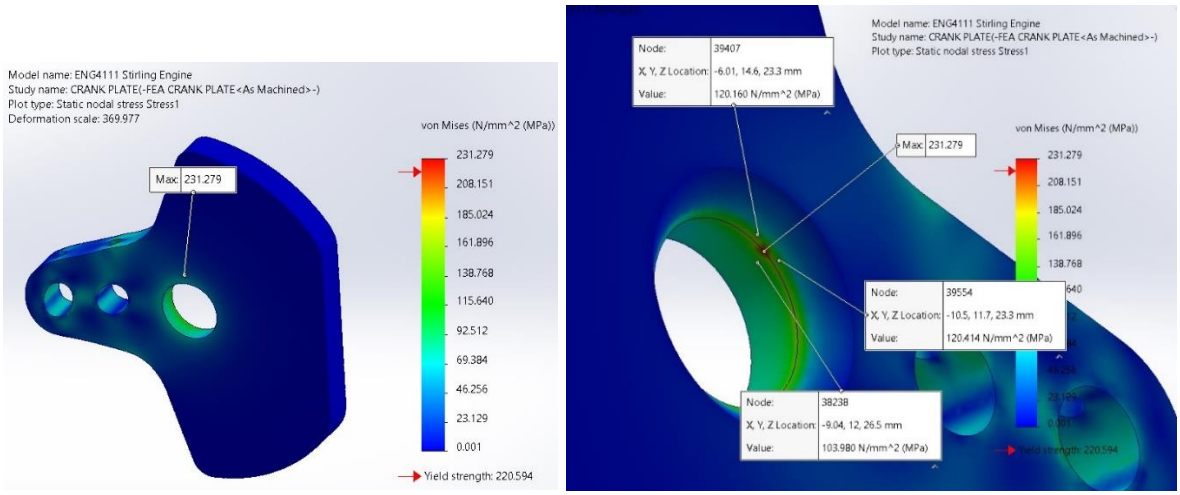

Figure 5.40: Von mises stress plot for crank plate (MPa).

Figure 5.41 shows the von mises stress at the 17 mm holes. It can be seen that the stress here is approximately 68 MPa and represents a safety factor of 5.15 as Grade 350 steel is used. The depth of the cross section increases between the outer 17 mm hole and the centre hole as the bending stress increases towards the centre hole. The analysis suggests that the stress remains approximately constant which is a good result.

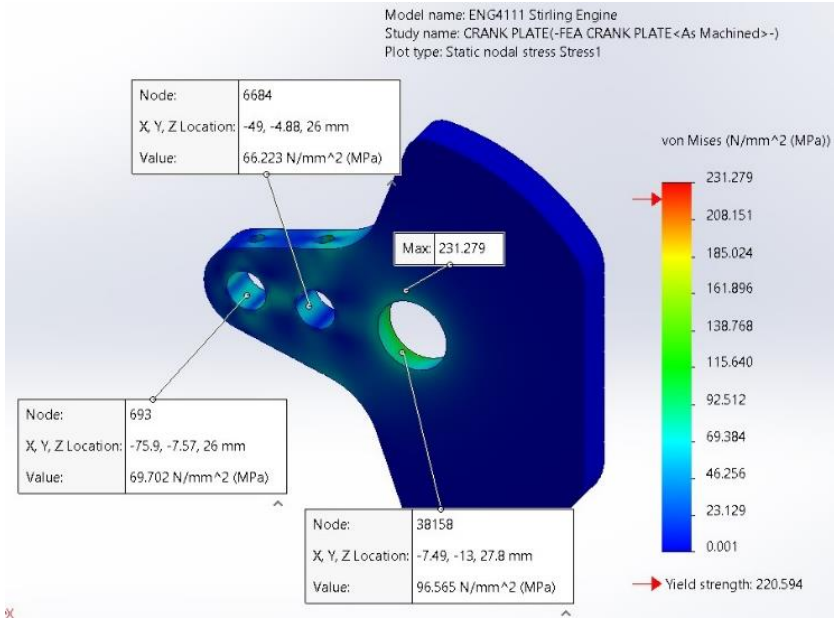

Figure 5.41: Von mises stress at 17 mm holes (MPa).

Figure 5.42 shows iso clipping of the crank plate stress at 50 MPa and 100 MPa. It can be seen that the stress values over 100 MPa are very localised and therefore can be ignored. Significant parts of the component are stressed above 50 MPa, however as the stress is less than 100 MPa at these locations the values are still safely below the yield strength of 350 MPa.

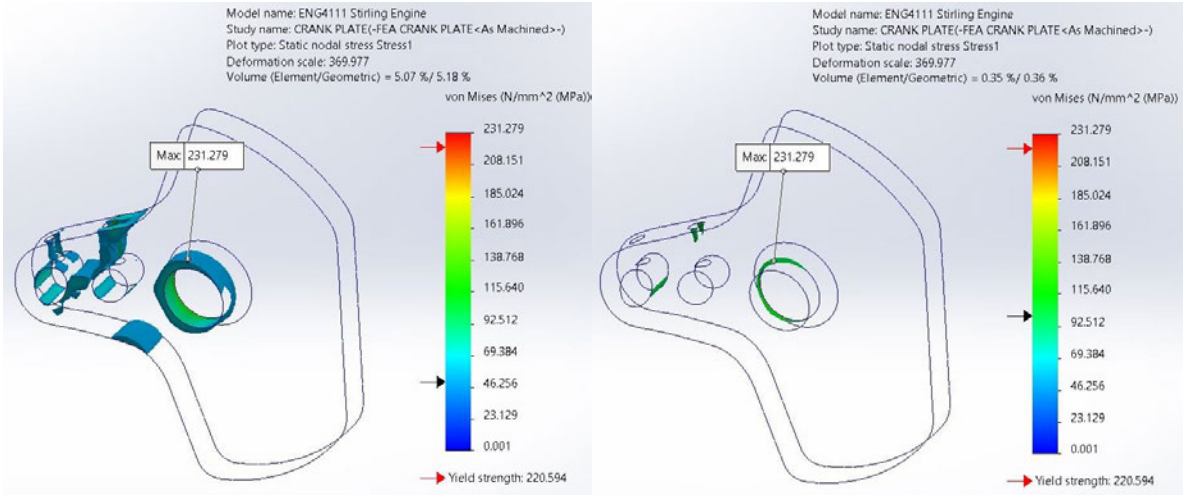

Figure 5.42: Crank plate iso clipping at 50 MPa (left) and 100 MPa (right).

5.4.6 Output Shaft

The FEA of the output shaft follows a similar procedure to the hand calculations in Section 5.2.9. Figures 5.43 and 5.44 show the bearing supports applied to the shaft in SolidWorks. The sections of the shaft which are supported by the bearings are restricted from moving in both radial and axial directions. This is realistic as grub screws are used to lock the shaft axially. Self-alignment is allowed as the insert bearings are self-aligning.

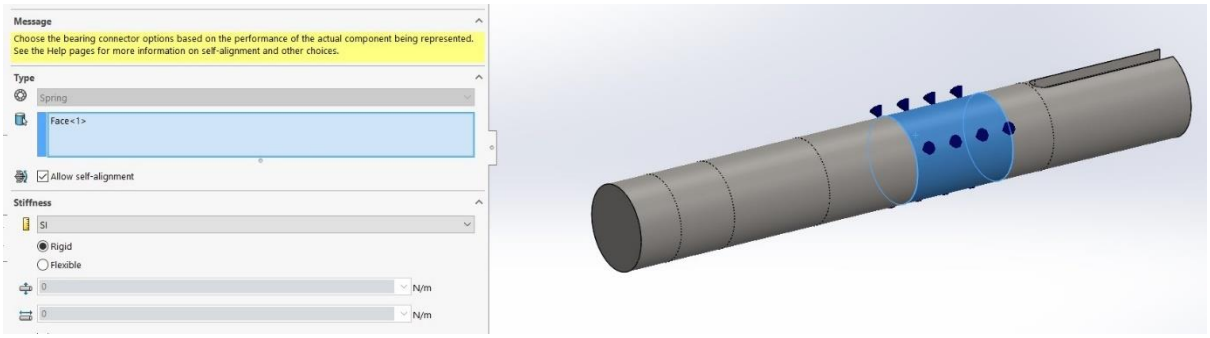

Figure 5.43: Outer bearing support on output shaft.

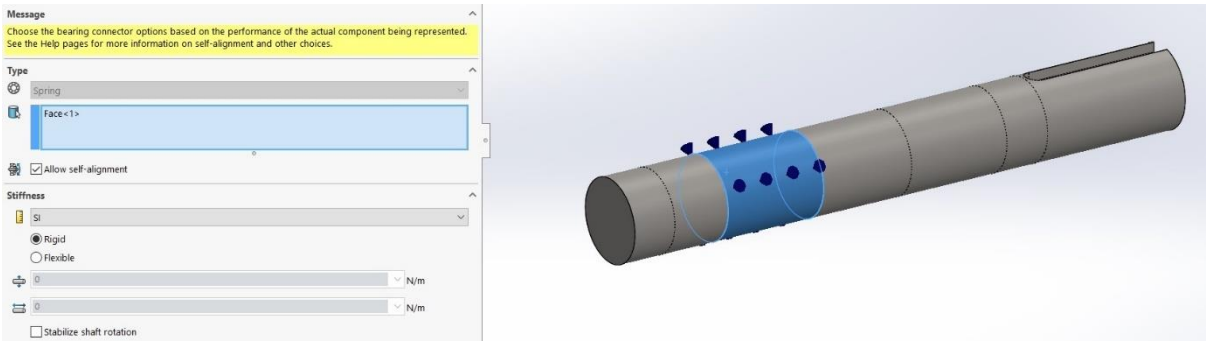

Figure 5.44: Inner bearing support on output shaft.

As shown in Figures 5.45 and 5.46, the outer end of the shaft is fixed while the torque and force is applied to the inside end of the shaft where the crank plate is welded. This will cause shear stresses to develop in the shaft for the purposes of stress analysis.

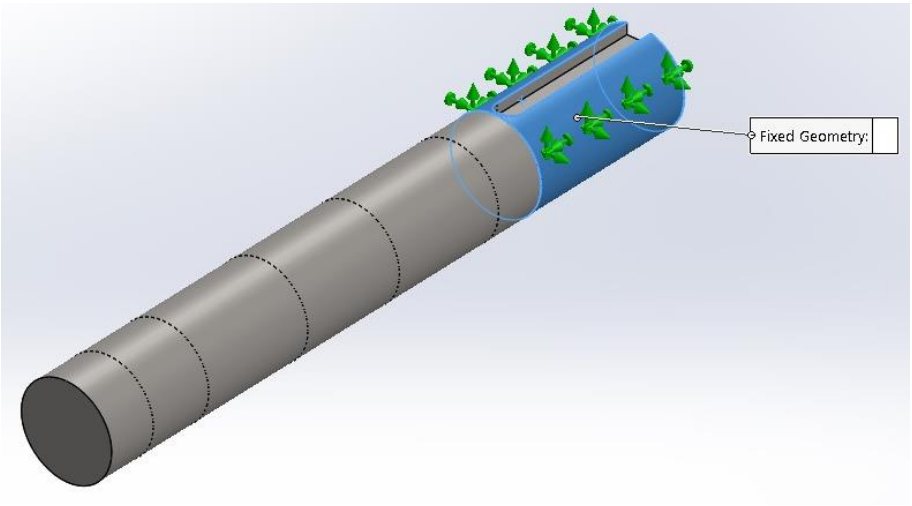

Figure 5.45: Fixed end of output shaft.

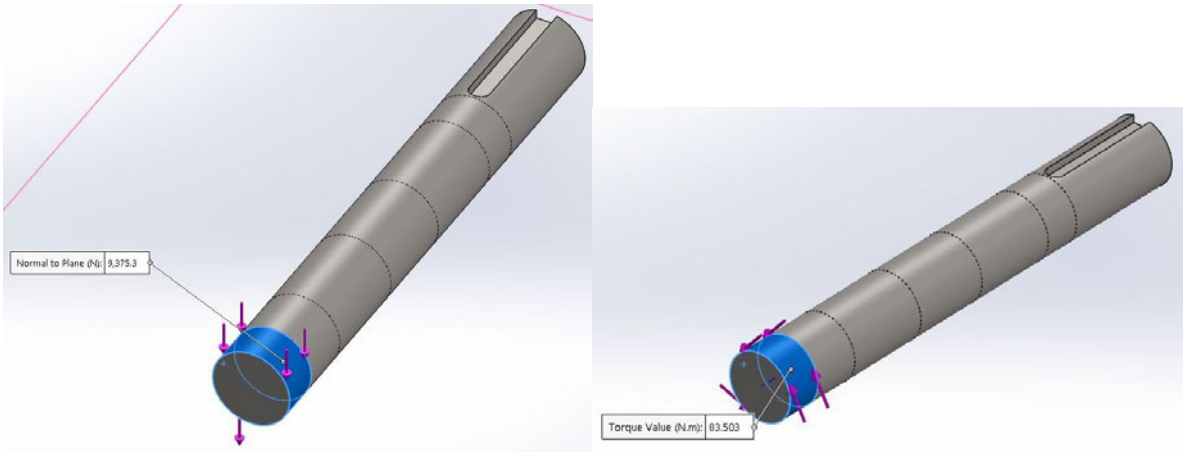

Figure 5.46: Application of torque and force in output shaft FEA.

Figure 5.47 shows the final mesh of the output shaft. The maximum and minimum element sizes are 2.5 mm and 1 mm respectively, which yields a very fine mesh that should yield accurate results. The keyway could be removed for the purposes of the FEA, however it does not appear to affect the results or computational requirements.

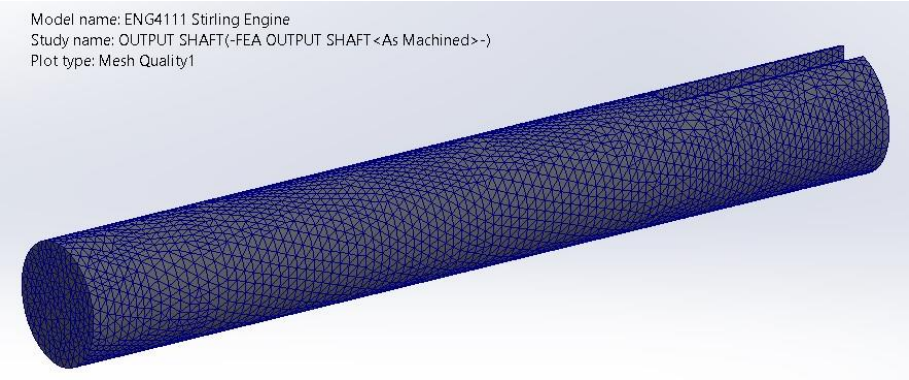

Figure 5.47: Final mesh of output shaft.

As shown in Figure 5.48, the analysis suggests a maximum von mises stress of 242.76 MPa. As predicted by the hand calculations, the maximum stress occurs around the internal bearing support. The high stress values right at the edge of the supports may represent stress singularities and be higher than the actual stresses experienced. Figures 5.49 and 5.50 show probes of stress values around these points and they suggest that the stress may be closer to 190 MPa. This agrees with the hand calculations as a von mises stress of 180.45 MPa which was found in (5.29).

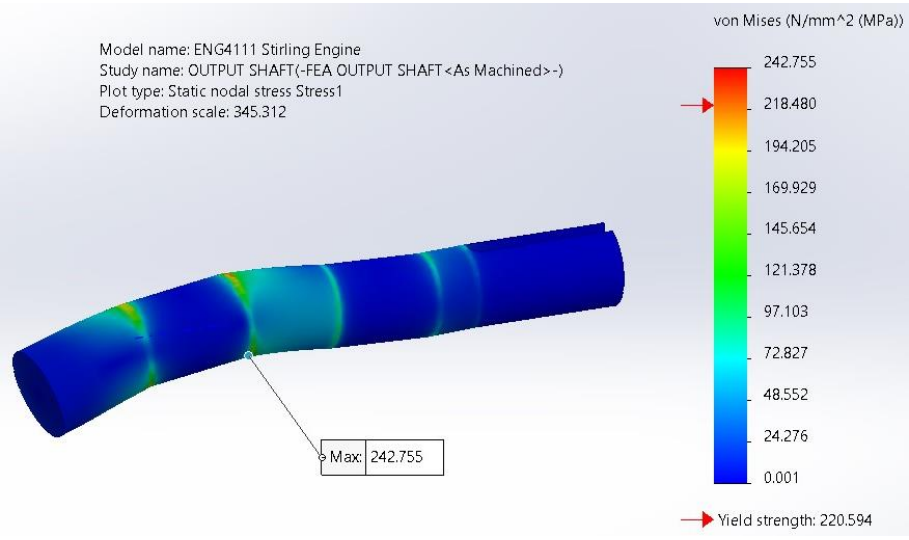

Figure 5.48: Von mises stress plot of output shaft (MPa).

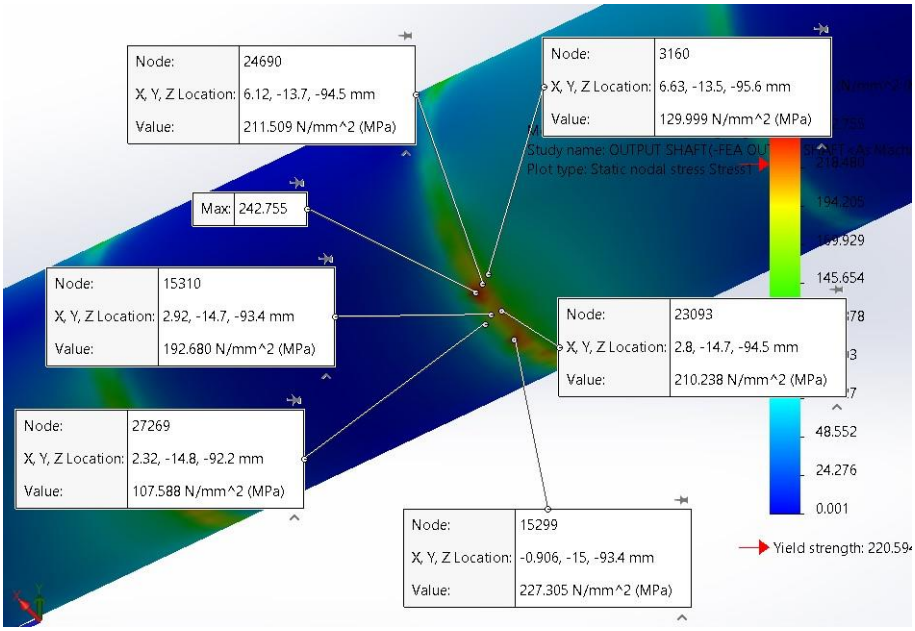

Figure 5.49: Von mises stress around internal bearing support of output shaft (MPa).

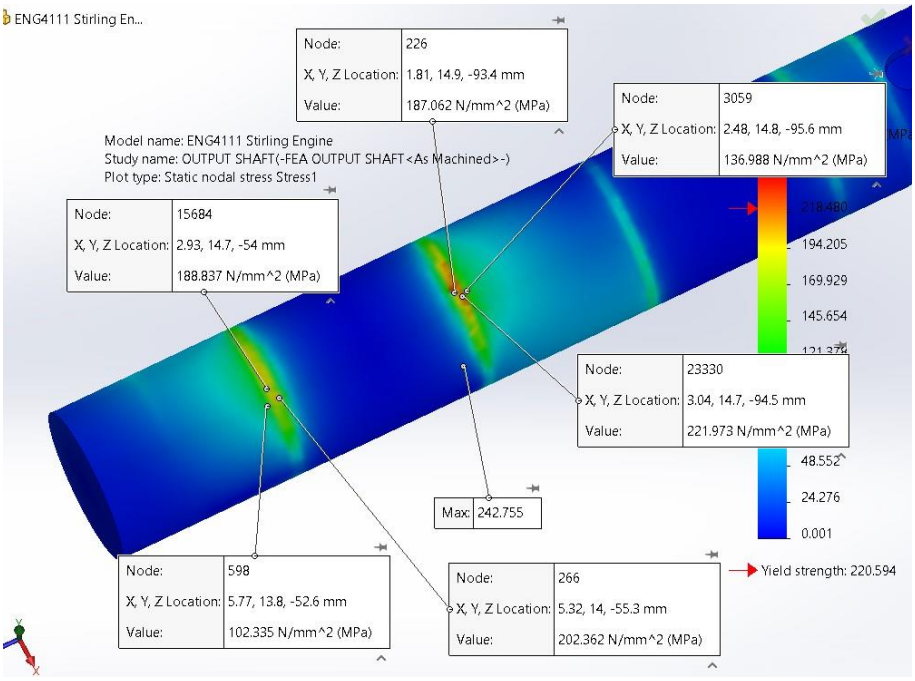

Figure 5.50: Von mises stress around internal bearing support of output shaft (MPa).

Figure 5.51 shows iso clipping of the output shaft stress at 100 MPa and 175 MPa. It can be seen that the stress values over 100 MPa are found around the internal bearing support. The values of stress over 175 MPa are extremely localised and can be ignored by Saint Venant's principle.

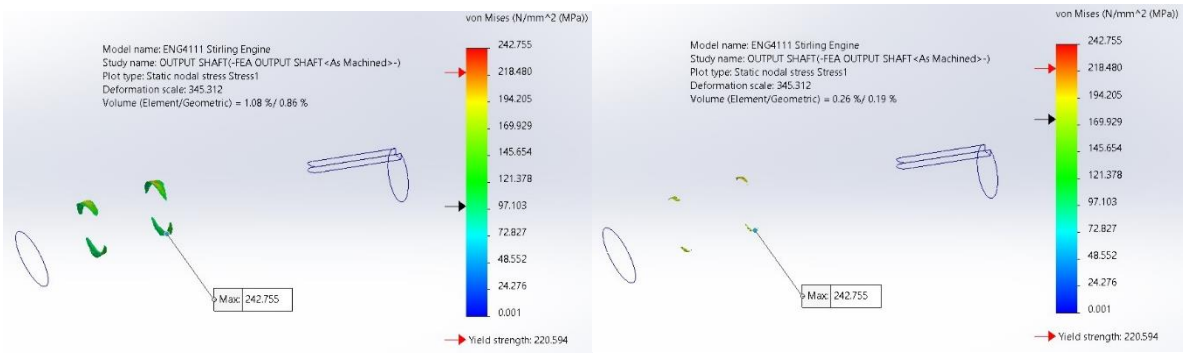

Figure 5.51: Output shaft iso clipping at 100 MPa (left) and 175 MPa (right).

5.5 Technical drawings

Technical detail and assembly drawings have been produced for the manufacture of all components and final assembly of the engine. Appendix C contains the complete set of final revision drawings which were used in producing the prototype engine.

5.6 Fabrication of components

All of the components for the engine were fabricated using the drawings contained in Appendix C as per the manufacturing processes outlined in Section 5.2. This section shows photos of all manufactured components before being assembled as shown in Section 5.7.

Figure 5.52: Hot cylinder fabrication as per Drawing MS-SE-01 Revision B.

Figure 5.53: Cold cylinder fabrication as per Drawing MS-SE-02 Revision A.

Figure 5.54: Engine body fabrication as per Drawing MS-SE-03 Revision B.

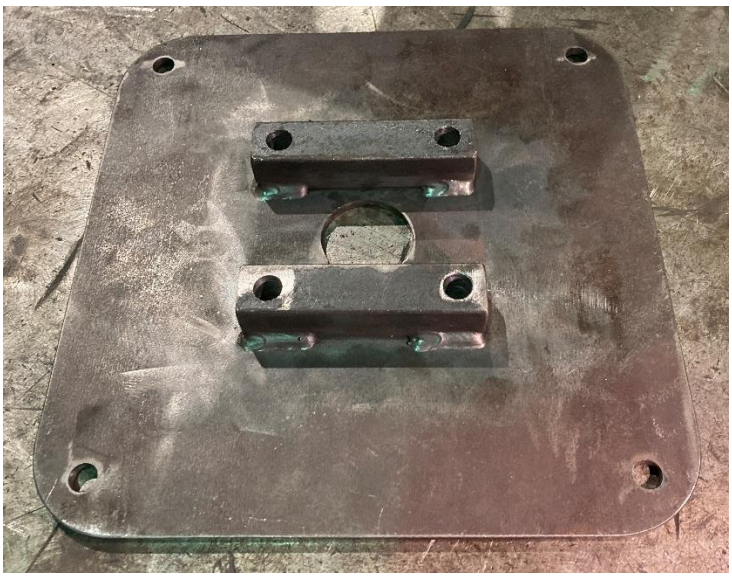

Figure 5.55: Bearing plate fabrication as per Drawing MS-SE-04.

Figure 5.56: Crank pin fabrication as per Drawing MS-SE-05.

Figure 5.57: Connecting rod fabrication as per Drawing MS-SE-06.

Figure 5.58: Bronze bush fabrication as per Drawing MS-SE-08.

Figure 5.59: Connecting air tube with regenerator fabrication as per Drawing MS-SE-10.

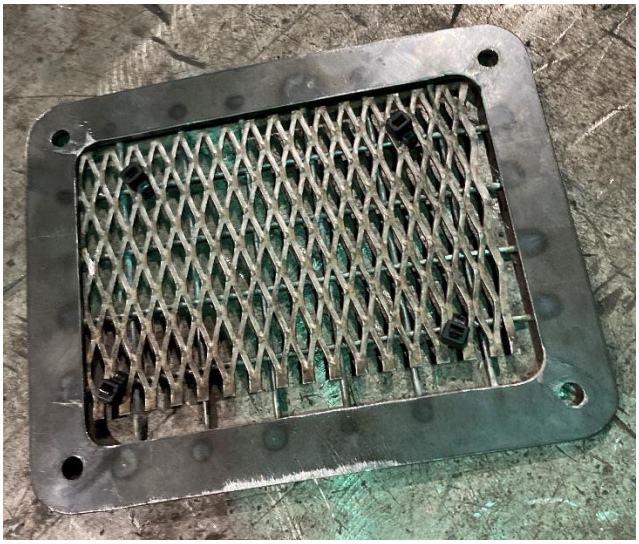

Figure 5.60: Cover fabrication as per Drawing MS-SE-11.

Figure 5.61: Output shaft and crank plate fabrication as per Drawing MS-SE-12 Revision B.

Figure 5.62: Idler shaft and crank plate fabrication as per Drawing MS-SE-13 Revision B.

Figure 5.63: Heater fabrication as per Drawing MS-SE-15.

Figure 5.64: Key fabrication as per Drawing MS-SE-18.

Figure 5.65: Bronze shim fabrication as per Drawing MS-SE-20.

5.7 Assembly

This section shows photos of the engine assemblies in the order that the components were assembled. The subassemblies were put together first before completing assembly of the entire engine.

The connecting rod and piston subassemblies were assembled initially and are shown in Figure 5.66.

Figure 5.66: Connecting rod and piston assembly as per Drawing MS-SE-16.

The output and flywheel shaft assemblies were completed next and are shown in Figures 5.67 and 5.68.

Figure 5.67: Flywheel shaft assembly as per Drawing MS-SE-17.

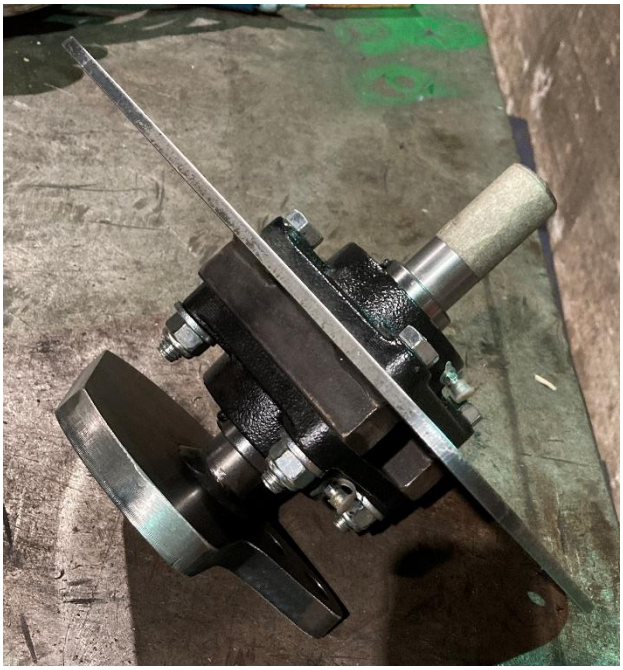

Figure 5.68: Output shaft assembly as per Drawing MS-SE-19.

The complete engine assembly was completed next utilising all the fabricated components and subassemblies as shown in Figures 5.69 to 5.76. The first step was to fit the connecting rod and piston assemblies into the hot and cold cylinders with the heater already screwed into the hot cylinder. It was found that the best sealing occurred with three compression rings and the friction was not overly restrictive. After the pistons had been inserted into the cylinders, the hot and cold cylinders were bolted to the engine body which had already been bolted down to a bench.

The connecting air tube was then fitted to the two cylinders and the crank pin was then inserted through both connecting rods with the three bronze shims being placed as shown in Drawing MS-SE-GA. The flywheel and output shaft assemblies were then bolted onto the engine body with the drilled hole in each of the crank plates being fitted onto the crank pin. The external circlips were then fitted onto the crank pin and the grub screws fitted into the crank plates and tightened against the crank pin. Finally, the cover was bolted onto the side of the engine body.

Figure 5.69: Heater head fitted to hot cylinder.

Figure 5.70: Assembly of piston and connecting rod assemblies in hot and cold cylinders.

Figure 5.71: Assembly of cylinder assemblies onto engine body and air tube fitted to cylinders.

Figure 5.72: Crank pin inserted through bearings in connecting rods with bronze shims.

Figure 5.73: Flywheel shaft assembly fitted to engine body and crank pin inserted into hole on crank plate.

Figure 5.74: Output shaft assembly fitted to engine body and crank pin inserted into hole on crank plate.

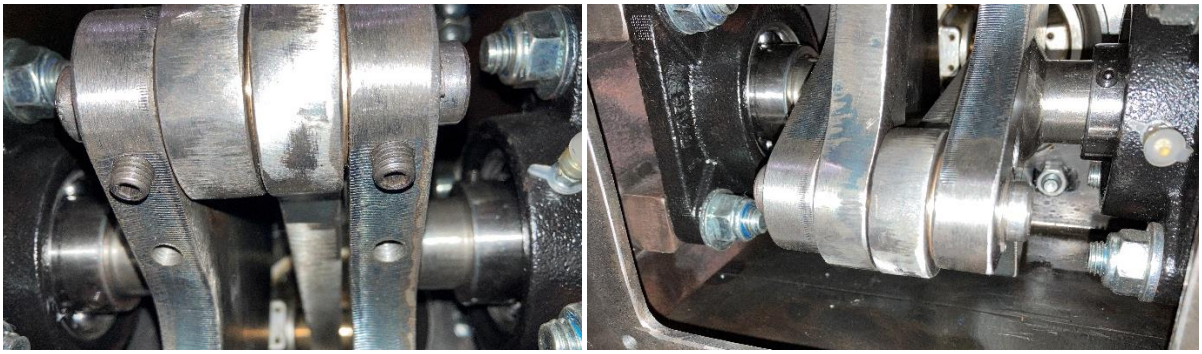

Figure 5.75: Circlips and grub screws fitted to retain crank pin.

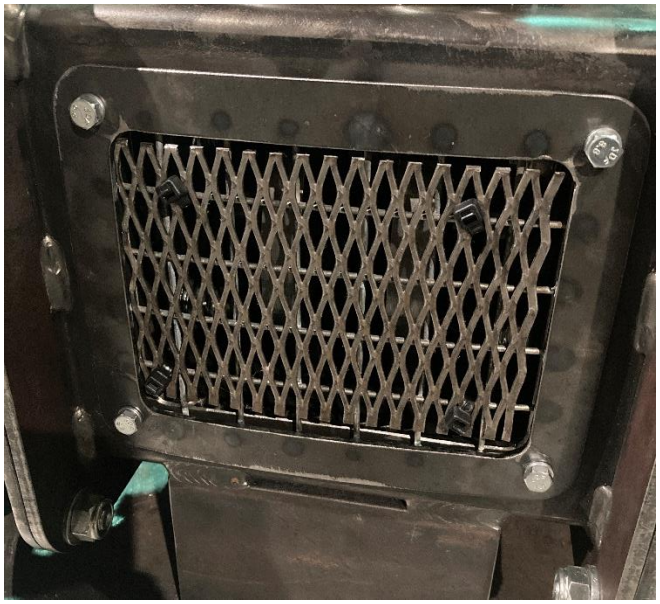

Figure 5.76: Cover bolted over access hatch.

Figures 5.77 and 5.78 show photos of the engine fully assembled.

Figure 5.77: Photos of fully assembled engine.

Figure 5.78: Photos of fully assembled engine.

5.8 Chapter Summary

This chapter has outlined the detailed design of all engine components based on the initial design presented in Chapter 4. The 3D solid models produced in SolidWorks are shown along with stress analysis of each component based on the material selection. Design choices such as material selection and functionality have been discussed with respect to best practice outlined in the literature. FEA of all critical components was carried out and the results have been presented and compared with the initial hand calculations. Finally, the fabrication and assembly of the engine has been presented with photos and descriptions of each stage of manufacture.

Chapter 6

Testing and Discussion

6.1 Chapter overview

This chapter discusses the results of testing the engine with an applied temperature to simulate hydrogen combustion as the heat source. Section 6.2 outlines how the engine performed when temperature was applied and Section 6.3 discusses the limitations which were observed as the temperature increased significantly. Section 6.4 outlines modifications which were made to the engine after initial testing and how the engine responded after these changes had been made. Sections 6.5 and 6.6 outline revised power calculations for the varied geometry, and the revised drawings which were produced. Section 6.7 provides a discussion of the results and Section 6.8 discusses further optimisation which could be done to the engine. Section 6.9 outlines some potential real-world applications for the design if the target power output were to be achieved.

6.2 Engine performance

In this section, results from all tests which were carried out are presented. It was verified in each case that air was travelling through the connecting air tube as expected by unscrewing the fittings at each point and verifying that air escaped when the working gas was compressed by the pistons.

6.2.1 Initial engine response and friction

Ross (1993) suggests that mechanical detail is very important in the successful operation of a Stirling Engine. The pistons should seal well and as the engine turns over compression it should feel “bouncy”. Furthermore, friction should be minimised and any kinks or binds in the mechanism should be corrected.

On initial assembly, the pistons were inserted into the cylinders with two compression rings fitted. When the engine was turned over without the air tube connected (so that no compression would occur), the mechanism seemed relatively free and there was not a great deal of friction. The mechanism seemed quite smooth however some resistance was noted when the pistons were at bottom dead centre. After

the connecting air tube was fitted, significant compression was felt in the engine as the flywheel was rotated and the pistons compressed the gas in the working space when swept volume was at a minimum. Some air loss could be heard on compression as air escaped past the pistons, particularly at bottom dead centre.

6.2.2 Initial testing

During initial testing, the heater head had not been included in the design and heat was applied directly to the end wall of the hot cylinder of the engine with an oxy-acetylene torch as outlined in the methodology. An Accud AC-IT700 infrared thermometer was used to measure the temperature of the end wall of the hot cylinder, and the device was set to an emissivity of 0.95. The end wall was slowly heated to a maximum temperature of 600° C before heating was ceased due to concerns of distorting the walls of the hot cylinder. The crank was rotated by using a pull cord to turn the flywheel as shown in Figure 6.1, however the results were not promising.

Figure 6.1: Photo of the “pull cord” wrapped around the flywheel to crank the engine.

The engine crank did not rotate any further by itself beyond the initial inertia given to the flywheel by the pull cord. Two potential shortcomings were identified, namely: the absence of a heater with additional surface area to deliver heat to the working gas; and air leakage past the pistons. Ross (1993)

identifies the efficiency of the heater and piston sealing as critical factors for engine operation and so modifications were made in these areas as a starting point. In an attempt to rectify these shortcomings, a heater head was designed and fitted as described in Chapter 5 and a third compression ring as well as an oil ring was fitted to both pistons.

6.2.3 Second test with heater head design and additional piston rings

After fitting the third compression ring and oil ring to the pistons, the friction in the mechanism was significantly more noticeable. However, the air leakage problem had improved as no air could be heard escaping past the pistons at bottom dead centre. The heater head was fitted to the hot cylinder and the engine was tested again. As the heater moved the heat source further away from the hot cylinder and connecting air tube, more heat could be applied to the heater with less potential for distortion of the cylinder. Figure 6.2 shows a photo of heat being applied to the heater head with the oxy-acetylene heating torch.

Figure 6.2: Heat being applied to heater head with oxy-acetylene heating torch.

The heater was heated to approximately 700° C before cracking was observed in the end plate of the heater and the testing was ceased. Again, multiple attempts were made to start the engine as the heat was applied and the temperature increased to the maximum value of 700° C for this test, but unfortunately the engine would not run. Some improvement was observed as the crank rotated a couple of turns by itself after the flywheel's initial inertia had been consumed, however it was not significant to suggest that the engine would operate further.

The original heater head design was 135 mm overall length with a 5 mm Grade 250 steel plate as the welded end plate. The heater was modified to 103 mm overall length in an attempt to reduce dead volume and improve the efficiency of the heater by moving the heat source closer to the working gas, which reduces the amount of conduction required. The end plate was redesigned as 8 mm thick 1045 steel to reduce the potential of cracking occurring. As the air leakage was minimal, the oil ring was removed from both pistons to reduce the friction while still maintaining a good seal.

6.2.4 Third test with modified heater head and oil ring removed

After fitting the shortened heater and removing the oil ring from both pistons, the engine was retested. This time, a maximum temperature of 800° C was achieved without damage occurring to the heater head, however testing was ceased as the oxy-acetylene torch was unable to heat the heater beyond this temperature. Some air loss past the pistons was noted but it was still an improvement over the initial testing which utilised only two compression rings. The mechanism felt freer to rotate, which was likely aided by the removal of the oil rings.

Again, the engine would not run despite reaching a maximum temperature of 800° C. The crank behaved similarly to the second test as it rotated a couple of times by itself before stopping after initial cranking.

It was noticed during this test that as the pistons moved to bottom dead centre, the bottom of the piston became unsupported as it moved past the end of the cylinder. This may have been causing air loss and increasing resistance in the mechanism as the connecting rods pushed the back into the cylinders. Therefore, for the subsequent test the crank radius length was shortened to reduce the length of piston which extended beyond the cylinder at bottom dead centre. This changes the work and power output calculations and revised values are presented in Section 6.5. The crank radius was shortened by drilling a second hole in the crank plates at 42 mm from the centre of the output shaft and fitting the crank pin through this hole. Figure 6.3 shows an image of the crank plate with a second hole drilled.

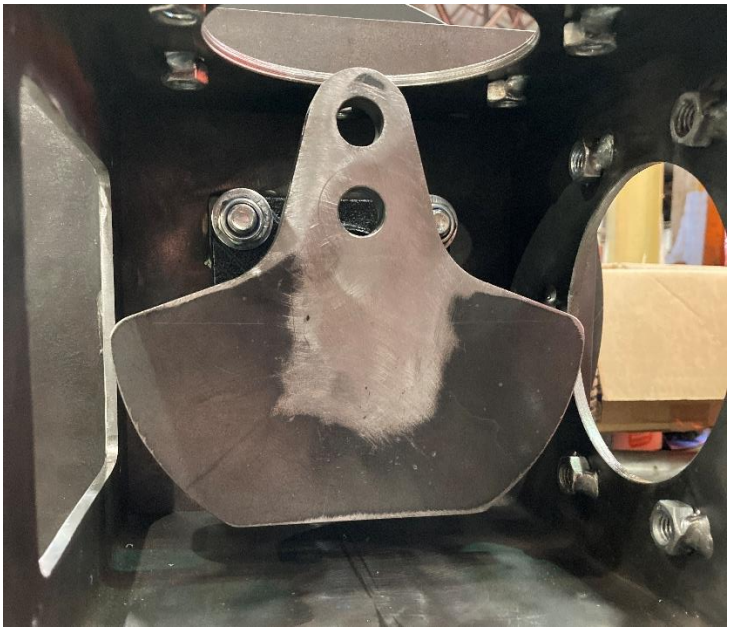

Figure 6.3: Second hole drilled in crank plate for crank pin at 42 mm from the centre of the output shaft.

6.2.5 Fourth test with shortened crank radius and original conrods

With the crank pin fitted at a shorter radius from the centre of the output shaft, the stroke of the piston is reduced and therefore so is the swept volume. The modified assembly is shown in Figure 6.4. Theoretically, this will reduce the power output of the engine however will reduce resistance caused by compression. When the flywheel was turned with the connecting air tube fitted, the mechanism felt freer which suggests that less compression was occurring and resistance in the mechanism had been reduced as intended. The heater head was heated again to a maximum temperature of 800° C and the engine was tested multiple times as the temperature increased.

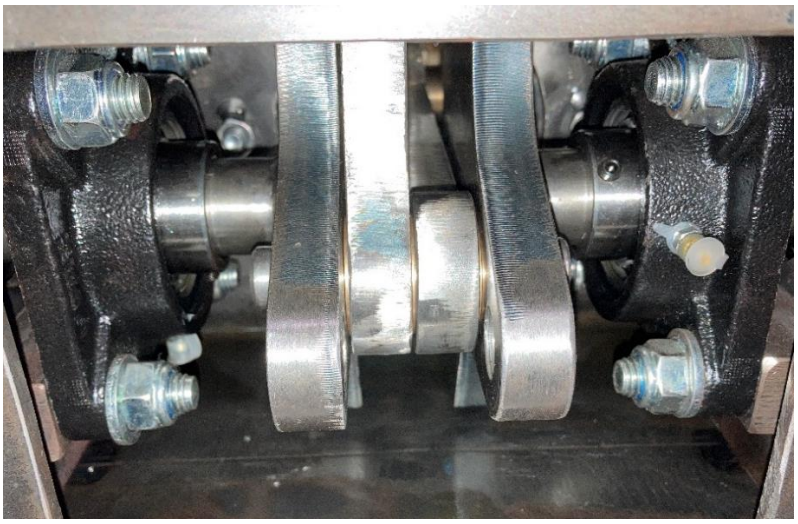

Figure 6.4: Crank pin fitted at 42 mm from centre of output shaft.

This configuration showed the most promise as the engine ran by itself for approximately 4 seconds at 700° C and approximately 5 seconds at 800° C before decelerating to a stop. Ross (1993) suggests that at high compression ratios the engine is harder to start, but with high enough hot temperatures significant power and speed can be achieved. Although the modified configuration did not decrease the compression ratio, it is possible that the decrease in swept volume made it easier for the engine to run despite the decrease in potential power output. If a higher temperature could be achieved, better results may occur and this could be accomplished in future work. However, despite the limitations to the temperature produced by the oxy-acetylene torch, some cracking of the thread in the heater head was observed and it was welded to the hot cylinder for subsequent testing. For future work, a better heater head could be designed which can withstand higher temperatures.

6.2.6 Fifth test with shortened crank radius and longer conrods

For the fifth test, longer connecting rods with a centre distance of 214 mm were fitted to decrease the amount of dead volume in the engine and increase the amount of compression. This also had the added benefit of retaining the pistons within the cylinder at bottom dead centre, and therefore they are always fully supported. The resistance created by compression increased when the flywheel was rotated without heat applied.

The heater head was heated to 800° C and the engine was cranked again multiple times during heating. The engine showed little promise of running and only rotated a couple of times after being cranked, similarly to the second and third tests. After 800° C was achieved the testing was ceased as some resistance was noted as the mechanism was rotated and it was thought that distortion was occurring in the hot cylinder due to the applied heat.

6.3 Heating Temperatures

The engine was cranked at various temperatures between 500° C and 800° C but unfortunately there was limited success in terms of engine performance. The temperature was measured using the infrared temperature gun, and examples of temperature reads during testing are shown in Figures 6.5 and 6.6. The maximum temperature was limited by the durability of the heater head and the oxy-acetylene torch. For future testing, a more robust heater head could be designed and a way of applying more heat to the heater could be utilised. If the heater could be heated to 1 100° C, there may be sufficient energy for the engine to run.

Figure 6.5: Heater head heated to 500° C and 600° C during testing.

Figure 6.6: Heater head heated to 700° C and 800° C during testing.

6.4 Modifications made

A list of the modifications made after the initial testing are summarised below in the order that they were made. These modifications were made in an attempt to optimise the engine and get it to run under the applied heat.

- Designed and added heater head
- Added compression and oil ring to pistons
- Removed oil ring from pistons to reduce friction
- Shortened heater head and made the end plate thicker and from a different material
- Reduced the crank radius by drilling a second hole for the crank pin at 42 mm from the centre of the output shaft
- Made new connecting rods with a longer centre to centre distance of 214 mm

The original design, which is detailed in the drawings contained in Appendix C, was tested in the third test, while the first and second tests used this configuration except with superseded heater designs.

Drawing number MS-SE-GA Revision A shows the assembly with the crank pin at the shorter radius and the shorter connecting rods fitted. This assembly was utilised in the fourth test.

The longer connecting rods are shown in drawing number MS-SE-21 in Appendix D, and the updated piston/connecting rod assembly is shown in drawing number MS-SE-22. Drawing number MS-SE-GA Revision B shows the assembly with the crank pin at the shorter radius and the longer connecting rods fitted. This assembly was utilised in the fifth test.

6.5 Revised power calculations

As the geometry changed for the fourth and fifth tests, the work and power output calculations will differ. Table 6.1 shows the modified dimensional values for the engine tested in the fourth test (drawing number MS-SE-GA Revision A) while Table 6.2 shows the modified dimensional values for the engine tested in the fifth test (drawing number MS-SE-GA Revision B).

Table 6.1: Geometric values for engine as per drawing number MS-SE-GA Revision A).

Description	**Symbol**	**Value**	**Units**
Crank Radius Expansion Piston	r_1	4.2	cm
Crank Radius Compression Piston	r_2	4.2	cm
Connecting Rod Length Expansion Piston	l_1	18.75	cm
Connecting Rod Length Compression Cylinder	l_2	18.75	cm
Phase Angle	α	90	degrees
Expansion Cylinder Radius	E_r	4.445	cm
Compression Cylinder Radius	C_r	4.445	cm
Length from crank centre to TDC of expansion piston	OE	22.95	cm
Length from crank centre to TDC of compression piston	OD	22.95	cm

Table 6.2: Geometric values for engine as per drawing number MS-SE-GA Revision B).

Description	**Symbol**	**Value**	**Units**
Crank Radius Expansion Piston	r_1	4.2	cm
Crank Radius Compression Piston	r_2	4.2	cm
Connecting Rod Length Expansion Piston	l_1	21.4	cm
Connecting Rod Length Compression Cylinder	l_2	21.4	cm
Phase Angle	α	90	degrees
Expansion Cylinder Radius	E_r	4.445	cm
Compression Cylinder Radius	C_r	4.445	cm
Length from crank centre to TDC of expansion piston	OE	25.6	cm
Length from crank centre to TDC of compression piston	OD	25.6	cm

The same procedure was carried out as outlined in Chapter 4 for the initial engine design and the power output values calculated are shown in Tables 6.3 and 6.4. It can be seen that the power output predicted for both engines is quite similar. This is because the swept volume is equal in both cases and the amount of dead volume is the only difference. The dead volume in the regenerator tube is equal to 80.54 cm^3, the dead volume in the heater head is 167.63 cm^3 and the dead volume in each cylinder when the piston is at top dead centre is approximately 328.17 cm^3. The only analysis which takes these dead volumes into account is the Schmidt equation, and some difference is seen between the two engines in the results using this analysis.

Table 6.3: Power output for engine with 42 mm crank radius and connecting rod length of 187.5 mm from centre to centre.

Th (° C)	n (rev/s)	P-V Power, $L_{S,PV}$ (W)	Schmidt Power $L_{S,S}$ (W)	Beale Power, $L_{S,B}$ (W)	West Power, $L_{S,W}$ (W)
500	7.645	1218.39	1136.57	335.50	345.09
600	8.043	1524.83	1458.02	386.98	441.09
700	8.421	1841.83	1801.83	440.81	543.77
800	8.781	2167.59	2165.26	496.74	652.55
900	9.126	2501.05	2546.99	554.79	767.22
1000	9.459	2841.85	2945.88	614.99	887.63
1100	9.682	3156.87	3326.44	670.39	1003.24

Table 6.4: Power output for engine with 42 mm crank radius and connecting rod length of 214 mm from centre to centre.

Th (° C)	n (rev/s)	P-V Power, $L_{S,PV}$ (W)	Schmidt Power $L_{S,S}$ (W)	Beale Power, $L_{S,B}$ (W)	West Power, $L_{S,W}$ (W)
500	7.663	1234.55	1154.90	340.27	349.99
600	8.062	1545.12	1480.87	392.36	447.22
700	8.440	1866.37	1829.13	446.77	551.12
800	8.801	2196.62	2197.60	503.39	661.28
900	9.146	2534.63	2584.04	562.06	777.27
1000	9.479	2880.12	2987.92	622.94	899.09
1100	9.697	3197.89	3371.69	678.65	1015.60

When comparing the power output values in Tables 6.3 and 6.4 to the calculated values for the initial design in Table 4.8, it can be seen that the anticipated power output is lower in all cases for the revised geometry. This is because the swept volume is smaller due to the reduced crank radius. The lowest power output values expected are found by the Beale equation and range from 340.27 W at 500° C to 678.65 W at 1 100° C. These values are lower than for the initial design but the engine with these dimensions may be easier to start, particularly at lower temperatures.

6.6 Revised technical drawings

Appendix D contains a technical detail drawing of the longer connecting rod, as well as assembly drawings with the different crank and connecting rod configurations.

6.7 Discussion of results

A number of modifications were made to the engine but unfortunately the engine failed to run. Although the power output predicted in Chapter 4 was in the range of 750 – 1 000 W, the engine was unable to

produce enough power to rotate even under no load. It should be noted that the maximum temperature which was achieved in testing was only 800° C due to limitations in the heater head material and the heat output of the oxy-acetylene torch. It is possible that if higher temperatures could be achieved the engine might run and further work could explore these possibilities.

As discussed, the literature mentions a few major factors which have a significant impact on the success or failure of a Stirling Engine. Thombare and Verma (2008) state that some of the key considerations affecting engine performance are regenerator effectiveness, working fluid, fluid leakage and fluid friction. The regenerator material and porosity affect both the regenerator effectiveness and fluid friction due to the restriction to the flow of the working gas. Therefore, this aspect of the design may require more consideration as a relatively small copper mesh regenerator was utilised and the porosity was not investigated. Tlili (2012) observed that by increasing the regenerator volume efficiency is improved as more effective heat exchange occurs, and therefore a larger regenerator volume may improve the results. The ability of the working gas to pass through the regenerator was assessed by unscrewing one end of the air connecting tube and compressing the other piston which was still connected to the tube. The working gas was able to flow with minimal restriction noted. Some fluid leakage was noted as air could be heard bypassing the pistons. This may require new cylinders to be fabricated with a tighter tolerance as leakage still occurred even with three compression rings fitted.

The other major contributors to engine performance according to Thombare and Verma (2008) are mean cycle pressure, dead volumes, thermal losses and mechanical losses. It was found that the power output and the mean cycle pressure in a Stirling engine is directly related, and the pressure required to achieve high power values and densities is in the range of 10 to 20 MPa (Erbay & Yavuz, 1997). Therefore, increasing the pressure of the working gas by pressurising the system could lead to better results. Dead volumes have been minimised as much as possible, but they could be reduced further by making the diameter of the connecting air tube smaller and redesigning the heater head. Thermal losses could be reduced by improving the design of the heater head.

Mechanical losses have been minimised as much as possible by lubricating the pistons and bushes and using ball bearings wherever possible. Friction could be further minimised by reducing the number of compression rings fitted to the piston. This was tried during testing however it resulted in too much air leakage past the pistons. Another potential way to reduce losses in the mechanism could be to consider another mechanism altogether. Tlili (2012) investigates the Ross Yoke mechanism and shows that by way of design, this linkage reduces the lateral forces imposed on the pistons by minimising the lateral movement of the connecting rods. Egas & Clucas (2018) suggest that an alpha type engine utilising a Ross Yoke mechanism can achieve higher compression ratios and therefore may be more suited to high temperature applications. Therefore, the use of this mechanism could reduce some of the losses

associated with the crank slider design however high temperatures must be achievable to produce an efficient engine.

The best result in terms of running time occurred in the fourth test. This configuration had the highest dead volume and a shorter crank radius than the original design. Organ (2014) suggests that an increase in the pressure ratio which can occur as a result of a larger dead volume, may lead to a net increase in performance, although little exploration has been made into this phenomenon. Organ (2014) also states that by choosing a lower compression ratio, the mechanical friction in the mechanism is reduced and therefore less power loss would occur. This is in opposition to most Stirling Engine theory such as Cheng & Yang (2012) which suggests that dead volume should be minimised to increase the net work output. This could be a potential explanation for the increased performance in the fourth test, however further investigation is required. Another explanation may be offered by Ross (1993), who suggests that at high compression ratios and high enough hot temperatures, the engine will be harder to start but significant power and speed can be achieved. Therefore, higher hot cylinder temperature and working gas pressure may be required to improve the performance of the original engine design.

As was shown in Egas & Clucas (2018), the volume ratio of the engine should not be higher than the temperature ratio. As the volume ratio of the initial design was 4.62, the temperature ratio will not reach this value until approximately 1 100° C. While it should be noted that an engine can still run despite the volume ratio being higher than the temperature ratio, it will not be as efficient as negative work will be introduced. Therefore, if the volume ratio of the engine was reduced, better performance may result.

6.8 Optimisation

Given the potential sources of power loss discussed in Section 6.7, various optimisations could be made to the engine to improve the performance. Some potential options are listed and discussed below.

SIZE OF REGENERATOR TUBE DIAMETER

As stated in Cheng & Yang (2012), the dead volume should be minimised to improve the net work per cycle. Other literature agrees with this, stating that an exponential drop in power is experienced with an increase in the dead volume (Abdullah et al. 2005). Decreasing the diameter of the connecting air tube would decrease the dead volume the engine. However, as the diameter is decreased, the amount of pressure loss due to fluid friction increases. This is undesirable as a decrease in working gas pressure reduces the work output per cycle. Therefore, a balance must be found between the two losses.

LENGTH OF REGENERATOR

Decreasing the length of the regenerator would also decrease dead volume within the engine. With the design adopted, the length was minimised as much as possible, however further reduction in length may be possible.

IMPROVE DESIGN OF CYLINDER

As mentioned, the internal bore of the cylinder may have a tolerance which is too large, and therefore air is allowed to pass by the pistons on compression. Both Ross (1993) and Organ (2014) emphasize the importance of eliminating air leakage, and therefore this area may be of particular interest for improving the performance of the engine.

IMPROVE DESIGN OF HEATER

Rinker (2018) states that losses at the heater must be minimised in order to maximise the efficiency of a Stirling engine, and the temperature must be high. Also, Hirata et al. (2001) suggest that significant pressure loss can occur at the heater head and may affect engine performance. The heater head has been designed to maximise the amount of surface area in the internal working space while minimising the amount of dead volume that would decrease the pressure. However, a more complex heat exchanger design may be required to deliver sufficient heat at a specified temperature to the working gas and produce more work. For future heater designs, the temperature inside the cylinder could be tested to assess the efficiency of the heat exchanger.

MINIMISE FRICTION IN THE CRANK SLIDER MECHANISM

Any friction in the crank mechanism should be minimised as much as possible to reduce the resistance opposing the piston motion. It is believed that this was achieved quite well with the design as most components were self-aligning and low friction bearings were utilised. Some kinks were noted at certain points in the cycle, particularly when the pistons were moving away from bottom dead centre. The geometry and design of the crank case and cylinders could be modified to improve the support of the piston at this point. Furthermore, an alternative mechanism like the Ross Yoke mechanism could be considered as discussed in Section 6.7.

STARTER MOTOR

The engine was cranked by pulling a rope which was wrapped around the flywheel. Better results may be seen with the use of a starter motor to crank the engine. More rotations could be completed and more initial energy given to the flywheel.

PRESSURISATION OF THE WORKING GAS

As discussed in Section 6.7, pressures in the range of 10 to 20 MPa may be required to achieve high power output density (Erbay & Yavuz, 1997). Gicquel (2011) concurs, stating that control of the machine's power output can be achieved by varying the pressure, and in general this is done to produce very high pressures. Tlili (2012) provides further evidence of this, stating that by increasing the mass of working gas within the engine, more power is achieved. There is a limit however and at some critical value of mass the power starts to decrease due to the increased pressure loss with occurs. Therefore, some investigation into pressurising the working gas during operation may yield a solution which improves the performance of the engine. Given that the maximum expected pressure was 1.5104 MPa, charging the working space to a pressure of 10 MPa will create much higher stresses in the components and may require the redesign of some or all parts.

PHASE ANGLE AND VOLUME RATIO

While it would require a complete redesign of the engine geometry, Organ (2014) suggests that the standard phase angle of 90 degrees and volumetric ratio of one may not necessarily yield the best performance. Adjusting these values may vary the theoretical power output but may improve the performance of the engine.

6.9 Real world applications

Although successful operation of the engine was not achieved, some real-world applications have been investigated should the target power be attained. Given the requirement for a supply of hydrogen fuel, the engine must be located where it has access to a fuel source. Furthermore, careful handling of hydrogen is required, and this should be considered in the design of any hydrogen storage and combustion system.

Electricity generation is a potential application for this engine given that it can produce continuous power output provided that the heat source is maintained. As discussed in Section 4.2, a typical residential solar panel installation in Australia generates 3-5 kW, and therefore the installation of one or more engines coupled with generators could provide a similar amount of electricity. This is extremely prevalent given that the amount of solar panel waste which ends up in landfill is approximately 6 to 7 million tonnes per year in Australia, with an average lifespan of 21 years per panel (Latten & Lillywhite, 2021). Kropiwnicki and Szewczyk (2016) supports the potential for residential installation, stating that typical electricity generation devices which are installed in a residential setting produce less

than 1 kW of power. Therefore, this engine could be utilised in the generating electricity for the residential market.

The engine may be able to replace electric motors in some applications. The engine can be utilised for mechanical propulsion however the nature of the power output must be considered. The engine can provide continuous long term power output, however is unable to achieve rapid changes in speed or power. The power output can be varied by adjusting the temperature of the heat source or adjusting the charge pressure applied to the working space as discussed earlier. Therefore, it can be used in applications where a varied mechanical power source is required.

As outlined in the Literature Review, Stirling Engines are being used for combined heat and power (CHP) applications where heat and electricity are simultaneously generated for different purposes. This type of application can be found in residential, commercial, and industrial applications. Current CHP technologies range from 1 to 5.5 kW and therefore a similar opportunity exists for utilising the hydrogen powered Stirling Engine in this application either as a single engine or multiple can be used to produce more power as required (De Paepe et al., 2006). Thimsen (2002) suggests that most Stirling Engine technology is targeted at base-load or back-up power and the target power output range of 750 – 1 000 W is well suited to relatively small-scaled electricity generation, but as mentioned multiple engine systems can be utilised to generate more power if required.

6.10 Chapter summary

This chapter has outlined the performance of the engine during testing by applying heat to the heater head of the engine. The different responses observed are described after making modifications to the engine in an attempt to get it to run by itself. Revised power calculations and drawings are presented for the modified components and engine assemblies and it can be seen that an engine with a shorter crank radius performed slightly better than the original design, despite the reduction in predicted power output. In the end, the engine failed to run and a discussion has been presented about how to further optimise the engine and what could be hindering its operation. Some potential real world applications have been discussed if the target power output is able to be achieved with optimisation.

Chapter 7

Conclusions and Further Work

7.1 Conclusions

The aims and objectives of the project outlined in Chapter 1 and Appendix A have been addressed in carrying out the required project work and producing this dissertation. Background information and analytical theory on Stirling Engines was gathered in the Literature Review and an understanding of the design requirements and considerations was achieved at this stage. Solar energy as a fuel source for Stirling Engines was researched to understand current technologies, applications engine requirements before hydrogen as a fuel was research to evaluate its potential for powering a Stirling Engine. The properties of hydrogen combustion were obtained and compared with those of concentrated solar to compare the two energy sources and justify the potential for hydrogen in this application. It was found that Stirling Engines can generate significant power when sufficient heat can be generated, and hydrogen combustion is more than capable of achieving these temperatures. Thus, it was concluded that given the applications for concentrated solar Stirling Engines, a hydrogen powered Stirling Engine could be designed, tested, and assessed for commercial viability.

The background information and theory obtained in the Literature Review was then applied in designing a Stirling Engine utilising hydrogen as the fuel source. The configuration selection was justified based on criteria proposed in the literature, and work and power output calculations were completed. The alpha type Stirling Engine was chosen for the configuration and a target power output was chosen based on typical Stirling Engine applications. Various analytical methods were obtained in the Literature Review and analyses were made to determine the work output using the P-V Diagram method, the Schmidt Equation, the Beale Number and the West Number. After calculating and comparing the net work per cycle found using these analyses, the optimum rotational speed was found using the method outlined in Hirata et al. (2001) and thus the expected power output was determined. The lowest predictor of power output was the Beale Number, and the values were within the target power range.

After completing initial calculations, a physical engine was designed, fabricated and tested. Material selections was discussed for each component and the final design was justified by stress analysis and Finite Element Analysis of critical components. Technical detail and assembly drawings were produced for all components and the engine assembly, and were utilised in manufacturing the engine. The engine was tested by heating the heater head of the engine using an oxy-acetylene torch and a maximum

temperature of 800° C was achieved before limitations in the design and heat source occurred. Unfortunately, the engine failed to run by itself during testing and as such the initial power calculations were unable to be verified. Modifications were made to the engine in an attempt to improve its performance and generate results, and while some improvement was seen the engine still would not run. The modifications made are discussed in Chapter 6 and revised power calculations and drawings were completed. Some further suggestions for improvements or modifications to the engine are also outlined to understand why the engine would not run. Despite the engine failing to run, some potential applications have been investigated should the targeted power output be achieved.

7.2 Further work

In order to further progress the hydrogen powered Stirling Engine towards commercial viability, further work is required. The following sections outline potential areas where further work can be conducted which was either outside the scope of this project or continues work already commenced during this project.

7.2.1 Further engine development and testing

As discussed, the engine failed to run during testing despite modifications made to the components. One drawback of the testing process was the limitation to the maximum temperature of 800° C achieved at the heater head. Further design and development could be conducted to increase the temperature achievable and observe the results at higher temperatures.

7.2.2 Optimisation

Optimisation of the engine components can be investigated to improve its performance and reduce losses. Section 6.8 outlines potential areas for optimisation including: size of the regenerator tube diameter; length of the regenerator; cylinder design; heater design; friction in the crank slider mechanism; starter motor; pressurisation of the working gas; and phase angle and volume ratio. These areas have been identified in the literature as major contributing factors to the success of the engine, and further research and development in these aspects may lead to success in terms of engine operation.

7.2.3 Hydraulic combustion system

Although hydrogen was investigated as a fuel source for powering a Stirling Engine in this project, the design and incorporation of a hydrogen combustion system was outside the scope. This will require significant system and control design not just in terms of operation, but also in terms of making the engine viable for applications in industry. Other considerations include delivery of hydrogen fuel to the system, the use of liquid or gaseous hydrogen, and fuel/oxidiser ratio to control the flame temperature.

7.2.4 Commercial viability

The ultimate goal of the concept investigated in this project is the development of a commercially viable engine which can serve a useful purpose in industry while reducing harmful emissions released into the environment. Making the engine commercially viable involves various aspects including but not limited to efficiency, engine life, applications, economic viability and sustainability. Further work can be completed in transitioning the concept from the initial design and testing conducted in this report to a commercially viable engine.

References

Abdullah, S, Yousif, BF & Sopian, K 2005, 'Design consideration of low temperature differential double-acting Stirling engine for solar application', *Renewable energy*, vol. 30, no. 12, pp. 1923-41.

Aggarwal, S 2010, 'Hydrogen-assisted Combustion and Emission Characteristics of Fossil Fuels', in M Lackner, et al. (eds), *Handbook of Combustion: Gaseous and Liquid Fuels*, WILEY-VCH Verlag GmbH & Co. KGaA, Weinheim, vol. 3, pp. 305-57.

Aksoy, F, Karabulut, H, Çınar, C, Solmaz, H, Özgören, YÖ & Uyumaz, A 2015, 'Thermal performance of a Stirling engine powered by a solar simulator', *Applied thermal engineering*, vol. 86, pp. 161-7.

Air and Gas Duct Structural Design Committee 2020, *Structural Design of Air and Gas Ducts for Power Stations and Industrial Boiler Applications*, Second edn, American Society of Civil Engineers, Reston, Virginia.

Australian Trade and Investment Commission 2022, *Australia a global first with dual-fuel hydrogen power plant*, , Australian Government, Canberra, viewed 22 September 2022, <https://www.austrade.gov.au/news/success-stories/australia-a-global-first-with-dual-fuel-hydrogen-power-plant>.

Bapat, SL, Kedare, SB & Shendage, DJ 2011, 'Investigations on Performance of Stirling Engine Regenerator Matrix', *Proceedings of the ASME/JSME 2011 8th Thermal Engineering Joint Conference*, Hawaii, USA.

Bataineh, K 2018, 'Mathematical formulation of alpha -type Stirling engine with Ross Yoke mechanism', *Energy (Oxford)*, vol. 164, pp. 1178-99.

Beer, FP, Johnston, RE, Dewolf, JT & Mazurek, DF 2015, *Mechanics of materials*, Seventh Edition in SI Units. edn, McGraw-Hill Education, New York, NY.

Boretti, A 2021, 'α-Stirling hydrogen engines for concentrated solar power', *International journal of hydrogen energy*, vol. 46, no. 29, pp. 16241-7.

Boundy, AW 2012, *Engineering Drawing*, 8th edition. edn, McGraw-Hill Australia, North Ryde.

Catapano, F, Perozziello, C & Vaglieco, BM 2021, 'Heat transfer of a Stirling engine for waste heat recovery application from internal combustion engines', *Applied thermal engineering*, vol. 198, p. 117492.

Cengel, Y & Boles, M 2015, *Thermodynamics: An Engineering Approach*, 8 edn, McGraw-Hill, New York.

Cengel, Y, Combala, J & Turner, R 2016, *Fundamentals of Thermal-Fluid Sciences*, 5 edn, McGraw-Hill, New York.

Cheng, CH & Yang, HS 2012, 'Optimization of geometrical parameters for Stirling engines based on theoretical analysis', *Applied energy*, vol. 92, pp. 395-405.

Department of Climate Change, Energy, the Environment and Water 2022, *Photovoltaic systems*, Australian Government, Canberra, viewed 26 September 2022, < https://www.yourhome.gov.au/energy/photovoltaic-systems>.

De Paepe, M, D'Herdt, P & Mertens, D 2006, 'Micro-CHP systems for residential applications', *Energy conversion and management*, vol. 47, no. 18, pp. 3435-46.

Dinesh, K, Gowtham, RR, Naresh, M, Rakesh, N & Sriram, R 2014, 'Design and Fabrication of Low Cost Stirling Engine for Low Duty Industrial Applications', *International Journal of Scientific & Technology Research*, vol. 3, no. 3, pp. 75-78.

Dong, H, Guo, J, Liu, J, Meng, T, Li, M, Chen, X, Li, N & Alavi, H 2021, 'Energy generation and storing electrical energy in an energy hybrid system consisting of solar thermal collector, Stirling engine and thermoelectric generator', *Sustainable cities and society*, vol. 75, p. 103357.

Drell, I & Belles, F 1958, *Survey of hydrogen combustion properties*, Washington.

Egas, J & Clucas, DM 2018, 'Stirling engine configuration selection', *Energies (Basel)*, vol. 11, no. 3, p. 584.

Erbay, LB & Yavuz, H 1997, 'Analysis of the stirling heat engine at maximum power conditions', *Energy (Oxford)*, vol. 22, no. 7, pp. 645-50.

Ertas, A & Jones, JC 1996, *The engineering design process*, 2nd ed. edn, Wiley, New York.

Formosa, F & Despesse, G 2010, 'Analytical model for Stirling cycle machine design', *Energy conversion and management*, vol. 51, no. 10, pp. 1855-63.

FSEC 2014, *Hydrogen Basics*, University of Central Florida, Florida, viewed 22 May, <http://www.fsec.ucf.edu/en/consumer/hydrogen/basics/utilization.htm>.

Furmanek, M & Kropiwnicki, J 2021, 'Stirling engines - the state of technology development and computational models', *Combustion Engines*.

Gadré, I & Maiorana, J 2014, *Price Model of the Stirling Engine*, Bachelor Thesis, KTH School of Industrial Engineering and Management, Stockholm, viewed 23 August 2022, <https://www.diva-portal.org/smash/get/diva2:735271/FULLTEXT01.pdf>.

Gicquel, R 2011, *Energy systems: a new approach to engineering thermodynamics*, First edition. edn, CRC Press, an imprint of Taylor and Francis, Boca Raton, FL.

He, MM 2016, 'Stirling Engine for Solar Thermal Electric Generation', ProQuest Dissertations Publishing.

Hirata, K 1998, *Simple Performance Prediction Method for Stirling Engine*, Koichi Hirata, Japan, viewed 23 July 2022, <http://www.bekkoame.ne.jp/~khirata/academic/simple/simplee.htm>.

Hirata, K, Iwamoto, S & Toda, F 2001, 'Performance of Stirling Engines', *JSME International Journal*, vol. 44, no. 1, pp. 140-7.

Hoag, K & Dondlinger, B 2016, *Vehicular engine design*, Second edition. edn, Springer, New York.

Hosford, WF 2010, *Solid mechanics*, Cambridge University Press, Cambridge.

Ipci, D & Karabulut, H 2018, 'Thermodynamic and dynamic analysis of an alpha type Stirling engine and numerical treatment', *Energy conversion and management*, vol. 169, pp. 34-44.

Johansson, P 2019, *New piston ring solution for Stirling engines*, Master's thesis, Lulea University of Technology.

Juvinall, RC & Marshek, KM 2012, *Fundamentals of machine component design*, 5th ed. edn, John Wiley & Sons, Hoboken, NJ.

Keveny, M 2011, *Animated Engines*, viewed 14 January, <http://animatedengines.com/>.

Kiesgen, G, Leinhos, D & Rottengruber, H 2008, 'Internal Combustion Engines', in A Zuttel, et al. (eds), *Hydrogen as a Future Energy Carrier*, WILEY-VCH Verlag GmbH & Co. KGaA, Weinheim, pp. 371-80.

Kolin, I 1991, *Stirling Motor: History-Theory-Practice*, Inter University Center, Dubrovnik, Croatia.

Kropiwnicki, J & Szewczyk, A 2016, 'Stirling Engines Powered by Renewable Energy Sources', *Applied Mechanics and Materials*, vol. 831, no. Advances in Mechanical and Energy Engineering, pp. 263-9.

Laazaar, K & Boutammachte, N 2020, 'New approach of decision support method for Stirling engine type choice towards a better exploitation of renewable energies', *Energy conversion and management*, vol. 223, p. 113326.

Latten, M & Lillywhite, B 2021, *Solar panel waste: where are we heading?*, Corrs Chambers Westgarth, Sydney, Australia, viewed 2 October 2022, <https://www.corrs.com.au/insights/solar-panel-waste-where-are-we-heading>.

Lister 2000, *Instruction Manual & Parts List: Air Cooled Diesel Engines*, Book 1029/470, Hawker Siddeley, Dursley, England.

Lovegrove, K, Nathan, G & Zapata, J 2022, *Concentrating solar thermal*, Australian Academy of Science, Australia, viewed 23 May, <https://www.science.org.au/curious/technology-future/concentrating-solar-thermal>.

Martini, W 1983, *Stirling Engine Design Manual*, 2 edn, US Department of Energy, Washington.

MEC4104 2021, *Renewable Energy Technology: course notes*, University of Southern Queensland, Toowoomba.

Moya, EZ 2012, 'Parabolic-trough concentrating solar power (CSP) systems', in pp. 197-239.

NTN Corporation 2020, *Ball and Roller Bearings*, Cat. No. 2203/E, NTN Corporation, Japan.

Organ, AJ 2014, *Stirling cycle engines: inner workings and design*, John Wiley & Sons Inc., Chichester, West Sussex, United Kingdom.

Puech, P & Tishkova, V 2011, 'Thermodynamic analysis of a Stirling engine including regenerator dead volume', *Renewable energy*, vol. 36, no. 2, pp. 872-8.

Rand, DAJ, Rand, DAJ & Dell, RM 2007, *Hydrogen Energy: challenges and prospects*, vol. 1, NBN International, Cambridge.

Reddy, DS & Khan, MK 2022, 'Stationary point focus solar concentrators—A review', *International journal of energy research*, vol. 46, no. 5, pp. 5678-702.

RedFluid 2022, *The definitive guide to differentiate BSPP or Gas, BSPT, and NPT threads*, RedFluid, Spain, viewed 24 August 2022, < https://redfluid.es/en/differences-bspp-gas-bspt-npt-threads/>.

Rinker, GT 2018, 'Design and Optimization of a 1 kW Stirling Engine', ProQuest Dissertations Publishing.

Ross, A 1993, *Making Stirling Engines*, Ross Experimental, Ohio.

Rutczyk, B, Szczygieł, I & Kabaj, A 2020, 'Evaluation of an α type stirling engine regenerator using a new differential model', *Energy (Oxford)*, vol. 209, p. 118369.

Schefer, RW, White, C & Keller, J 2008, 'Lean Hydrogen Combustion', in D Dunn-Rankin (ed.), *Lean Combustion: Technology and Control*, Elsevier, San Diego, California, pp. 213-54.

Senft, JR 2002, 'Optimum Stirling engine geometry', *International journal of energy research*, vol. 26, no. 12, pp. 1087-101.

Senviboon, V, Silpsakoolsook, B & Kwankaomeng, S 2018, 'Optimization of geometrical parameter for V-type alpha Stirling engine based on dimensionless analysis', *MATEC Web of Conferences*, vol. 192, p. 2044.

Thimsen, D 2002, *Stirling Engine Assessment*, Electric Power Research Institute, California.

Thombare, DG & Verma, SK 2008, 'Technological development in the Stirling cycle engines', *Renewable & sustainable energy reviews*, vol. 12, no. 1, pp. 1-38.

Thombare, DG & Karmare, SV 2012, 'Theoretical and experimental investigation of Alfa type bio mass Stirling engine with effect of regenerator effectiveness, heat transfer, and properties of working fluid', *Journal of renewable and sustainable energy*, vol. 4, no. 4, p. 43126.

Tlili, I 2012, 'A numerical investigation of an alpha stirling engine using the ross yoke linkage', *Heat and Technology*, vol. 30, no. 1, pp. 23-35.

Twidell, J & Weir, T 2015, *Renewable Energy Resources*, 3 edn, Routledge, Oxon.

Urieli, I & Berchowitz, D 1984, *Stirling cycle engine analysis*, Adam Hilger Ltd, Bristol.

Valves Tubes Fittings 2022, *3" 3000lb NPT Black Carbon Steel Sch80 Barrel Nipple (4" Long)*, Valves Tubes Fittings, Bolton, England, viewed 27 August 2022, <https://www.valvestubesfittings.com/screwed-pipe-fittings/black-threaded-3000lb-fittings/3000lb-black-threaded-barrel-nipples/npt-sch80-barrel-nipple-4-inches-long-threaded-both-ends-black-bs3799-astm-a106-6254n080>.

Verhoeven, JD 2007, *Steel metallurgy for the non-metallurgist*, ASM International, Materials Park, OH.

Vineeth, C 2012, *Stirling Engines: A Beginner's Guide*, College of Engineering Thiruvananthapuram, Thiruvananthapuram.

Walker, G 1994, *The Stirling alternative: power systems, refrigerants, and heat pumps*, Gordon and Breach Science, Yverdon, Switzerland.

Wessels, WR 2010, *Practical reliability engineering and analysis for system design and life-cycle sustainment*, CRC Press, Boca Raton, Fla.

Wischnewski, B 2022, *Calculation of thermodynamic state variables of air*, Peace Software, Berlin, Germany, viewed 23 July 2022, <https://www.peacesoftware.de/einigewerte/luft_e.html>.

Wu, F, Chen, L, Wu, C & Sun, F 1998, 'Optimum performance of irreversible stirling engine with imperfect regeneration', *Energy conversion and management*, vol. 39, no. 8, pp. 727-32.

Yetter, RA, Glassman, I & Glumac, NG 2014, *Combustion*, Academic Press.

Zhu, S, Yu, G, Liang, K, Dai, W & Luo, E 2021, 'A review of Stirling-engine-based combined heat and power technology', *Applied energy*, vol. 294, p. 116965.

Appendix A

Project Specification and Timeline

Appendix A contains the Project Specification and Timeline which were produced during the planning phase.

ENG4111/4112 Research Project

Project Specification

For: Michael Sheehan

Title: Fabrication and design of a Stirling Engine powered by hydrogen

Major: Mechanical Engineering

Supervisors: Dr. Belal Yousif

Enrollment: ENG4111 – EXT S1, 2022

ENG4112 – EXT S2, 2022

Project Aim: To investigate the potential of using hydrogen as a fuel source for powering a Stirling Engine, and to design and fabricate a Stirling Engine to evaluate its performance and suitability for use in real world applications.

Programme: Version 1, 16th March 2022

Objectives

1. Research background information relating to Stirling Engine types and applications.
2. Evaluate literature on using hydrogen as a fuel source and identify the maximum difference in temperature which can be attained for powering the engine.
3. Evaluate literature on using solar concentration technology to generate heat from solar energy.
4. Compare maximum temperature difference achievable using solar or hydrogen as the input fuel source.
5. Select best engine configuration depending on fuel source input temperature.
6. Design engine parameters depending on power output requirements.
7. Research potential materials which could be utilised for engine components.
8. Design engine components and produce drawings for manufacture.
9. Fabricate and test the engine by simulating the temperature difference achievable with hydrogen as a fuel source.
10. Analyse data from testing and compare results with expected values from earlier calculations.
11. Evaluate suitability of the engine for use in real world applications.

If time and resource permit:

12. Optimisation of the engine components and parameters.
13. Research the hydrogen combustion process and technology and consider its incorporation within the engine.
14. Research the typical power generated by a PV solar system and compare with a hydrogen powered Stirling Engine.

Task	ENG4111 - Semester 1																			ENG4112 - Semester 2													
	Week (commencing 21 Feb 2022)																																
	1	2	3	4	5	6	7	8	9	10	11	12	13	14	15	16	17	18	19	20	21	22	23	24	25	26	27	28	29	30	31	32	33	34	35
1. Project Preparation phase																																			
Receive approval for project - Submit Planning Document 1																																			
Planning and preparation - Submit Planning Document 2																																			
Literature review - research Stirling Engines and potential fuel sources (hydrogen and solar)																																			
Evaluate and compile relevant literature with applicable equations																																			
Outline methodology, detailed risk assessment, identify resource requirements, revise project timeline																																			
Submit project progress report																																			
2. Calculation and Design of Prototype																																			
Calculate maximum temperatures with different fuel sources and compare, consider power requirements and applications																																			
Calculate engine parameters																																			
Detailed engine design and method of testing																																			
Acquire resources																																			
3. Fabrication and Testing																																			
Fabricate engine and test jig																																			
Test engine and collect data																																			
Modify prototype as required and retest																																			
Collate data in graphs, tables, figures etc																																			
4. Analysis of Results																																			
Analyse data and results																																			
Compare initial calculations with experiment data																																			
Evaluate engine for use in real world applications, research further if necessary																																			
(Time permitting) Optimisation of the engine and retest																																			
(Time permitting) Research hydrogen combustion process and consider incorporation within engine, reconsider design if necessary																																			
(Time permitting) Research typical PV solar system and compare with SE, reconsider design if necessary																																			
5. Dissertation and presentation of results																																			
Prepare discussion and link with literature review and results																																			
Prepare draft dissertation																																			
Presentation in Professional Practice 2																																			
Submit completed dissertation																																			

Appendix B

Risk Management Plan

Appendix B contains the Risk Management Plan which was produced and authorized for managing risk throughout the project.

University of Southern Queensland — Read Only View

USQ Safety Risk Management System

Close | Develop as new RMP

Version 2.0

Safety Risk Management Plan

Risk Management Plan ID:	Status:	Current User:	Author:	Supervisor:	Approver:
RMP_2022_6748	Approve	i:0#.w|usq\[redacted]	i:0#.w|usq\[redacted]	i:0#.w|usq\[redacted]	i:0#.w|usq\[redacted]

Assessment Title:	SRMP for Research Project	Assessment Date:	14/03/2022
Workplace (Division/Faculty/Section):	204070 - School of Mechanical and Electrical Engineering	Review Date:	(5 years maximum)

Approver:	Supervisor: (for notification of Risk Assessment only)
Belal Yousif;	Belal Yousif;

Context

DESCRIPTION:

What is the task/event/purchase/project/procedure?	ENG4111/4112 Research Project & Dissertation		
Why is it being conducted?	Undergraduate Dissertation		
Where is it being conducted?	Toowoomba, QLD		
Course code (if applicable)	ENG4111 & ENG4112	Chemical Name (if applicable)	

WHAT ARE THE NOMINAL CONDITIONS?

Personnel involved	Michael Sheehan
Equipment	Heating Device, Power Measuring Device, Data Recording Device, Computer, Hand Tools, Power Tools, Stirling Engine Test Model
Environment	Test Lab or Workshop
Other	
Briefly explain the procedure/process	Stirling Engine to be fabricated and tested for power output. Manufacture of the components of the engine will be completed by qualified tradesmen or USQ staff. Most components will require machining or fabrication which will be completed by a professional. After the engine components have been made, I (the student) will need to assemble the engine onto a test jig. This may require some hand tools and/or power tools. Heat must be provided to the engine using a heating device, and the power output measured using a suitable device. Data will be recorded and output to a computer. A computer will also be required for design and drafting of the engine. As well as research and producing documentation etc.

Assessment Team - who is conducting the assessment?

Assessor(s):	Belal Yousif
Others consulted: (eg elected health and safety representative, other personnel exposed to risks)	

Risk Matrix

Probability	Consequence				
	Insignificant No Injury 0-$5K	Minor First Aid $5K-$50K	Moderate Med Treatment $50K-$100K	Major Serious Injury $100K-$250K	Catastrophic Death More than $250K
Almost Certain 1 in 2	M	H	E	E	E
Likely 1 in 100	M	H	H	E	E
Possible 1 in 1,000	L	M	H	H	H
Unlikely 1 in 10,000	L	L	M	M	M
Rare 1 in 1,000,000	L	L	L	L	L

Recommended Action Guide	
Extreme:	**E**= Extreme Risk – Task ***MUST NOT*** proceed
High:	**H** = High Risk – Special Procedures Required (Contact USQSafe) Approval by VC only
Medium:	**M**= Medium Risk - A Risk Management Plan/Safe Work Method Statement is required
Low:	**L**= Low Risk - Manage by routine procedures.

Risk Register and Analysis

	Step 1	Step 2	Step 2a	Step 2b	Step 3			Step 4				
	Hazards: From step 1 or more if identified	The Risk: What can happen if exposed to the hazard without existing controls in place?	Consequence: What is the harm that can be caused by the hazard without existing controls in place?	Existing Controls: What are the existing controls that are already in place?	Risk Assessment: Consequence x Probability = Risk Level			Additional Controls: Enter additional controls if required to reduce the risk level	Risk assessment with additional controls: Has the consequence or probability changed?			
					Probability	Risk Level	ALARP		Consequence	Probability	Risk Level	ALARP
	Example											
	Working in temperatures over 35^{0} C	Heat stress/heat stroke/exhaustion leading to serious personal injury/death	catastrophic	Regular breaks, chilled water available, loose clothing, fatigue management policy.	possible	high	No	temporary shade shelters, essential tasks only, close supervision, buddy system	catastrophic	unlikely	mod	Yes
1	Heating device	Burns/Skin injuries	Moderate	Isolate heating device so it can't be touched, warning signals on device to show when it is hot	Unlike	Med ...	☐	First aid kit nearby, warning signs around area, complete isolation of heating unit	Moder	Rare	Low	☑
2	Sharp tools/abrasives	Cuts/Lacerations /Abrasions	Minor	Wear appropriate PPE when using sharp tools or abrasives, use tools appropriately and in a safe manner	Possib	Med ...	☐	First aid kit nearby	Minor	Unlil	Low	☑
3	Power measuring device	Electrical shock/Injury to hands	Moderate	Make sure device is used properly and safely, isolate all electrical components so they can't be touched, build covers over rotating test parts so no injury can occur	Unlike	Med ...	☐	First aid kit nearby, wear appropriate PPE	Moder	Rare	Low	☑
4	Reciprocating parts	Injury to body parts	Minor	Build covers over reciprocating parts so that they can't be touched, include warning signs	Unlike	Low	☐					☑
5	Hot engine parts	Burns/Skin injuries	Moderate	Build covers over all hot parts to restrict access, wear appropriate PPE when conducting tests, warning signs	Unlike	Med ...	☐					☑
6	Power tools	Cuts/Lacerations /Abrasions	Moderate	Wear appropriate PPE, work safely, ensure safety guards are fitted	Unlike	Med ...	☐	First aid kit nearby	Moder	Unlil	Me ...	☑
7	Computer ergonomics	Muscle or skeletal pain	Insignifica	Take regular breaks, use good posture	Rare	Low	☐					☑

Step 5 - Action Plan (for controls not already in place)

	Additional Controls:	Exclude from Action Plan: (repeated control)	Resources:	Persons Responsible:	Proposed Implementation Date:
1	First aid kit nearby, warning signs around area, complete isolation of heating unit	☐	First Aid Kit, Warning Signs, Covers or guards	Michael Sheehan	16/03/2022
2	First aid kit nearby	☑			
3	First aid kit nearby, wear appropriate PPE	☑			
6	First aid kit nearby	☑			

Supporting Attachments

View Attachments

Click here to attach a file

Step 6 – Request Approval

Drafters Name: Michael Sheehan

Draft Date: 14/03/2022

Drafters Comments:

Assessment Approval: All risks are marked as ALARP

Maximum Residual Risk Level: Medium - Cat 4 delegate or above Approval Required

Document Status: Approve

Step 6 – Approval

Approvers Name: Belal Yousif

Approvers Position Title:

Approvers Comments:

I am satisfied that the risks are as low as reasonably practicable and that the resources required will be provided.

Approval Decision: Approve

Approve / Reject Date: 14/03/2022

Document Status: Approve

Appendix C

Detail and Assembly Drawings of Engine Design

Appendix C contains all detail and assembly drawings produced for manufacturing the Stirling engine as outlined in Chapter 5.

ITEM NO.	DESCRIPTION	DRAWING NUMBER	QTY.
1	ENGINE BODY	MS-SE-03	1
2	HOT CYLINDER	MS-SE-01	1
3	COLD CYLINDER	MS-SE-02	1
4	REGENERATOR TUBE	MS-SE-10	1
5	COVER	MS-SE-11	1
6	PISTON CONROD ASSEMBLY	MS-SE-16	2
7	CRANK PIN	MS-SE-05	1
8	OUTPUT SHAFT ASSEMBLY	MS-SE-19	1
9	CONROD SHIM	MS-SE-20	3
10	17mm EXTERNAL CIRCLIP		2
11	FLYWHEEL SHAFT ASSEMBLY	MS-SE-17	1
12	HEATER HEAD	MS-SE-15	1
13	M8 x 10 GRUB SCREW		2
14	M12 x 35 BOLT GR8.8 w/ NYLOC NUT & WASHER 2x		8
15	M10 x 40 BOLT GR8.8 w/ NYLOC NUT & WASHER 2x		12
16	M12 x 50 BOLT GR8.8 w/ NYLOC NUT & WASHER 2x		4
17	M6 x 12 BOLT GR8.8 w/ SPRING WASHER		4

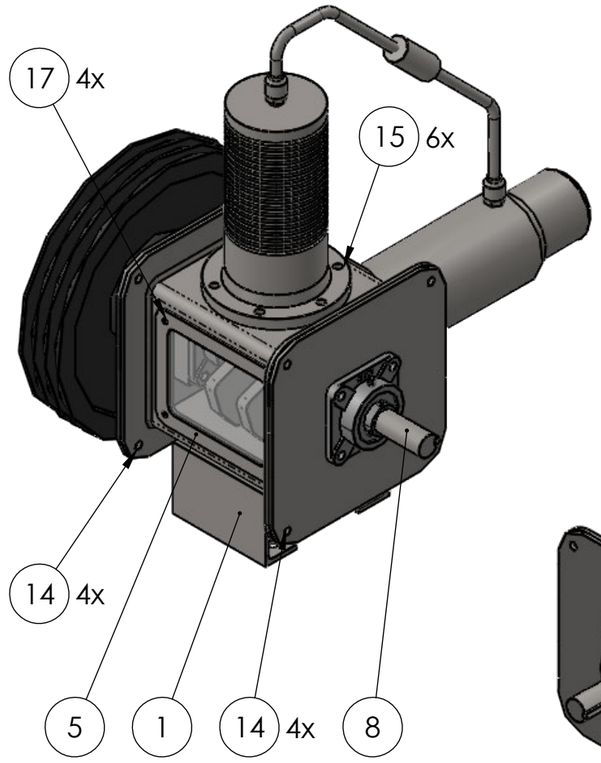

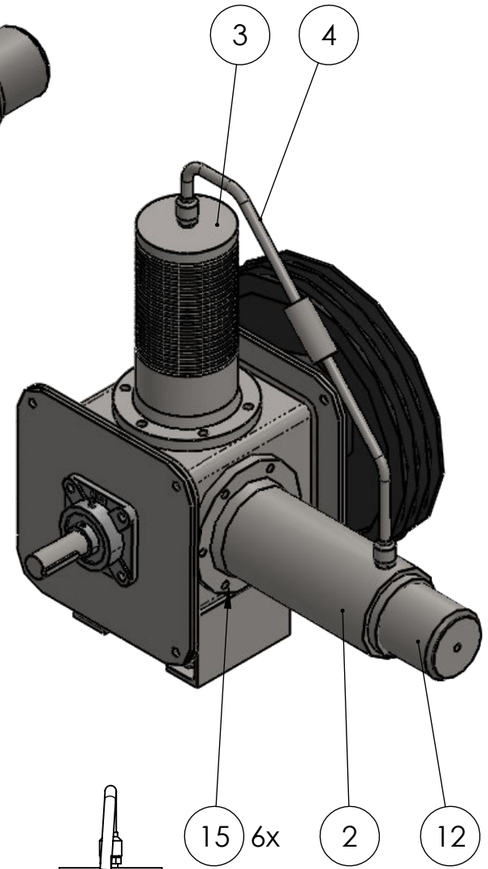

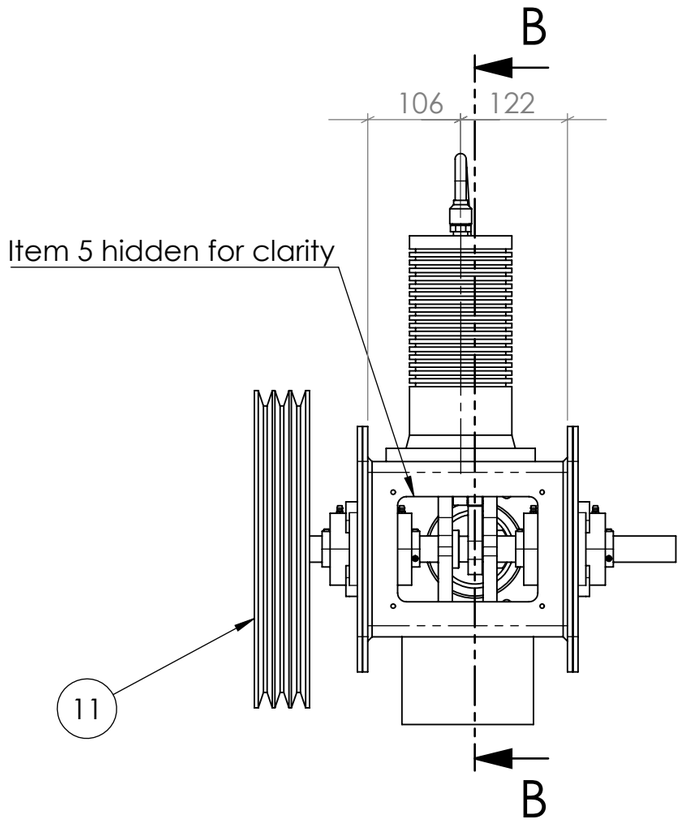

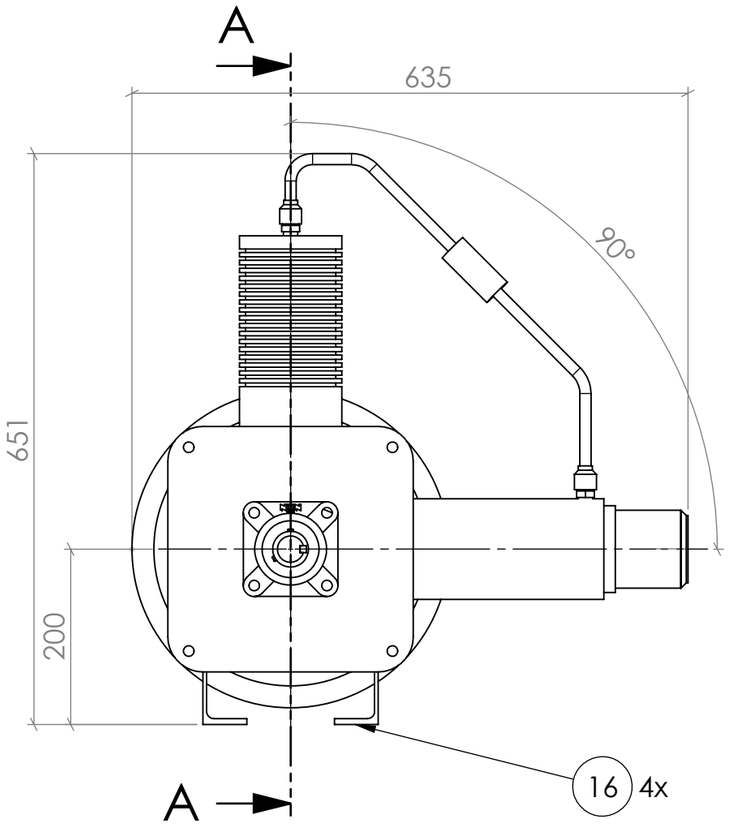

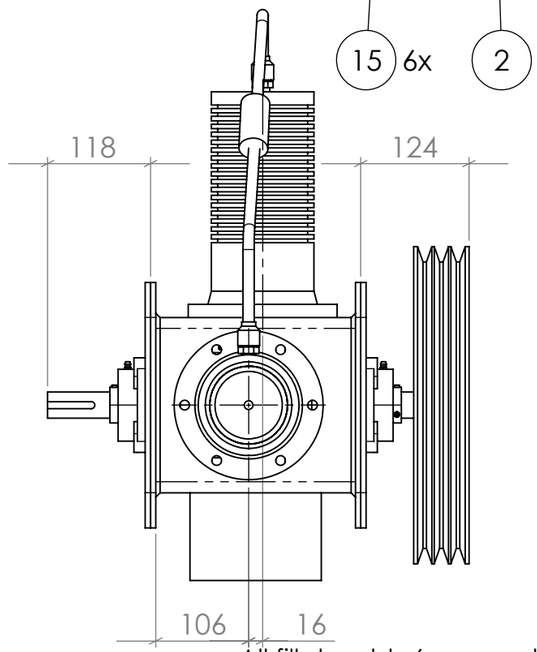

All fillet welds 6mm continuous U.N.O.

APPROVED FOR CONSTRUCTION
SIGNED:
DATE: / /
Drawing is not valid unless signed

No.	DATE	CHANGES	BY
-	-		

3RD ANGLE PROJECTION U.N.O.
ALL DIM'S IN mm U.N.O.
DO NOT SCALE

Drawn: MJS
Date: Sep 22
Scale: 1:7

SITE 6 , 528-560 ALDERLEY Street.
TOOWOOMBA, QLD 4350 Australia.
Fax: (07) 46352004
Phone: (07) 46352660
EMAIL:

Michael Sheehan
STIRLING ENGINE GENERAL ASSEMBLY
SHEET 1 OF 2
Job Number:

Drawing No. **MS-SE-GA**
Rev. -

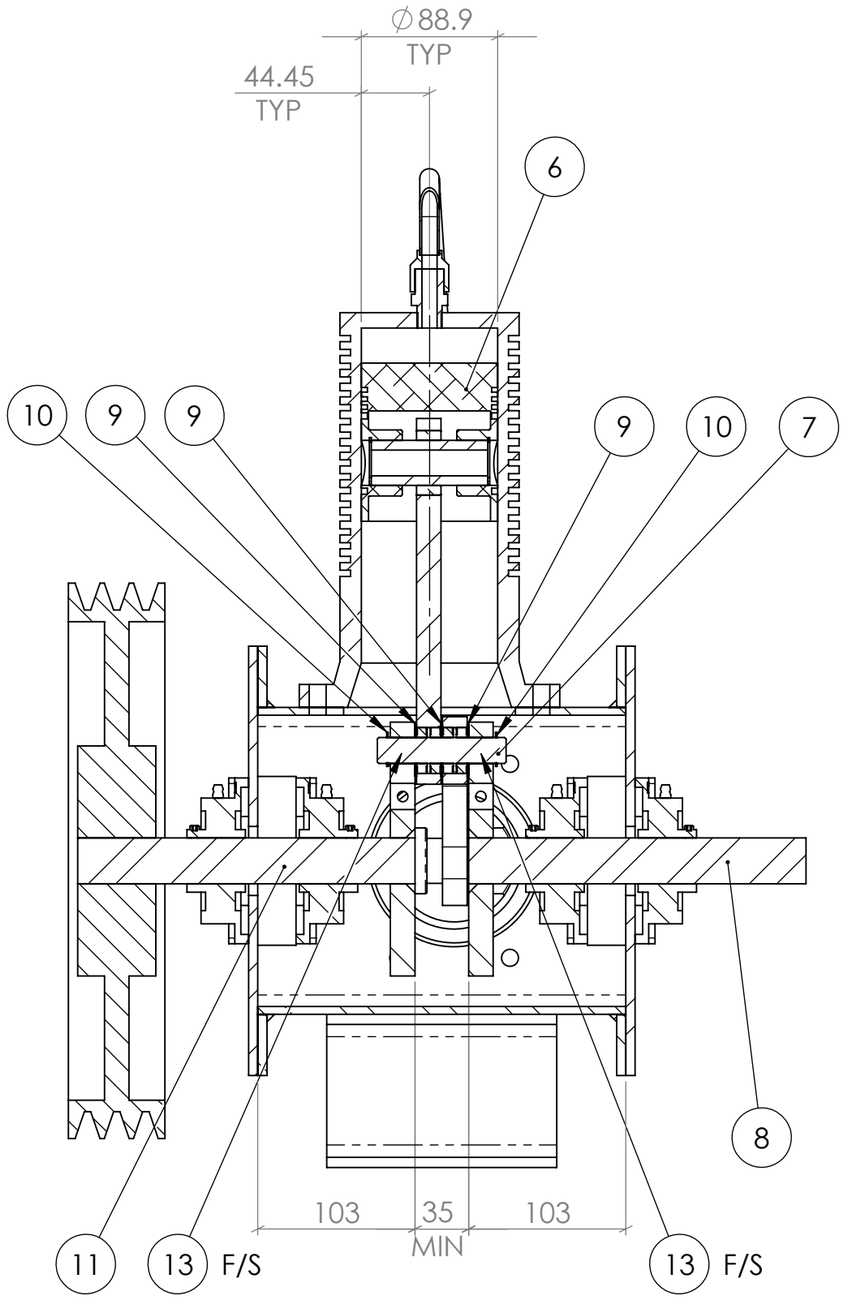

SECTION A-A

SCALE 1 : 4

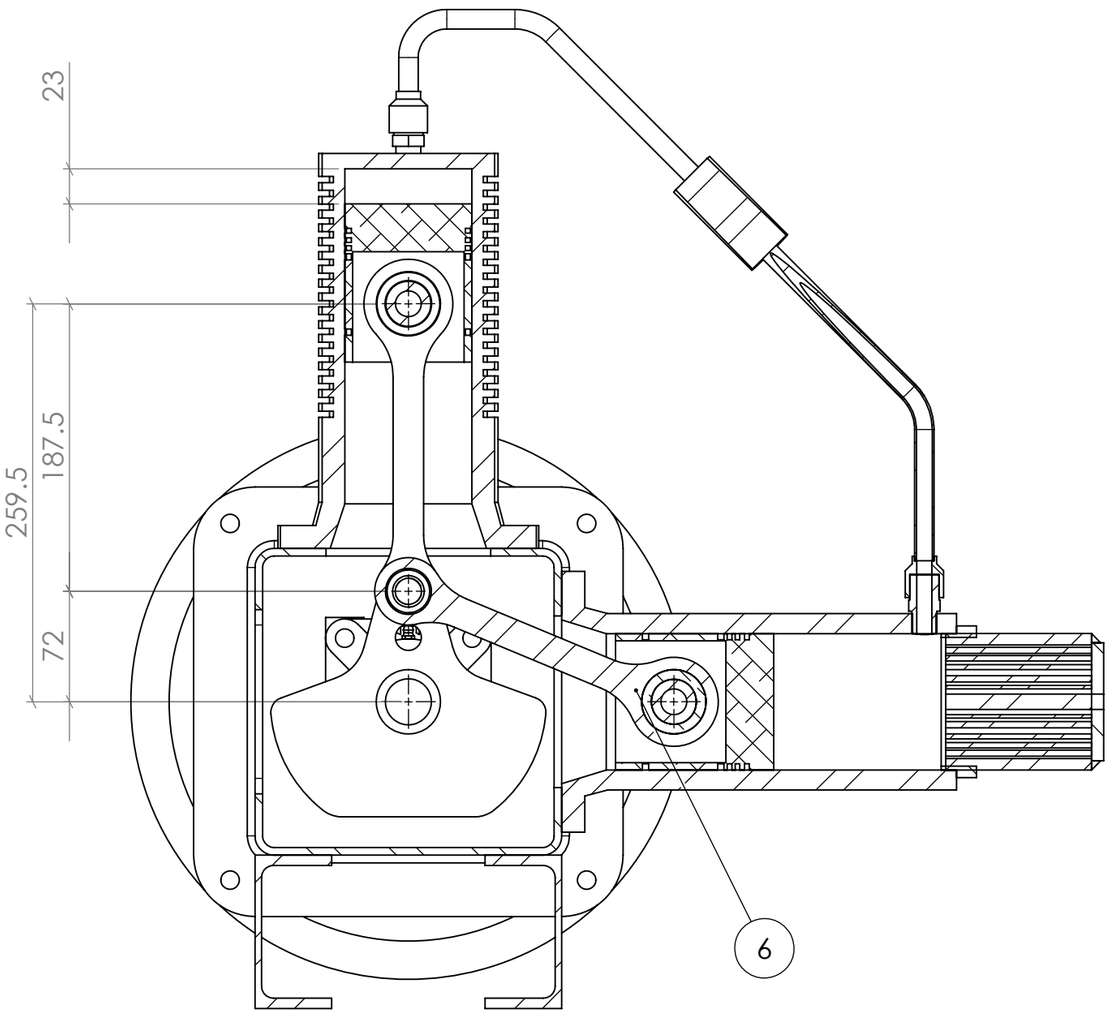

SECTION B-B

SCALE 1 : 4

All fillet welds 6mm continuous U.N.O.

APPROVED FOR CONSTRUCTION
SIGNED:
DATE: / /
Drawing is not valid unless signed

No.	DATE	CHANGES	BY
-	-		

3RD ANGLE PROJECTION U.N.O.
ALL DIM'S IN mm U.N.O.
DO NOT SCALE

Drawn: MJS
Date: Sep 22
Scale: 1:7

SITE 6 , 528-560 ALDERLEY Street.
TOOWOOMBA, QLD 4350 Australia.
Fax: (07) 46352004
Phone: (07) 46352660
EMAIL:

OZTEC Manufacturing
STIRLING ENGINE
GENERAL ASSEMBLY
SHEET 2 OF 2
Job Number:

Drawing No. **MS-SE-GA**
Rev. **-**

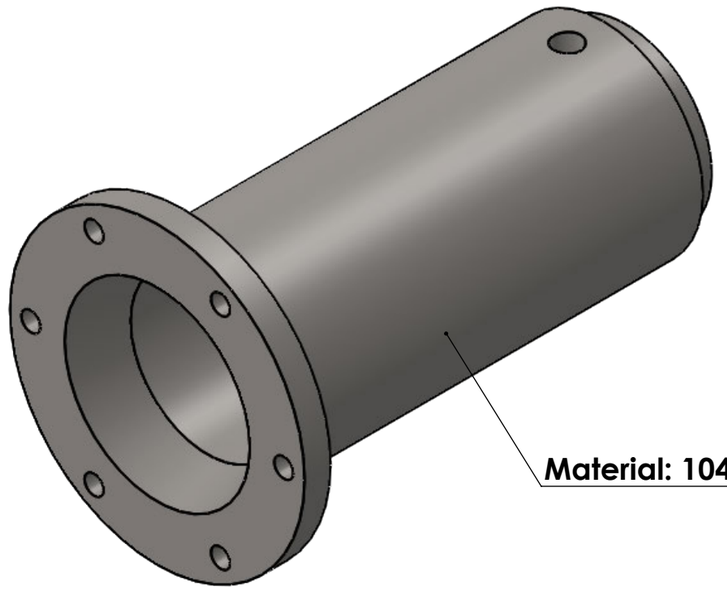

Material: 1045 Black Steel Bar

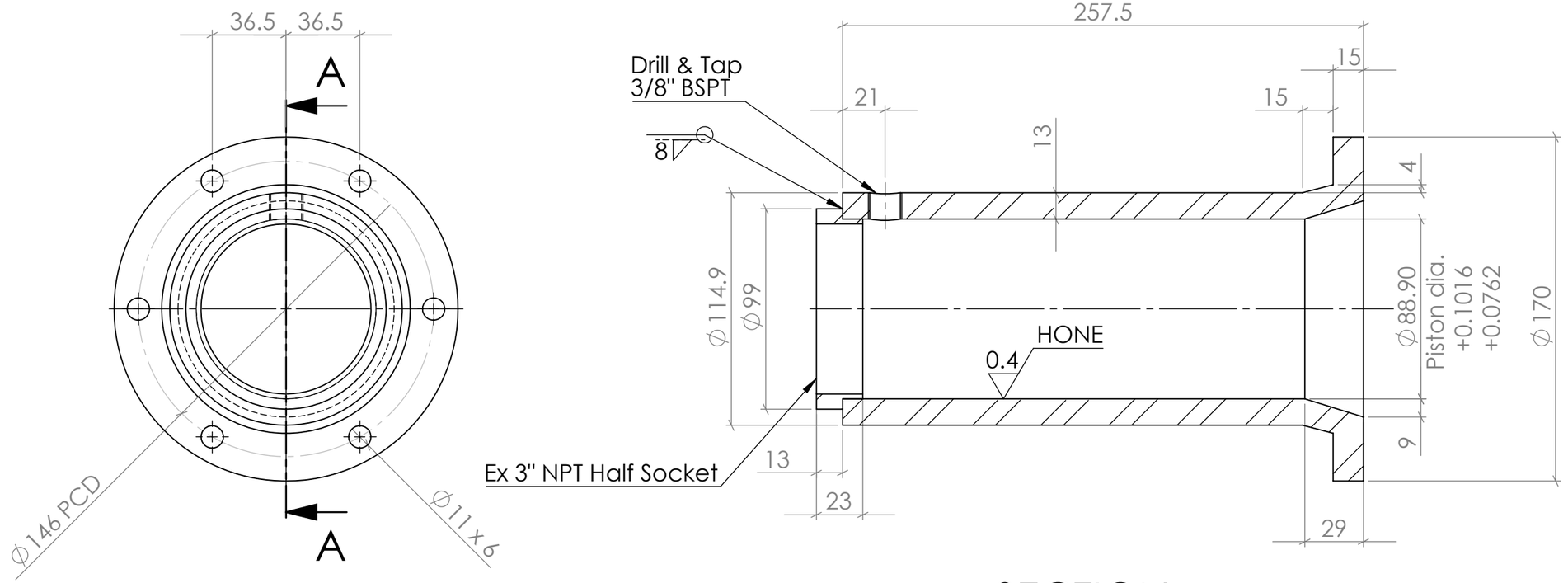

SECTION A-A

All fillet welds 6mm continuous U.N.O.

APPROVED FOR CONSTRUCTION

SIGNED:

DATE: / /

Drawing is not valid unless signed

No.	DATE	CHANGES	BY
B	Sept 22	Added welded half socket	MJS
A	Aug 22	Changed bore tolerance	MJS

3RD ANGLE PROJECTION U.N.O.

ALL DIM'S IN mm U.N.O.

DO NOT SCALE

Drawn: MJS

Date: July 2022

Scale: 2:5

USQ ENG4111/2 Research Project
TOOWOOMBA, QLD 4350 Australia
Student Number: 0061080388
Ph: 0455142395
EMAIL: U1080388@umail.usq.edu.au

Michael Sheehan

Stirling Engine

HOT CYLINDER

SHEET 1 OF 1

Job Number:

Drawing No. **MS-SE-01**

Rev. **B**

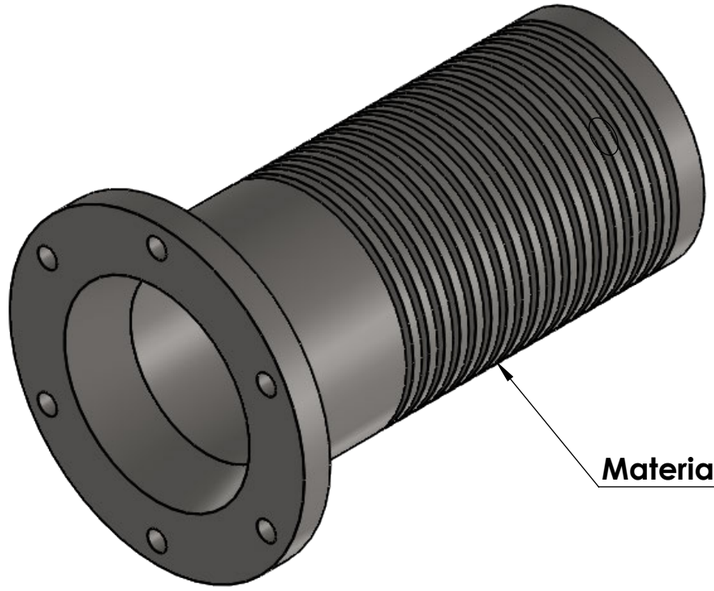

Material: 1045 Black Bar

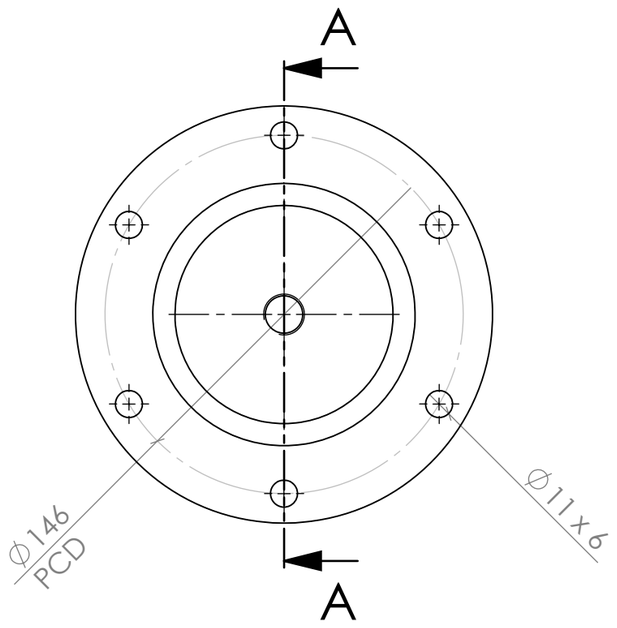

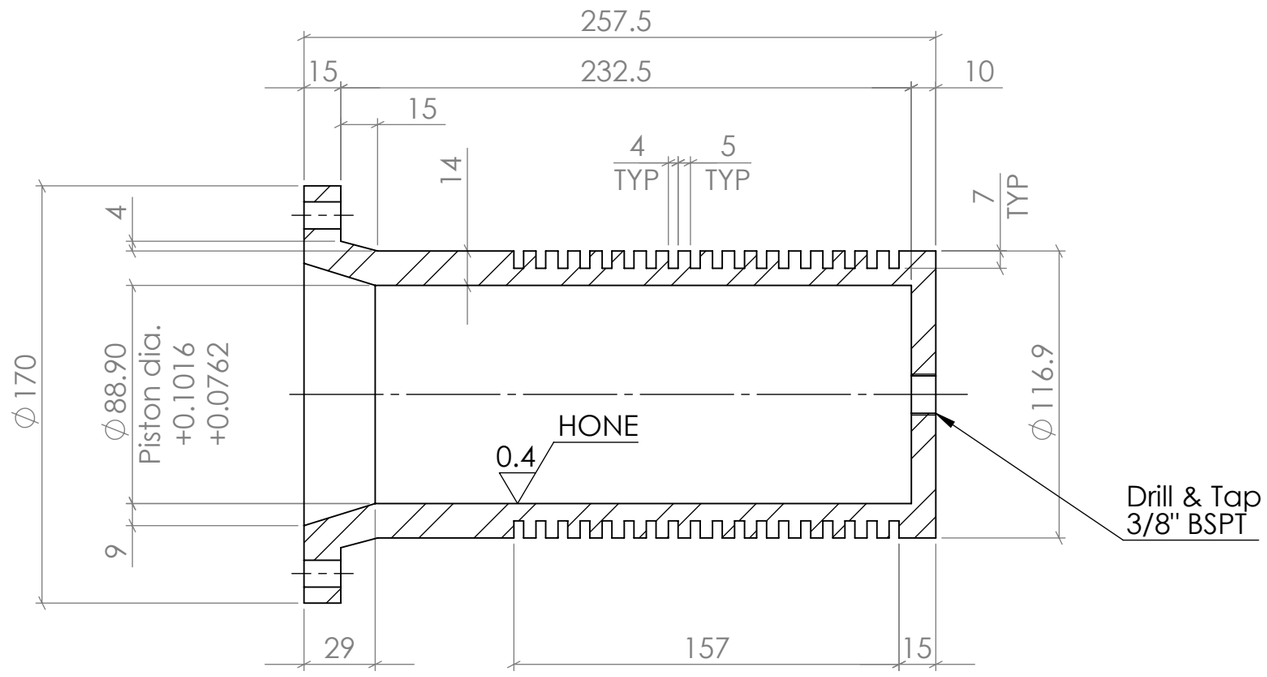

SECTION A-A

All fillet welds 6mm continuous U.N.O.

APPROVED FOR CONSTRUCTION
SIGNED:
DATE: / /
Drawing is not valid unless signed

No.	DATE	CHANGES	BY
A	Aug 22	Changed bore tolerance	MJS

3RD ANGLE PROJECTION U.N.O.
ALL DIM'S IN mm U.N.O.
DO NOT SCALE

Drawn: MJS
Date: July 2022
Scale: 2:5

USQ ENG4111/2 Research Project
TOOWOOMBA, QLD 4350 Australia
Student Number: 0061080388
Ph: 0455142395
EMAIL: U1080388@umail.usq.edu.au

Michael Sheehan
Stirling Engine
COLD CYLINDER
SHEET 1 OF 1
Job Number:

Drawing No. **MS-SE-02**
Rev. **A**

ITEM NO.	QTY.	DESCRIPTION	LENGTH
1	1	200x200x5.0 SHS	240
2	2	STEEL PLATE GR250, 6 x 280 x 280	
3	2	100 PFC	150

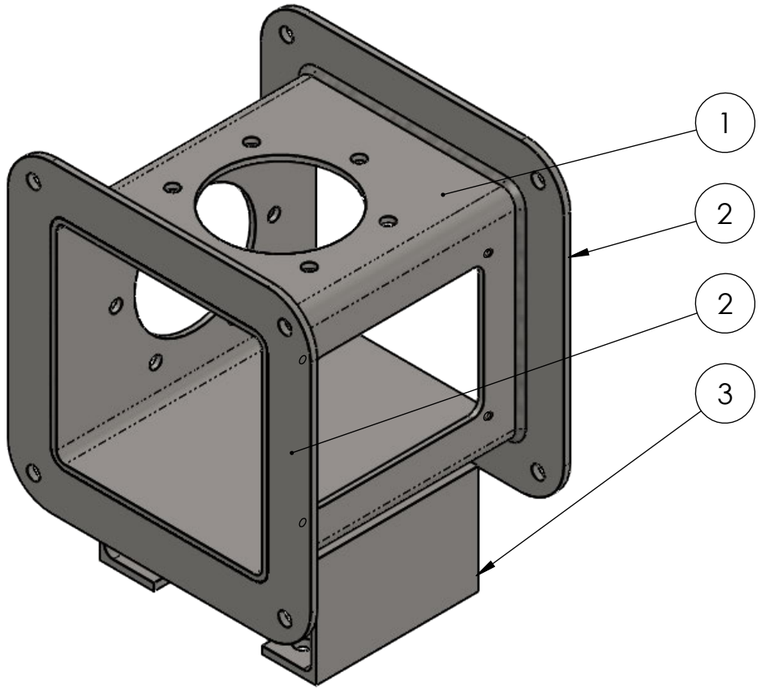

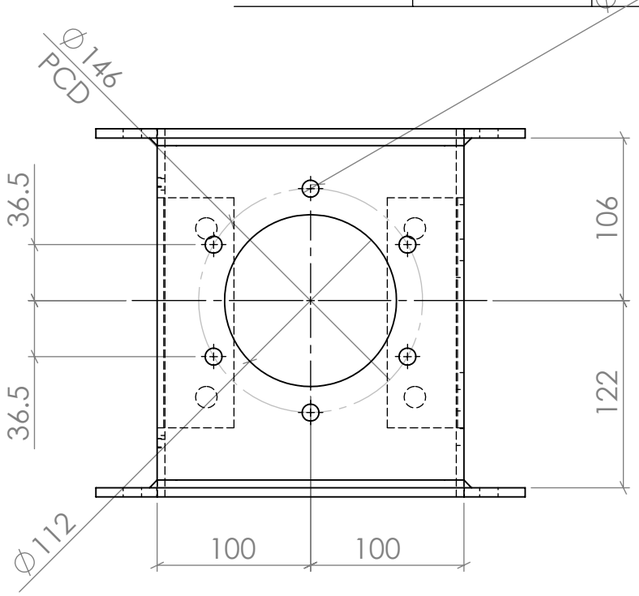

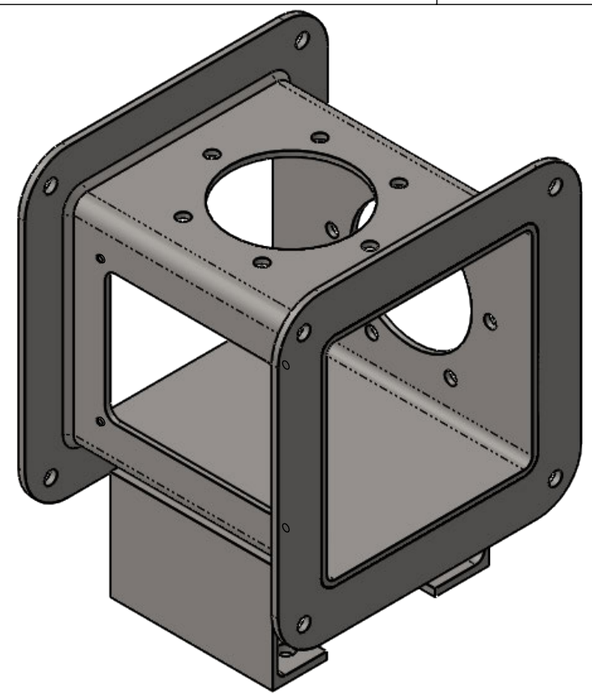

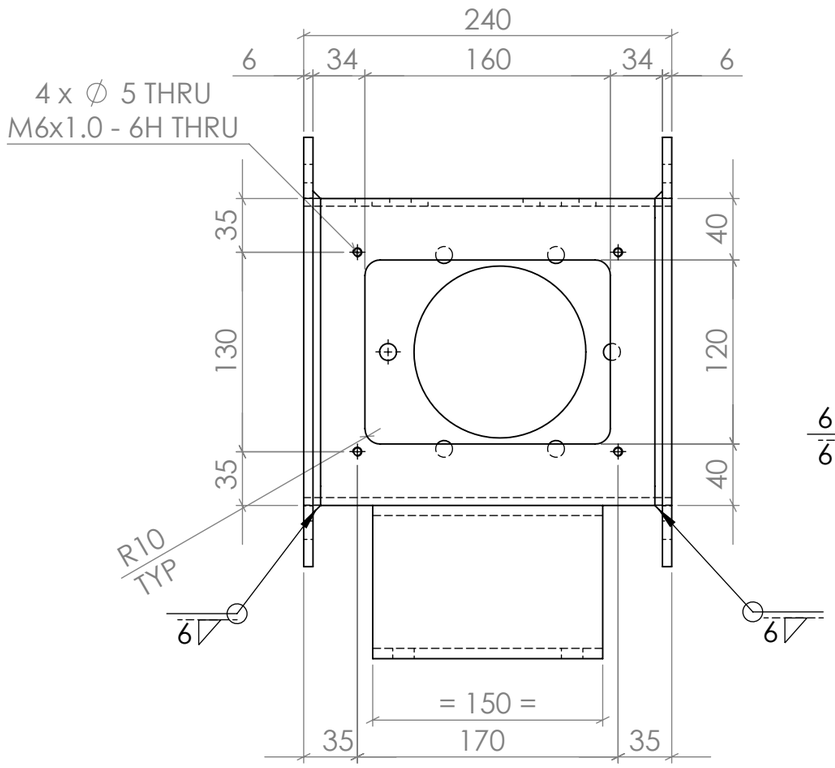

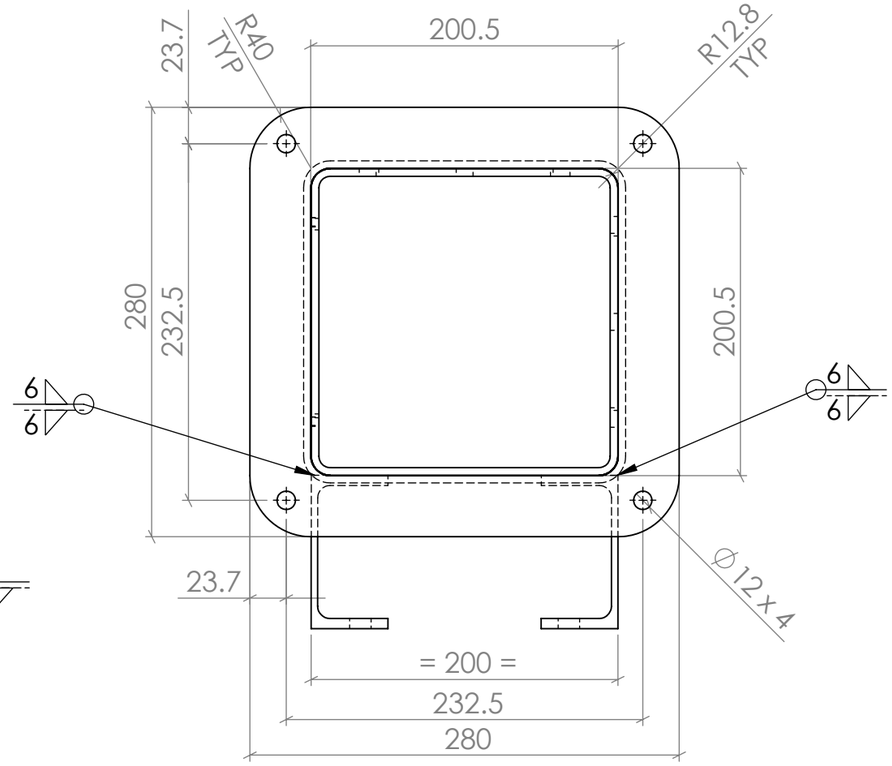

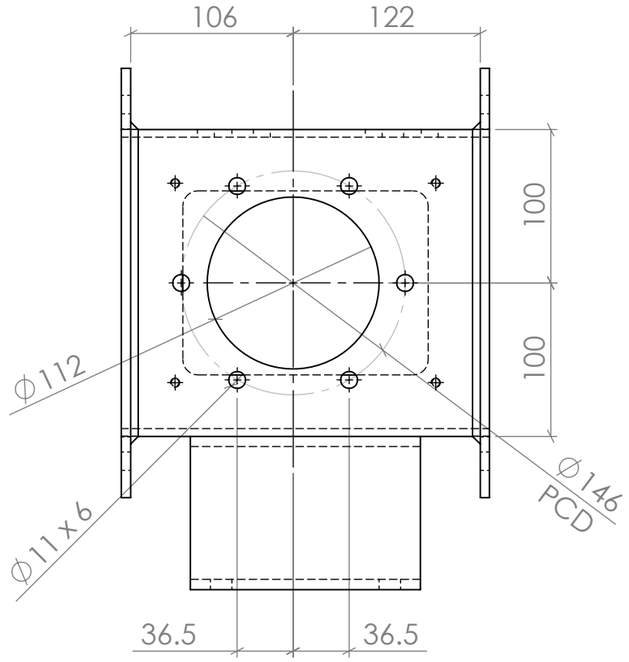

All fillet welds 6mm continuous U.N.O.

APPROVED FOR CONSTRUCTION
SIGNED:
DATE: / /
Drawing is not valid unless signed

No.	DATE	CHANGES	BY
B	Aug 22	Changed circular cutout dimension	MJS
A	Aug 22	Added PFC legs	MJS

3RD ANGLE PROJECTION U.N.O.
ALL DIM'S IN mm U.N.O.
DO NOT SCALE

Drawn: MJS
Date: July 22
Scale: 1:4

USQ ENG4111/2 Research Project
TOOWOOMBA, QLD 4350 Australia
Student Number: 0061080388
Ph: 0455142395
EMAIL: U1080388@umail.usq.edu.au

Michael Sheehan
Stirling Engine
BODY
SHEET 1 OF 2

Job Number:

Drawing No. **MS-SE-03**
Rev. **B**

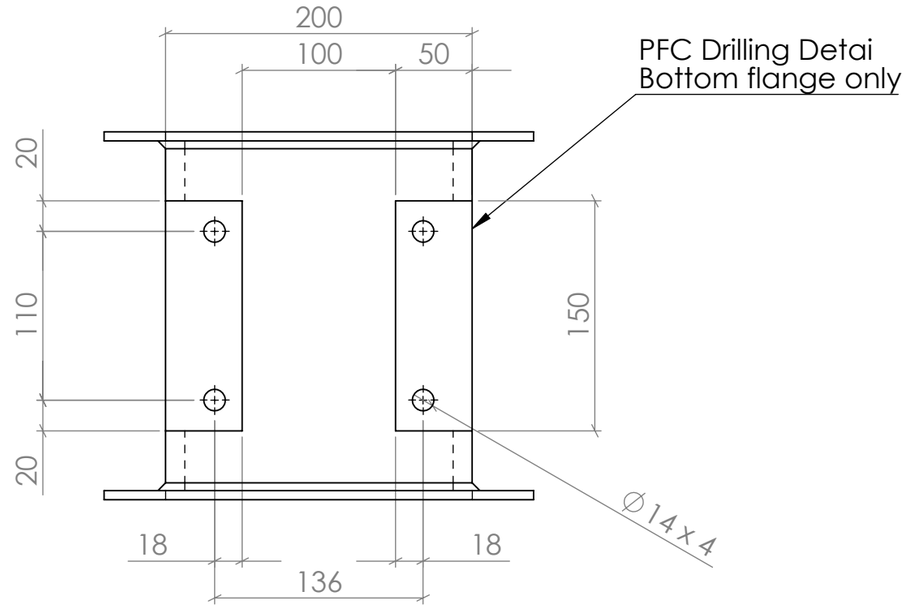

All fillet welds 6mm continuous U.N.O.

APPROVED FOR CONSTRUCTION

SIGNED:

DATE: / /

Drawing is not valid unless signed

No.	DATE	CHANGES	BY
B	Aug 22	Changed circular cutout dimension	MJS
A	Aug 22	Added PFC legs	MJS

3RD ANGLE PROJECTION U.N.O.

ALL DIM'S IN mm U.N.O.

DO NOT SCALE

Drawn: MJS

Date: July 22

Scale: 1:4

USQ ENG4111/2 Research Project
TOOWOOMBA, QLD 4350 Australia
Student Number: 0061080388
Ph: 0455142395
EMAIL: U1080388@umail.usq.edu.au

Michael Sheehan

Stirling Engine

BODY

SHEET 2 OF 2

Job Number:

Drawing No. **MS-SE-03**

Rev. **B**

ITEM NO.	QTY.	DESCRIPTION	LENGTH
1	1	STEEL PLATE GR250, 6 x 280 x 280	
2	2	25 SQ Bar	110

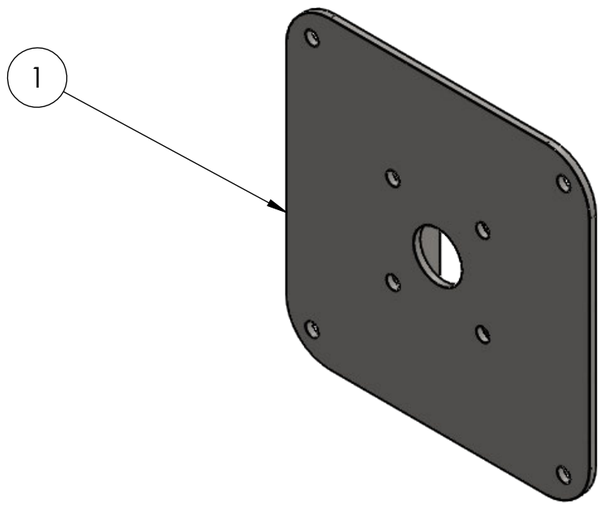

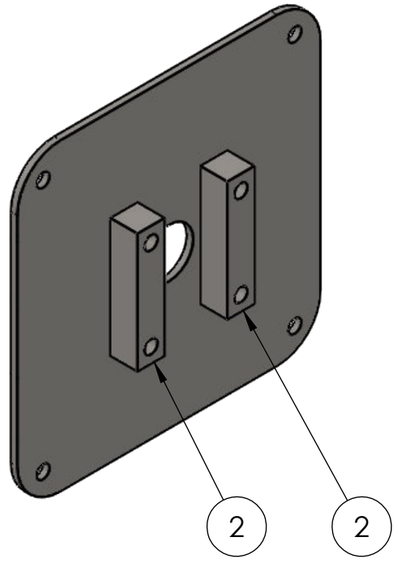

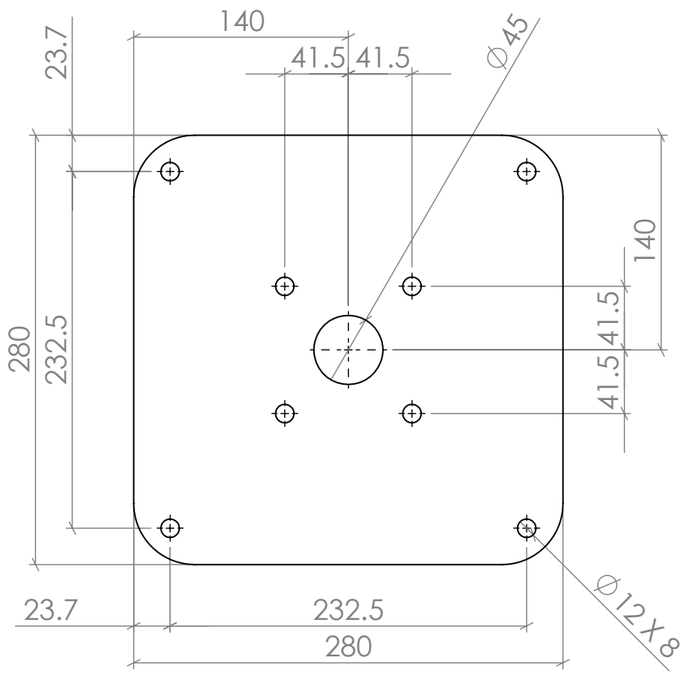

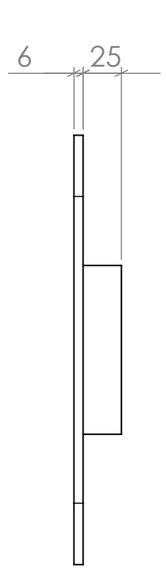

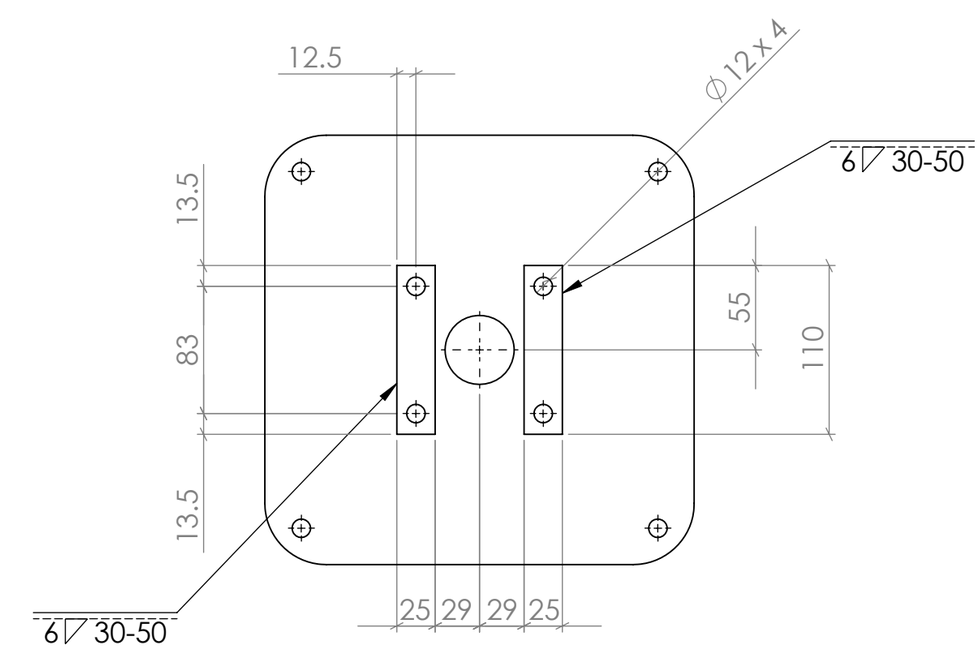

All fillet welds 6mm continuous U.N.O.

APPROVED FOR CONSTRUCTION
SIGNED:
DATE: / /
Drawing is not valid unless signed

No.	DATE	CHANGES	BY
-	-		

3RD ANGLE PROJECTION U.N.O.
ALL DIM'S IN mm U.N.O.
DO NOT SCALE

Drawn: MJS
Date: July 2022
Scale: 1:4

USQ ENG4111/2 Research Project
TOOWOOMBA, QLD 4350 Australia
Student Number: 0061080388
Ph: 0455142395
EMAIL: U1080388@umail.usq.edu.au

Michael Sheehan
Stirling Engine
BEARING PLATE
SHEET 1 OF 1
Job Number:

Drawing No. **SE-SE-04**
Rev. -

ITEM NO.	QTY.	DESCRIPTION	LENGTH	MATERIAL
1	1	Ø17 Solid Round Bar	84	4140 P&P

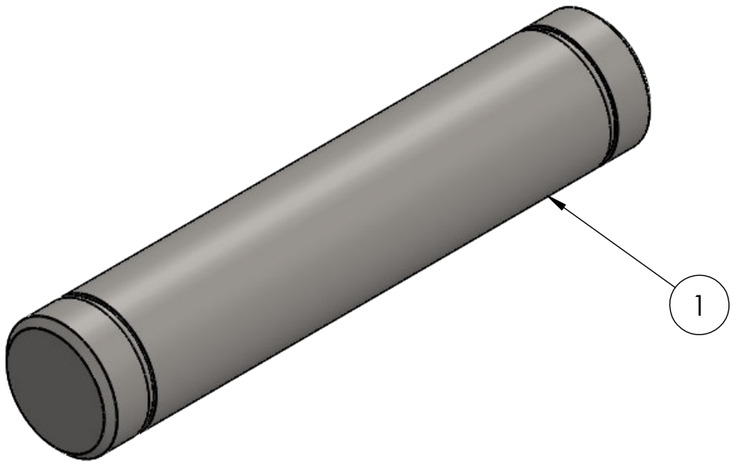

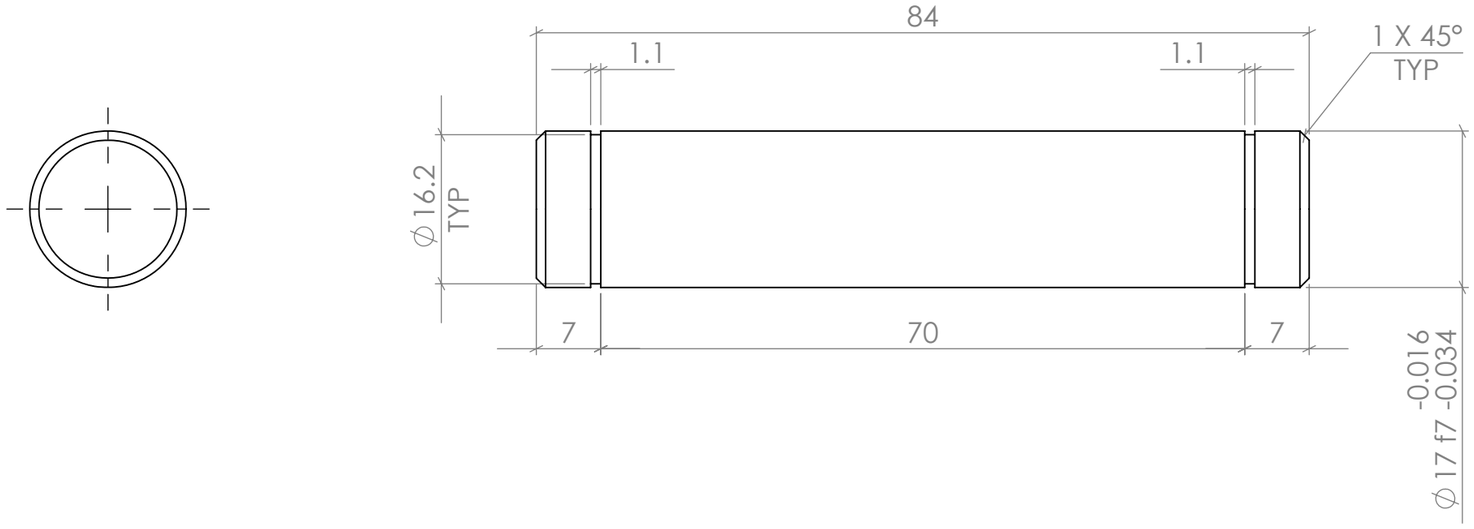

All fillet welds 6mm continuous U.N.O.

APPROVED FOR CONSTRUCTION

SIGNED:

DATE: / /

Drawing is not valid unless signed

No.	DATE	CHANGES	BY
-	-		

3RD ANGLE PROJECTION U.N.O.

ALL DIM'S IN mm U.N.O.

DO NOT SCALE

Drawn: MJS

Date: July 2022

Scale: 3:2

USQ ENG4111/2 Research Project
TOOWOOMBA, QLD 4350 Australia
Student Number: 0061080388
Ph: 0455142395
EMAIL: U1080388@umail.usq.edu.au

Michael Sheehan

Stirling Engine

CRANK PIN

SHEET 1 OF 1

Job Number:

Drawing No. **MS-SE-05**

Rev. **-**

ITEM NO.	QTY.	DESCRIPTION	LENGTH
1	1	16 PL GR350	

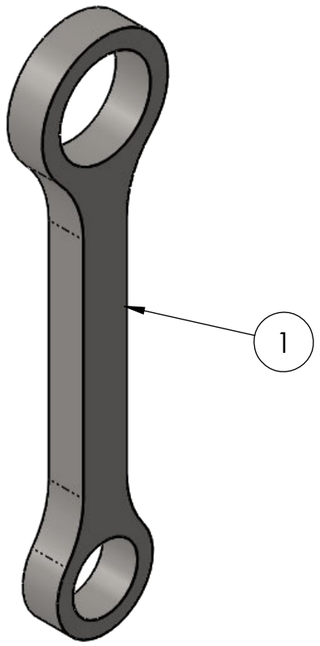

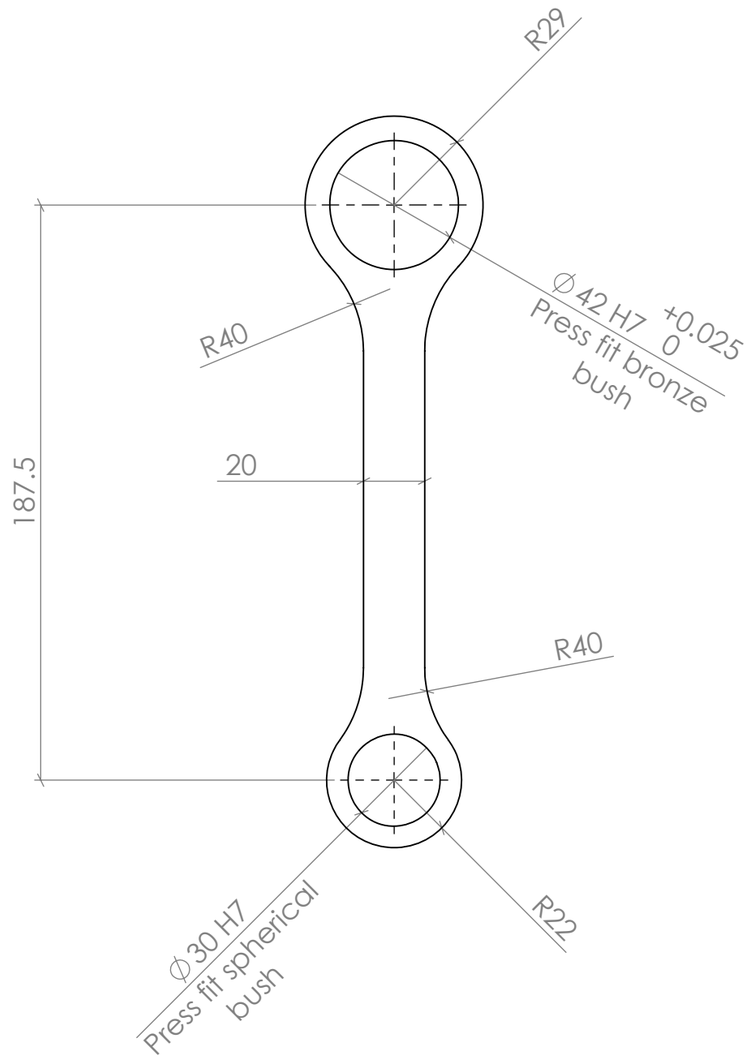

All fillet welds 6mm continuous U.N.O.

APPROVED FOR CONSTRUCTION
SIGNED:
DATE: / /
Drawing is not valid unless signed

No.	DATE	CHANGES	BY
-	-		

3RD ANGLE PROJECTION U.N.O.
ALL DIM'S IN mm U.N.O.
DO NOT SCALE

Drawn: MJS
Date: July 2022
Scale: 1:2

USQ ENG4111/2 Research Project
TOOWOOMBA, QLD 4350 Australia
Student Number: 0061080388
Ph: 0455142395
EMAIL: U1080388@umail.usq.edu.au

Michael Sheehan
Stirling Engine
CON ROD
SHEET 1 OF 1
Job Number:

Drawing No. **MS-SE-06**
Rev. **-**

ITEM NO.	QTY.	DESCRIPTION	LENGTH
1	1	LG2 Bronze Bush	16

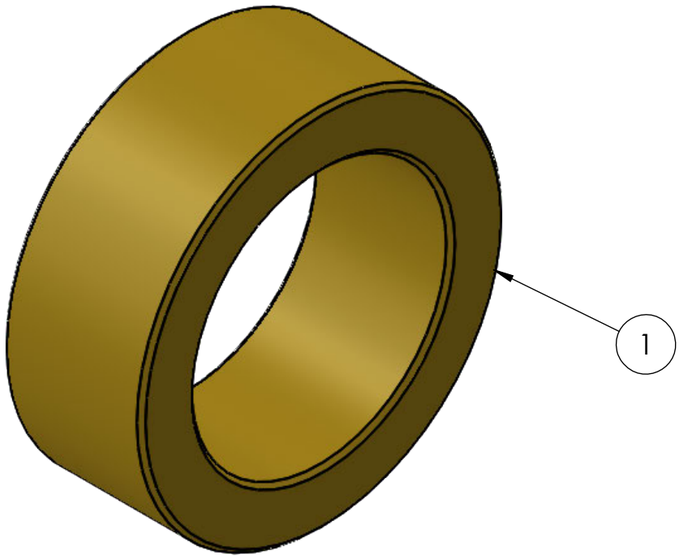

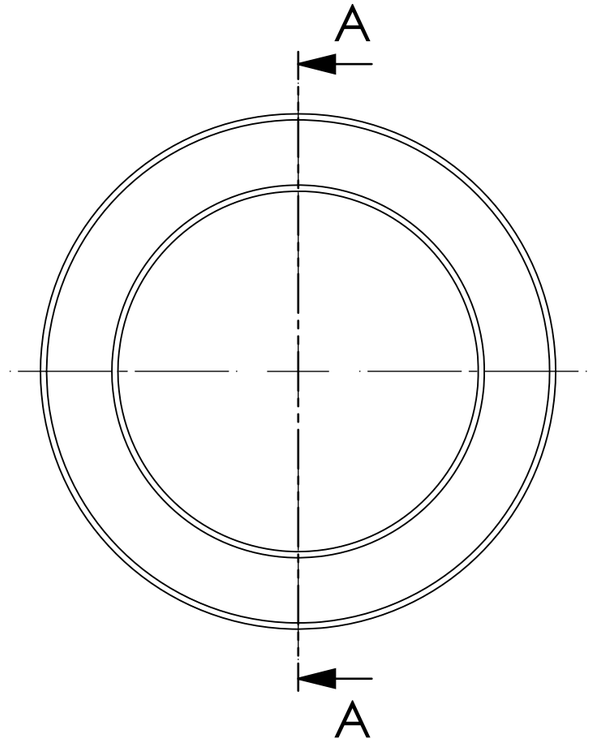

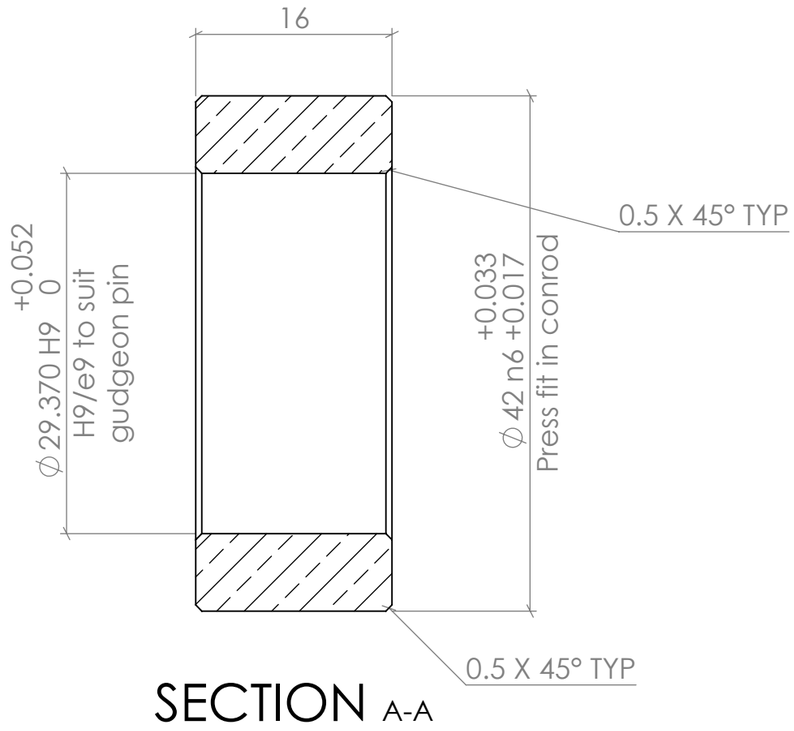

SECTION A-A

All fillet welds 6mm continuous U.N.O.

APPROVED FOR CONSTRUCTION
SIGNED:
DATE: / /
Drawing is not valid unless signed

No.	DATE	CHANGES	BY
-	-		

3RD ANGLE PROJECTION U.N.O.
ALL DIM'S IN mm U.N.O.
DO NOT SCALE

Drawn: MJS
Date: July 2022
Scale: 2:1

USQ ENG4111/2 Research Project
TOOWOOMBA, QLD 4350 Australia
Student Number: 0061080388
Ph: 0455142395
EMAIL: U1080388@umail.usq.edu.au

Michael Sheehan
Stirling Engine
WRIST PIN BUSH
SHEET 1 OF 1
Job Number:

Drawing No. **MS-SE-08**
Rev. -

ITEM NO.	QTY.	DESCRIPTION	LENGTH
1	2	3/8" BSPT x 3/4" JIC NIPPLE M/M (CB2-0612)	
2	2	3/4" JIC F x 1/2" Tubeweld (C87-1208)	
3	1	1/2" OD x 1.22mm wt Steel Tube	
4	1	3/4" BSP Heavy Socket x 72mm long	

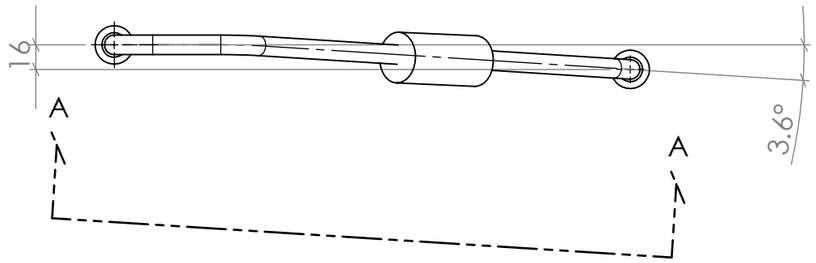

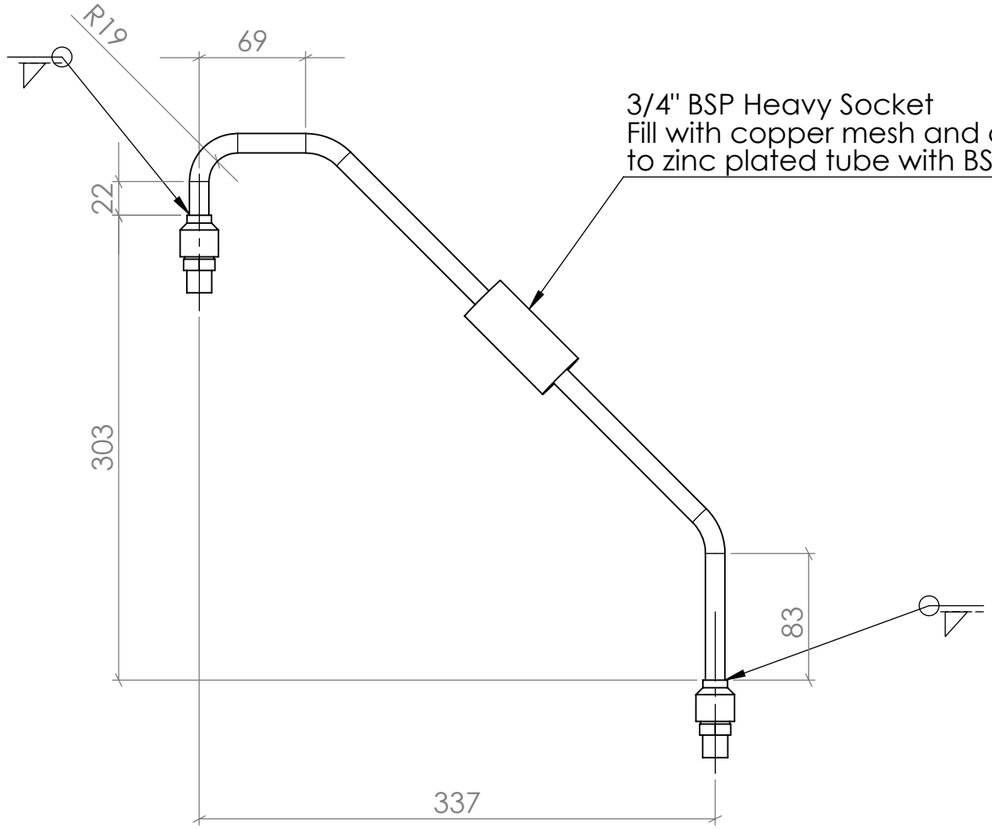

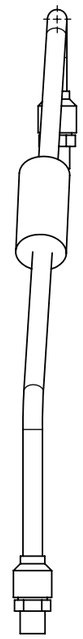

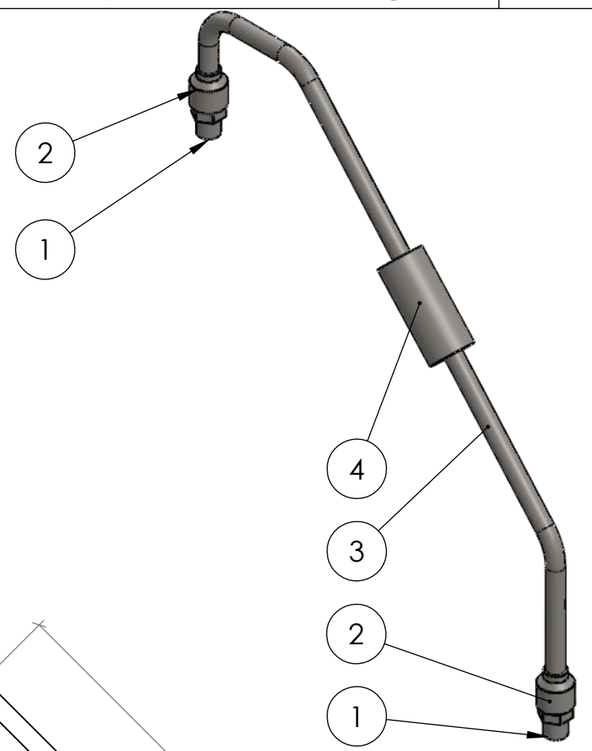

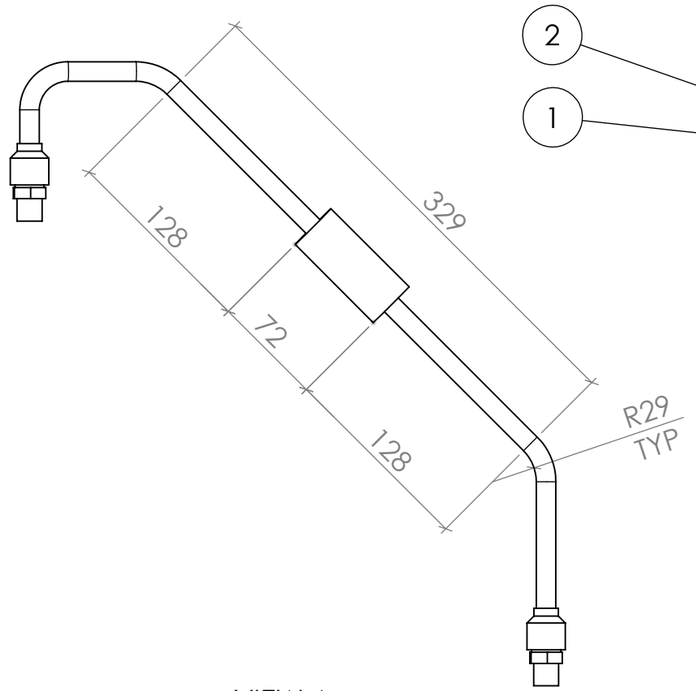

VIEW A
3.63°

All fillet welds 6mm continuous U.N.O.

APPROVED FOR CONSTRUCTION
SIGNED:
DATE: / /
Drawing is not valid unless signed

No.	DATE	CHANGES	BY
-	-		

3RD ANGLE PROJECTION U.N.O.
ALL DIM'S IN mm U.N.O.
DO NOT SCALE

Drawn: MJS
Date: July 2022
Scale: 1:4

USQ ENG4111/2 Research Project
TOOWOOMBA, QLD 4350 Australia
Student Number: 0061080388
Ph: 0455142395
EMAIL: U1080388@umail.usq.edu.au

Michael Sheehan
Stirling Engine
REGENERATOR TUBE
SHEET 1 OF 1
Job Number:

Drawing No. **MS-SE-10**
Rev. -

ITEM NO.	QTY.	DESCRIPTION	LENGTH
1	1	PLATE, 3 x 160 x 200	
2	1	Steel Expanded Metal 19 x 5 opening, 120 x 160	

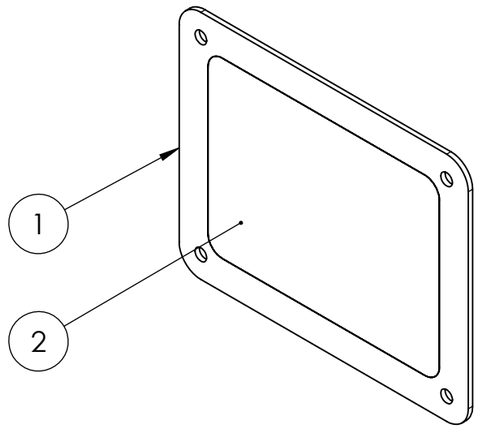

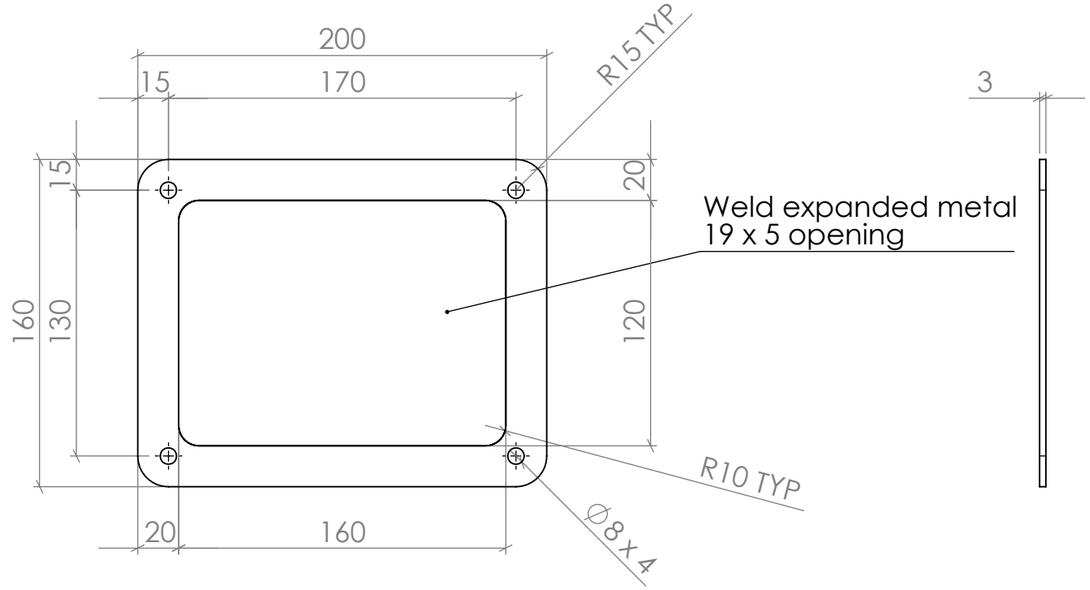

All fillet welds 6mm continuous U.N.O.

APPROVED FOR CONSTRUCTION
SIGNED:
DATE: / /
Drawing is not valid unless signed

No.	DATE	CHANGES	BY
-	-		

3RD ANGLE PROJECTION U.N.O.
ALL DIM'S IN mm U.N.O.
DO NOT SCALE

Drawn: MJS
Date: July 2022
Scale: 1:3

USQ ENG4111/2 Research Project
TOOWOOMBA, QLD 4350 Australia
Student Number: 0061080388
Ph: 0455142395
EMAIL: U1080388@umail.usq.edu.au

Michael Sheehan
Stirling Engine
COVER
SHEET 1 OF 1
Job Number:

Drawing No. **MS-SE-11**
Rev. **-**

ITEM NO.	QTY.	DESCRIPTION	LENGTH
1	1	STEEL GR350 PLATE, 16 x 155.69 x 162.89	
2	1	Ø30.00 1045 Bright Bar	220.00

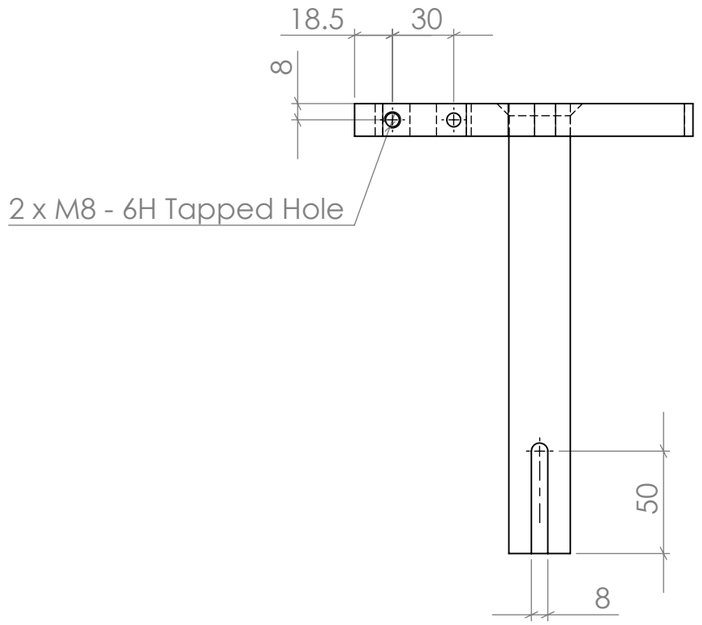

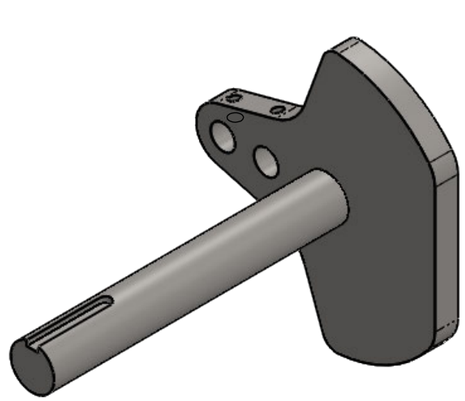

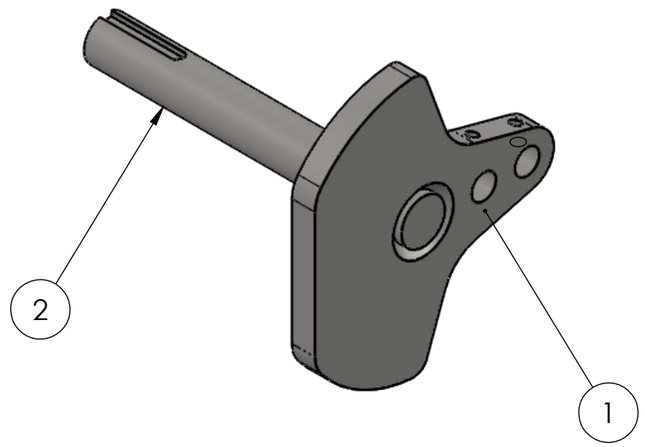

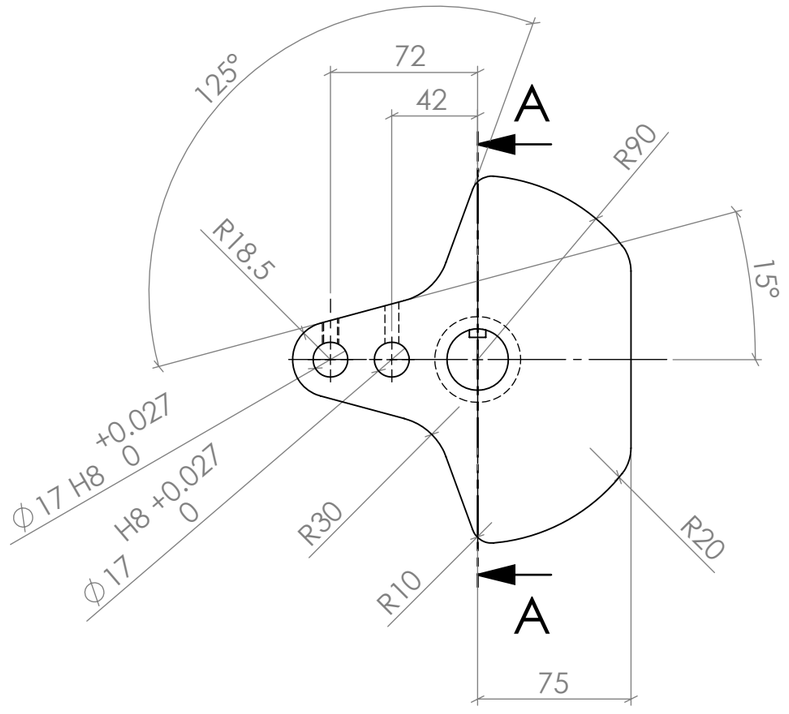

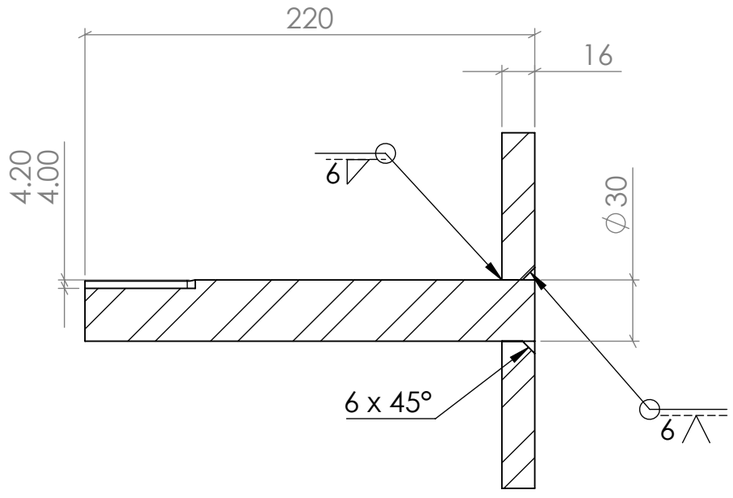

SECTION A-A

All fillet welds 6mm continuous U.N.O.

APPROVED FOR CONSTRUCTION
SIGNED:
DATE: / /
Drawing is not valid unless signed

No.	DATE	CHANGES	BY
B	Sep 22	Added second hole for crank pin at 42mm radius	MJS
A	Sep 22	Changed profile of crank plate	MJS

3RD ANGLE PROJECTION U.N.O.
ALL DIM'S IN mm U.N.O.
DO NOT SCALE

Drawn: MJS
Date: July 2022
Scale: 1:3

USQ ENG4111/2 Research Project
TOOWOOMBA, QLD 4350 Australia
Student Number: 0061080388
Ph: 0455142395
EMAIL: U1080388@umail.usq.edu.au

Michael Sheehan
Stirling Engine
OUTPUT SHAFT
SHEET 1 OF 1
Job Number:

Drawing No. **MS-SE-12**
Rev. **B**

ITEM NO.	QTY.	DESCRIPTION	LENGTH
1	1	STEEL GR350 PLATE, 16 x 155.69 x 162.89	
2	1	Ø30.00 1045 Bright Bar	220.00

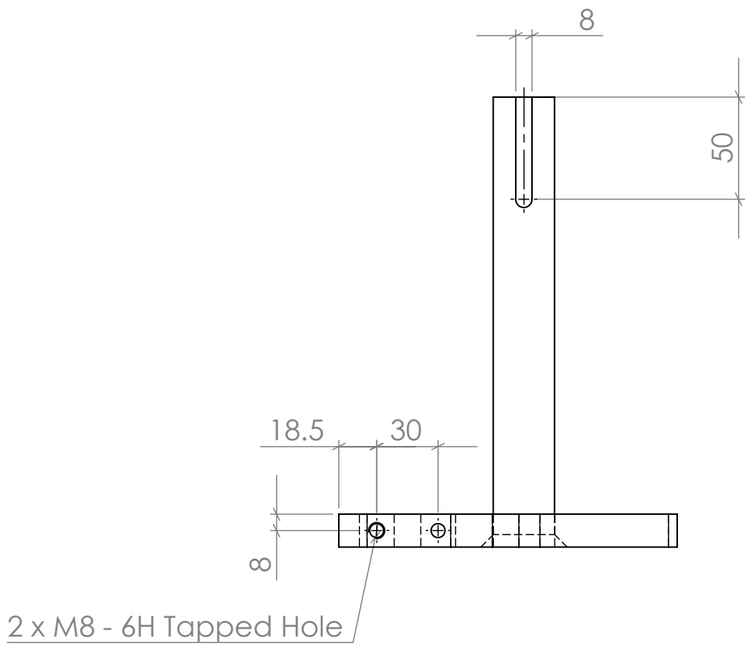

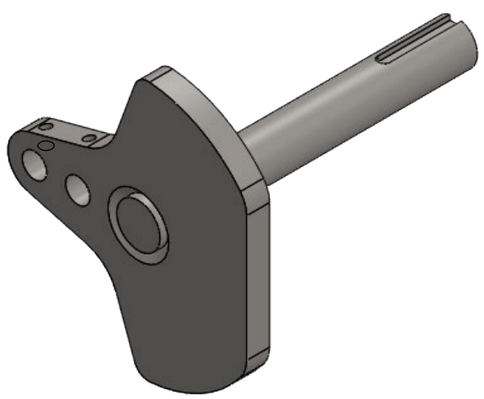

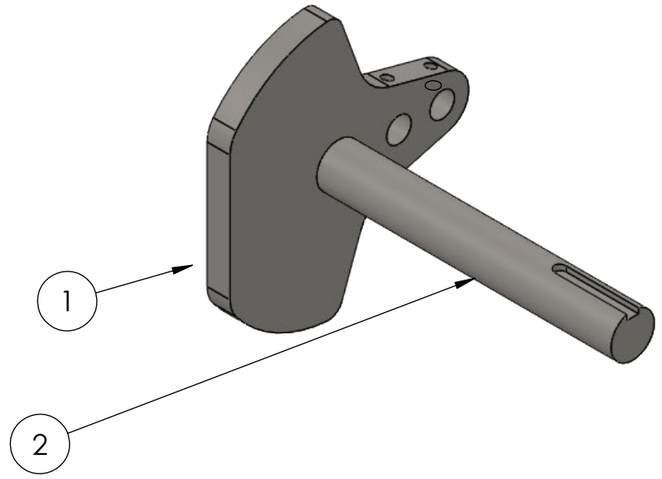

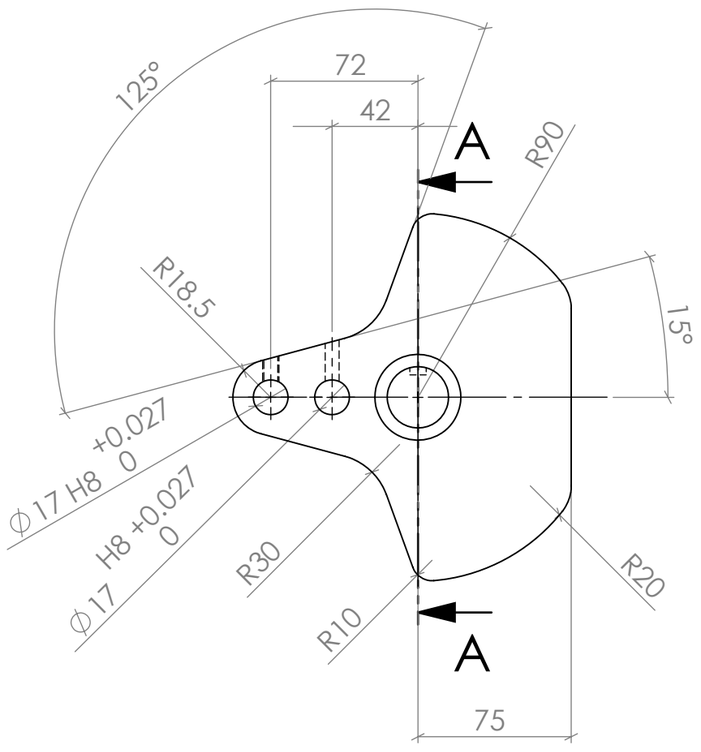

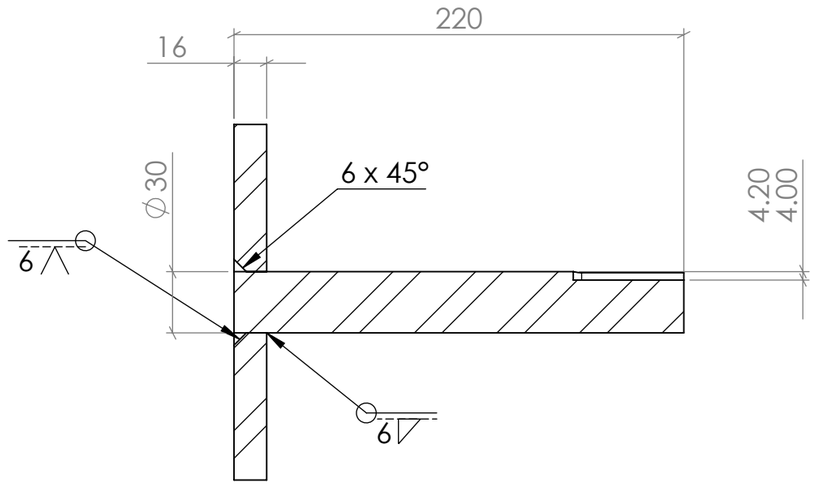

SECTION A-A

All fillet welds 6mm continuous U.N.O.

APPROVED FOR CONSTRUCTION
SIGNED:
DATE: / /
Drawing is not valid unless signed

No.	DATE	CHANGES	BY
B	Sep 22	Added second hole for crank pin at 42mm radius	MJS
A	Sep 22	Changed profile of crank plate	MJS

3RD ANGLE PROJECTION U.N.O.
ALL DIM'S IN mm U.N.O.
DO NOT SCALE

Drawn: MJS
Date: July 2022
Scale: 1:3

USQ ENG4111/2 Research Project
TOOWOOMBA, QLD 4350 Australia
Student Number: 0061080388
Ph: 0455142395
EMAIL: U1080388@umail.usq.edu.au

Michael Sheehan
Stirling Engine
IDLER SHAFT
SHEET 1 OF 1
Job Number:

Drawing No. **MS-SE-13**
Rev. **B**

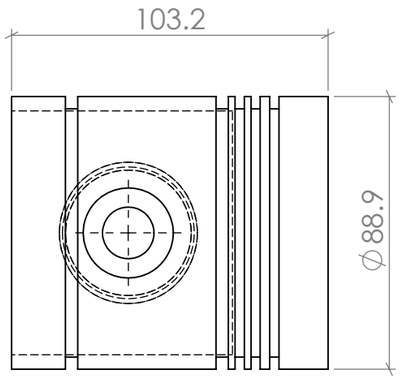

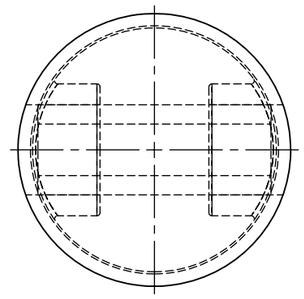

AS SUPPLIED

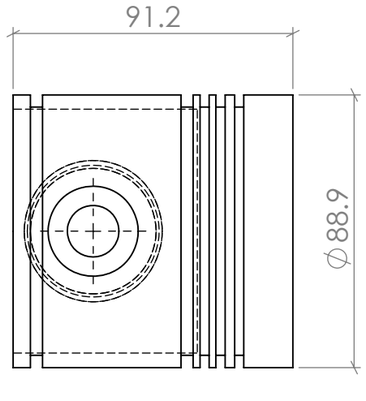

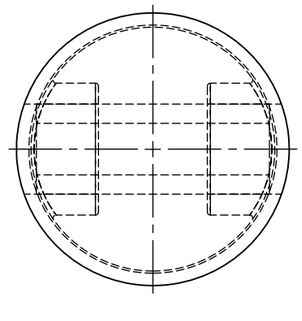

POST MACHINING

All fillet welds 6mm continuous U.N.O.

APPROVED FOR CONSTRUCTION
SIGNED:
DATE: / /
Drawing is not valid unless signed

No.	DATE	CHANGES	BY
-	-		

3RD ANGLE PROJECTION U.N.O.
ALL DIM'S IN mm U.N.O.
DO NOT SCALE

Drawn: MJS
Date: July 2022
Scale: 1:2

USQ ENG4111/2 Research Project
TOOWOOMBA, QLD 4350 Australia
Student Number: 0061080388
Ph: 0455142395
EMAIL: U1080388@umail.usq.edu.au

Michael Sheehan
Stirling Engine
Piston PA483506 STD
SHEET 1 OF 1
Job Number:

Drawing No. **MS-SE-14**
Rev. **-**

ITEM NO.	QTY.	DESCRIPTION	LENGTH
1	1	1045 STEEL, 8 x 77 x 77	
2	1	3" NPT Barrel Nipple	95
3	1	STEEL PIPE 71.0 X 63.0	95
4	1	STEEL PIPE 60.3 X 53.1 (50 NB Med)	95
5	1	STEEL PIPE 48.3 x 41.9 (40 NB Med)	95
6	1	STEEL PIPE 33.7 x 25.7 (25 NB Heavy)	95
7	1	STEEL PIPE 21.3 x 16.7 (20 NB Light)	95
8	1	10mm Steel Solid Round Bar	95

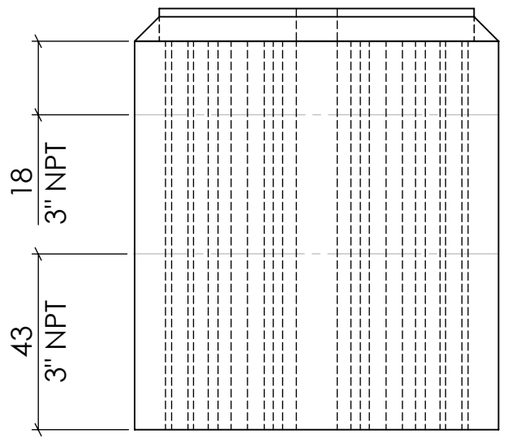

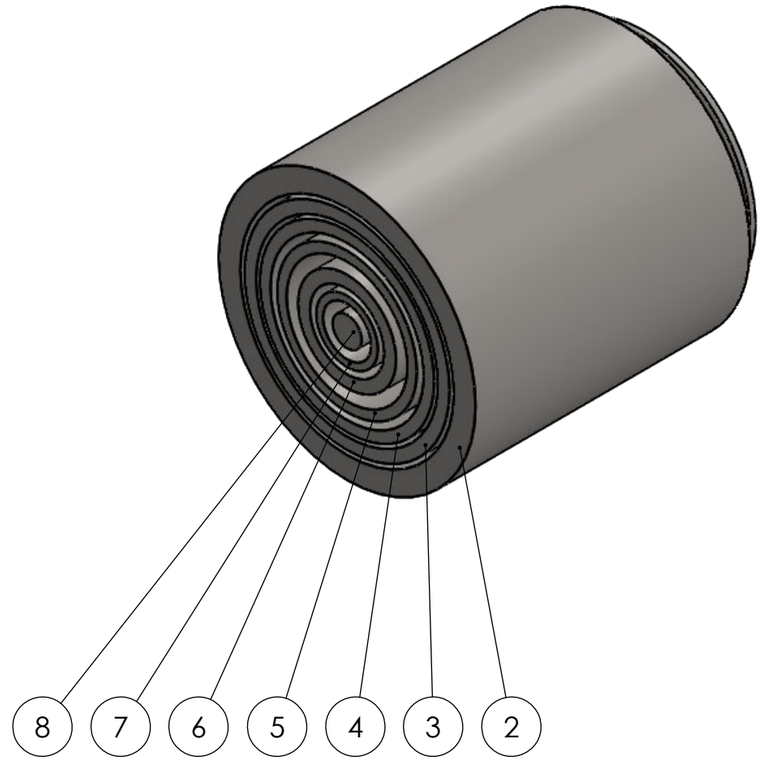

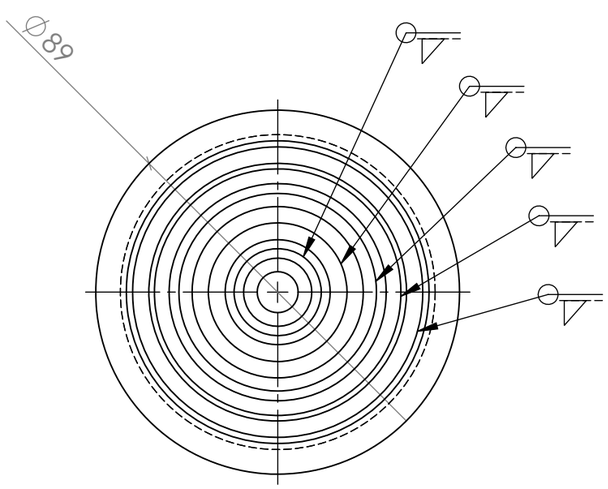

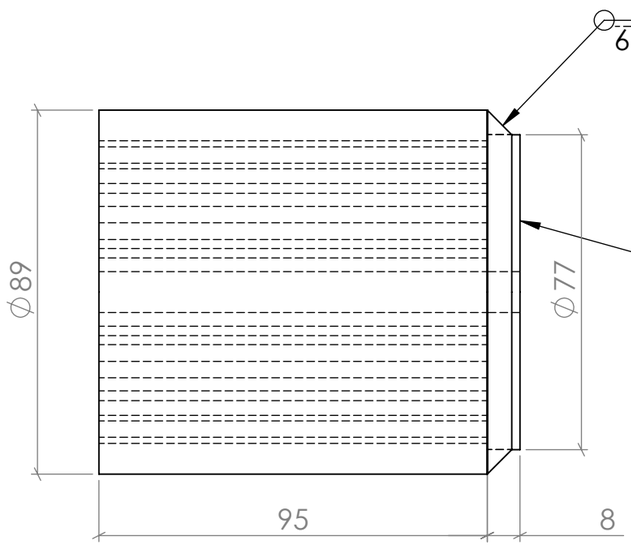

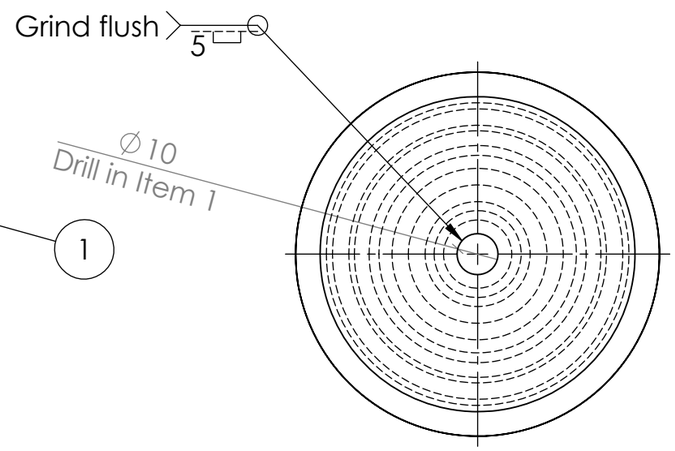

All fillet welds 6mm continuous U.N.O.

APPROVED FOR CONSTRUCTION
SIGNED:
DATE: / /
Drawing is not valid unless signed

No.	DATE	CHANGES	BY
-	-		

3RD ANGLE PROJECTION U.N.O.
ALL DIM'S IN mm U.N.O.
DO NOT SCALE

Drawn: MJS
Date: July 2022
Scale: 2:3

USQ ENG4111/2 Research Project
TOOWOOMBA, QLD 4350 Australia
Student Number: 0061080388
Ph: 0455142395
EMAIL: U1080388@umail.usq.edu.au

Michael Sheehan
Stirling Engine
HEATER HEAD
SHEET 1 OF 1
Job Number:

Drawing No. **MS-SE-15**
Rev. **-**

ITEM NO.	DESCRIPTION	DRAWING NUMBER	QTY.
1	CONROD	MS-SE-06	1
2	CONROD BUSH	MS-SE-08	1
3	BEARING 6903 (30 x 17 x 7)		2
4	PISTON PA483506 STD	MS-SE-14	1
5	INTERNAL CIRCLIP 29.37mm		2

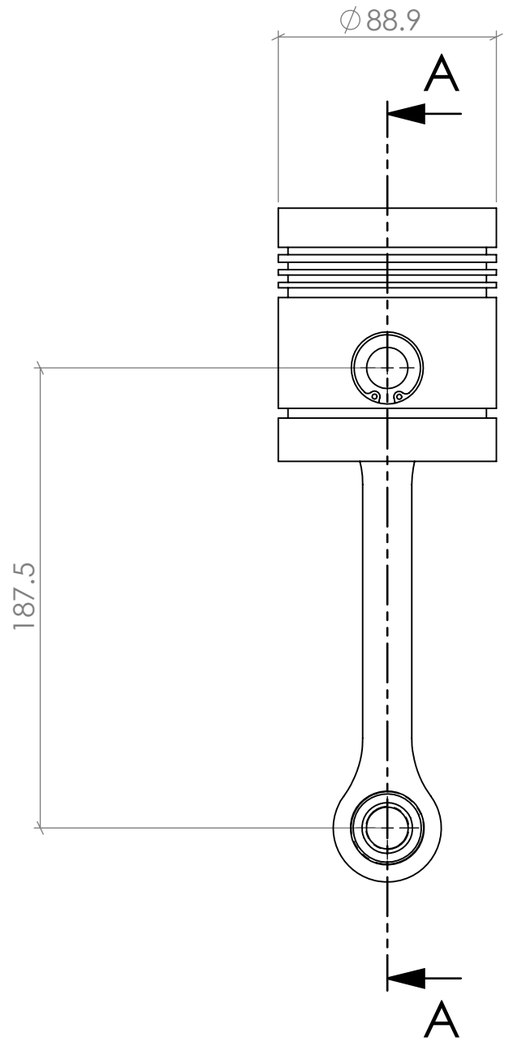

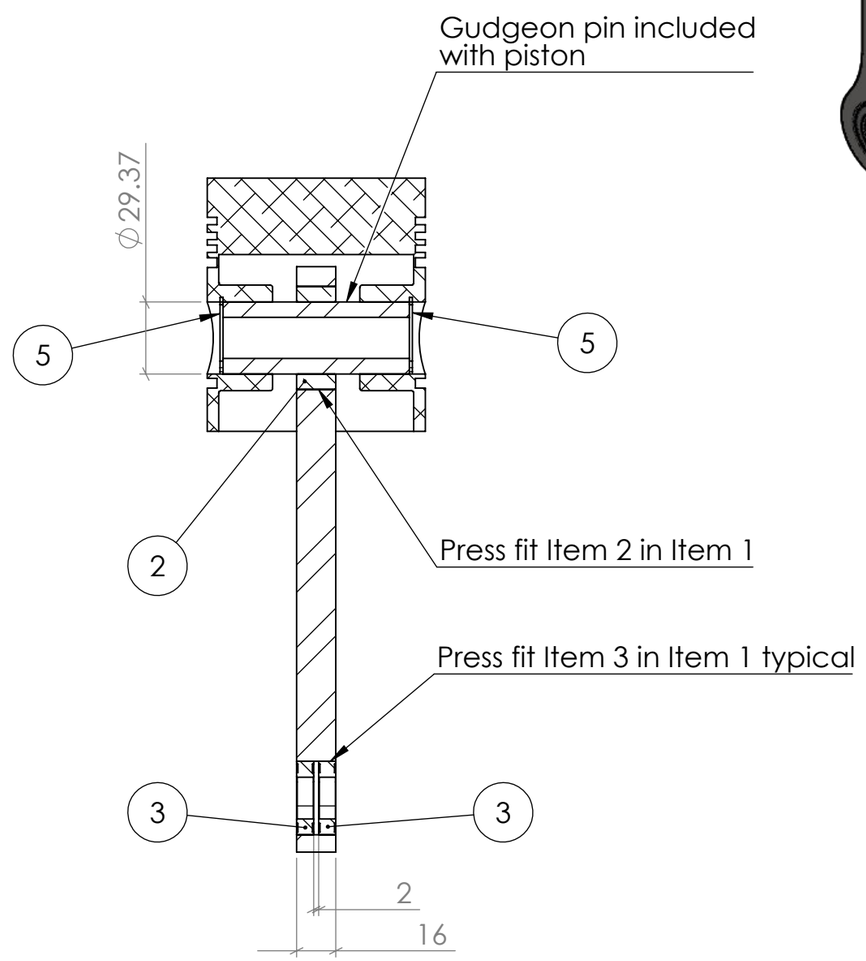

SECTION A-A

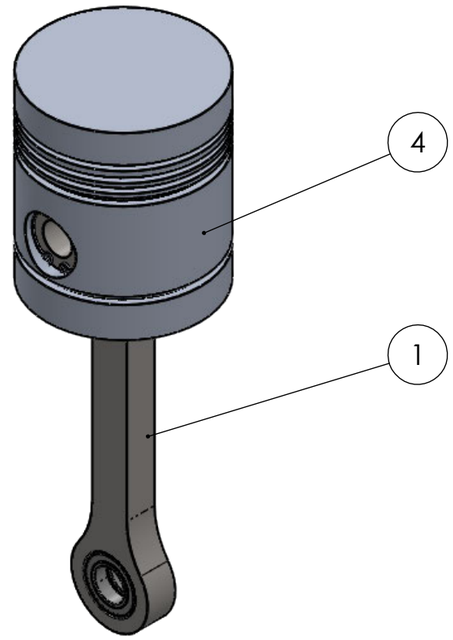

All fillet welds 6mm continuous U.N.O.

APPROVED FOR CONSTRUCTION
SIGNED:
DATE: / /
Drawing is not valid unless signed

No.	DATE	CHANGES	BY
-	-		

3RD ANGLE PROJECTION U.N.O.
ALL DIM'S IN mm U.N.O.
DO NOT SCALE

Drawn: MJS
Date: Sep 22
Scale: 2:5

USQ ENG4111/2 Research Project
TOOWOOMBA, QLD 4350 Australia
Student Number: 0061080388
Ph: 0455142395
EMAIL: U1080388@umail.usq.edu.au

Michael Sheehan
Stirling Engine
Piston Conrod Assembly
SHEET 1 OF 1 Job Number:

Drawing No. **MS-SE-16**
Rev. **-**

ITEM NO.	DESCRIPTION	DRAWING NUMBER	QTY.
1	BEARING PLATE	MS-SE-04	1
2	IDLER SHAFT	MS-SE-13	1
3	UCF206-30		2
4	FLYWHEEL	SPB-3 355 V-Belt Pulley w/ 3020-30mm Taper Lock Bush	1
5	KEY	MS-SE-18	1
6	M10 x 80 BOLT GR8.8 w/ NYLOC NUT & WASHER 2X		4

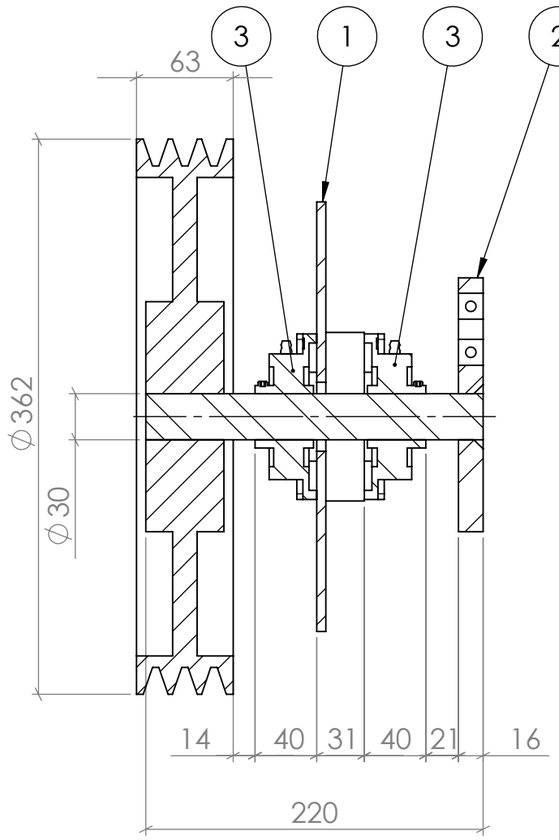

SECTION A-A

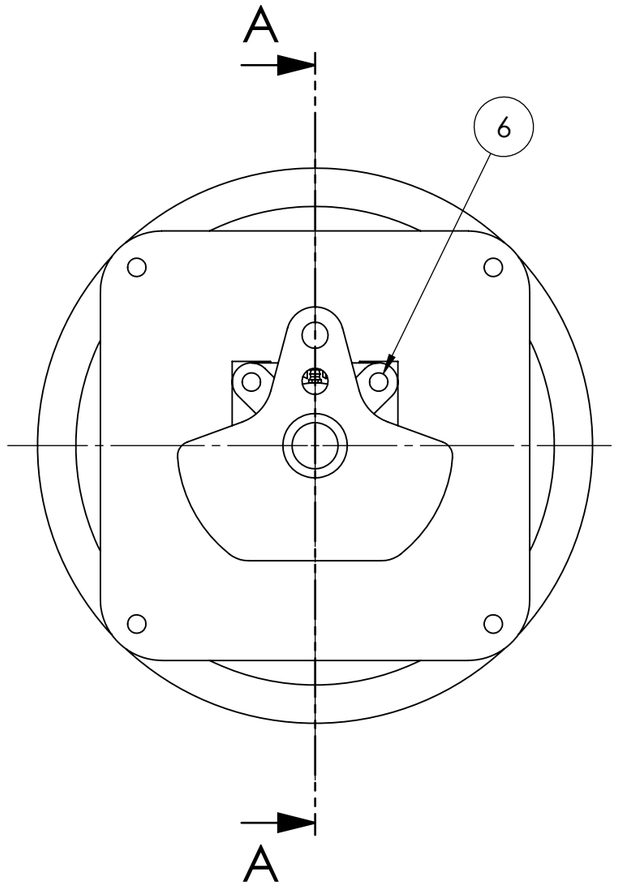

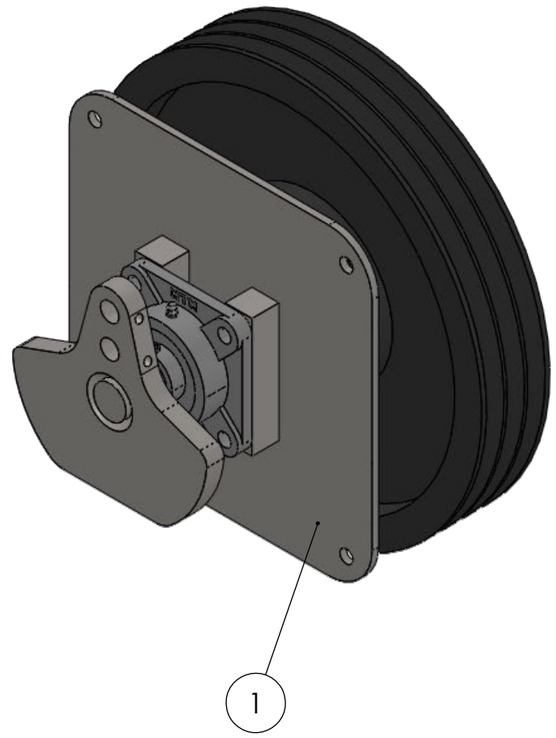

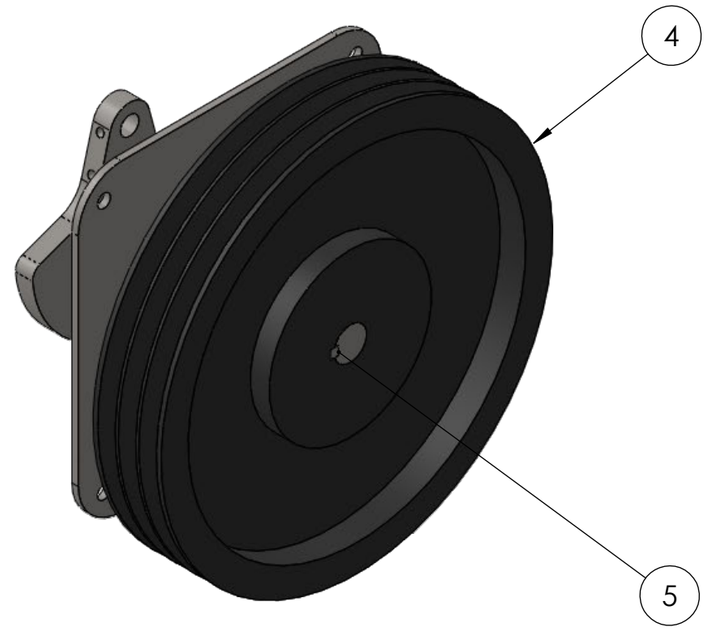

All fillet welds 6mm continuous U.N.O.

APPROVED FOR CONSTRUCTION
SIGNED:
DATE: / /
Drawing is not valid unless signed

No.	DATE	CHANGES	BY
-	-		

3RD ANGLE PROJECTION U.N.O.
ALL DIM'S IN mm U.N.O.
DO NOT SCALE

Drawn: MJS
Date: Sep 22
Scale: 1:4

USQ ENG4111/2 Research Project
TOOWOOMBA, QLD 4350 Australia
Student Number: 0061080388
Ph: 0455142395
EMAIL: U1080388@umail.usq.edu.au

Michael Sheehan
Stirling Engine
FLYWHEEL SHAFT ASSEMBLY
SHEET 1 OF 1
Job Number:

Drawing No. **MS-SE-17**
Rev. -

ITEM NO.	QTY.	DESCRIPTION	LENGTH
1	1	8 x 7 KEYSTEEL	54

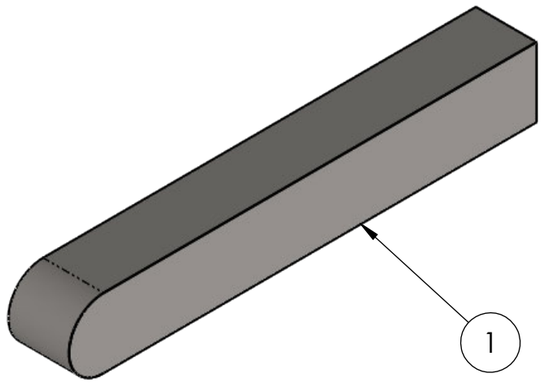

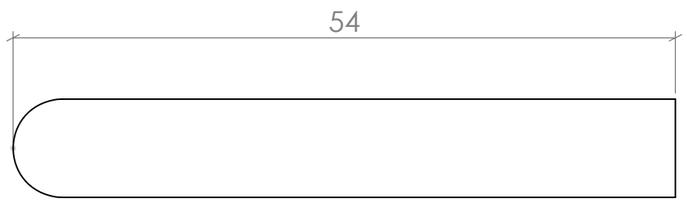

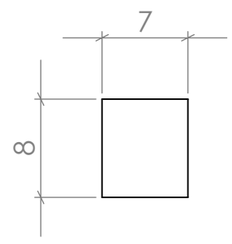

All fillet welds 6mm continuous U.N.O.

APPROVED FOR CONSTRUCTION
SIGNED:
DATE: / /
Drawing is not valid unless signed

No.	DATE	CHANGES	BY
-	-		

3RD ANGLE PROJECTION U.N.O.
ALL DIM'S IN mm U.N.O.
DO NOT SCALE

Drawn: MJS
Date: Sep 22
Scale: 2:1

USQ ENG4111/2 Research Project
TOOWOOMBA, QLD 4350 Australia
Student Number: 0061080388
Ph: 0455142395
EMAIL: U1080388@umail.usq.edu.au

Michael Sheehan
Stirling Engine
KEY
SHEET 1 OF 1
Job Number:

Drawing No.
MS-SE-18
Rev.
-

ITEM NO.	PART NUMBER	DESCRIPTION	QTY.
1	BEARING PLATE	MS-SE-04	1
2	OUTPUT SHAFT	MS-SE-12	1
3	UCF206-30		2
4	KEY	MS-SE-18	1
5	M10 x 80 BOLTS GR8.8 w/ NYLOC NUT & WASHER 2X		4

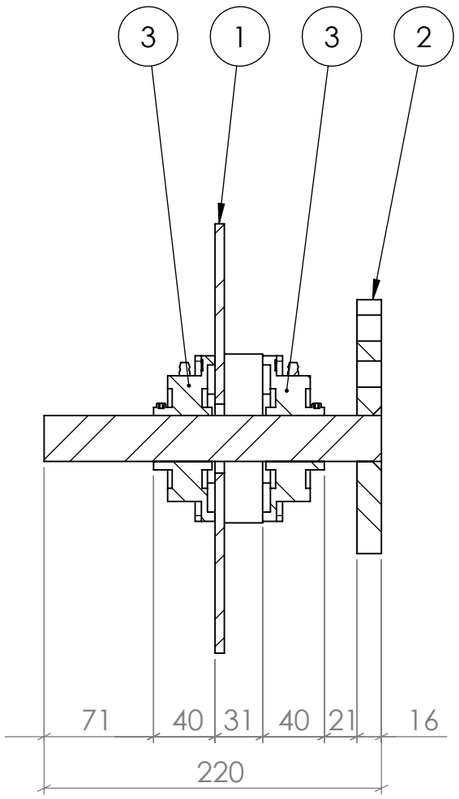

SECTION A-A

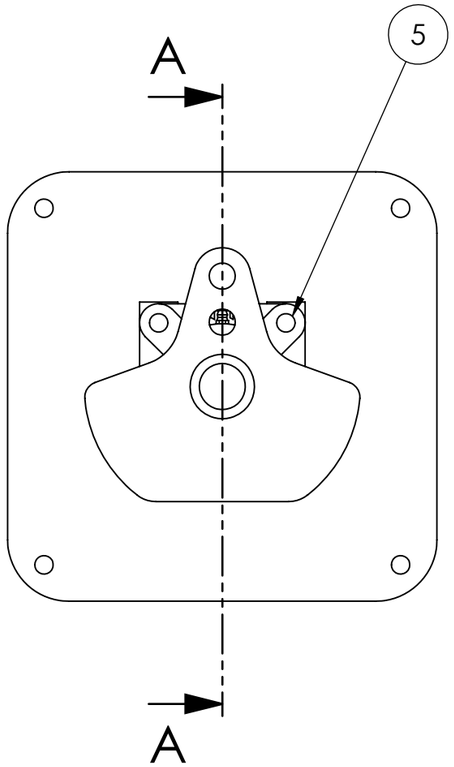

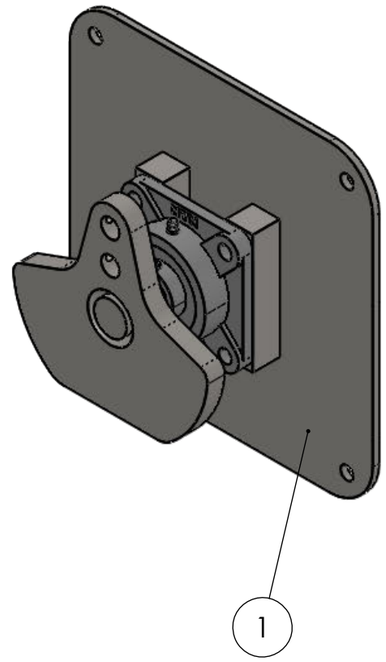

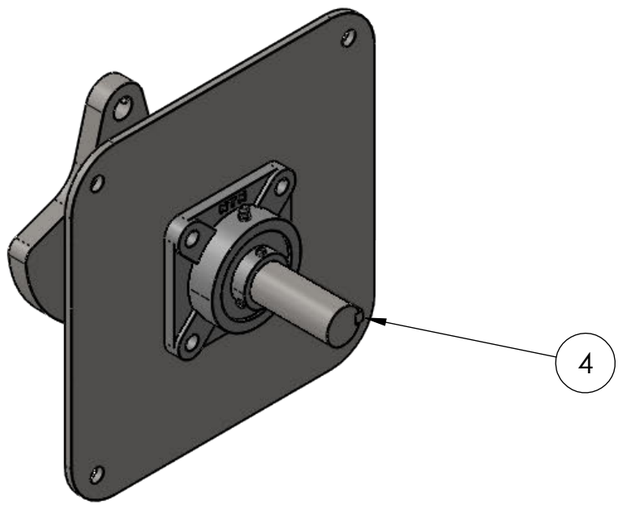

All fillet welds 6mm continuous U.N.O.

APPROVED FOR CONSTRUCTION
SIGNED:
DATE: / /
Drawing is not valid unless signed

No.	DATE	CHANGES	BY
-	-		

3RD ANGLE PROJECTION U.N.O.
ALL DIM'S IN mm U.N.O.
DO NOT SCALE

Drawn: MJS
Date: Sep 2022
Scale: 1:4

USQ ENG4111/2 Research Project
TOOWOOMBA, QLD 4350 Australia
Student Number: 0061080388
Ph: 0455142395
EMAIL: U1080388@umail.usq.edu.au

Michael Sheehan
Stirling Engine
OUTPUT SHAFT ASSEMBLY
SHEET 1 OF 1
Job Number:

Drawing No. **MS-SE-19**
Rev. -

ITEM NO.	QTY.	DESCRIPTION	LENGTH
1	1	LG2 BRONZE	1

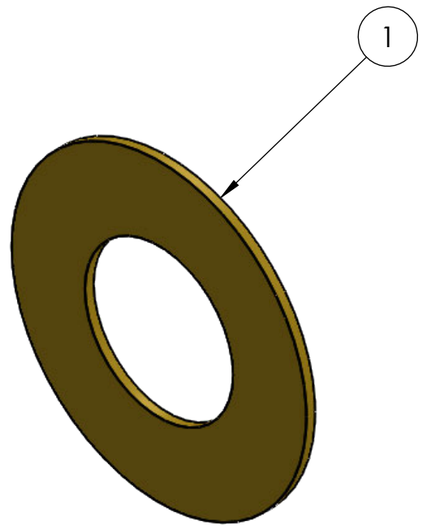

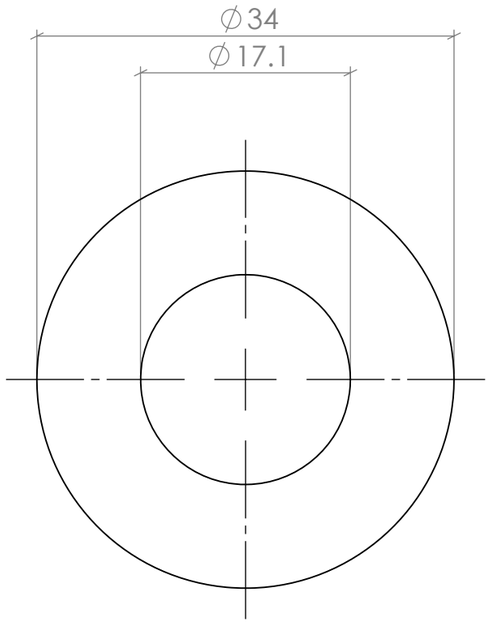

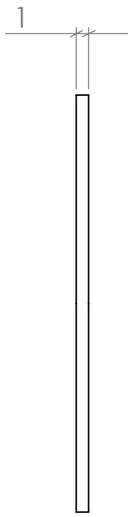

All fillet welds 6mm continuous U.N.O.

APPROVED FOR CONSTRUCTION
SIGNED:
DATE: / /
Drawing is not valid unless signed

No.	DATE	CHANGES	BY
-	-		

3RD ANGLE PROJECTION U.N.O.
ALL DIM'S IN mm U.N.O.
DO NOT SCALE

Drawn: MJS
Date: Sep 22
Scale: 2:1

USQ ENG4111/2 Research Project
TOOWOOMBA, QLD 4350 Australia
Student Number: 0061080388
Ph: 0455142395
EMAIL: U1080388@umail.usq.edu.au

Michael Sheehan
Stirling Engine
BRONZE SHIM
SHEET 1 OF 1
Job Number:

Drawing No.
MS-SE-20
Rev.
-

Appendix D

Detail and Assembly Drawings of Modified Components

Appendix D contains detail and assembly drawings for engine components which were modified during testing as discussed in Chapter 6.

ITEM NO.	DESCRIPTION	DRAWING NUMBER	QTY.
1	ENGINE BODY	MS-SE-03	1
2	HOT CYLINDER	MS-SE-01	1
3	COLD CYLINDER	MS-SE-02	1
4	REGENERATOR TUBE	MS-SE-10	1
5	COVER	MS-SE-11	1
6	PISTON CONROD ASSEMBLY	MS-SE-16	2
7	CRANK PIN	MS-SE-05	1
8	OUTPUT SHAFT ASSEMBLY	MS-SE-19	1
9	CONROD SHIM	MS-SE-20	3
10	17mm EXTERNAL CIRCLIP		2
11	FLYWHEEL SHAFT ASSEMBLY	MS-SE-17	1
12	HEATER HEAD	MS-SE-15	1
13	M8 x 10 GRUB SCREW		2
14	M12 x 35 BOLT GR8.8 w/ NYLOC NUT & WASHER 2x		8
15	M10 x 40 BOLT GR8.8 w/ NYLOC NUT & WASHER 2x		12
16	M12 x 50 BOLT GR8.8 w/ NYLOC NUT & WASHER 2x		4
17	M6 x 12 BOLT GR8.8 w/ SPRING WASHER		4

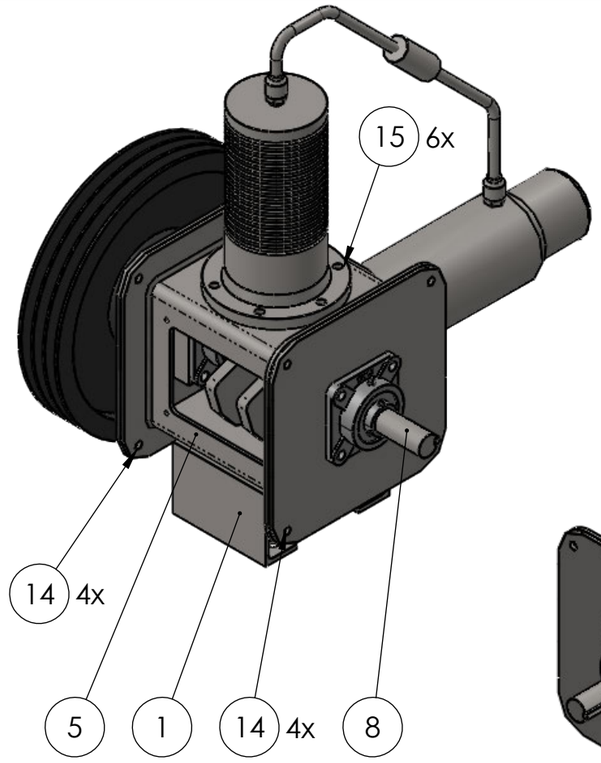

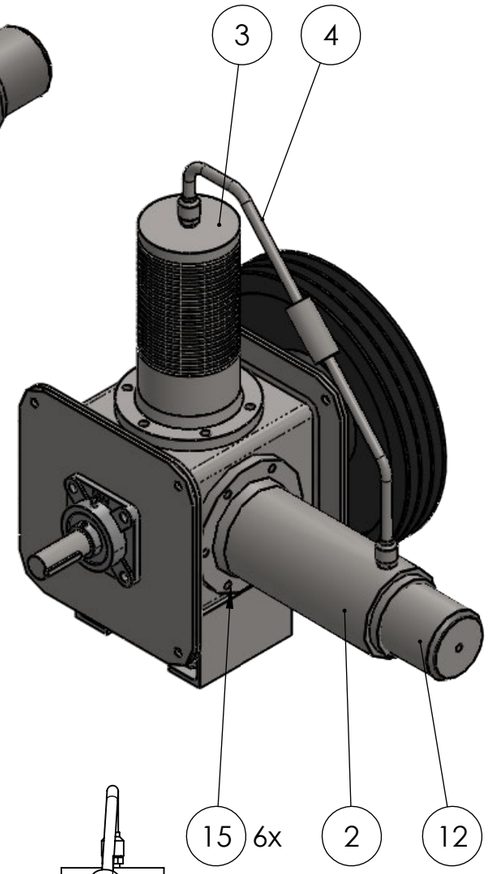

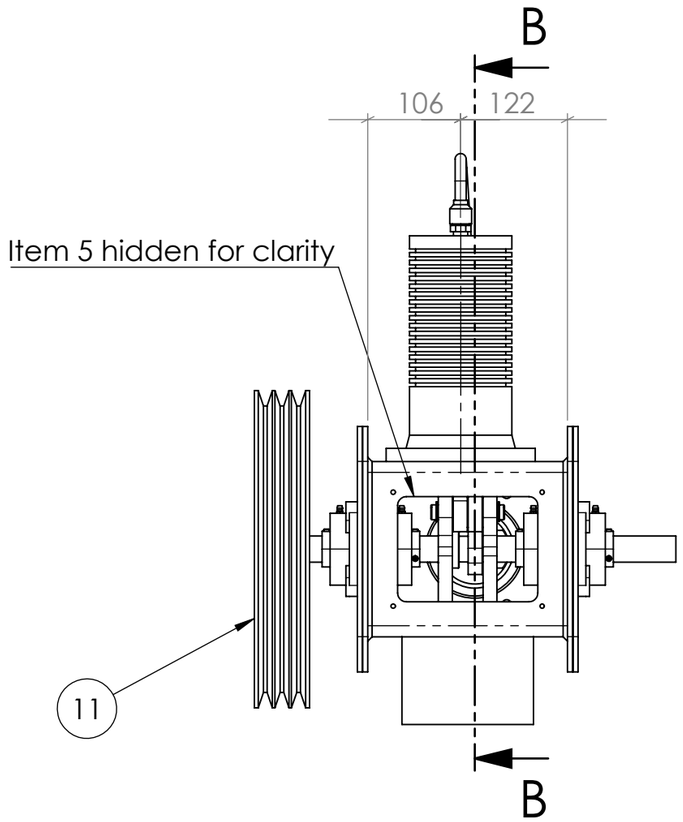

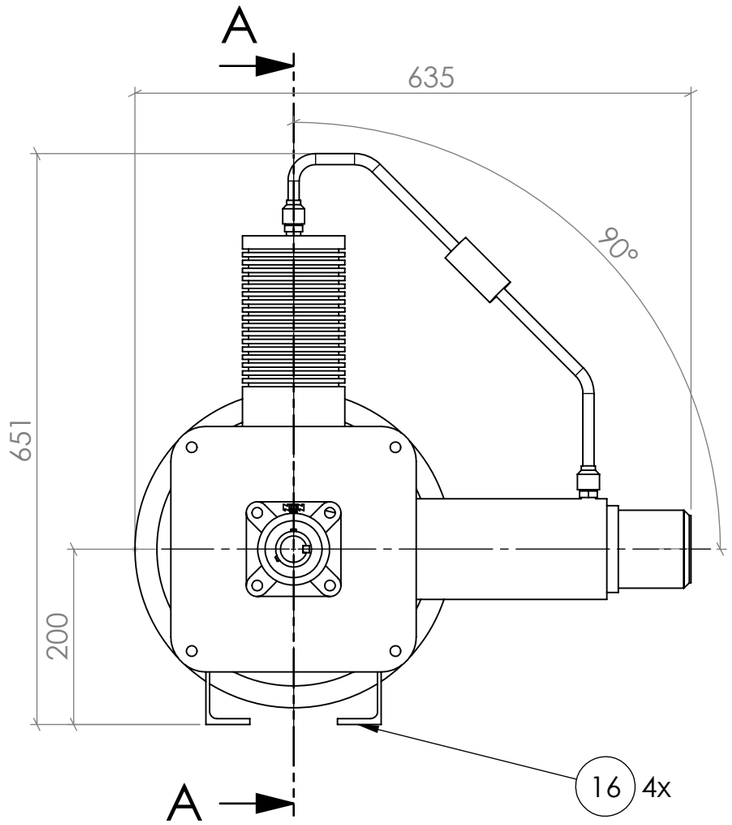

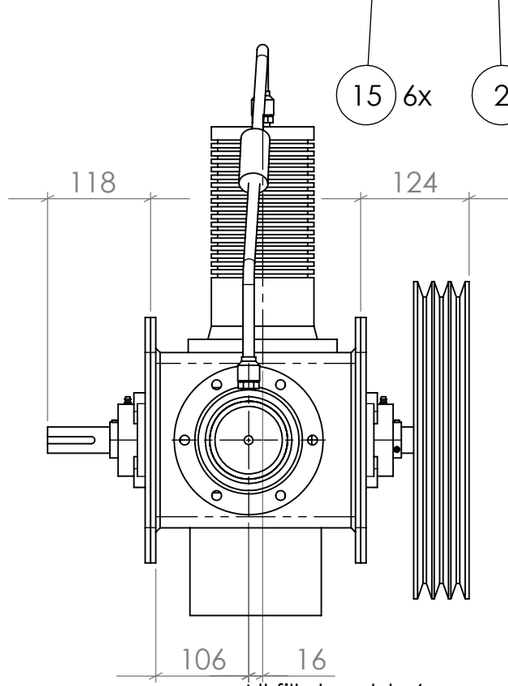

All fillet welds 6mm continuous U.N.O.

APPROVED FOR CONSTRUCTION
SIGNED:
DATE: / /
Drawing is not valid unless signed

No.	DATE	CHANGES	BY
A	Sep 22	Crank pin at shorter crank radius of 42 mm	MJS

3RD ANGLE PROJECTION U.N.O.
ALL DIM'S IN mm U.N.O.
DO NOT SCALE

Drawn: MJS
Date: Sep 22
Scale: 1:7

SITE 6 , 528-560 ALDERLEY Street.
TOOWOOMBA, QLD 4350 Australia.
Fax: (07) 46352004
Phone: (07) 46352660
EMAIL:

Michael Sheehan
STIRLING ENGINE GENERAL ASSEMBLY
SHEET 1 OF 2
Job Number:

Drawing No. **MS-SE-GA**
Rev. **A**

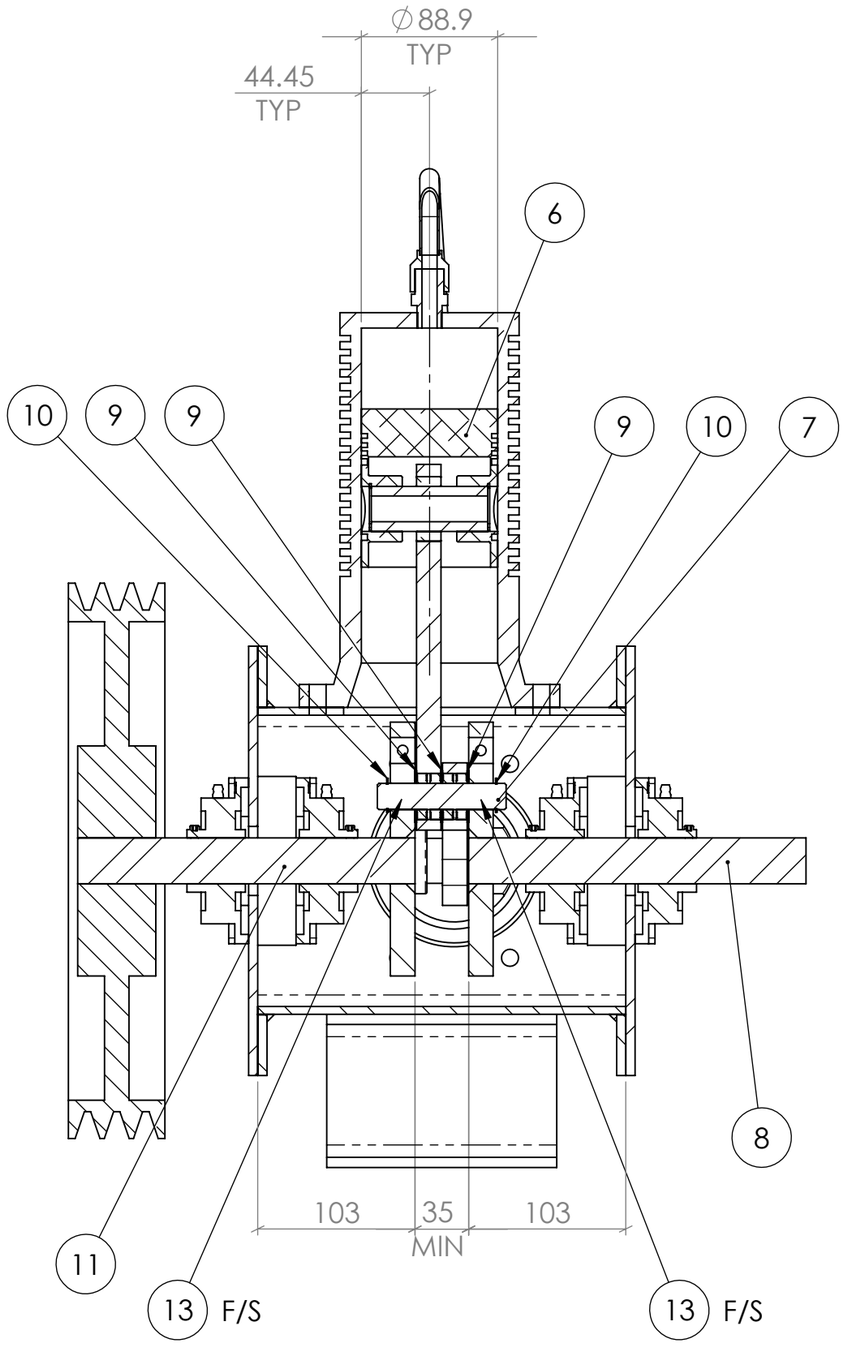

SECTION A-A

SCALE 1 : 4

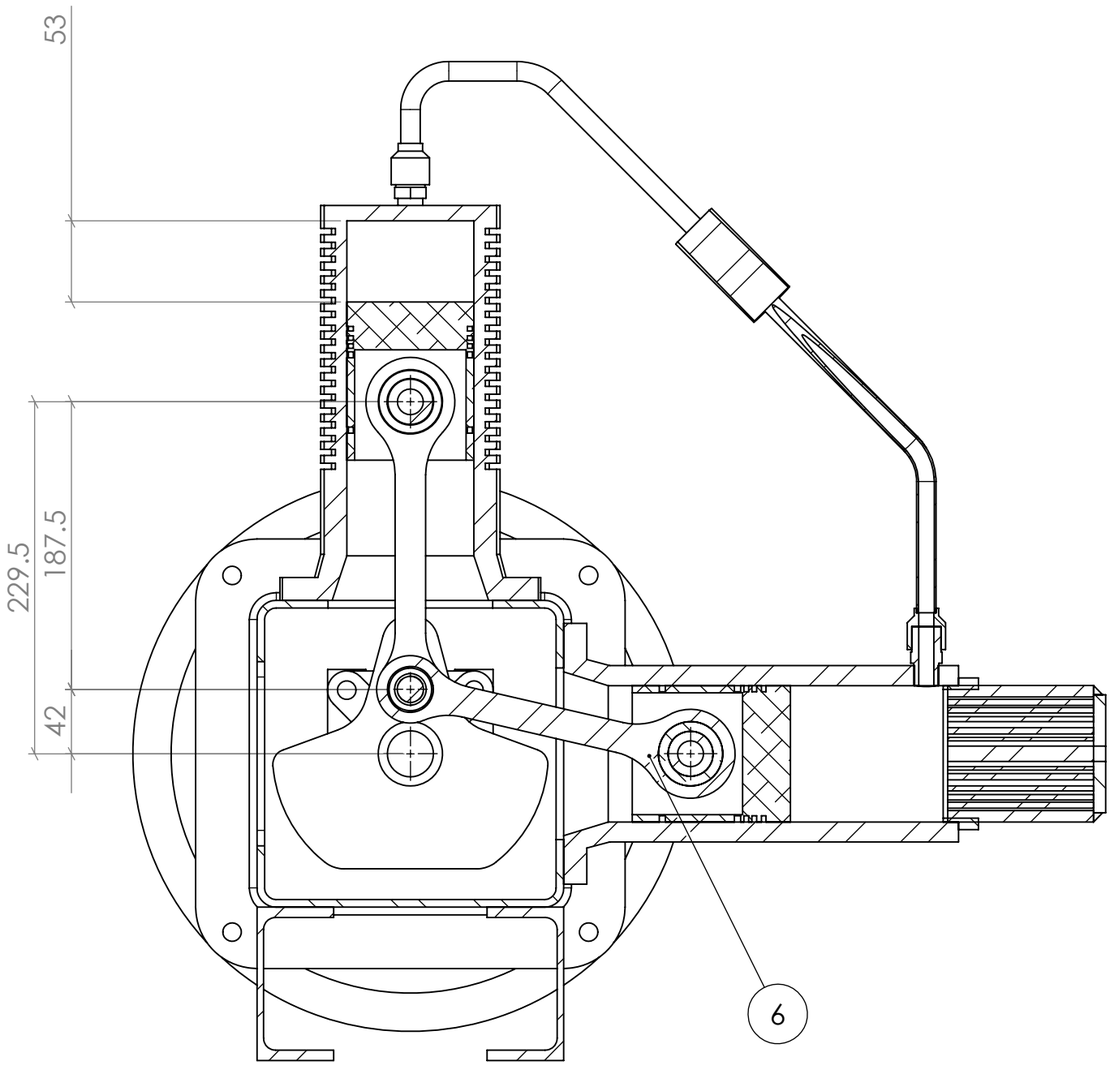

SECTION B-B

SCALE 1 : 4

All fillet welds 6mm continuous U.N.O.

APPROVED FOR CONSTRUCTION

SIGNED:

DATE: / /

Drawing is not valid unless signed

No.	DATE	CHANGES	BY
A	Sep 22	Crank pin at shorter crank radius of 42 mm	MJS

3RD ANGLE PROJECTION U.N.O.

ALL DIM'S IN mm U.N.O.

DO NOT SCALE

Drawn: MJS

Date: Sep 22

Scale: 1:7

SITE 6 , 528-560 ALDERLEY Street.
TOOWOOMBA, QLD 4350 Australia.
Fax: (07) 46352004
Phone: (07) 46352660
EMAIL:

OZTEC Manufacturing

STIRLING ENGINE

GENERAL ASSEMBLY

SHEET 2 OF 2

Job Number:

Drawing No. **MS-SE-GA**

Rev. **A**

ITEM NO.	DESCRIPTION	DRAWING NUMBER	QTY.
1	ENGINE BODY	MS-SE-03	1
2	HOT CYLINDER	MS-SE-01	1
3	COLD CYLINDER	MS-SE-02	1
4	REGENERATOR TUBE	MS-SE-10	1
5	COVER	MS-SE-11	1
6	LONG PISTON CONROD ASSEMBLY	MS-SE-22	2
7	CRANK PIN	MS-SE-05	1
8	OUTPUT SHAFT ASSEMBLY	MS-SE-19	1
9	CONROD SHIM	MS-SE-20	3
10	17mm EXTERNAL CIRCLIP		2
11	FLYWHEEL SHAFT ASSEMBLY	MS-SE-17	1
12	HEATER HEAD	MS-SE-15	1
13	M8 x 10 GRUB SCREW		2
14	M12 x 35 BOLT GR8.8 w/ NYLOC NUT & WASHER 2x		8
15	M10 x 40 BOLT GR8.8 w/ NYLOC NUT & WASHER 2x		12
16	M12 x 50 BOLT GR8.8 w/ NYLOC NUT & WASHER 2x		4
17	M6 x 12 BOLT GR8.8 w/ SPRING WASHER		4

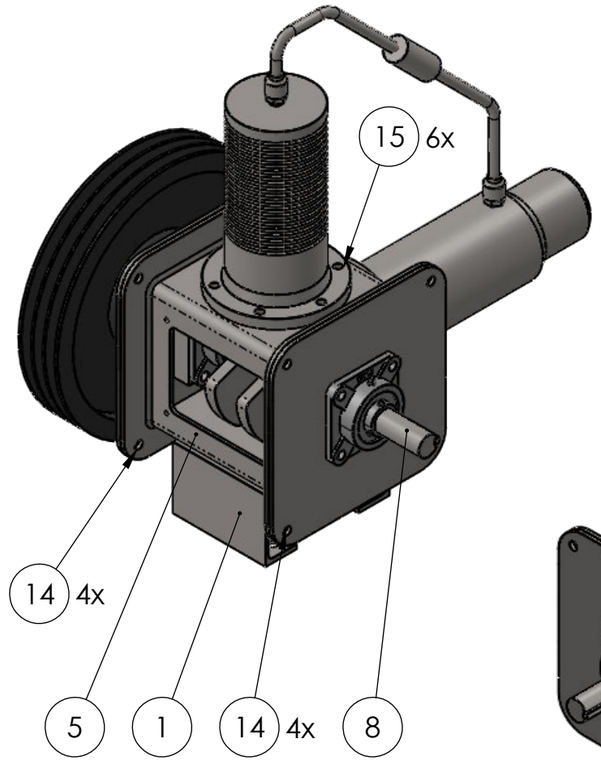

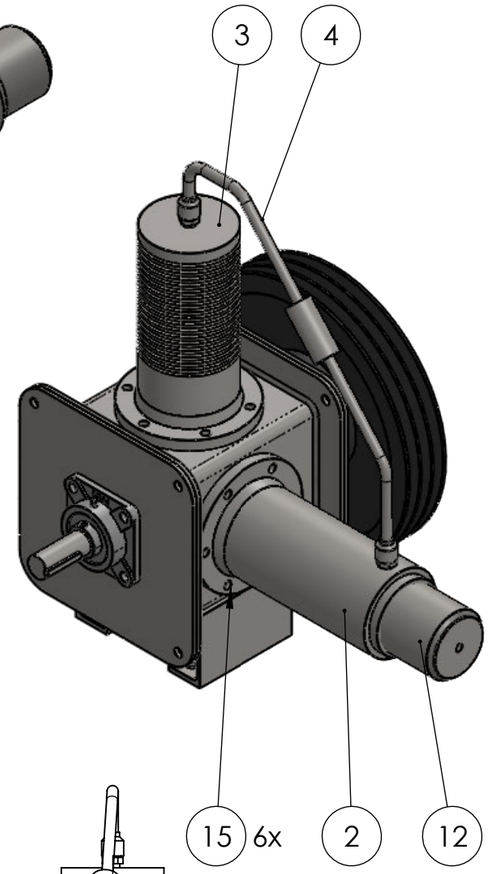

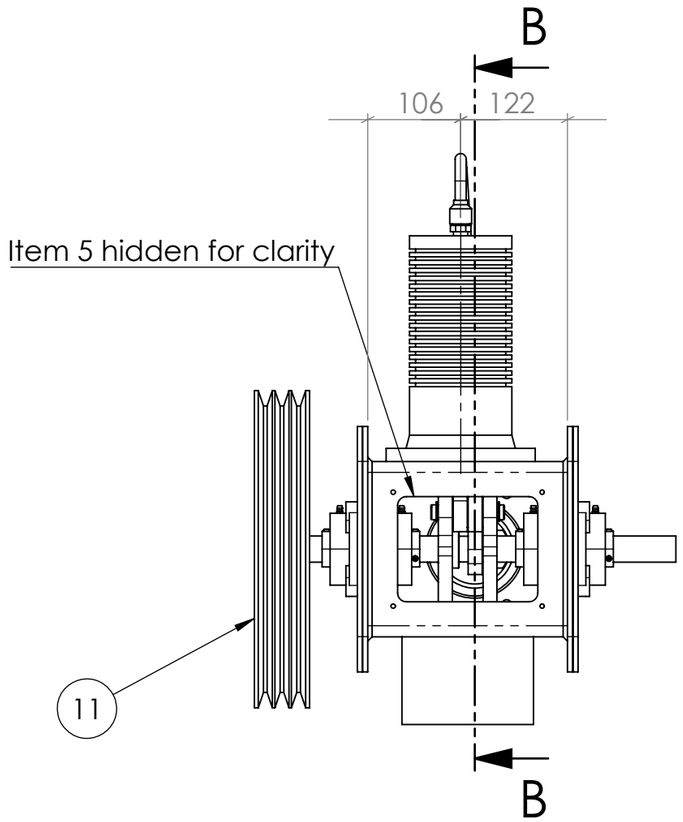

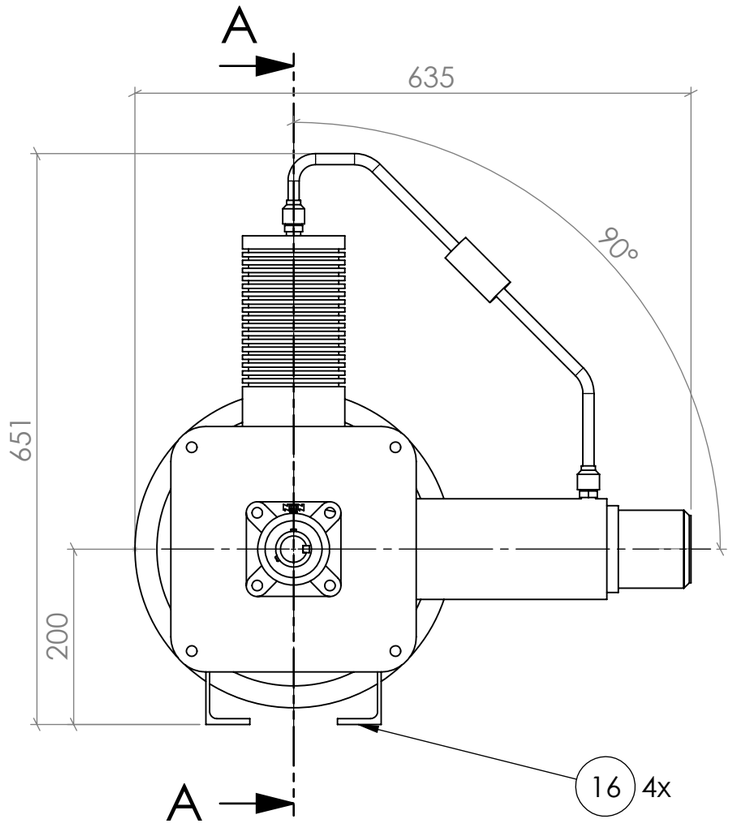

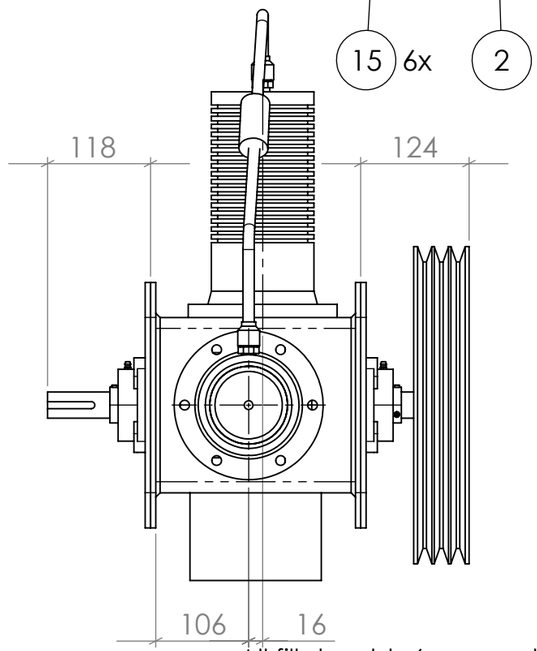

All fillet welds 6mm continuous U.N.O.

APPROVED FOR CONSTRUCTION
SIGNED:
DATE: / /
Drawing is not valid unless signed

No.	DATE	CHANGES	BY
B	Sep 22	Longer connecting rod with 214 mm centre distance	MJS
A	Sep 22	Crank pin at shorter crank radius of 42 mm	MJS

3RD ANGLE PROJECTION U.N.O.
ALL DIM'S IN mm U.N.O.
DO NOT SCALE

Drawn: MJS
Date: Sep 22
Scale: 1:7

SITE 6 , 528-560 ALDERLEY Street.
TOOWOOMBA, QLD 4350 Australia.
Fax: (07) 46352004
Phone: (07) 46352660
EMAIL:

Michael Sheehan
STIRLING ENGINE GENERAL ASSEMBLY
SHEET 1 OF 2
Job Number:

Drawing No. **MS-SE-GA**
Rev. **B**

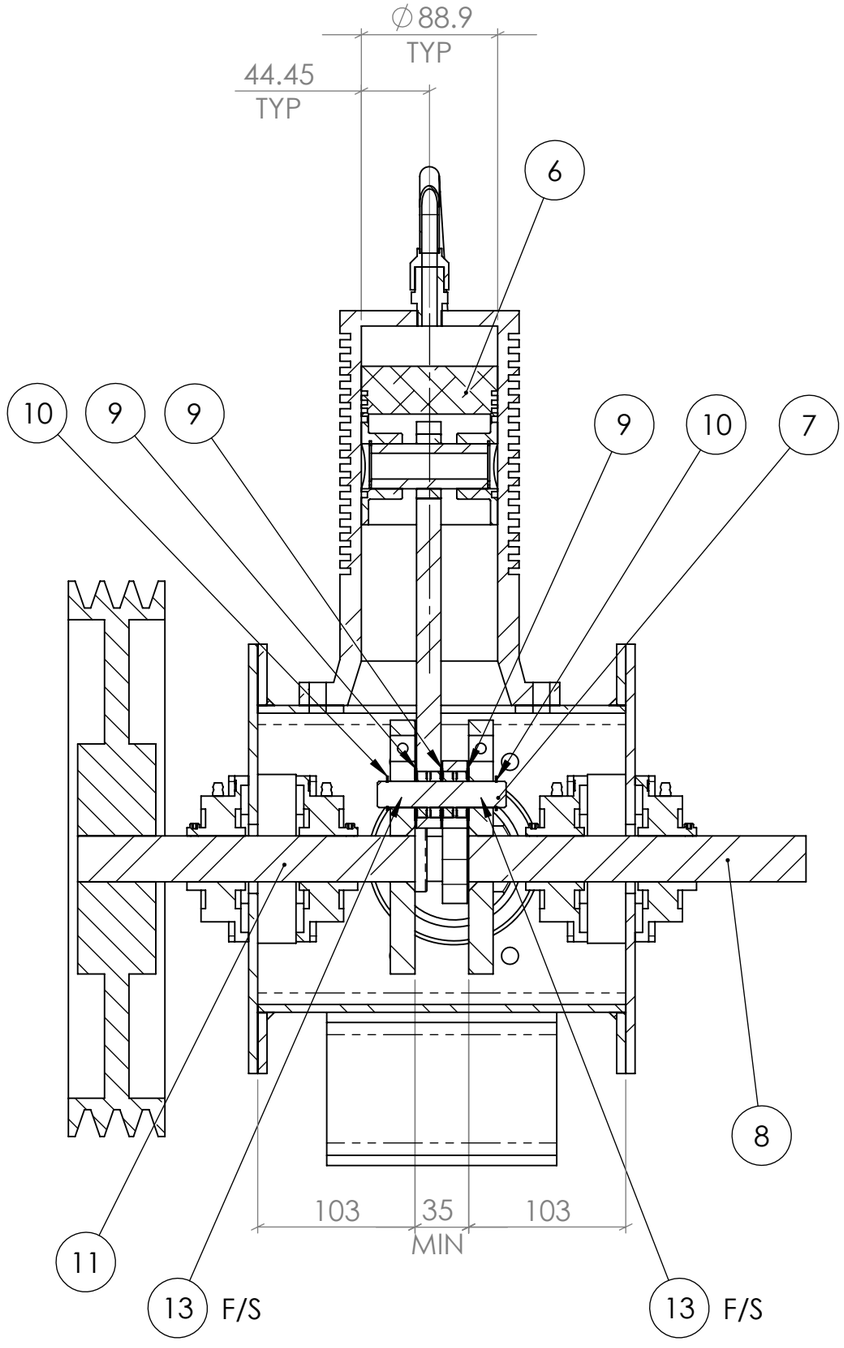

SECTION A-A

SCALE 1 : 4

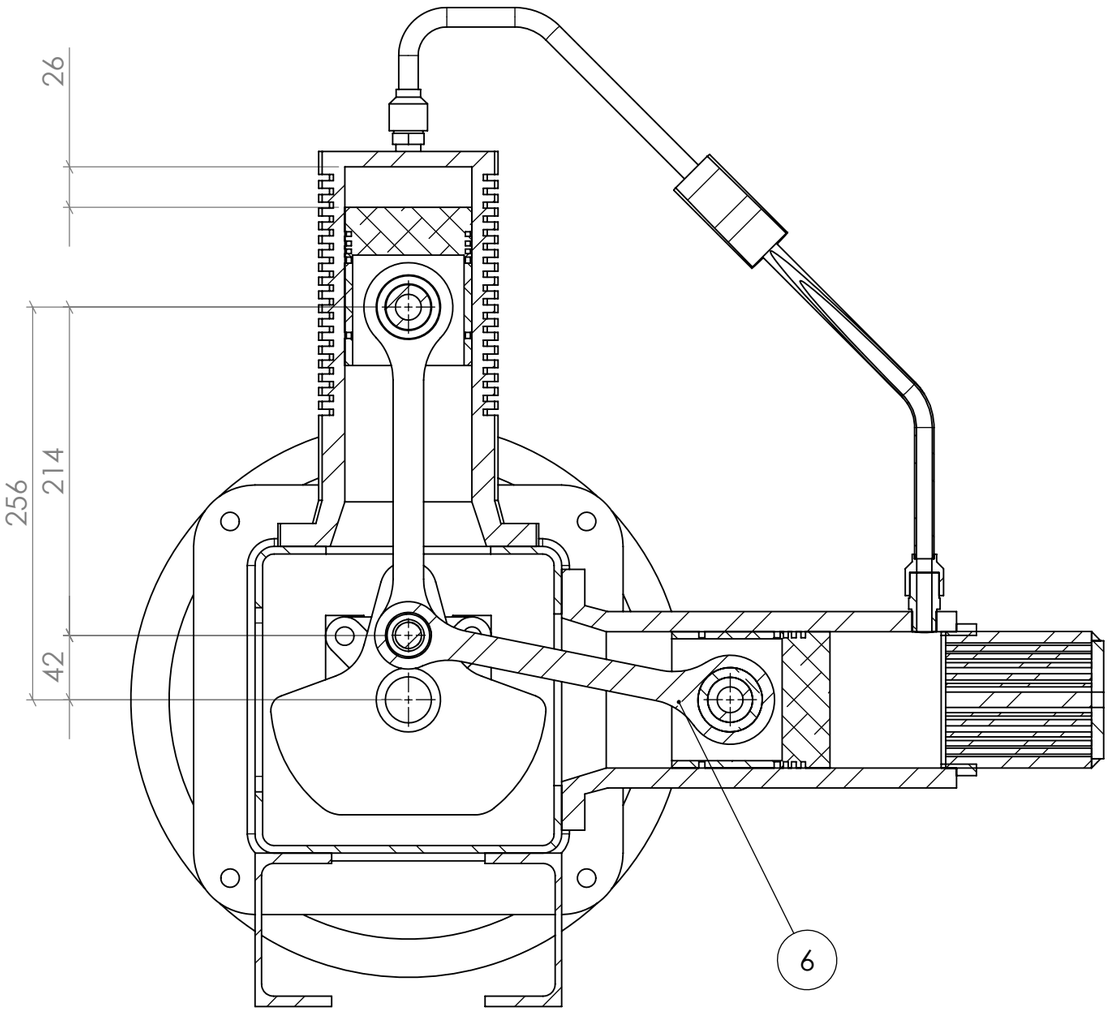

SECTION B-B

SCALE 1 : 4

All fillet welds 6mm continuous U.N.O.

APPROVED FOR CONSTRUCTION

SIGNED:

DATE: / /

Drawing is not valid unless signed

No.	DATE	CHANGES	BY
B	Sep 22	Longer connecting rod with 214 mm centre distance	MJS
A	Sep 22	Crank pin at shorter crank radius of 42 mm	MJS

3RD ANGLE PROJECTION U.N.O.

ALL DIM'S IN mm U.N.O.

DO NOT SCALE

Drawn: MJS

Date: Sep 22

Scale: 1:7

SITE 6 , 528-560 ALDERLEY Street.
TOOWOOMBA, QLD 4350 Australia.
Fax: (07) 46352004
Phone: (07) 46352660
EMAIL:

OZTEC Manufacturing

STIRLING ENGINE

GENERAL ASSEMBLY

SHEET 2 OF 2

Job Number:

Drawing No. **MS-SE-GA**

Rev. **B**

ITEM NO.	QTY.	DESCRIPTION	LENGTH
1	1	16 PL GR350	

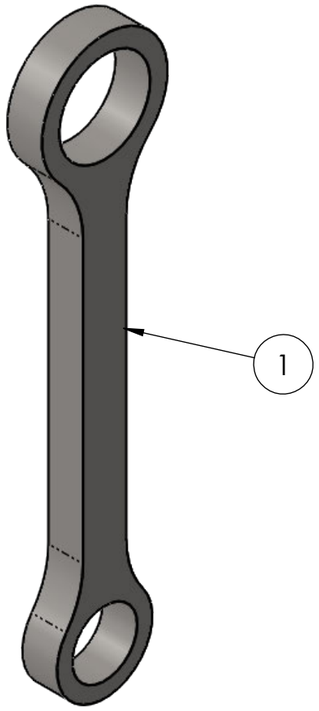

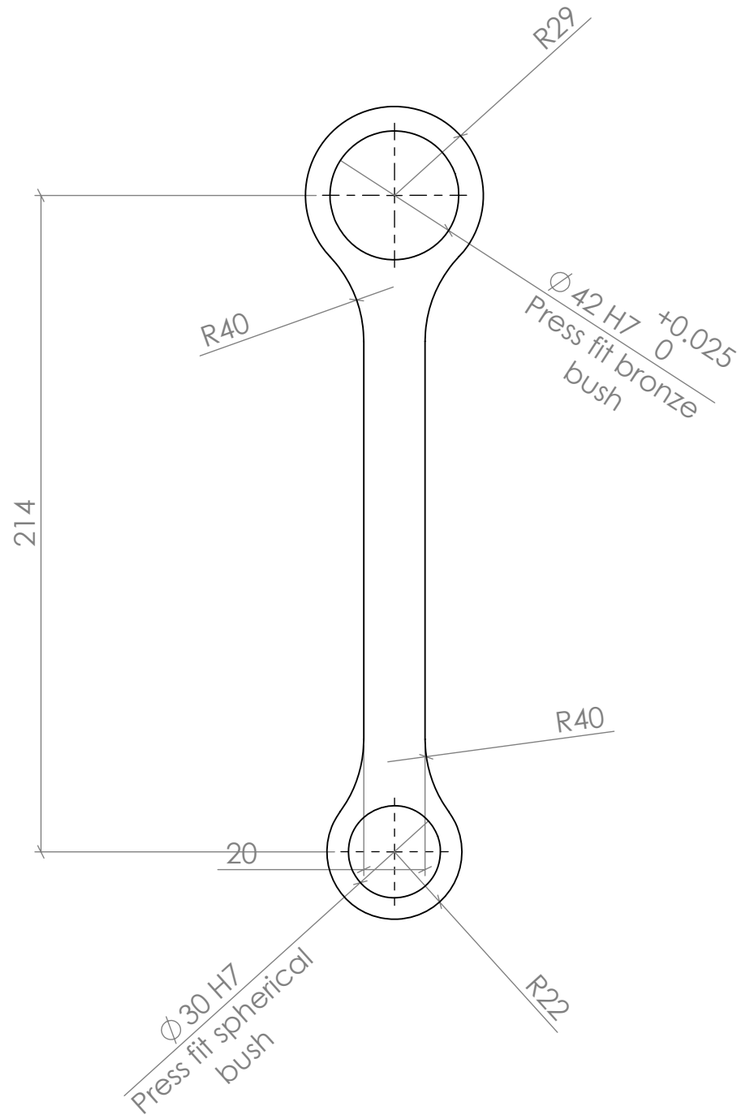

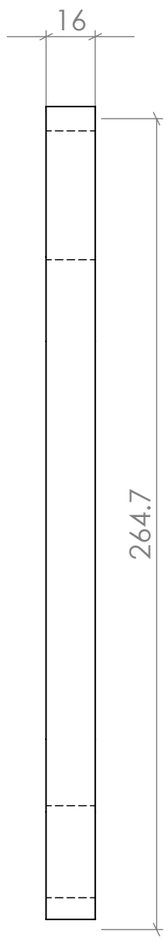

All fillet welds 6mm continuous U.N.O.

APPROVED FOR CONSTRUCTION
SIGNED:
DATE: / /
Drawing is not valid unless signed

No.	DATE	CHANGES	BY
-	-		

3RD ANGLE PROJECTION U.N.O.
ALL DIM'S IN mm U.N.O.
DO NOT SCALE

Drawn: MJS
Date: Sep 2022
Scale: 1:2

USQ ENG4111/2 Research Project
TOOWOOMBA, QLD 4350 Australia
Student Number: 0061080388
Ph: 0455142395
EMAIL: U1080388@umail.usq.edu.au

Michael Sheehan
Stirling Engine
LONG CON ROD 214 mm
SHEET 1 OF 1
Job Number:

Drawing No. **MS-SE-21**
Rev. **-**

ITEM NO.	DESCRIPTION	DRAWING NUMBER	QTY.
1	LONG CON ROD 214 mm	MS-SE-20	1
2	CONROD BUSH	MS-SE-08	1
3	BEARING 6903 (30 x 17 x 7)		2
4	PISTON PA483506 STD	MS-SE-14	1
5	INTERNAL CIRCLIP 29.37mm		2

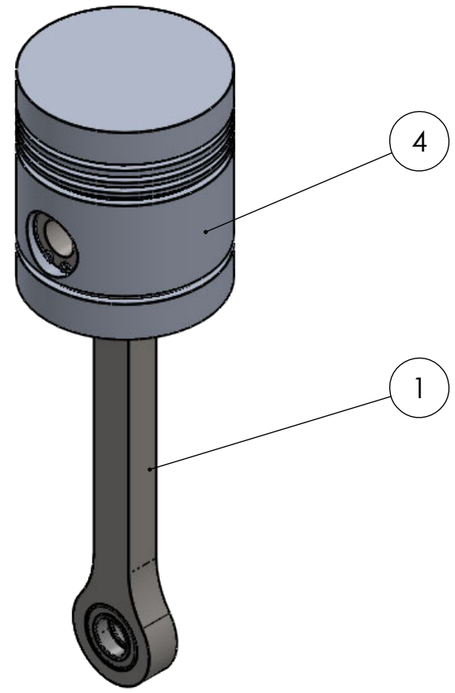

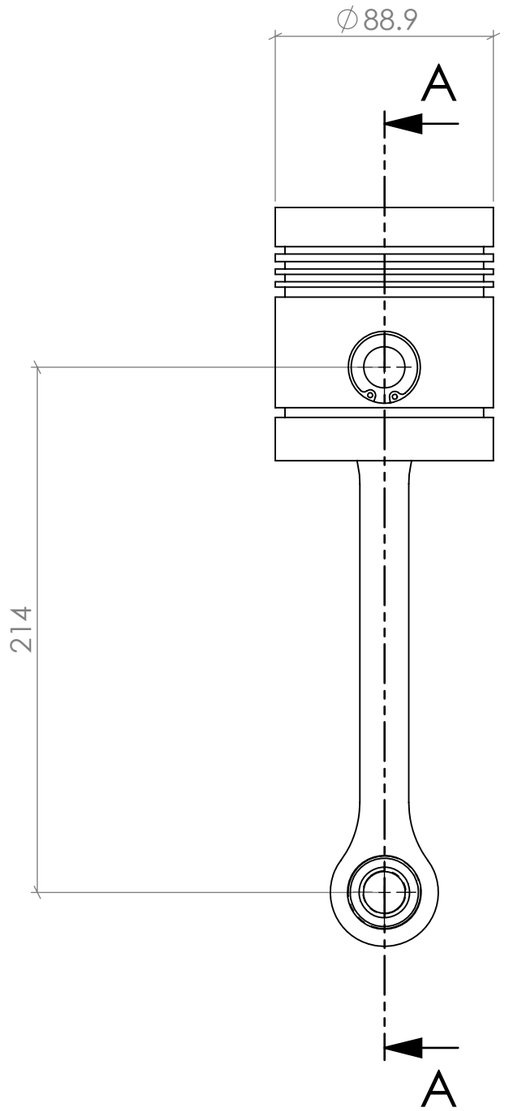

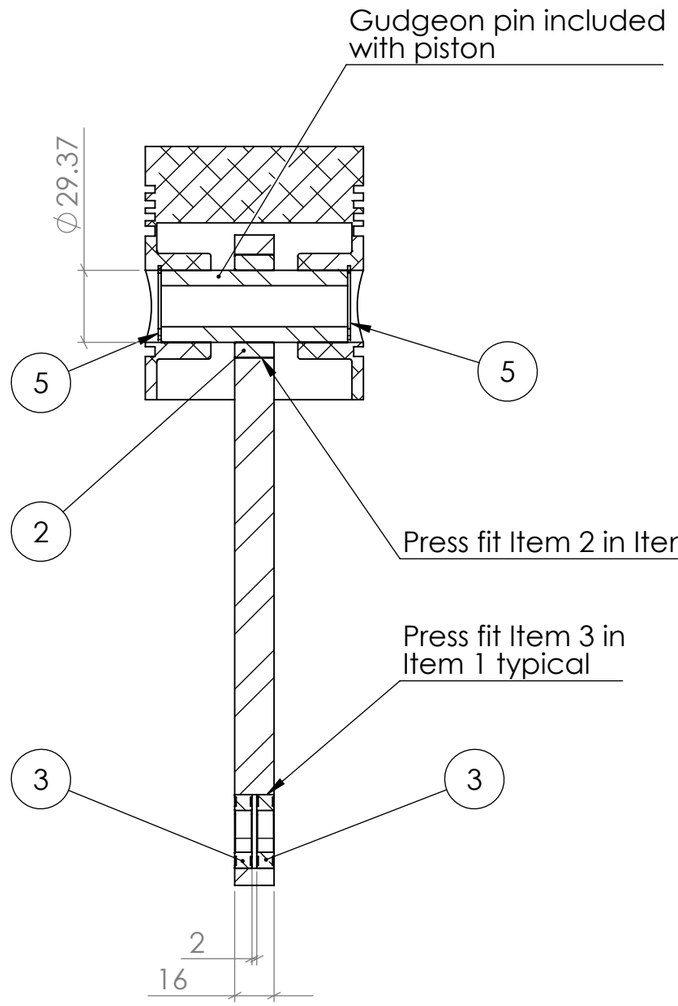

SECTION A-A

All fillet welds 6mm continuous U.N.O.

APPROVED FOR CONSTRUCTION
SIGNED:
DATE: / /
Drawing is not valid unless signed

No.	DATE	CHANGES	BY
-	-		

3RD ANGLE PROJECTION U.N.O.
ALL DIM'S IN mm U.N.O.
DO NOT SCALE

Drawn: MJS
Date: Sep 22
Scale: 2:5

USQ ENG4111/2 Research Project
TOOWOOMBA, QLD 4350 Australia
Student Number: 0061080388
Ph: 0455142395
EMAIL: U1080388@umail.usq.edu.au

Michael Sheehan
Stirling Engine
LONG Piston Conrod Assembly
SHEET 1 OF 1 Job Number:

Drawing No. **MS-SE-22**
Rev. **-**